PERFORMANCE-BASED PLASTIC DESIGN OF EARTHQUAKE RESISTANT STEEL STRUCTURES: CONCENTRICALLY BRACEDFRAMES, TALL MOMENT FRAMES, PLATE SHEAR WALL FRAMES

By

MOHAMMAD REZA BAYAT

Presented to the Faculty of the Graduate School of

The University of Texas at Arlington in Partial Fulfillment

of the Requirements

for the Degree of

DOCTOR OF PHILOSOPHY

THE UNIVERSITY OF TEXAS AT ARLINGTON

December 2010

Dedicated to my family

ACKNOWLEDGEMENTS

The author wishes to express his sincere gratitude to his doctoral advisors, Professors Shih-Ho Chao and Subhash Goel, for their consistent support and guidance during the course of his Ph.D. studies. Without them, this research work would not have been possible. It has been the author's great pleasure and honor to have the opportunity to work with both of them. The author hopes he can continue working with them for many years to come not only as colleagues, but also as friends. Many appreciations are due to Professor Chao, who along with financial support has provided the author with great academic resources at UT Arlington to pursue his studies. The author is most indebted to Professor Goel, his advisor from The University of Michigan, for his exemplary guidance, mentorship, and support throughout all this time which have greatly benefited the author both personally and professionally.

The author would also like to express his sincere gratitude to Professor Ali Abolmaali, member of doctoral committee, for his consistent guidance and encouragement. His generous advices have always been helpful and have greatly helped the author in pursuing his professional goals.

In addition, author's warm appreciation is extended to his doctoral committee members, Professors John H. Matthys, Frank K. Lu, and Guillermo Ramirez for their time, guidance, and helpful suggestions.

The author also acknowledges the partial funding support provided by G. S. Agarwal Fellowship Fund at The University of Michigan, NUCOR Research and Development, and American Institute of Steel Construction for the research work in this dissertation.

Last, but not least, the author wishes to extend his utmost heartfelt appreciation to his family, to whom this dissertation is dedicated, for their endless love, encouragement, and support. They have always been the great source of inspiration to him.

November 5, 2010

ABSTRACT

PERFORMANCE-BASED PLASTIC DESIGN OF EARTHQUAKE RESISTANT STEEL STRUCTURES: CONCENTRICALLY BRACED FRAMES, TALL MOMENT FRAMES, PLATE SHEAR WALL FRAMES

Mohammad Reza Bayat, Ph.D.

The University of Texas at Arlington, 2010

Supervising Professors: Shih-Ho Chao, Subhash C. Goel

It is well known that structures designed by current codes experience large inelastic deformations during major earthquakes. However, current seismic design practice in the U.S. is based on elastic structural behavior and accounts for inelastic behavior only in an indirect manner through certain modification factors such as R, I, and C_d. Under moderate to severe earthquakes, inelastic activity, including severe yielding and buckling of structural members can be unevenly distributed in the structure which may result in global collapse or costly repair work. Recently, a new design method has been developed and referred to as Performance-Based Plastic Design (PBPD). This method directly accounts for inelastic behavior by using pre-selected target drift and yield mechanism as key performance limit states.

In this research work, the application of PBPD is successfully extended to design of mid-rise to tall steel Concentrically Braced Frames (CBF) with increased confidence level against collapse and also to tall steel Moment Frames (MF). The PBPD procedure for design of Steel Plate Shear Walls (SPSW) is also developed.

The PBPD method is extended to design of mid-rise to tall CBF structures by proposing several key modifications in the calculation of design base shear. These include: consideration of column axial deformations in estimation of yield and target drifts, lateral force distribution to prevent large story drifts at upper stories due to higher mode effects, and target drift by proposed λ-factor to account for pinched hysteretic behavior. Moreover, different methods are suggested to enhance the confidence level of mid- to high-rise CBF structures against collapse. These methods include: increase in design base shear by using slightly larger λ-factor for mid- to high-rise frames, using Split-X configuration for braces, and increasing the minimum required fracture life, N_f.

Application of PBPD method in design of tall MF structures is successfully carried out. Modifications for design of tall MF systems, primarily on design of columns, are proposed to achieve this goal. The current PBPD procedure for design of columns in steel MF structures works well for low-rise frames, but results in overdesigned sections for mid- to high-rise frames. It is shown that by applying the proposed modifications in design of tall MF, excellent seismic performance under pushover as well as time-history analyses can be achieved.

The PBPD procedure for design of SPSW, an emerging lateral load resisting system, is developed. This procedure uses target drift and yield mechanism as key

performance limit states. The pinched hysteretic behavior of SPSW is directly accounted for in this method by using the proposed λ-factor method. By applying this method in the design of a 4-story SPSW frame, it was shown that the proposed PBPD procedure works very well for design of these systems. The performance criteria of target drifts and yield mechanisms were successfully met for the PBPD designs. In addition, with the proposed PBPD procedure, multiple level design based on appropriate target drifts for each hazard level, can be easily implemented. In general, the PBPD designed frames showed improved performance compared to the code designed SPSW frame, especially under MCE ground motions.

TABLE OF CONTENTS

LIST OF FIGURES

LIST OF TABLES

CHAPTER 1

INTRODUCTION

1.1 Background and Motivation

Current seismic design practice is generally based on elastic structural behavior with inelastic behavior only considered indirectly through certain modification factors. However, it is well known that the structures designed by current codes experience large inelastic deformations during major earthquakes (e.g. Gupta and Krawinkler, 1999). Code design base shear in current U.S. seismic design practice is calculated by using specified elastic spectra, and then modified by appropriate response modification factor, *R,* and importance factor, *I*. After design of members (which is generally done based on elastic analysis results), the inelastic drift is estimated by multiplying the elastic drift by a deflection amplification factor, C_d. This estimated drift should not exceed the code specified drift limits (on the order of 2% for moment frames). It has been found that the structures designed by such procedures experience large inelastic deformations under severe earthquake ground motions (e.g. Goel and Leelataviwat, 1998; Gupta and Krawinkler, 1999). In other words, the behavior of structures subjected to design level ground motions can be somewhat unpredictable and uncontrolled even after all of the current code criteria are satisfied. Inelastic activity, including severe yielding and buckling of structural members can be unevenly distributed in the structure which may

result in global collapse or costly repair work. Therefore, the current design approaches may not lead to structures with intended behavior under major ground motions.

Due to the increased demand levels on performance, safety, and economy needed in structural design, especially in the aftermath of the 1994 Northridge and the 1995 Kobe earthquakes, the new building codes are finding their way toward Performance-Based Design (PBD) framework. As a result, there is an increasing demand for new analysis/design procedures which are capable of predicting structural behavior in a more accurate way such that they can be implemented in PBD practice. This is due to the fact that the main goal of PBD is to have desirable and predictable structural responses. Currently, PBD is carried out by performing series of design and evaluations in an iterative manner, which may not always give the desired result because an initial good design is needed to arrive at the targeted design after iterations (Krawinkler and Miranda, 2004). It should also be noted that the current seismic design procedures focus mainly on the demand to capacity ratios at the member and component level rather than the global (system) level. Accordingly, the overall structural performance may be strongly affected by the weakest or least-ductile elements (Hamburger at al., 2004).

In order to achieve more predictable structural performance under strong earthquake ground motions, knowledge of the ultimate structural behavior, such as nonlinear relations between force and deformation, and yield mechanism of the structure are essential. Accordingly, design factors such as determination of appropriate design lateral forces, selection of desirable yield mechanism, and structure strength and drift etc., for given hazard levels should become part of the design process right from the

beginning. One such complete design methodology, which accounts for structural inelastic behavior directly and practically eliminates the need for any assessment or iteration after initial design, has been developed by S. C. Goel and his associates at The University of Michigan during the last ten years or so (Leelataviwat et al., 1999; Lee and Goel, 2001; Dasgupta et al., 2004; Chao and Goel, 2005; Chao and Goel, 2006a; Goel and Chao, 2008). The method is called Performance-Based Plastic Design (PBPD).

This method directly accounts for inelastic behavior and eliminates the need for any assessment after initial design. The method uses pre-selected target drift and yield mechanism as key performance limit states. The design base shear for selected hazard level(s) is calculated by equating the work needed to take the structure monotonically up to the target drift to that required by an equivalent elastic-plastic single degree of freedom (EP-SDOF) system to achieve the same state. In addition, a new lateral force distribution has been developed based on the relative distribution of maximum story shears obtained from inelastic dynamic analysis (Chao et al., 2007). Plastic design and appropriate capacity approach are then carried out to detail the yielding members and other frame members (including connections) respectively, in order to achieve the intended yield mechanism and behavior. More details of this method can be found in Chapter 3.

The method has been successfully applied to steel Moment Frames (MF), Buckling Restrained Braced Frames (BRBF), Eccentrically Braced Frames (EBF), Special Truss Moment Frames (STMF). Its application to conventional concentrically braced frames (CBF) with degrading hysteretic behavior due to brace buckling is currently being developed with the encouraging results thus far. In all cases, the frames

developed the desired strong column-weak beam/yielding member mechanisms as intended, and the story drifts/ductility demands were well within the selected design values, thus meeting the selected performance objectives. Comparisons of responses with corresponding baseline frames designed by current practice have consistently shown superiority of the proposed methodology, in terms of achieving the desired behavior (Goel and Chao, 2008).

The research work presented herein proposes several important improvements in the application of the PBPD method in design of CBF and tall steel MF systems. In addition, the PBPD procedure for design of Steel Plate Shear Wall (SPSW) systems has been developed in this research work. The modifications for steel MF systems are mainly on the design of columns in tall frames. Although the current PBPD procedure for design of columns in steel MF systems works well for low-rise frames, it results in significantly overdesigned sections for mid-rise to tall frames. For CBF structures, modifications to the calculation of the PBPD design base shear are proposed to account for the pinched hysteretic response and also the varying yield drift ratios due to column axial deformation of such systems. These modifications are especially beneficial in applying the PBPD method to taller CBF structures. Moreover, different methods to increase the confidence level of mid to high-rise CBF structures against collapse are proposed and their efficiencies in enhancing the confidence level are evaluated. Furthermore, the PBPD procedure for design of SPSW systems is developed. This procedure uses target drift and yield mechanism as key performance limit states. Using the proposed PBPD method,

SPSW structures can be designed such that they can meet the desired performance criteria (target drift and intended yield mechanism) for given hazard levels.

1.2 Objectives and Organization of the Dissertation

The purposes of this study were to further improve the newly developed Performance-Based Plastic Design (PBPD) procedure and also to develop the procedure for application of this method to new steel structural systems. The main objectives were: (1) To refine the design of columns, as part of the PBPD procedure, in tall steel Moment Frames (MF); (2) To modify the application of PBPD procedure for Concentrically Braced Frames (CBF), especially for taller CBF; (3) To enhance the confidence level of taller CBF structures against collapse; and (4) To develop the PBPD procedure for design of steel plate shear walls (SPSW), an emerging lateral load resisting system. The organization of the dissertation follows:

- Chapter 1 provides background and motivations, objectives and the organization of the dissertation.
- Chapter 2 presents a review of the current seismic procedures. Previous studies on the problems with the current code procedures along with the new PBPD method are summarized. In addition, the performances of steel MF and CBF in past earthquakes are reviewed. Moreover, the analytical and experimental studies on Steel Plate Shear Wall (SPSW) systems are reviewed.
- Chapter 3 presents an introduction to the PBPD procedure along with the discussion on different components of this method.

- Chapter 4 presents the results of reliability-based performance evaluation or confidence level analysis of two sets of CBF, the NEHRP design and the PBPD design. The confidence levels of the PBPD frames against global collapse are obtained using the procedure outlined in FEMA 351 (FEMA, 2000b). These confidence levels are then compared with those of code-compliant NEHRP frames.

- In Chapter 5, the PBPD procedure for CBF systems is evaluated and several modifications are proposed. A new configuration for the gusset plate connection, in which the gusset plate is only connected to the column, is proposed such that the total unbalanced moment on the column would be reduced. Also, the current capacity design method for columns in CBF based on the accumulative axial forces is evaluated by comparing the column moments from pushover and dynamic analyses. In addition, a proposed method to account for pinching hysteretic behavior of CBF in PBPD approach, with the capability to be applied to other types of systems with degrading behavior, is introduced. For design base shear calculation in CBF systems, a procedure to estimate the varying yield drift ratio (due to flexural deformation caused by axial deformation of columns) at the beginning of design for braced systems is proposed. The target drift ratio for such systems is modified accordingly, based on the original definition of the target drift used in the work-energy equation in PBPD. The suggested PBPD approach is utilized to design the 9-story SAC building by using CBF as the lateral load resisting system. The performance of this design is then evaluated using 10%/50yrs (DBE) and 2%/50yrs (MCE) SAC LA ground motions. Moreover, the seismic performance of the 9-story braced frame designed by PBPD with rigid and pinned beam to column connections

are studies. Finally, the performance of the PBPD designed 9-story CBF is evaluated by using the FEMA 351 (FEMA, 2000b) procedure and its confidence level against collapse is obtained.

- In Chapter 6, several methods in design of mid to high-rise CBF structures are proposed in order to improve their confidence level against collapse. The efficiency of each method in increasing the confidence level is evaluated. These include modification in the PBPD design base shear calculation for taller CBF by revising the λ-factor initially estimated in Chapter 5, and considering alternate brace configuration of two story X-pattern (Split-X). Also, the effect of increasing the minimum brace fracture life, N_f , on the confidence level studied.

- Chapter 7 presents modifications to the current PBPD procedure for design of Non-Designated Yielding Members (Non-DYMs), such as columns, in tall MF structures such that their final design better matches with the expected performance. Two main issues are addressed in this chapter: (1) Calculation of base column plastic moment, M_{pc}, to prevent formation of soft-story mechanism and also to achieve a more realistic column design moment profile over the height of the structure; and (2) P-Delta effect for design of Non-DYMs. These modifications are then applied to redesign the 20-story SAC LA building by the PBPD method using suggested modifications. The performance of the original SAC frame and the PBPD frame under nonlinear static and dynamic analyses are then evaluated and compared.

- In Chapter 8, the PBPD procedure for design of SPSW systems are presented. The procedure presents a systematic approach for analysis and design of such systems,

using target drift and yield mechanism as key performance limit states. The pinching behavior of SPSW is directly accounted for in this method by using the proposed λ-factor method. Using the developed PBPD method, a dual level design based on appropriate target drift for each hazard level can be easily implemented to obtain the desired performance at different hazard levels for SPSW systems. The proposed procedure is then applied to design of SPSW structures and the performances of these systems are evaluated using nonlinear static and dynamic analyses.

- Chapter 9, the final chapter, presents the summary and conclusions of this study along with suggestions for future studies.

CHAPTER 2

LITERATURE REVIEW

2.1 General

The current seismic design procedures are mainly based on elastic structural behavior analyses under seismic horizontal forces and account for inelastic behavior in a rather indirect manner. Such Equivalent Lateral Force Procedures are specified in the recent seismic codes such as Uniform Building Code (UBC, 1997), NEHRP Recommended Provisions (NEHRP, 1997), and NEHRP 2003 (BSSC, 2003). These procedures offer rather simplified methods to obtain the design base shear from the code-specified spectral accelerations by assuming elastic behavior for the structure and then reducing the design base shear by a force modification factor, *R*, obtained based on the expected ductility of the structural system.

The structures designed by using such procedures may have adequate strength and stiffness to meet the serviceability requirements. However, it is well known that the structures designed to the current codes can experience inelastic deformations under severe earthquakes in a somewhat uncontrolled manner. Such inelastic deformations can be disproportionately and widely distributed in the structure. This can prevent the structure from forming the intended failure mode which may result in less than expected ductility and energy dissipation capacity. In addition, rather undesirable and unpredictable response including total collapse of the structure can occur.

Current code design philosophy is to provide sufficient strength and stiffness for the structure such that it remains serviceable during small and frequent earthquakes and also provides life safety for the occupants under the event of a severe earthquake.

In the following sections of this chapter, the performances of steel MF and CBF in past earthquakes are reviewed. The current code seismic design methods are discussed. Previous studies on the issues with the current code procedures along with the new PBPD method are summarized. In addition, the analytical and experimental studies on Steel Plate Shear Wall (SPSW) systems are reviewed.

2.2 Seismic Performance of Moment Frames

2.2.1 Performance of Moment Frames in Past Earthquakes

Due to their architectural flexibility and ease of constructability, steel moment frames (SMF) are one of the most common structural systems used in the United States and other places in the world as the lateral load resisting system. The performance of these frames seemed to be good in some major earthquakes before the 1994 Northridge earthquake, such as 1964 Alaska, 1971 San Fernando, and 1989 Loma Prieta earthquakes. These observations appear to confirm the common opinion about SMFs that they have ductile and stable behavior under earthquake loading and led to the belief that these systems present outstanding seismic performance (Malley, Yu, and Moore, 2004). As a result, welded SMF structures with welded beam-to-column connections were widely used by engineers as lateral load resisting system for major buildings in the areas with high seismicity. It was believed that the earthquake induced damage in these systems

would be limited to the ductile yielding of members and connections and their collapse under earthquake was not deemed to be possible. The 1994 Northridge earthquake significantly questioned this view. Following this earthquake, several welded SMF buildings were discovered to have experienced brittle fractures of beam-to-column connections. The height of the damaged buildings ranged from one story to 26 stories, and their age ranged from buildings as old as 30 years to structures being erected at the time of the earthquake. Such damages were often associated with no or very little architectural damage which were making them difficult to be revealed. Such findings also raised concerns about the possibility of similar damages from previous earthquakes. Later investigations verified the occurrence of such damages in a number of buildings under 1992 Landers, 1992 Big Bear, and 1989 Loma Prieta earthquakes (FEMA 355E, 2000c). Similar damages to SMF buildings were reported after 1995 Kobe earthquake in Japan. This earthquake was more severe than the Northridge earthquake and caused about 10% of the welded SMFs to collapse (Malley, Yu, and Moore, 2004; FEMA 355E, 2000c).

Although no case of collapse occurred in welded SMF structures in the US under earthquakes, the findings after Northridge earthquake led to growing concerns about the safety of such buildings in the event of a larger earthquake. Consequently, a 6-year project, funded by Federal Emergency Management Agency (FEMA), and based on an agreement between FEMA and SAC Joint Venture, was defined to carry out the investigation, and develop guidelines for inspection, evaluation, rehabilitation and construction of SMF structures. These collaborative efforts resulted in the development of several guidelines and documents for design, evaluation, and rehabilitation of SMFs

such as the Recommended Seismic Design Criteria for New Steel Moment Frame Buildings, FEMA 351 (FEMA, 2000b) and many other useful documents (Malley, Yu, and Moore, 2004).

2.2.2 Current Code Design Method

The current code seismic design procedures in the United States are mainly based the NEHRP Recommended Provisions published in 2003, also called FEMA-450 (BSSC, 2003). It should be noted that the seismic design criteria in ASCE/SEI 7-05 (ASCE, 2005) is exclusively based on the NEHRP 2003 Recommended Provisions. The ASCE/SEI 7-05 is the document that the International Building Code, IBC 2006 (ICC, 2006) is referring to for minimum design load criteria.

2.2.2.1 Equivalent Lateral Force Procedure (NEHRP-2003)

The NEHRP Recommended Provisions for Seismic Regulations for New Buildings and Other Structures (BSSC, 2003) specify the seismic requirements for design and construction of new structures. The required design base shear, V, in a given direction is obtained in accordance with the following equation:

$$V = C_s W \tag{2.1}$$

where C_s is the seismic response coefficient and W is the total dead load and applicable permanent portions of live loads which are expected to be present at the time of earthquake. The seismic response coefficient, C_s, is determined as:

$$C_s = \frac{S_{DS}}{R/I} \tag{2.2}$$

where S_{DS} is the design spectral response acceleration parameter in the short period range, R is the response modification factor, and I is the occupancy importance factor. S_{DS} is obtained as:

$$S_{DS} = \frac{2}{3} S_{MS} = \frac{2}{3} F_a S_S \tag{2.3}$$

where S_{MS} is the maximum considered earthquake spectral response acceleration for short periods and obtained by multiplying the site coefficient, F_a, and the mapped maximum considered earthquake spectral response acceleration at short periods, S_S. The values of site coefficient, F_a, are determined as a function of site class and mapped maximum considered earthquake spectral response acceleration at short periods.

The value of the seismic response coefficient computed in accordance with Equation 2.2 need not exceed the following:

$$C_s = \frac{S_{D1}}{T(R/I)} \quad \text{for} \quad T \le T_L \tag{2.4}$$

$$C_s = \frac{S_{D1} T_L}{T^2 (R/I)} \quad \text{for} \quad T > T_L \tag{2.5}$$

where S_{D1} is the design spectral response acceleration parameter at a period of 1.0 second, T is the fundamental period of the structure (in seconds), T_L is Long-period transition period (in seconds). C_s shall not be taken less than 0.01.

S_{D1} is determined as:

$$S_{D1} = \frac{2}{3} S_{M1} = \frac{2}{3} F_v S_1 \tag{2.6}$$

where S_{M1} is the maximum considered earthquake spectral response acceleration at 1.0 second and obtained by multiplying the site coefficient, F_v, and the mapped maximum considered earthquake spectral response acceleration at 1.0 second, S_1.

For buildings and structures located where S_1 is equal to or greater than 0.6g, C_s shall not be taken less than:

$$C_s = \frac{0.5S_1}{R/I} \tag{2.7}$$

where S_1 is the mapped maximum considered earthquake spectral response acceleration parameter.

For regular structures having 5 stories or less in height and having a period, T, of 0.5 seconds or less, the seismic response coefficient, C_s, is permitted to be calculated using values of 1.5 and 0.6, respectively, for the mapped maximum considered earthquake spectral response acceleration parameters S_S and S_1.

The fundamental period of the structure, T, can be approximately and conservatively estimated using the empirical formula given in the provisions. The approximate fundamental period for steel MF buildings is given by:

$$T_a = 0.028h_n^{0.8} \tag{2.8}$$

where h_n is the height in feet above the base to the highest level of the structure. There is also an upper bound limit for the estimated period form Equation 2.8. The estimated period should not exceed the product of C_u and T_a which are given in Section 5.2.2.1 of the provisions.

The response modification factor, R, values are given in Table 4-3.1 of the NEHRP 2003 provisions. For instance, the R value is given as 8 for special steel moment frames.

For deflection and drift limits, the NEHRP 2003 provisions require that the design story drift should not exceed the given allowable story drift. The basis of drift control is to provide both damage control and stability (against P-Delta effect) for the structure in the event that the design level earthquake occurs. The design of steel moment resisting frames is usually governed by drift limits rather than the strength criteria. According to the code, in calculation of the story drifts, for steel moment resisting frame systems, the contribution of panel zone deformations to overall story drift should be included.

The design story drift, Δ, is obtained as the difference of the deflections at the center of mass at the top and bottom of the story under consideration. The deflections of Level x, δ_x, should be determined in accordance with following equation:

$$\delta_x = \frac{C_d \delta_{xe}}{I} \tag{2.9}$$

where:

C_d = the deflection amplification factor from Table 4.3-1 of the provisions,

δ_{xe} = the deflections determined by an elastic analysis, and

The elastic analysis of the seismic-force-resisting system should be made using the prescribed seismic design forces. For structures, other than masonry shear wall or masonry wall frame structures, four stories or less in height with interior walls, partitions, ceilings, and exterior wall systems that have been designed to accommodate the story drifts, the story drifts are limited to the allowable story drift of Δ_a, equal to $0.025h_{sx}$ for

seismic use group I, $0.020h_{sx}$ for seismic use group II, and $0.015h_{sx}$ for seismic use group III, where h_{sx} is the story height below level x.

2.2.3 Summary of the Related Research

Many experimental and analytical studies have been done to study the seismic performance of SMF structures and the effect of design code procedures on the behavior of these systems under earthquake. In these studies, cyclic as well as dynamic tests have been done on components, full-scale and reduced-scale models. In addition, many analytical research works have been done on different aspects of seismic behavior of SMF structures. The focus in this literature review is mostly on the studies that consider revising the design procedures currently used in codes or developing new procedure for seismic design of SMF. Therefore, this review is done in two parts. In the first part, a summary of the previous studies on the performance of the SMF structures designed by the current code procedures, along with investigations and revisions on such procedures are presented.

In the second part, a review on the new design procedure based on target drift and yield mechanism proposed by Leelataviwat et al. (1999), and later modified by Lee and Goel (2001), and Chao et al. (2007) is given.

2.2.3.1 Related Research on Performance of SMFs

Studies by Park and Pauley (1975) and Lee (1996) have shown that the Strong Column-Weak Beam (SCWB) requirements in the modern codes (such as UBC-94) may

not be sufficient in preventing the formation of column plastic hinge or even soft story mechanism. This can be attributed to the localized code requirements to prevent soft story formation (i.e. SCWB requirement) which do not consider the actual overall distribution of beam plastic moments on the column. Park and Pauley (1975) showed that the usual assumption in design of columns that the points of contra-flexure are located approximately at the mid-height of the columns is not consistent with the distribution of column moments obtained from dynamic analyses (Figure 2.1). In this figure, the left diagram shows the column design moments obtained based on an elastic analysis for the equivalent static lateral forces. The other diagrams show the distribution of the moments in some significant instants under a nonlinear dynamic earthquake analysis. It can be seen that in many cases, the columns are actually in single curvature. It can also be seen that the column moments under dynamic analysis can be significantly larger than the design moments obtained from static analysis. Park and Pauley (1975) suggested that the sum of beam plastic moments should be used for design of only one column along with an adjusting factor, ranging from 0.8 to 1.3, which takes the higher modes into account.

Goel and Itani (1994) observed uneven distribution of yielding in the moment frames designed according to the modern codes. Difference in the distribution of the internal forces at the ultimate level and the design level was considered to be the main reason for this uneven yielding distribution.

A six story steel moment frame designed according to ATC 3-06 was studied by Lee (1996) under pushover analysis. It was seen that distribution of moments in column changed significantly from the elastic distribution after beam plastic hinges formed. It

was concluded that the ratio of sum of plastic moments used by the code in SCWB requirements cannot prevent the formation of plastic hinge in columns. Lee proposed a three-quarter rule to be used for SCWB design which states that three quarter of the sum of the girder plastic moment should be taken be the lower column.

Bondy (1996) obtained similar findings and showed that the current capacity design for columns significantly underestimates the moment demands on the columns. He concluded that the elastic column deformations as well as plastic moments of the beams need to be included in the capacity design of columns and proposed a method to design a column based on incremental displacement analysis using pushover method.

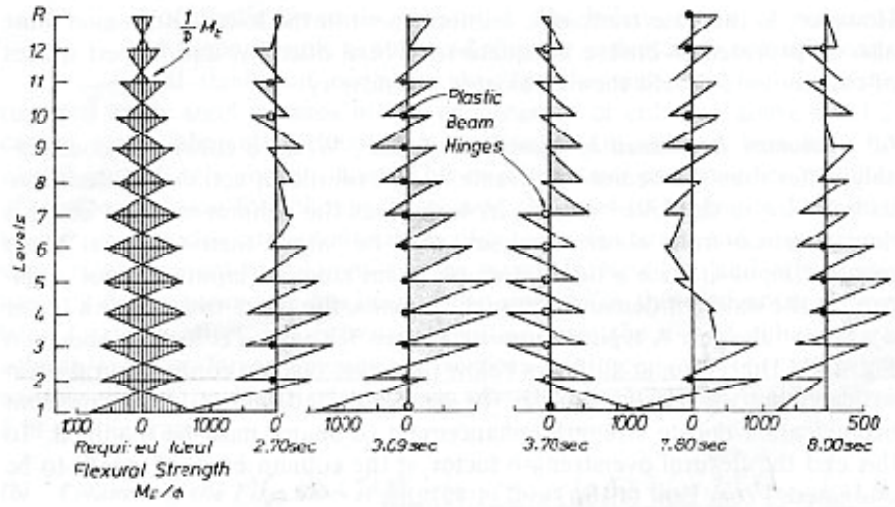

Figure 2.1. Comparison of Column Moment Patterns due to Horizontal Static and Dynamic Forces (Park and Pauley, 1975)

Gupta and Krawinkler (2000) carried out a comprehensive study on the seismic behavior of ductile SMF structures. The seismic responses of 3-story, 6-story, and 20-

story model SAC buildings with fully restrained connections at different hazard levels were obtained. The buildings were designed in three different seismic regions (Los Angeles, Seattle, and Boston) using the applicable code requirements for each site. Extensive inelastic pushover and nonlinear dynamic analyses were performed be using DRAIN-2DX software to study the response and performance of these frames under different intensity levels of earthquakes. SAC ground motions developed by Somerville et al. (1997) were used for dynamic analyses. Some important related findings to the current work are followed:

1) The current capacity design approach for columns based on the SCWB requirement cannot prevent the formation of plastic hinges in the columns. Major factors were considered to cause large moments in column along with high levels of axial force due to large overturning moments. More in depth research on the behavior of columns and column splices is needed.

2) A sensitivity study was carried out on the effects of the assumptions made in modeling and analysis assumptions on demand predictions.

3) The fundamental period for a SMF from the analytical model is much larger than the values obtained from code equations.

4) Pushover analysis was considered to be a very useful tool in evaluation of the structural seismic behavior and in initial prediction of seismic demands.

Also, a simplified procedure to estimate the global and local seismic demands was developed as a tool in the conceptual design stage to facilitate the decision making process. No modification to the current code procedures or new design procedures was

given. A procedure for identifying P-Delta sensitive cases and also recommendations for improvement in P-Delta response of flexible steel frames was introduced.

2.2.3.2 Study by Leelataviwat, Goel, and Stojadinovic (1999)

Leelataviwat et al. (1999) developed a new performance-based plastic design procedure using the concept of energy balance applied to a pre-selected yield mechanism with adequate strength and ductility. This method was later called Performance-Based Plastic Design (PBPD) method. In this procedure, the structure is designed at the ultimate limit state level. The ultimate design base shear for plastic analysis was derived based on a pre-selected yield mechanism and the corresponding target drift by using the input energy from the design pseudo-velocity spectrum. The proposed design concept was based on the plastic (limit) design theory and the corresponding design forces were derived by using the principle of energy conservation. The advantage of this approach is that the target story drift can be directly considered as a design parameter, without explicit checks for story drifts after the design. In addition, there is no need to use the controversial response modification factor, R, in this proposed procedure.

The performances of a mid-rise structure designed by the conventional method and the redesigned structure using the proposed method were compared. It was found that although both frames have similar total weights, the performance of the redesigned frame designed by the proposed method was much better than the original frame both under pushover and nonlinear dynamic analyses. In addition, it was found that the required

design based shear obtained from UBC-94 and UBC-97 were quite small and hence the validity values of *R*-factors in those codes were questioned.

Furthermore, the results showed that by using the proposed method, structures can be designed to meet a preselected performance objective. The method can be considered the first direct design, in line with the so-called Performance-Based Design approach, which actually uses the performance criteria to begin the design with. Therefore, the proposed method can be easily incorporated into a performance-based design framework with the performance objectives defined based on the seismic hazard levels and interstory drift level.

Two main factors are mentioned by Leelataviwat (1998) that cause most of the problems related with the seismic performance of SMF structures. One factor is the inconsistency between the strength and stiffness criteria (imposed drift limit). The drift limits govern the design of SMF most of the time, leaving the size of the beams relatively large compared to the size of columns. This can cause the inelastic activity (formation of plastic hinges) in columns. The other factor was mentioned to be the inability of the current elastic design method to capture the distribution of the inelastic internal forces. The combination of these two factors was deemed to result in the formation of undesirable and uncontrolled yield mechanism. The new design procedure proposed by Leelataviwat et al. (1999) was developed to resolve these two main issues of SMF structures by using more compatible strength and stiffness criteria and also more explicitly consideration of the global plastic distribution of internal forces. The proposed

method, which was later called PBPD, is based on the principle of conservation of energy and plastic analysis concept.

A column tree with the beam plastic moments and lateral forces applied to that is considered in this method in order to find the column design moments. The results showed that the proposed method works particularly well for mid-rise structures. However, the method appeared to result in over-estimate designs for high-rise structures and under-designed designs for low-rise structures.

The redesign of 20-story SAC frame was considered to further verify the validity of the design procedure. This 20-story frame was later redesigned by Lee and Goel (2001) and will be also considered in Chapter 8 of the current study. At first, this frame was designed using the proposed procedure by assuming 2% target drift. However, the design base shear and the column design moments were obtained to be excessively conservative such that appropriate sections could not be found from AISC-LRFD specifications, AISC 1994. As a result, the target drift was changed to 3% to be able to use standard member sections and to further verify the validity of the procedure for high-rise long period structures.

A comparison between the design column moments obtained by using the proposed procedure and the maximum column moment envelopes from time history analyses for the exterior and interior columns are shown in Figure 2.2. The computer program SNAP-2DX (Rai et al., 1996) which was developed at the University of Michigan was used for modeling. Four ground motions (El Centro, Newhall, Sylmar, and one synthetic ground motion) were used. As can be seen from this figure, the design

column moments obtained by using the proposed procedure are still too conservative. At some levels, these moments are almost three times larger than the column moments obtained from the nonlinear dynamic analyses. As was mentioned by Lee and Goel (2001), the main reason for such difference between the design column moments and the maximum column moment envelopes from time history analyses was using an inappropriate lateral force distribution which was inconsistent with the plastic design method employed.

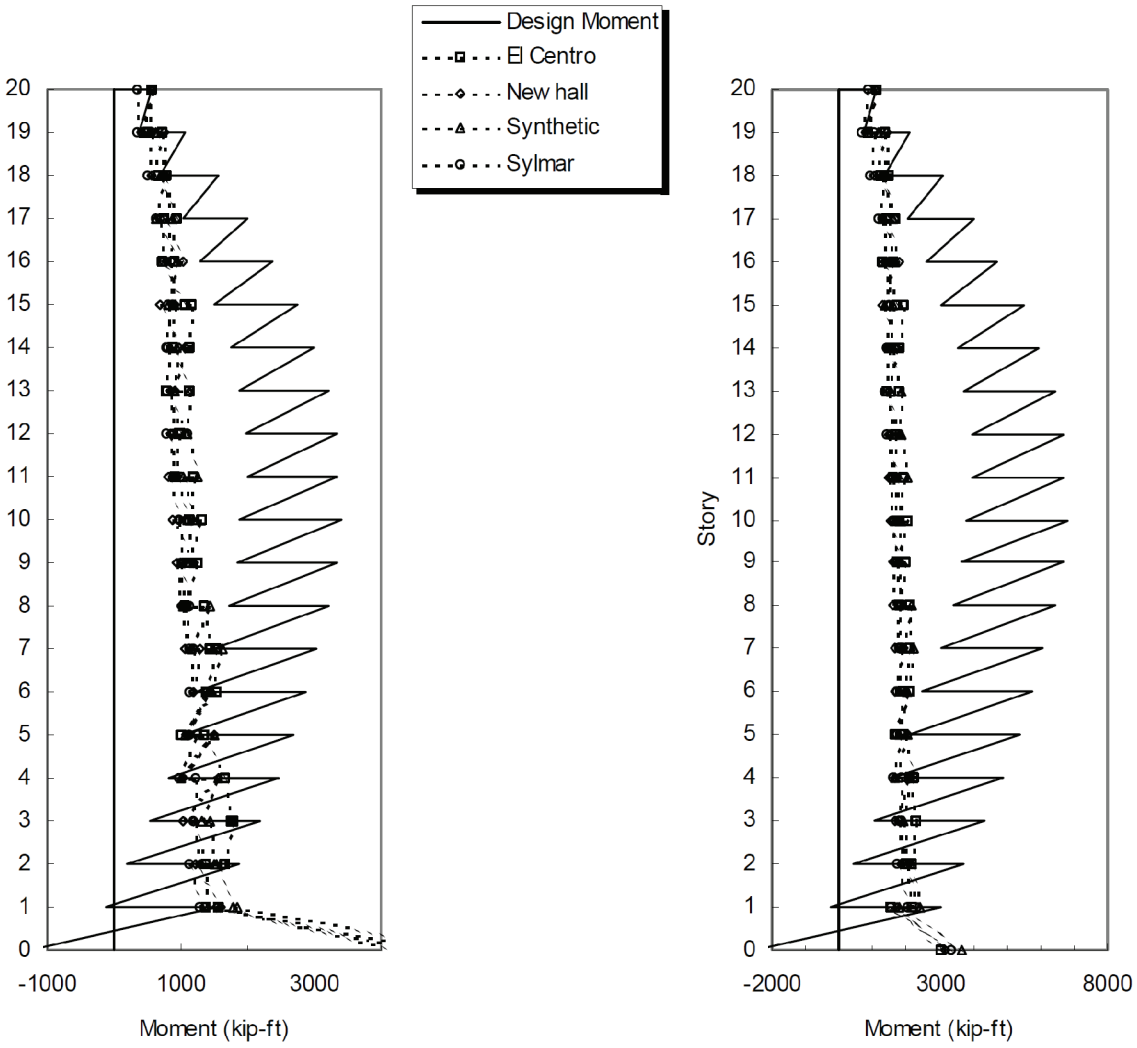

Figure 2.2. Design Column Moments by Leelataviwat et al.'s Procedure and Maximum Column Moment Envelopes from Time History Analyses for the 20-Story Frame (Leelataviwat et al., 1999): (a) Exterior; and (b) Interior Columns.

2.2.3.3 Study by Lee and Goel (2001)

In this study, Performance-Based Plastic Design (PBPD) using target drift and yield mechanism originally proposed by Leelataviwat et al. (1999) was reviewed and modified. As was mentioned in the previous section, the procedure proposed by Leelataviwat et al. (1999), although works very well for mid-rise structures, gives overly conservative design base shear and column design moments for the design of high-rise structures. A modified PBPD procedure was proposed in this study. A modification factor, as a function of the structural ductility factor and the ductility reduction factor, for the energy balance equation was derived.

A new lateral force distribution for the design procedure was developed from shear proportioning factors that were derived from the relative distribution of maximum story shears obtained from nonlinear dynamic analyses. Then, the equation of design base shear coefficient derived using the modified energy balance equation and the new lateral force distribution were used in the design.

In addition, a parametric study was performed to verify the validity of the proposed design procedure. The parametric results showed that the proposed method can be used to design structures which are not too conservative and also meet the pre-selected performance objective (target drift and yield mechanism).

It was seen in this study that the structures designed by the proposed PBPD method develop a uniform sway (beam yielding only) mechanism. Furthermore, as can be seen in Figure 2.3, the proposed procedure can give accurate estimation of the maximum column moment demands under actual earthquakes.

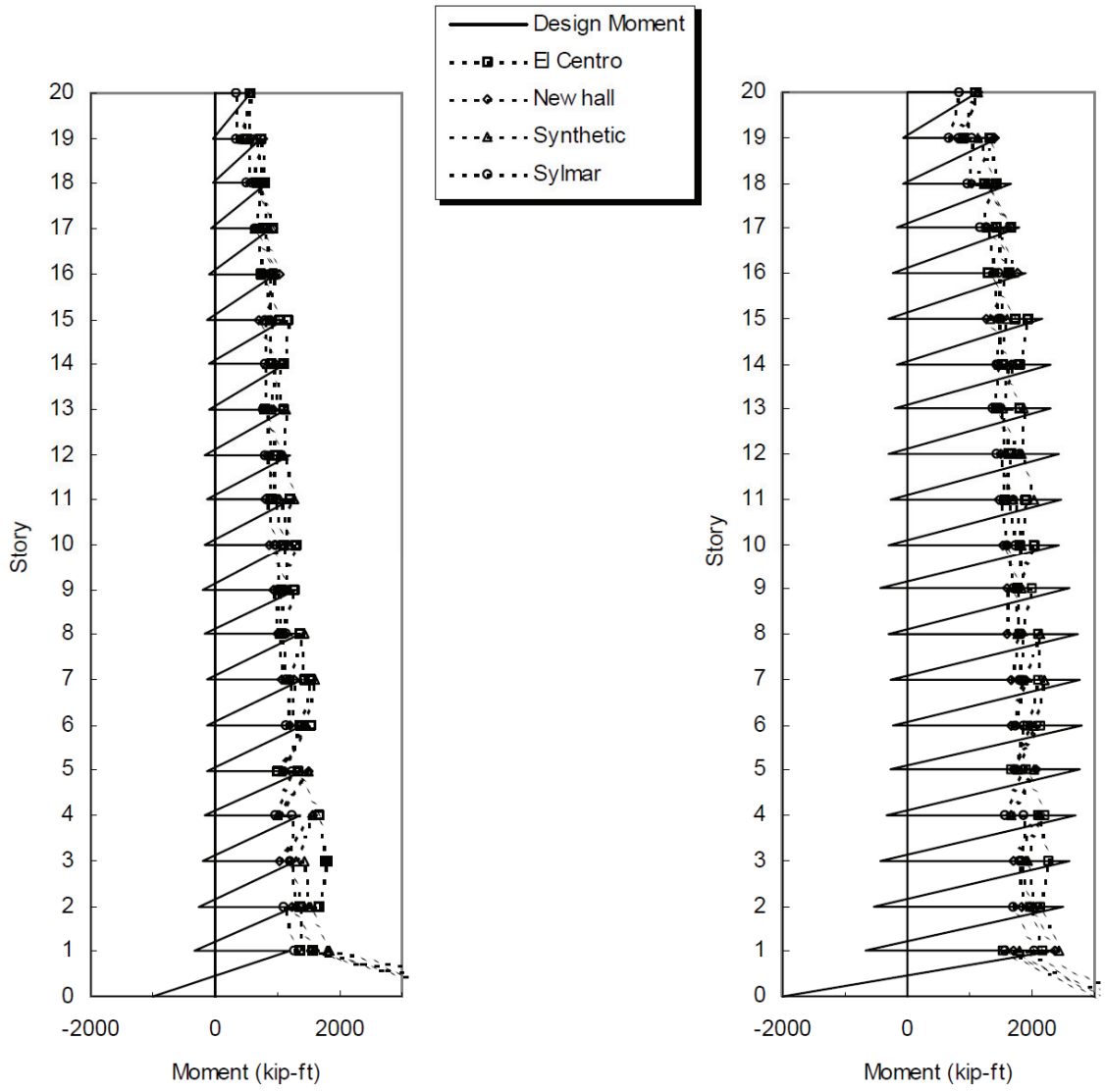

Figure 2.3. Design Column Moments versus Maximum Column Moment Envelopes from Nonlinear Dynamic Analyses for the 20-Story SAC Frame (Lee and Goel, 2001): (a) Exterior; and (b) Interior Columns.

2.2.3.4 Study by Chao, Goel, and Lee (2007)

It is shown in this study that code lateral force distributions do not represent the maximum force distributions that may be induced during nonlinear response, which may lead to inaccurate predictions of deformation and force demands. This may cause structures to behave in a rather unpredictable and undesirable manner. This study was done in line with the new lateral force distribution proposed by Lee and Goel (2001) to further validate the advantages of using a lateral force distribution based on the inelastic response. This new lateral force distribution is based on the inelastic behavior of the structure and was developed by using relative distribution of maximum story shears of the example structures subjected to a wide variety of earthquake ground motions.

In this study, extensive nonlinear dynamic analyses were carried out on different types of steel frames to verify the suggested distribution. The results showed that the suggested lateral force distribution, for the types of framed structures considered in this study, is more rational and gives a much better prediction of inelastic seismic demands at global as well as at element levels.

It is also noted that contrary to the current codes lateral distribution (which is derived based on first-mode elastic dynamic response) for all types of structures, the suggested lateral force distribution can be applied to most of the commonly used frame types, and it can also be modified for other structures by changing the value of the α factor.

It was seen that the maximum story shear distributions as given in the current codes, deviate significantly from the time-history dynamic analysis results regardless of

whether the structures respond in the elastic or inelastic range. On the other hand, different frames designed by using the suggested lateral force distribution resulted in maximum story shears that agreed well with those values obtained from nonlinear dynamic analyses. In addition, frames designed by the suggested lateral force distribution showed more uniform distribution of maximum story drifts along the height. Furthermore, the proposed column tree method for design of columns using the new design lateral force distribution, gives a very good estimation of maximum column moment demands when compared to the column moment demands induced by sever ground motions. The structures respond to severe ground motions which cause the structural response well into its inelastic stage. More details on this lateral force distribution can be found in Chapter 3.

2.3 Seismic Performance of Concentrically Braced Frames

Concentrically Braced Frames (CBFs) are among efficient steel structures commonly used to resist lateral loads due to earthquakes. However, these systems showed rather inferior performance under some major seismic events taken place in the US and Japan from late 1970s to mid late 1980s. Those observation, as will be discussed more in the following section, has led the engineering practice to move from CBFs to SMRFs, which were believed to be ductile and stable system at the time. It was after the 1994 Northridge earthquake that CBF system became more popular in engineering practice. CBFs, due to their large elastic stiffness, have been considered a desirable option to reduce the earthquake induced story drifts in structures.

It has been estimated that CBFs comprise about 40 percent of the newly built commercial construction in California during the last decade (Uriz, 2005). This change in the newly designed steel structures can be attributed to the simpler design of CBFs and also their high efficiency in resisting lateral load with reduced deflections compared to other systems such as SMRFs, especially after the 1994 Northridge earthquake.

In the early provisions adopted for CBFs, the elastic response of these systems was of more importance through providing increased brace strength and stiffness. More recently, requirements for ductility and energy dissipation capacity have been added to the seismic code provisions (e.g. AISC, 2005a) with introducing a new class of CBFs called Special Concentrically Braced Frames (SCBF) based on the research done by Goel and others (for instance, Goel, 1992a) in the last thirty years or so.

However, CBFs are generally considered less ductile seismic-resistant structures than other systems due to the buckling or fracture of the bracing members under large cyclic deformations. When designed by conventional elastic design methods, these structures can undergo excessive story drifts after buckling of bracing members. This can lead to early fractures of the bracing members, especially in those that popular rectangular tube sections (HSSs) are used for bracing members (Sabelli, 2000, Goel and Chao, 2008). A new design method, called Performance-Based Plastic Design (PBPD) method, has been recently applied to design of CBF systems which takes into account the inelastic behavior of the system in the design procedure (Chao and Goel, 2006b, Goel and Chao, 2008). The summary of these studies is given in Section 2.3.3. More details on

application of the PBPD method to CBFs can be found in Chapter 4. Further modification of this procedure can be found in Chapter 5.

A brief summary of the experimental result related to CBF systems is given in Section 2.3.2. Also, for a more complete literature review on experimental results relating to CBFs the reader is referred to Uriz (2005).

2.3.1 Summary of Experimental and Analytical Studies on CBF Structures

According to the commentary of AISC Seismic Provisions (AISC, 2005a) on Special CBFs, several connection failures were observed in CBF structures due to ground shaking caused by earthquakes. Similar connection failures were seen in cyclic testing of specimens designed using the current provisions for CBF (Astaneh-Asl, Goel, Hnason, 1985). Superior performance for the connections can be expected if eccentricities as well as brace cyclic post-buckling behavior are accounted for in the design. In addition, allowing the gusset plate to have free plastic rotations after out-of-plane buckling of the braces was considered necessary for desirable performance of the connection. A length of two times the gusset plate thickness was recommended as the free length between the end of the bracing member and the assumed line of restraint for the gusset plate (Astaneh-Asl, Goel, Hnason, 1985).

Other test results carried out by Lee and Goel (1987) showed that having plastic hinge in bracing member rather than the gusset plate by forcing in-plane buckling results in larger energy dissipation capacity. More findings can also be found in Astaneh-Asl (1998).

Aslani and Goel (1991) showed that in addition to more strict compactness criteria, closer spacing for stitches is also needed in order to achieve enhanced ductility for double-angle and double-channel braces. Their results also showed that the flexural strains and local buckling can be reduced by putting the double-angles in a toe-to-toe configuration (AISC, 2005a).

Extensive experimental and analytical studies done by S. C. Goel and others have shown that CBF structures, unlike common thinking, can achieve adequate ductility through proper member design and detailing. Mainly, limiting the width-to-thickness ratio of the brace section to minimize local buckling, closer spaces for stitches, and proper design and detailing for end connections can significantly improve the post-buckling behavior of CBF structures. Such results are basically the basis for the SCBF requirements (Goel, 1992a; Goel, 1992b; AISC, 2005a). By implementing the requirements in the AISC seismic provisions, premature brittle fracture of braces after global buckling (due to local buckling, connection fractures, and stability problems) can be prevented. Therefore these braces can undergo large inelastic deformations without early fracturing (AICS, 2005a).

Early failure of braces resulting in minor energy dissipation was seen in the analytical studies done by Tang and Goel (1987) and Hassan and Goel (1991). As was the case in experimental studies, failures occurred either at the plastic hinge due to local buckling or in the connections. On the other hand, stable hysteretic behavior without fracture was analytically obtained and verified by full-scale experiments for the brace

members designed to ensure ductile behavior (Tang and Goel, 1989). Wallace and Krawinkler (1985) found similar results in full-scale tests on CBF systems.

Sabelli (2000) conducted comprehensive analytical studies of 3-story and 6-story braced frames using the SNAP-2DX software for modeling (Rai et. al., 1996). This software has the capability of modeling brace fractures due to low cycle fatigue based on the fracture criterion for HSS braces (Tang and Goel, 1987). Brace fracture was considered to be a common feature in many of these dynamic analyses, especially those producing large or severe response. It was shown that early brace fractures may lead to excessively large story drifts and ductility demand on beams and columns when struck by strong ground motions. Similar results had been obtained by Goel (1992b). For more explanation on the result of this study, and also the fracture criterion used, the reader is referred to Chapter 4.

Uriz (2005) conducted series of analytical and experimental investigations in order to evaluate and improve the seismic performance of CBF structures. Following the procedure outlined in FEMA 351 (FEMA, 2000b) for performance evaluation of moment frames, the performance and also confidence level of conventionally designed 3-story and 6-story CBF and BRBF structures, originally designed by Sabelli (2000), were obtained. The summary of this reliability based performance assessment procedure is given in Chapter 4.

Widespread brace fractures were seen in CBF structures even under 10% in 50 year ground motions. Concentration of story drifts was seen in both CBF and BRBF, especially in low-rise frames. However, the confidence level of CBFs against collapse

was obtained to be significantly lower than BRBFs. This observation can be mainly attributed to brace fracture in CBFs. Confidence level assessment for CBFs designed by PBPD method are obtained in Chapter 4.

A physical theory brace model (force-based fiber element with distributed inelasticity) was developed to model the inelastic buckling behavior of steel members. Kinematic and isotropic hardening as well as Bauschinger effect can be captured by this proposed element model. The proposed model has the capability to characterize the buckling strength, post-buckling behavior, tensile strength, out-of-plane deformations, and overall hysteretic behavior of struts made from different cross sections (Uriz, 2005). Moreover, a numerical model was proposed, and validated by the experimental data, to capture the effects of low cycle fatigue in braces which eventually would lead to brace fracture.

Large-scale tests of three BRBFs and one CBF have been carried out. The test setup and the test specimen before testing are shown in Figure 2.2. Figure 2.3 shows the 2-story specimen at the last cycle of loading. In Figure 2.4, the fracture of beam-to-column connection in the last cycles of the loading can be seen. This fracture is due the fact that the rather large gusset plate changes the assumed simple beam-to-column connection into somewhat rigid connection which would consequently create considerable moment and rotation demands on the column. Since these demands have not been considered in the design of columns, which is typically done based on the axial force in CBFs, severe damage like shown in Figure 2.4 can occur.

In addition, including the low cycle fatigue in the model was considered essential to properly capture the actual behavior of the CBF system.

The proposed numerical models were calibrated based on the results of these large-scale tests, and later were used in the analytical studies for performance assessment of different steel braced systems. Several recommendations related to the design, detailing, modeling, and analyses of CBFs were given.

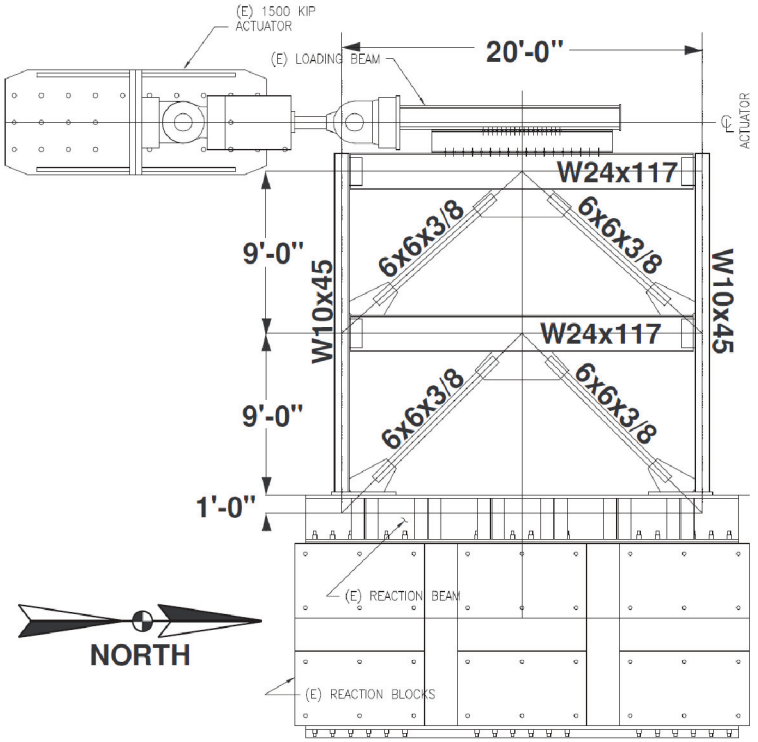

Figure 2.4. Test Setup for the 2-Story CBF (Uriz, 2005).

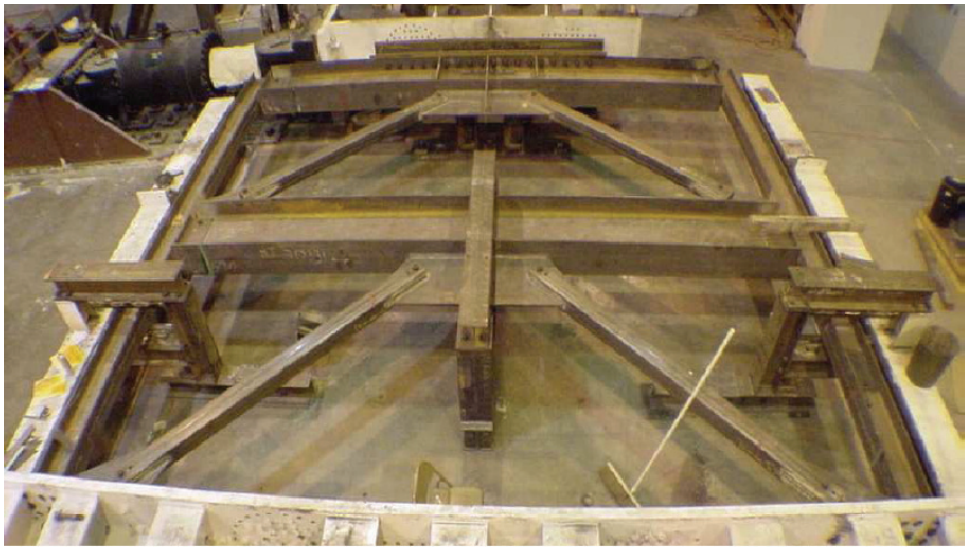

Figure 2.5. 2-Story CBF Test Setup and Specimen before Testing (Uriz, 2005).

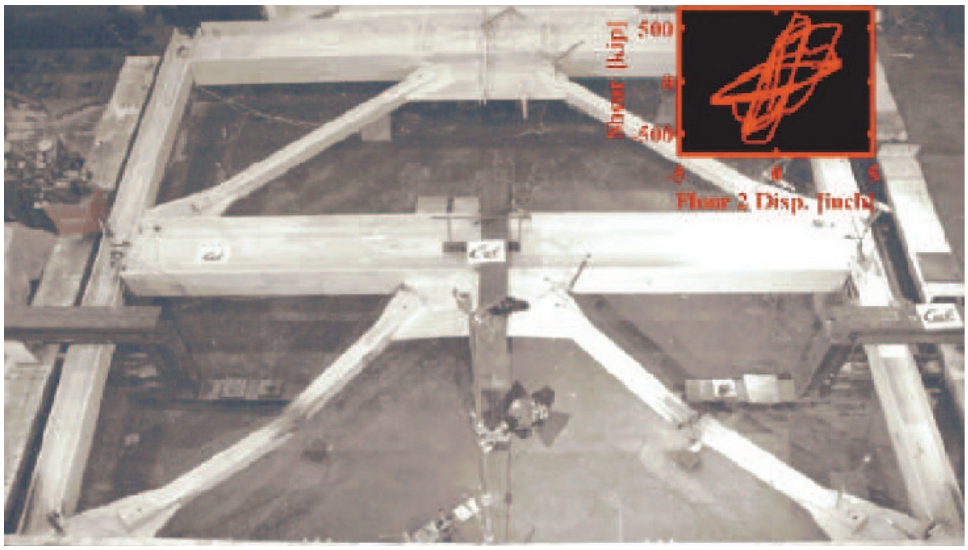

Figure 2.6. 2-Story CBF Test Specimen during Last Cycle of Loading (Uriz, 2005).

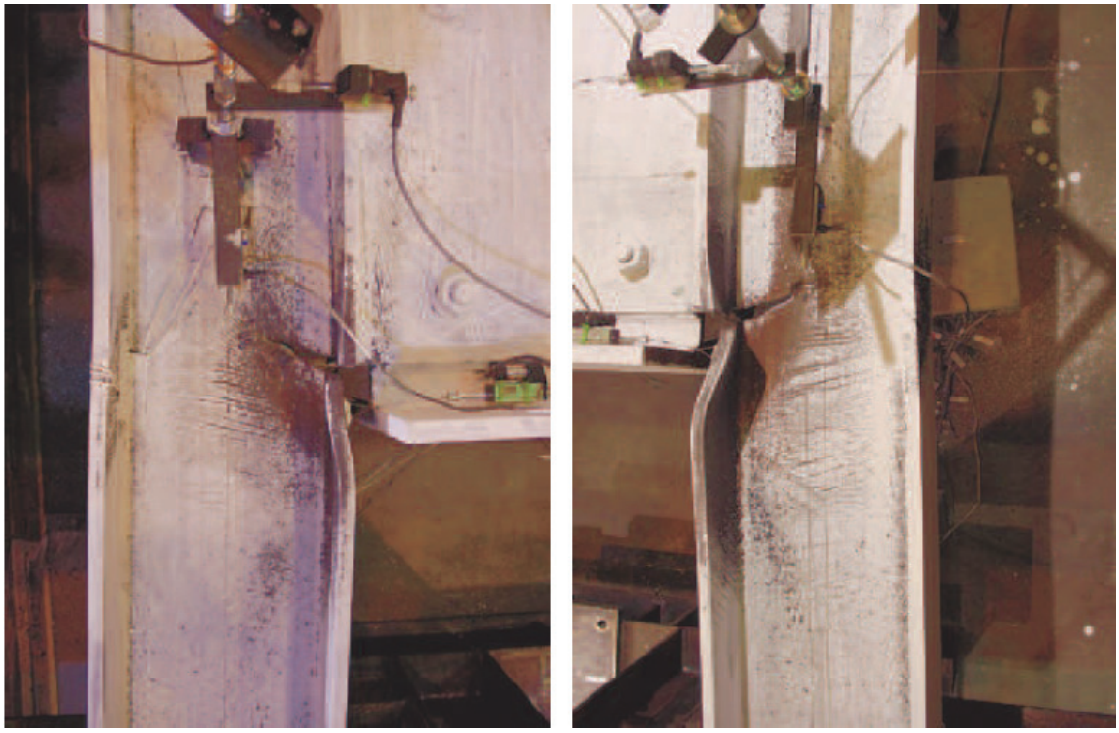

Figure 2.7. Fracture of Beam-to-Column Connection in the 2-story CBF Specimen (Uriz, 2005).

2.3.2 Application of PBPD Method to Design of CBFs (Chao and Goel, 2006b, Goel and Chao, 2008)

Chao and Goel applied the newly developed PBPD procedure to design of CBF systems (Chao and Goel, 2006b; and Goel and Chao, 2008). In the PBPD procedure, pre-selected target drift and yield mechanism are used as performance limit states. The design lateral forces are derived by using an energy equation where the energy needed to push the structure up to the target drift is calculated as a fraction of elastic input energy which is obtained from the selected elastic design spectra. Plastic design is then performed to detail the frame members in order to achieve the intended yield mechanism and behavior.

Buckling-type braces show somewhat pinched hysteresis loops under cyclic lateral loading. This pinched behavior has been considered in calculation of the design

base shear by introducing an energy modification factor (called η-factor) into the work-energy equation (Chao and Goel, 2006b).

In addition, modified brace and beam-to-column connection configurations are also suggested to further enhance the overall performance. A fracture life criterion is employed for the HSS braces to prevent premature fracture (Tang and Goel, 1987). Results from nonlinear time history analyses carried out on example 3-story and 6-story frames designed by the PBPD approach showed that the frames met all the desired performance objectives, including the intended yield mechanisms and story drifts while preventing brace fractures under varied hazard levels (Goel and Chao, 2008; and Chao and Goel, 2006b).

More detailed explanation of application of PBPD procedure in design of CBF structures can be found in Chapter 4.

2.4 Seismic Performance of Steel Plate Shear Walls

Unstiffened Steel Plate Shear Walls (SPSWs) are considered to be one of the emerging lateral load systems to resist earthquake. Unstiffened SPSWs can resist the lateral loads after the buckling of the plates through post-buckling tension-field action (TFA). These systems consist of steel web plates connected to the horizontal boundary elements (HBEs) and vertical boundary elements (VBEs), which are basically beams and columns (Figure 2.8). The connection between HBEs and VBEs can be either simple or rigid. However, AISC *Seismic Provisions* allows only the moment-resisting connection to be used in high seismic applications.

The first building code to adopt provisions for buckling type SPSWs was 1994 National building Code of Canada. More recently, provisions for this structural system are included in 2003 NEHRP *Recommended Provisions for Seismic Regulations for New Buildings and Other Structures* or FEMA-450 (FEMA, 2003) and also in AISC seismic provisions (AISC, 2005a). More explanation on the current AISC seismic provision (AISC, 2005a) requirements, which are basically based on the NEHRP 2003 (FEMA, 2003) provisions, will be given in Chapter 8.

Unstiffened SPSWs are considered among the most economical and efficient lateral load systems to resist winds and earthquakes. It has several advantages in terms of detailing costs, pace of construction, and providing adequate strength and stiffness with relatively less number of seismic bays (Berman et al., 2008).

In typical SPSWs used in today's practice, the web plates are unstiffened. From this point on in the text, SPSW would refer to unstiffened SPSW unless otherwise noted. Typical SPSW systems consist of three main components: 1) Steel web plates, 2) HBEs, and 3) VBEs. These components are shown in Figure 2.8 for a typical SPSW.

The analytical and experimental research work by several researchers on unstiffened SPSWs has been listed in AISC *Seismic Provisions* (AISC, 2005a) and also AISC Design Guide for SPSWs (Sabelli and Bruneau, 2007). These studies include both quasi-static and dynamic loading of these systems and demonstrated that the ductility and post-buckling strength of unstiffened web plates can be significant. As has been demonstrated in these studies, SPSWs show stable hysteretic responses under cyclic

loading (refer to Section 2.4.2). More explanation on the seismic design provisions for SPSWs in the US code along with the modeling techniques are given in Chapter 8.

2.4.1 Experimental Results on SPSWs

2.4.1.1 Component Tests

Timler and Kulak (1983) carried out a large-scale test on a single-story SPSW specimen. The main goal was to validate the adequacy of the proposed strip model developed by Thorburn et al. (1983) in which the resistance of the steel panel is obtained only based on post-buckling strength accompanied with the development of tension field action. Figure 2.9 shows the specimen used in this study. Simple beam-to-column connections were used in the specimen. The specimen was pushed monotonically up to the serviceability limit and then to failure. Tearing of the weld connecting the infill plate to the fish plate caused the failure for the specimen. Good agreement between the test results and proposed model was observed.

Tromposch and Kulak (1987) performed a large-scale test on a SPSW specimen with some modification compared to the specimen tested by Timler and Kulak (1983). They applied quasi-static cyclic load on the specimen up to 0.8% drift. Then the loading was increased monotonically up to the failure which was at 3.2% drift due to bolt slippage at the beam-to-column connection and also tearing of the welds between the infill plates and the fish plate. Very good correlation between the test results and the multi-strip model was observed. Pinched hysteresis behavior along with good ductility was reported for the specimen (Figure 2.10).

Roberts and Sabouri-Ghomi (1992) conducted 16 quasi-static cyclic tests on unstiffened steel plate shear panels with a circular opening at the center. They proposed equations to obtain the strength and stiffness reduction factor for perforated panels (having single or multiple holes) compared to the solid panel.

Berman and Bruneau (2003) used light-gauge, cold-rolled steel for the infill panels of a one-story SPSW specimen. The hysteresis loops with and without considering the boundary frame forces can be seen in Figures 2.11 and 2.12, respectively. The failure was due to the fracture in the infill panel propagating from the corners. The failure occurred at 3.7% drift, equivalent to a ductility of 12. With regard to this study, Berman et al. (2005) compared the hysteretic behavior of light-gauge SPSWs and CBFs in a series of cyclic tests. Totally six frames (four CBFs and two SPSWs) were tested (see Figure 2.13). It was observed that by scaling the hysteretic results to the same design base shear, the dissipated energy per cycle as well as the cumulative dissipated energy was almost similar for CBFs with tubular braces and flat plate SPSW. This observation was valid up to a ductility of four after which the tubular braces fractured (due to local buckling at mid-span). The flat plate SPSW was able to achieve a ductility of nine before its energy dissipation capacity per cycle started to decrease.

Vian and Bruneau (2005) investigated the behavior of perforated SPSW specimens, specimens with infill plate made form low-yield strength (LYS) steel, and specimens with reinforced cut-out corners. The effectiveness of these methods on reducing the demand on the VBEs was studied. Also, reduced beam section was used for the HBEs in these specimens to further reduce the demand on the VBEs. The hysteretic

response for the perforated and corner cut-out specimens is shown in Figure 2.14. As can be seen, the specimens in this study demonstrated stable hysteretic behavior with little pinching. Equations for estimating the stiffness reduction due to the presence of perforations in the infill plates were also developed in this study.

2.4.1.2 Tests on Multi-Story SPSWs

Caccese et al. (1993) studied the effects of panel slenderness ratio and also the type of beam-to-column connection on the performance of SPSWs. In their research, five three-story SPSWs with one-forth scale and different beam-to-column connection types were cyclically loaded up to 2% drift. The same cyclic displacement history was applied after first 24 cycles. The results on different plate thicknesses showed that the use of slender plates would result in more stable system. Also, Caccese at al. (1993) reported that the difference from using simple and moment-resisiting beam-to-column connection was small (Sabelli and Bruneau, 2007).

Driver et al. (1997) carried out experimental studies on a large-scale four-story, single bay SPSW specimen. Structural properties such as elastic stiffness, first yield, ultimate strength, and ductility and energy dissipation capacity for the specimen were studied. Moment-resisting connections were used in the specimen. 30 cycles of loading, including 20 cycles in the inelastic range were applied to the specimen as shown in Figure 2.15. Actuators were used at each floor in order to apply lateral cyclic loading. At four times the yield displacement, flange local buckling was observed at the bottom of lower story. However, the specimen was able to maintain more than 90% of its ultimate lateral strength until the failure occurred due to fracture of the weld at column base at

nine times the yield displacement (Figure 2.16). The SPSW specimen showed excellent ductility and energy dissipation capacity, along with stable behavior at large deformations.

Extensive analytical studies were also performed for the same specimen by using both finite element and strip-model methods. The analytical results generally showed good agreement with the experimental results (e.g. Figure 2.17). In addition, the hysteretic model for SPSWs was modified to result in better agreement with the test data.

Rezai (1999) conducted series of shake table tests on a four-story SPSW specimen with one-forth scale. Due to the movement limitations of the shake table, little inelasticity was seen in the system. The accuracy of finite element and strip models in predicting the response parameters were studied. Based on these studies, an alternative strip model was proposed (Figure 2.18) in order to capture the change in the inclination of the tension filed across the plate.

Lubell et al. (2000) conducted the testing of two single-story and one four-story SPSWs. The cyclic response of one of the single-story specimens is shown in Figure 2.19. In the test of four-story SPSW, it was found that anchoring of the tension field by using a considerably stiff beam at the top can significantly enhance the performance of the SPSW under lateral loading. It was also observed that similar to the results from Driver et al. (1997) and Rezai (1999), most of the damage was concentrated at the first story. From the “hourglass” deflected shape of the walls at the last stages of the test, it was concluded that capacity design is necessary for design of columns (Sabelli and Bruneau, 2007). The analytical modeling was done by using strip models. It was found

that the strip model can provide good estimation of the post-yield strength of the specimen. However, this simplified model underestimated the elastic stiffness.

Astaneh-Asl and Zhao (2001) tested a 1/2 scale 3-story SPSW assembly for the Century Tower project. The specimen was subjected to uniform shear force Figures 2.20 and 2.21). The first yielding occurred at 0.6% drift. Flange local buckling in the W-shape column was observed at 2.2% drift. The specimen was subjected to 40 elastic and 39 inelastic cycles. The maximum interstory drift was reported as 3.3% and the maximum shear strength was 917 kips. Figure 2.22 shows the cyclic response of the wall at the second floor. As shown in figure 2.23, fracture occurred in the upper floor coupling beam at the face of the column due to low-cycle fatigue.

Behbahanifard et al. (2003) tested a 3-story SPSW under combined simulated gravity load and quasi-static cyclic loading. Totally, 24 loading cycles were applied from which 14 were in the inelastic range. The specimen showed high initial stiffness aling with excellent ductility and energy absorption capacity. At 1.1 in. drift, a tear developed in the first story panel due to low cycle fatigue. Also flange local buckling at the column base and in the beam at the first level occurred at this drift. Beam flange showed fracture at 1.4 in. drift. The specimen at the end of the test is shown in Figure 2.24. The base shear-roof displacement response is also shown in Figure 2.25. A finite element model of the specimen was also developed based on nonlinear dynamic explicit formulation. After verifying the model against the experimental results (both monotonic and cyclic), a parametric study was performed using finite element models to study the effect of different parameters on the strength and stiffness of SPSWs. Column flexibility

parameter was reported to have significant effect on the response of SPSW. In addition, a model for taking into account the effect of overturning moment was proposed.

Qu et al. (2008) reported a two-phase experimental program done at the NCREE lab in Taiwan. In this test, a full-scale two-story SPSW with reduced beam section connections and composite floor was built. The main objectives of this program were identifying the capability of the infills to be replaced after a major earthquake, and also the seismic behavior of the intermediate beam. The specimen before the test and the test setup are shown in Figure 2.26. In the phase I of this test, the specimen was subjected to pseudo-dynamic testing under three ground motions. Buckling was developed in the infill plates. Then the buckled panels were replaced by new panels before applying a major earthquake on the specimen in the phase II of the testing program. As can be seen form Figure 2.27, the repaired SPSW system behaved quite similarly to the original system with the same stable hysteresis loops and energy dissipation capacity. It was observed that the specimen can show stable behavior up to story drifts of about 5%. In addition, the experimental results were compared to the results from analytical models (Figure 2.28). The dual strip model (with tension strips in both directions) was used to simulate the pseudo-dynamic results, while the 3D finite element model was used to obtain the monotonic pushover curve for the system. Both modeling techniques showed quite promising results in predicting the response of the SPSW structure.

Park et al. (2007) carried out cyclic testing on five 3-story single bay SPSWs with one-third scale. The typical test specimen is shown in Figure 2.29. Test parameters for these specimens were plate thickness and strength and compactness of the column.

Load-displacement curves for these specimens are shown in Figure 2.30. The specimens showed excellent initial stiffness, strength, ductility, and energy dissipation capacity. It was observed that local fracture of web plates did not have significant effect on the overall behavior. Final failures occurred at the beam-to-column connection or at the column base. It was shown that using noncompact sections for column would result in decrease in load-carrying and also deformation capacity of the SPSW due to early local buckling of the columns.

Choi and Park (2008) performed experiment on three SPSW specimens with three stories to evaluate the potential maximum ductility and energy dissipation capacity of thin steel plate walls. In addition, a concentrically braced frame (CBF) and a moment frame (MF) with similar beam and column sections were tested so that the results can be compared (Figure 2.31). Aspect ratio of the web plates and the shear strength of columns were considered as test parameters. Figure 2.32 shows the load-displacement results for the three SPSWs as well as the CBF and MF. It was observed that the values of dutility and energy dissipation of the FSPW2 (shear-dominated specimen) were 2.8 times and 5.8 times those of the CBF, and 3.3 times and 2.8 times those of the MF. The shear-dominated SPSW designed with ductile details showed excellent deformation capacity (close to that of MF). It was also observed that the shear strength and energy dissipation capacity of the SPSW got increased in proportion to the depth of infill plates.

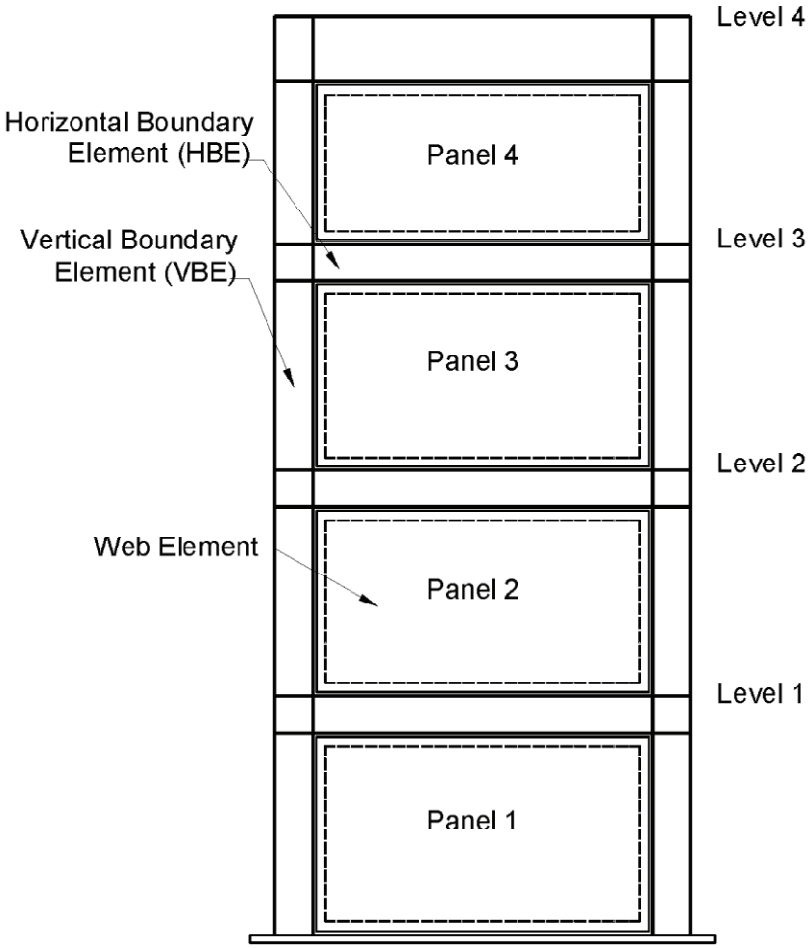

Figure 2.8. Components of a Typical SPSW (AISC, 2005a).

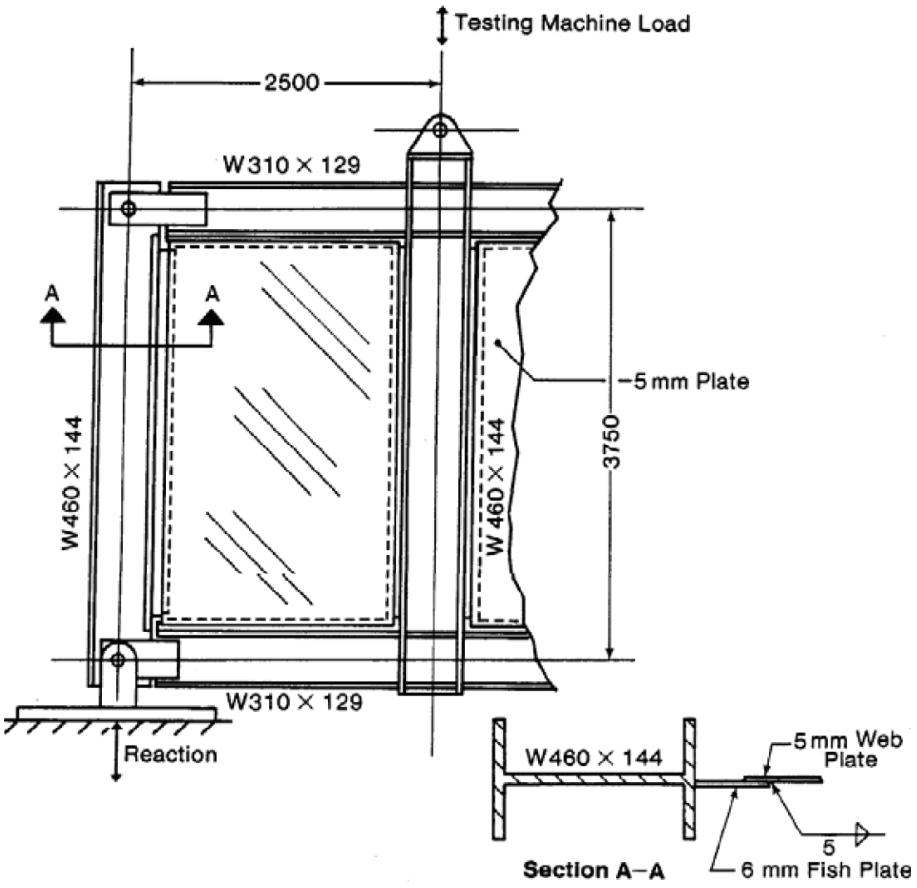

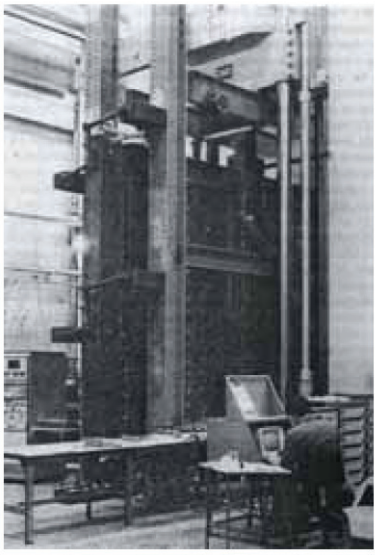

Figure 2.9. Two-Story Specimen Used by Timler and Kulak (1983).

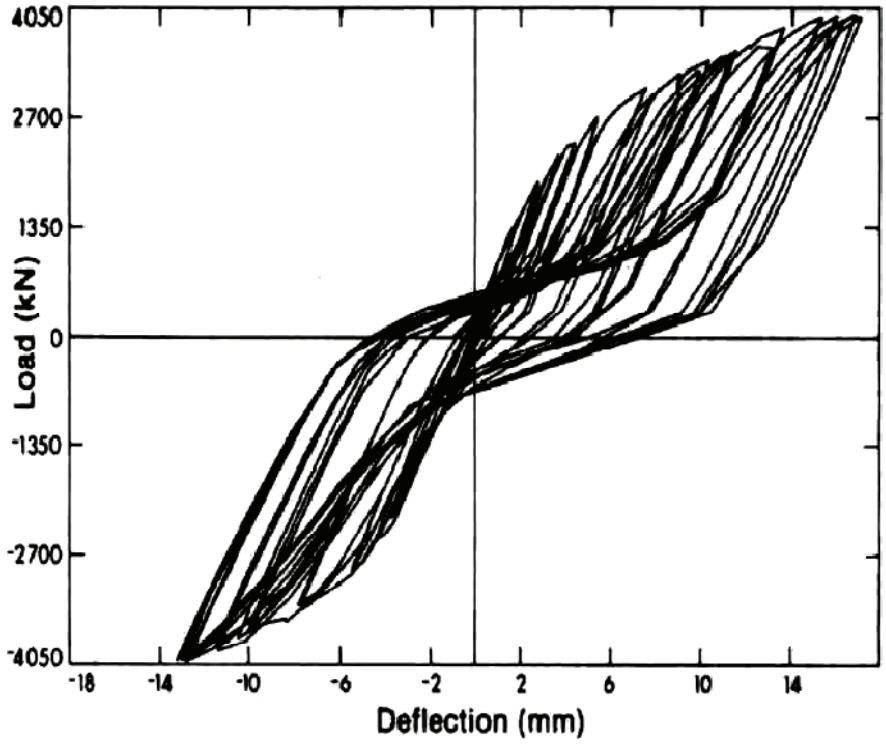

Figure 2.10. Cyclic Load-Displacement Response of SPSW Specimen Tested by Tromposch and Kulak (1987).

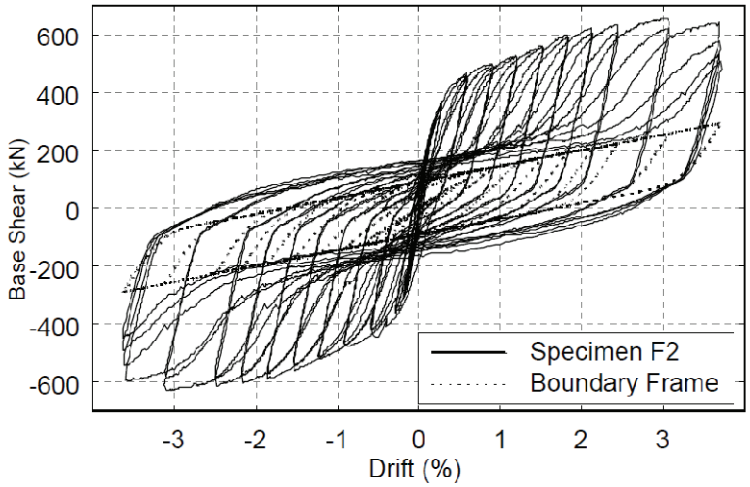

Figure 2.11. Light-Gauge SPSW and Boundary Frame Hysteresis (Berman and Bruneau, 2003).

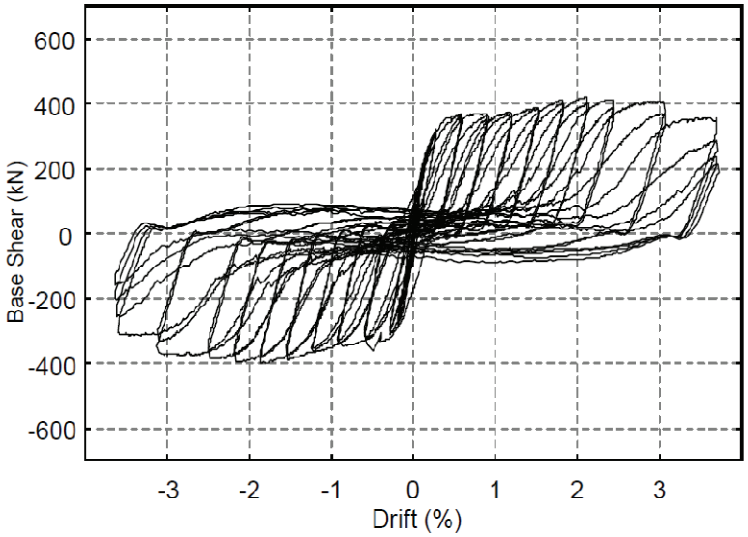

Figure 2.12. Light-Gauge SPSW Hysteresis- Infill Only (Berman and Bruneau, 2003).

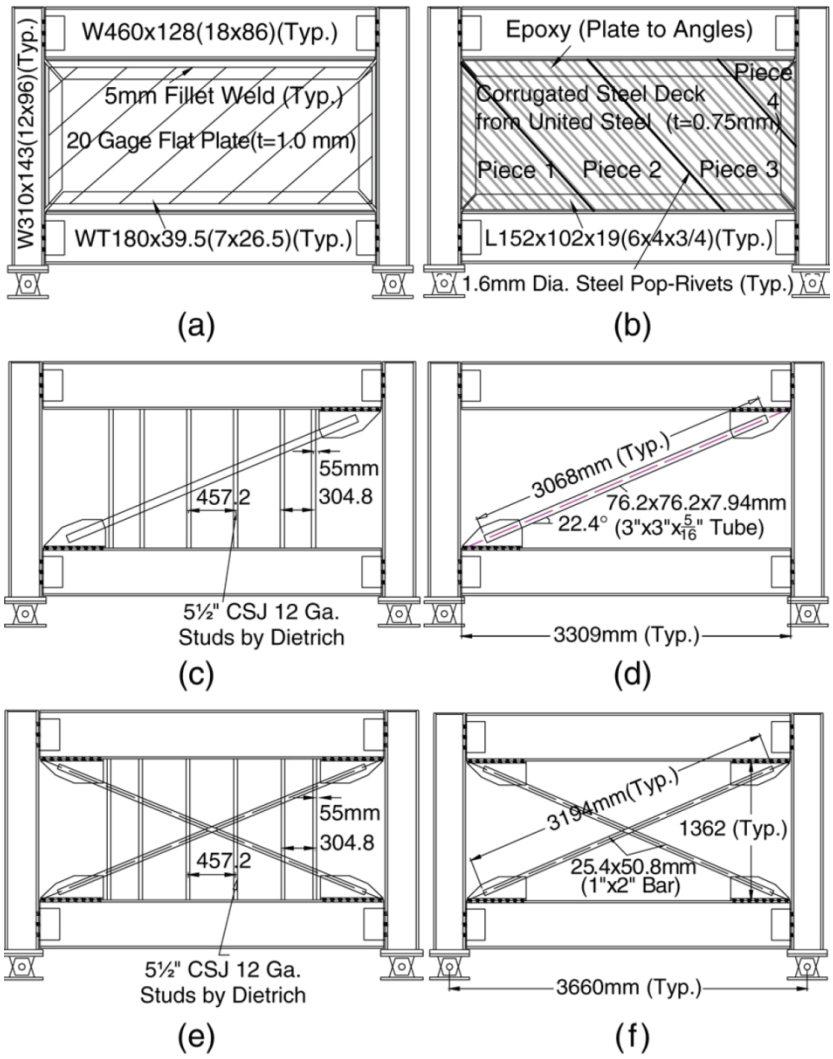

Figure 2.13. Six Specimens Tested under Cyclic Loading by Berman et al. (2005): (a) Flat Infill Plate; (b) Corrugated Infill Plate; (c) CBF with Single Tube and Vertical Studs; (d) CBF with Single without Studs; (e) CBF with X-Bracing and Vertical Studs; (f) CBF with X-Bracing and without Studs.

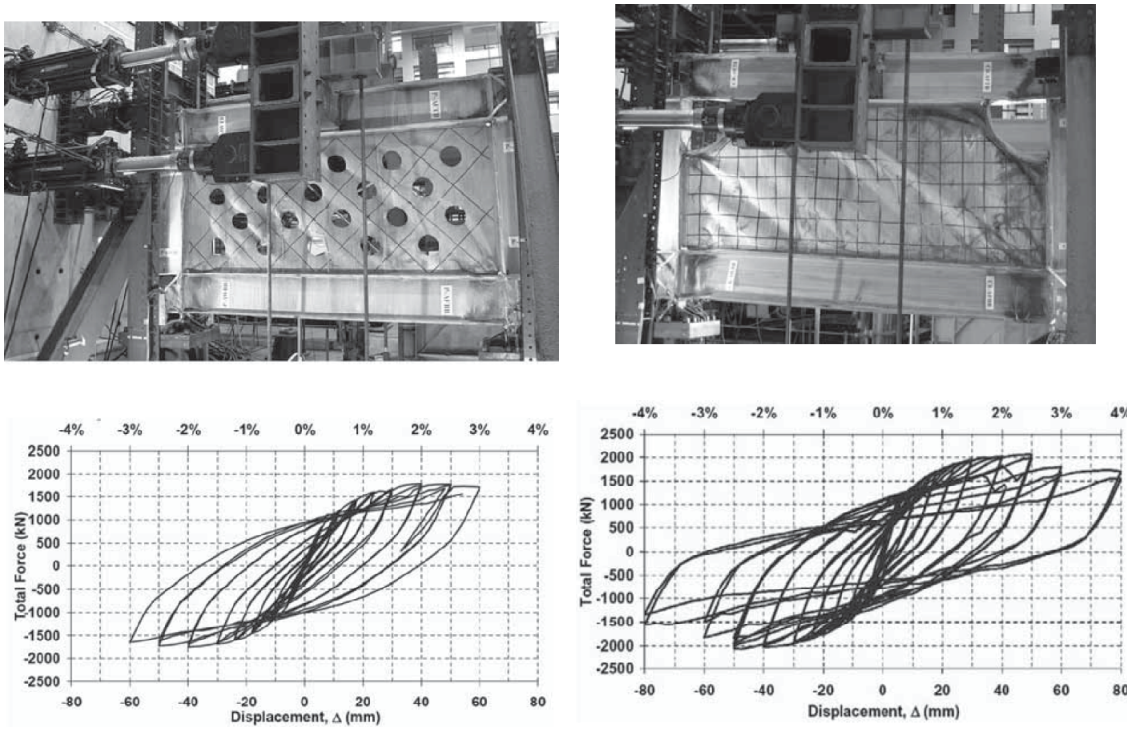

(a) (b)

Figure 2.14. (a) Perforated Specimen at 3% Drift; (b) Specimen with Reinforced Cut-Out Corners at 4% Drift (Vian and Bruneau, 2005).

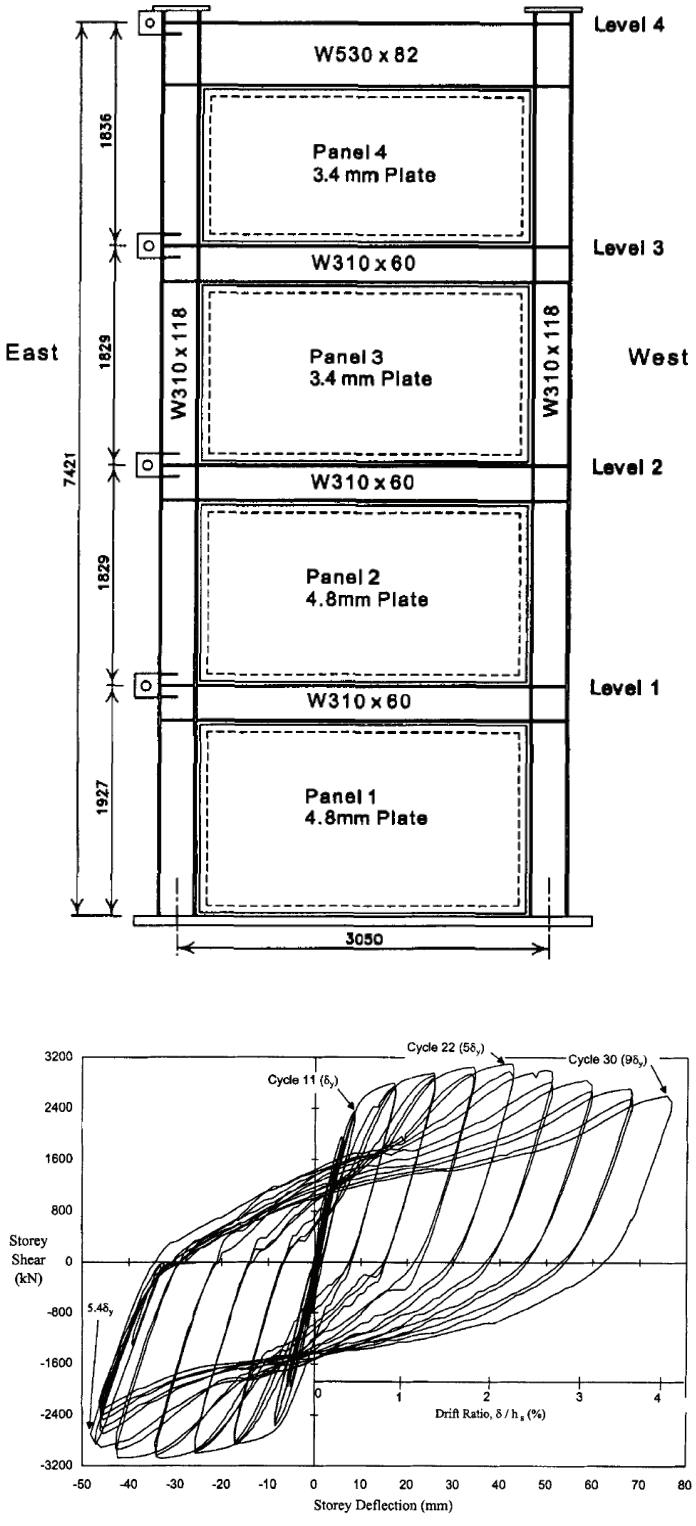

Figure 2.15. Test Setup and Cyclic Response of SPSW tested by Driver et al. (1998).

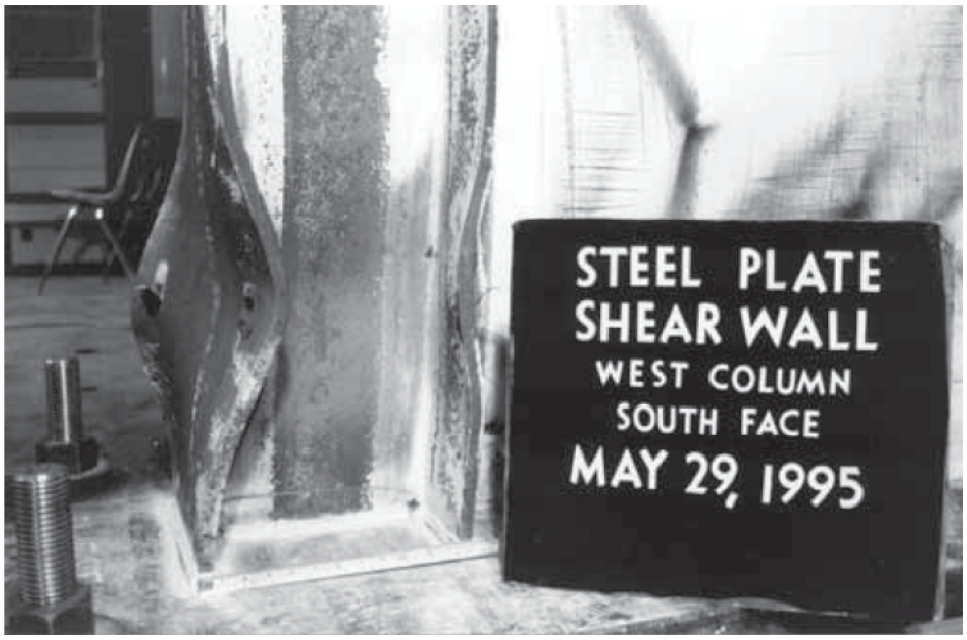

Figure 2.16. Local Buckling and Fracture of Column at the end of Test (Driver et al., 1997).

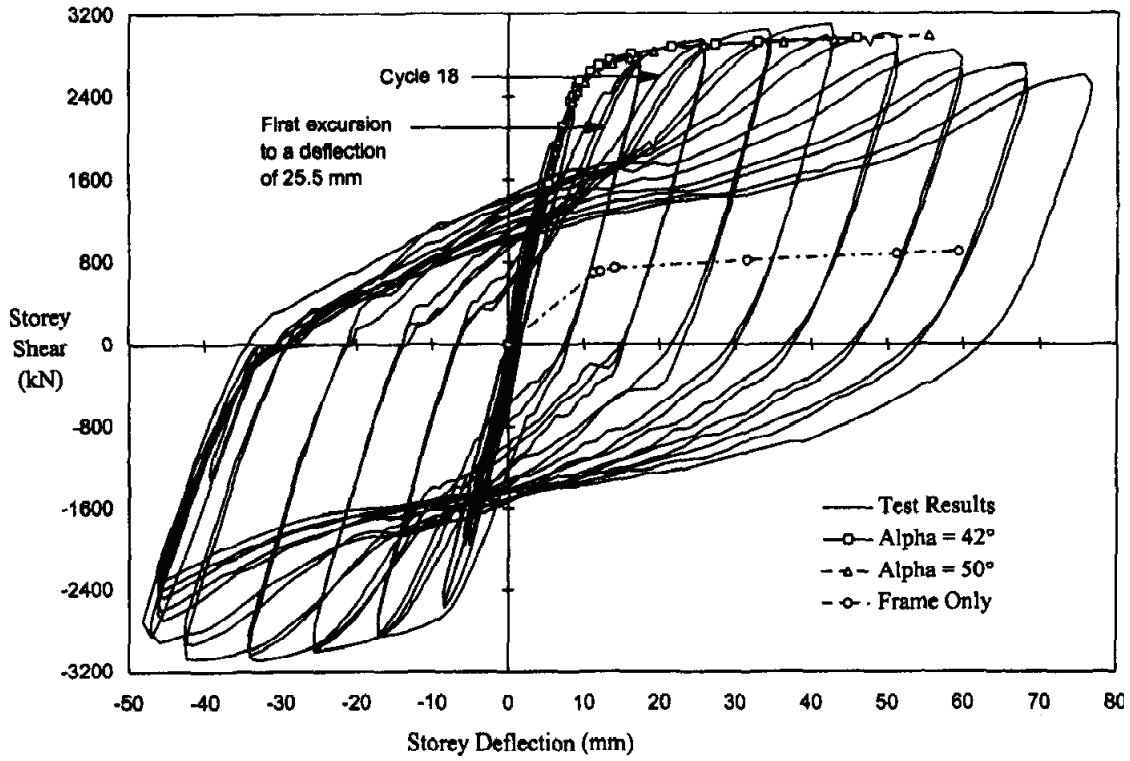

Figure 2.17. Comparison of Strip Model Analysis with Test Results (Driver et al., 1997).

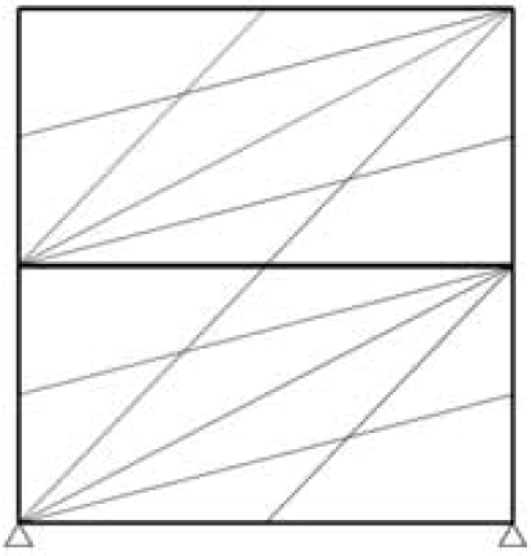

Figure 2.18. Modified Strip Model Proposed by Rezai (1999).

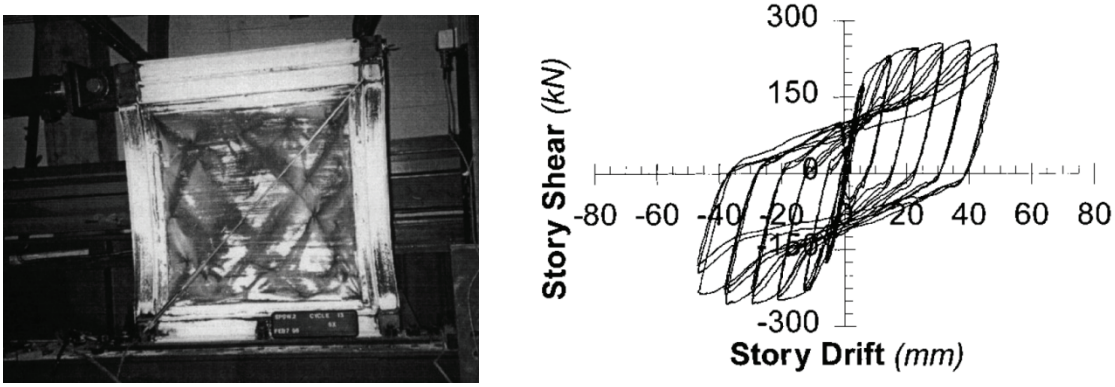

Figure 2.19. Test Setup and Cyclic Response of a Single-Story SPSW Tested by Lubell et al. (2000).

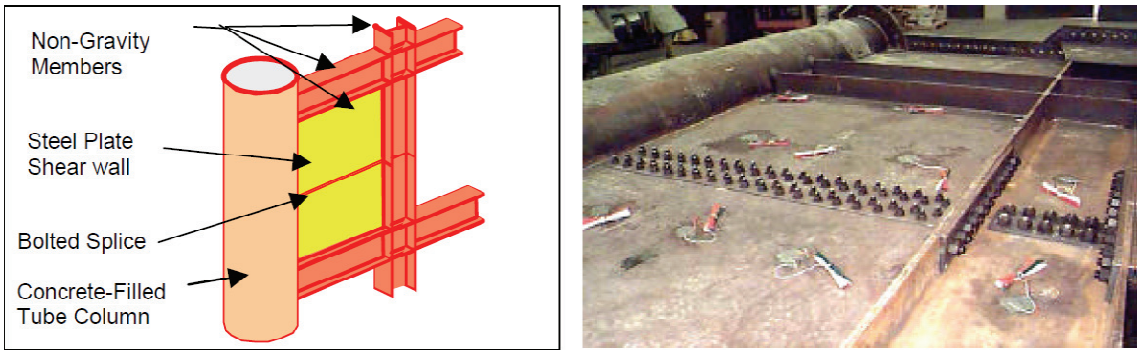

Figure 2.20. Components of the Test Specimen and Bolted Splice (Astaneh-Asl and Zhao, 2001).

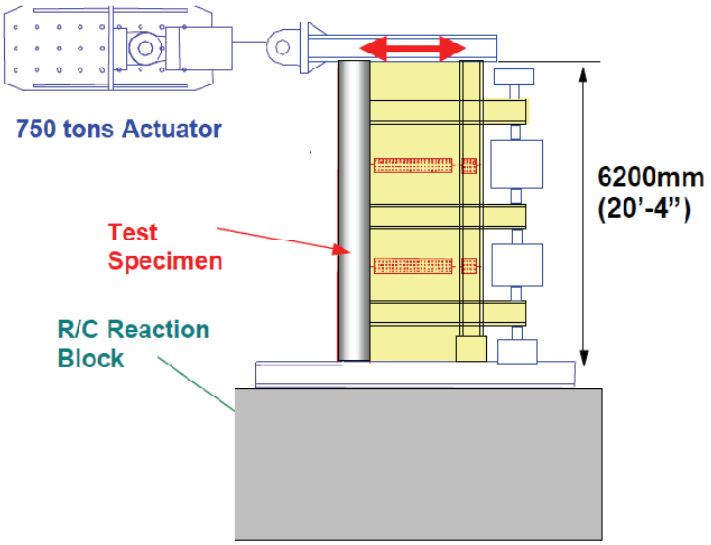

Figure 2.21. Test Setup for the SPSW Specimen (Astaneh-Asl and Zhao, 2001).

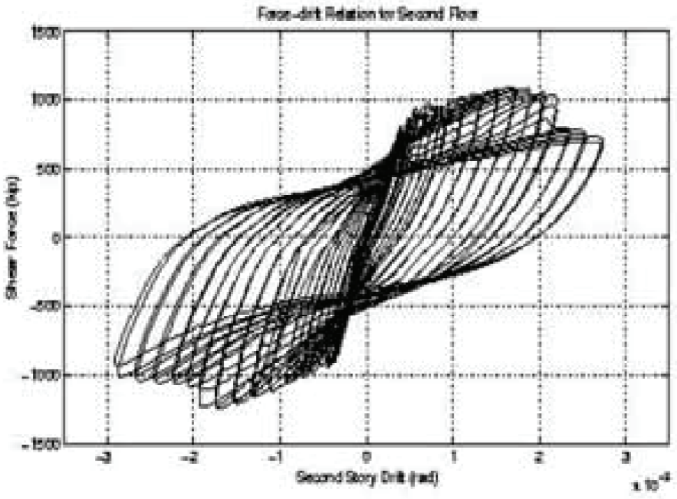

Figure 2.22. Hystertic Response at Second Floor (Astaneh-Asl and Zhao, 2001).

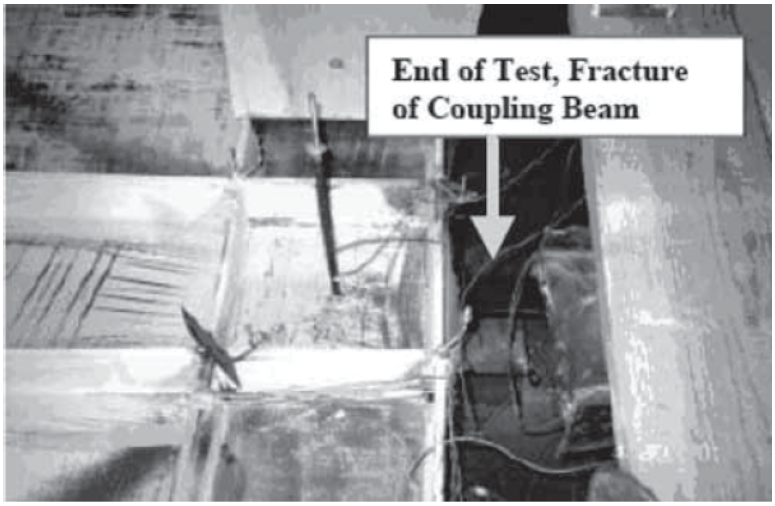

Figure 2.23. Fracture of Coupling Beam at the Face of the Column (Astaneh-Asl and Zhao, 2001).

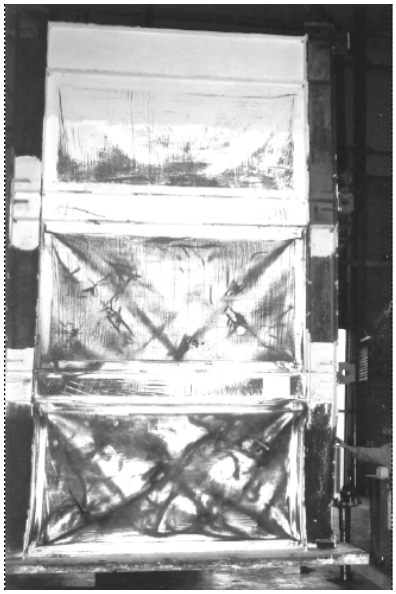

(a)

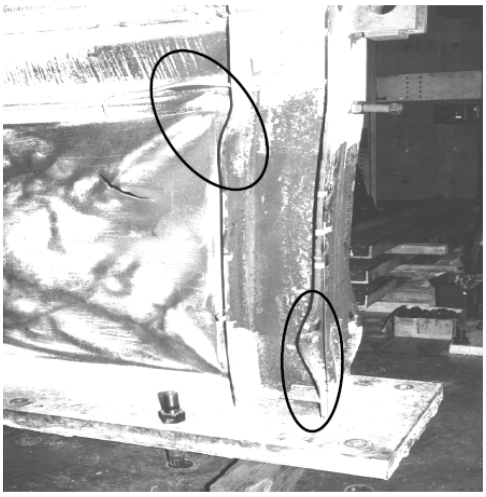

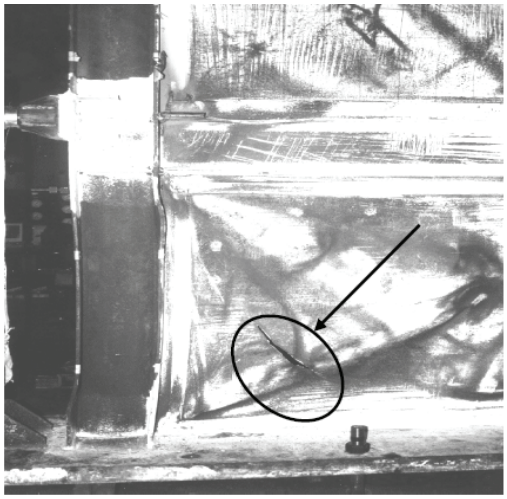

(b) (c)

Figure 2.24. 3-Story SPSW at the End of the Test: (a) Overall View; (b) Local Buckling of Column Flanges and Tear in Panel at 1st Story; (c) Tear at the Bottom of East Corner at 1st Story Panel (Behbahanifard et al., 2003).

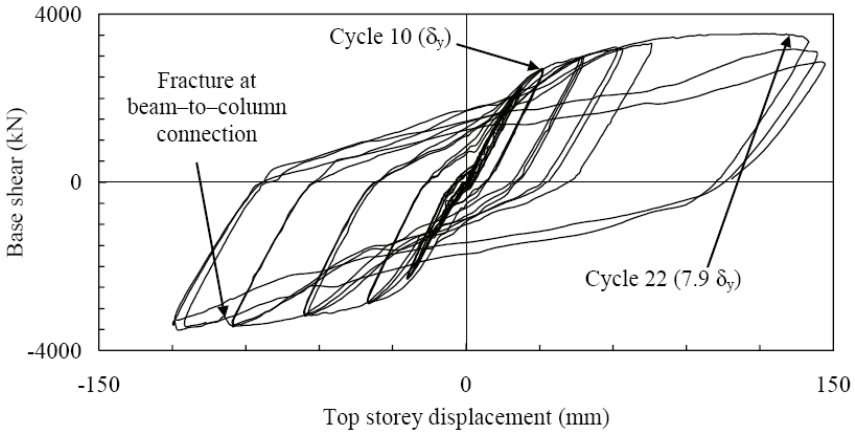

Figure 2.25. Base Shear vs Roof Displacement for 3-Story SPSW (Behbahanifard et al., 2003).

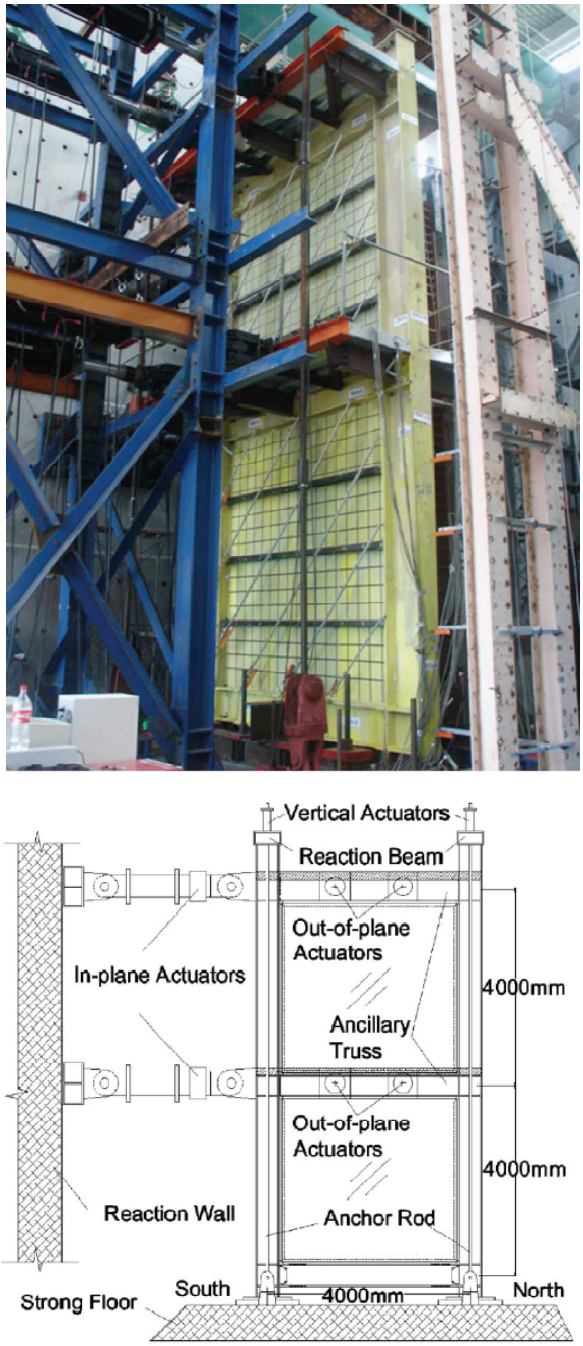

Figure 2.26. Specimen and the Test Setup (Qu et al., 2008).

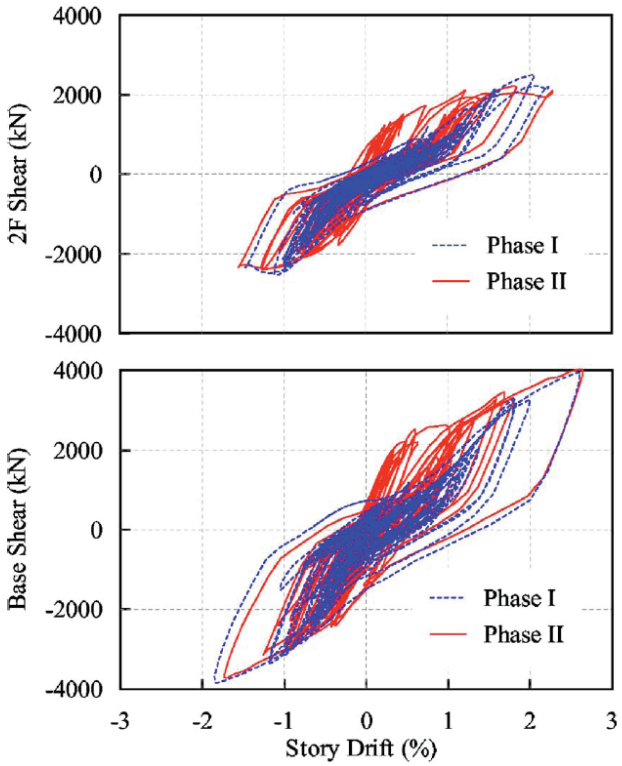

Figure 2.27. Comparing the Hysteresis Behavior of the Specimen in Phase I and Phase II (Qu et al., 2008).

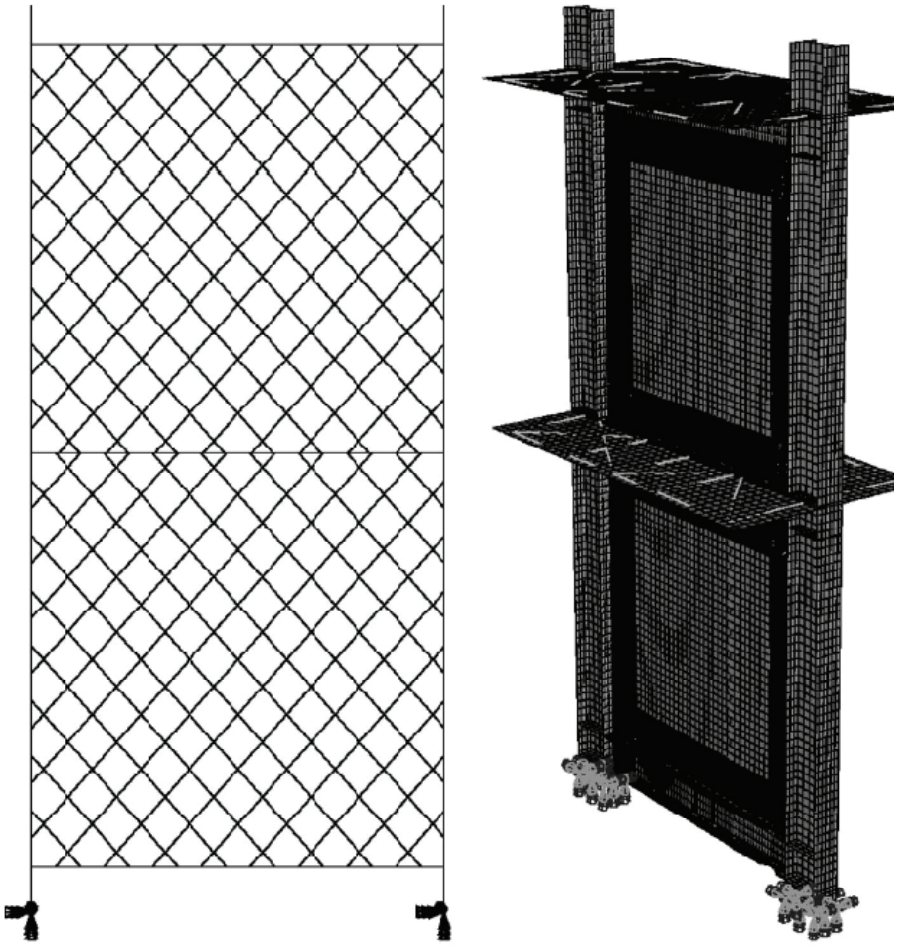

(a) (b)

Figure 2.28. Analytical Models of the Specimen: (a) Dual Strip Model; and (b) 3D FE Model (Qu et al., 2008).

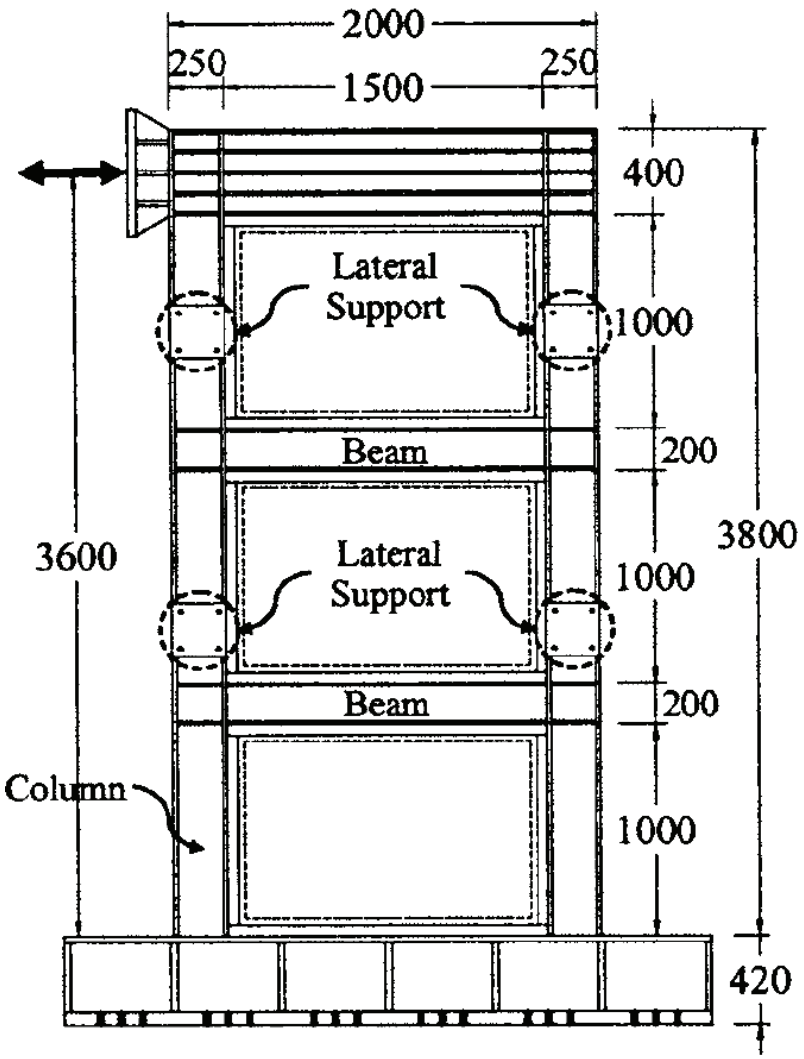

Figure 2.29. A Typical SPSW Test Specimen; Dimensions in mm (Park et al., 2007).

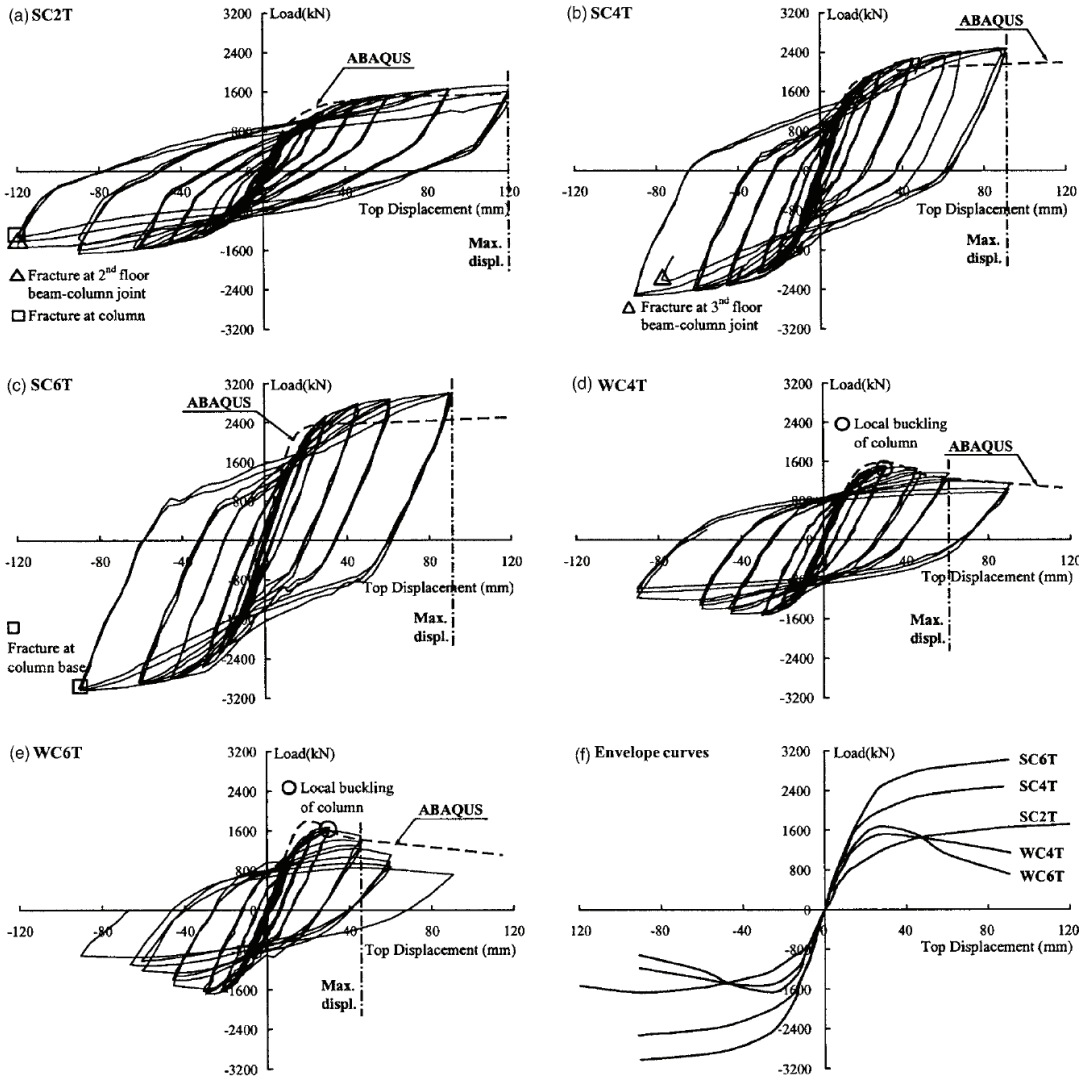

Figure 2.30. Load vs. Roof Displacement for SPSW Specimens (Park et al., 2007).

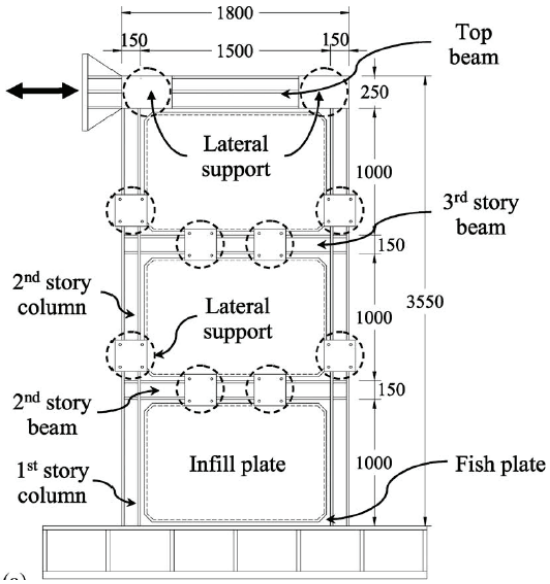

(a)

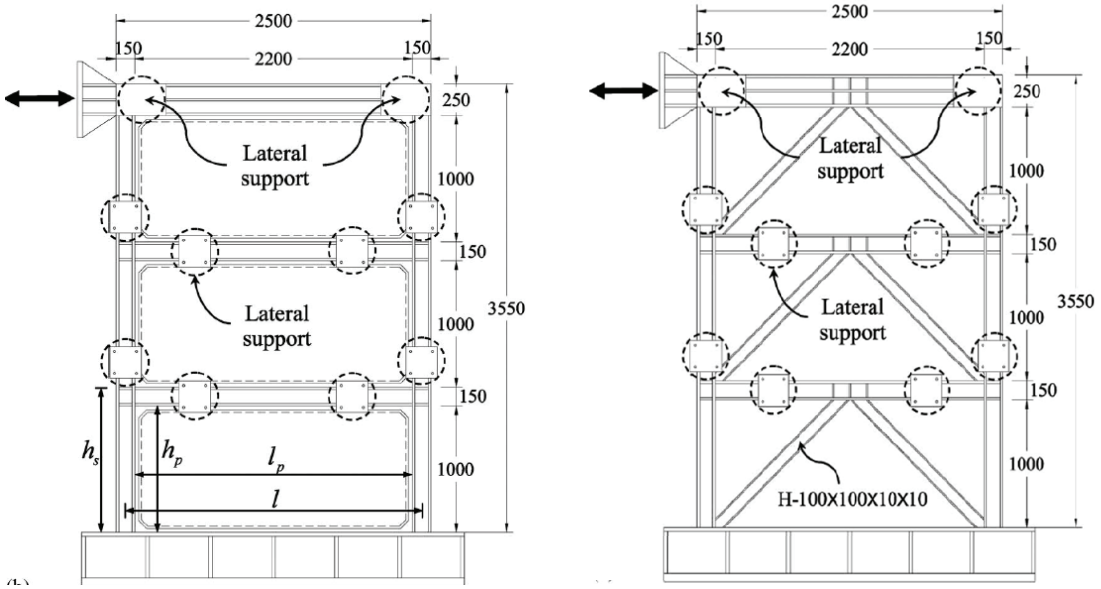

(b) (c)

Figure 2.31. Specimens Tested by Choi and Park (2008): (a) SPSW1; (b) SPSW2; and (c) CBF Specimens.

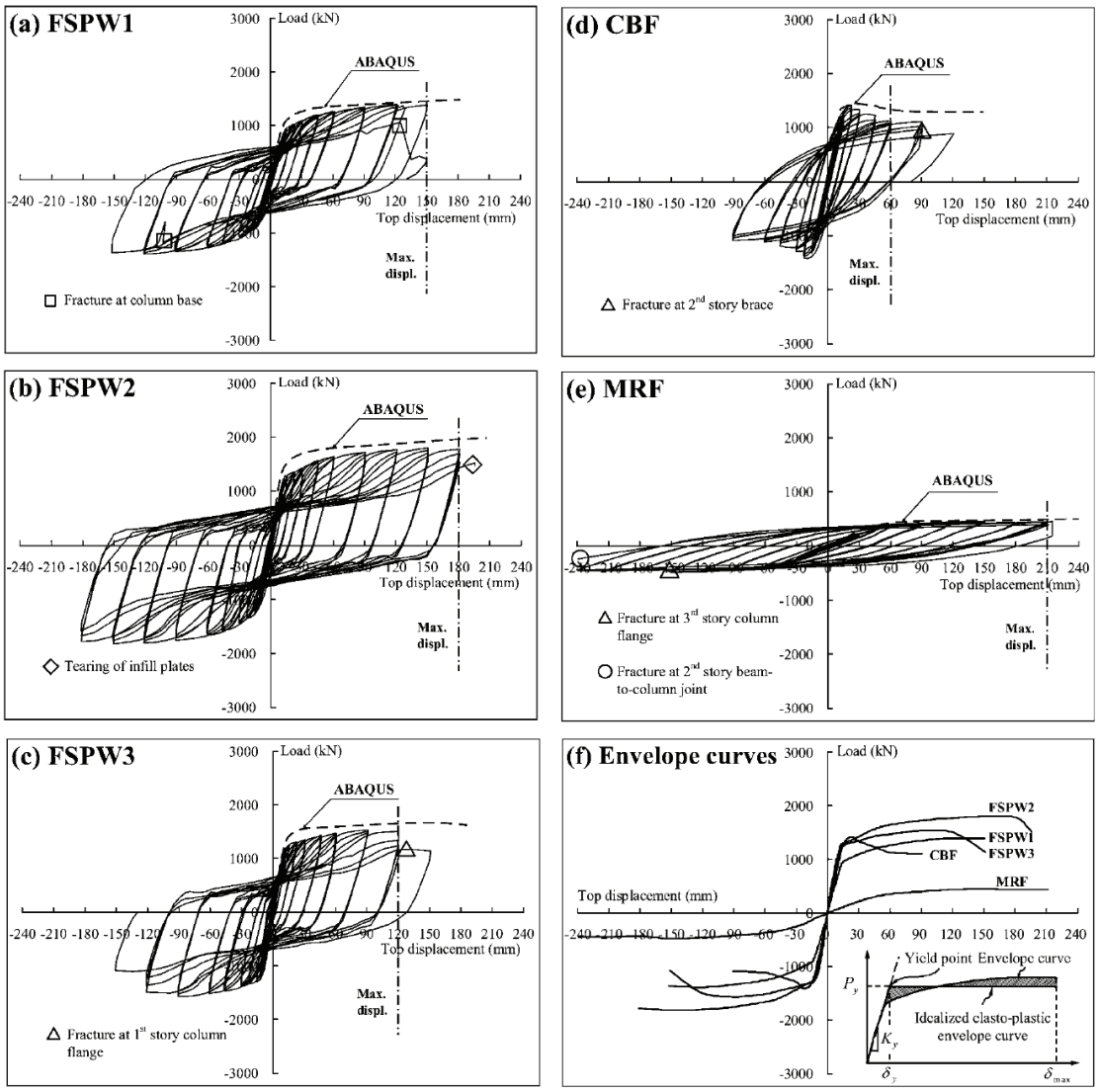

Figure 2.32. Load vs. Roof Displacement for SPSWs, CBF, and MRF Specimens (Choi and Park, 2008).

CHAPTER 3

PERFORMANCE-BASED PLASTIC DESIGN (PBPD) PROCEDURE

3.1 General

As mentioned in Chapter 1, the PBPD method uses pre-selected target drift and yield mechanism as key performance objectives. These two design parameters are directly related to the degree and distribution of structural damage. The design base shear for a specified hazard, which is generally given as design spectrum in the codes, is calculated by equating the work needed to push the structure monotonically up to the target drift to the energy required by an equivalent EP-SDOF to achieve the same state (Figure 3.1). Also, a new distribution of lateral design forces is used, which is based on relative distribution of maximum story shears calibrated by inelastic dynamic response results (Chao et al., 2007). Plastic design is then performed to detail the frame members and connections in order to achieve the intended yield mechanism and behavior. Thus, determination of design base shear, lateral force distribution, and plastic design are the three main components of the PBPD method. The outline of the step-by-step PBPD procedure is presented in this section, with more details to be discussed in the following sections in this chapter. More detailed discussions as well as the theoretical justification can be found in Goel and Chao (2008).

In this design procedure, the design base shear is determined by using the energy balance concept. The designer selects the target structural drifts (corresponding to

acceptable ductility and damage), and yield mechanism (for desirable response, and ease of post-earthquake damage inspection and reparability), and determines the design forces and frame member sizes for a given earthquake hazard (spectrum). There is no need for using factors, such as R, I, C_d, etc., as are required in the current design codes. Those factors are known to be based on a number of considerations including engineering judgment.

The step-by-step PBPD procedure is summarized as follows:

1. Select a desired yield mechanism and target drift for the structure consistent with the intended performance objectives for the design earthquake hazard. Assume idealized elastic-plastic (EP) force-displacement behavior and estimate yield drift ratio, θ_y, for the structure.

2. Estimate the natural period, T, of the structure and use an appropriate vertical distribution of design lateral forces.

3. With the information in Steps 1 and 2, along with the design spectral acceleration value, S_a, calculate the design base shear, V, by equating the work needed to monotonically push the structure up to the target drift (no pushover analysis needed) to the energy needed by an equivalent EP-SDOF to be displaced up to the same drift. A rational theory of inelastic seismic response of EP-SDOF can be used here, such as idealized inelastic response spectra by Newmark-Hall or others as preferred.

4. Modification for V is needed if the force-deformation behavior of the structure is different from the assumed EP behavior, such as for CBF or other framing systems.

5. Use plastic method to design the structural members that are expected to dissipate the earthquake energy inelastically (Designated Yielding Members, DYM), while

keeping the vertical distribution of lateral strength of the structure close to the distribution of design story shear distribution. Members that are required to remain elastic (non-DYM), such as columns, are designed by a capacity design approach, by accounting for the strain-hardening and material overstrength of the DYM as well as by including the frame deformation ($P-\Delta$) effects as appropriate.

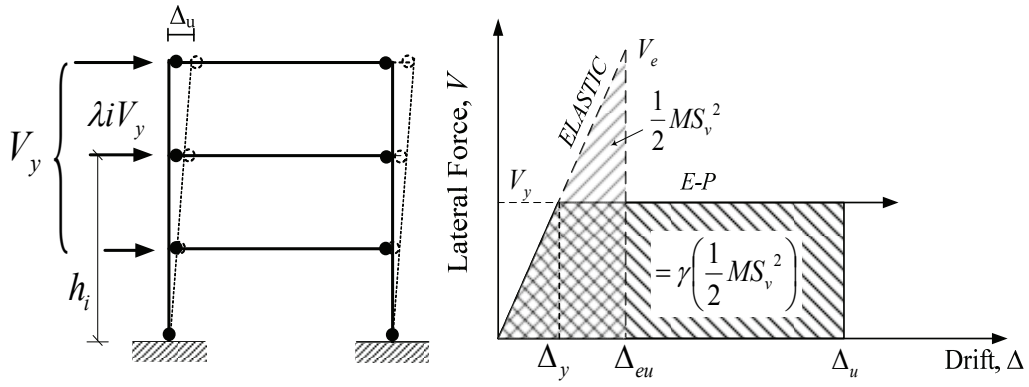

Figure 3.1. PBPD Concept: a) Yield Mechanism; b) Energy (Work) Balance Concept for SDOF.

3.2 PBPD Design Procedure

3.2.1 Target Yield Mechanism

The yield mechanism along with the target drift are the main design criteria in the PBPD procedure. The desired yield mechanism can be selected at the beginning of design. Figure 3.2 shows several typical structural systems subjected to design lateral forces and pushed to their target drift limit states (Goel and Chao, 2008). All inelastic deformations are intended to be confined within the Designated Yielding Members (DYMs) that are part of the selected yield mechanism, such as plastic hinges in beams or

yielding and buckling of bracing members in a CBF. Since the plastic hinges at column bases generally form during a major earthquake, the global yield mechanism of these structural systems also includes plastic hinges at those locations.

3.2.2 Design Lateral Forces

It is known that building structures designed according to current code procedures are expected to undergo large deformations in the inelastic range when subjected to major earthquakes. However, the equivalent static design lateral forces in the current codes are obtained from simplified models assuming that the structures behave elastically and primarily in the first mode of vibration (ATC 3-06, 1978; Clough and Penzien, 1993; Chopra, 2000; BSSC, 2003b), Thus, this leads such structures to experience lateral force distributions during earthquakes quite different from those given by the code formulas. In order to achieve the main goal of performance-based seismic design, *i.e.*, a desirable and predictable structural response, it is necessary to account for inelastic behavior of structures directly in the design process. The commonly used elastic analysis and design procedures in current practice, together with elastic design lateral force distributions, do not fulfill this goal in a realistic manner.

Unlike the force distribution in the current codes, the design lateral force distribution used in the PBPD method is based on maximum story shears as observed in nonlinear time-history analysis results (Chao et al., 2007). This new design lateral force distribution has been found suitable for MF, EBF, CBF, and STMF. Analytical results have shown that: 1) Frames designed by using this lateral force distribution experienced more uniform maximum interstory drifts along the height than the frames designed by

using current code distributions; 2) This force distribution also gives a very good estimate of maximum column moment demands when the structures are responding to severe ground motions and deform into the inelastic range; 3) Higher mode effects are well reflected in the proposed design lateral force distribution. This lateral force distribution is expressed as:

$$F_i = C'_{vi} V \tag{3.1}$$

where

$$C'_{vi} = (\beta_i - \beta_{i+1}) \left(\frac{w_n h_n}{\sum_{j=1}^{n} w_j h_j} \right)^{0.75T^{-0.2}} \quad \text{when } i = n,\ \beta_{n+1} = 0 \tag{3.2}$$

and

$$\beta_i = \frac{V_i}{V_n} = \left(\frac{\sum_{j=i}^{n} w_j h_j}{w_n h_n} \right)^{0.75T^{-0.2}} \tag{3.3}$$

In the above equations, β_i represents the shear distribution factor at level *i*; V_i and V_n, respectively, are the story shear forces at level *i* and at the top (*n*th) level; w_j is the seismic weight at level *j*; h_j is the height of level *j* from the base; w_n is the weight at the top level; h_n is the height of roof level from base; *T* is the fundamental period; F_i is the lateral force at level *i*; and *V* is the total design base shear.

3.2.3 Design Base Shear

Calculation of the required design base shear is one of the main steps in the PBPD procedure. The design base shear in this method is derived based on the inelastic state of the structure, with the drift control built-in. Therefore, no separate drift check is needed after design. In this approach the design base shear is determined by pushing the structure monotonically up to a target drift after the formation of a pre-selected yield mechanism. Note that no actual pushover analysis is needed for this as will be seen later. The amount of work needed is assumed as a factor γ times the elastic input energy $E\left(=\frac{1}{2}MS_v^2\right)$ for an equivalent EP-SDOF system (Housner, 1956 and 1960). It should be noted that the above mentioned work assumes no relationship with the actual energy dissipated during earthquake excitation, which has been used in energy-based procedures as proposed by a number of investigators (e.g. Akiyama, 1985; Uang and Bertero, 1988). However, those procedures have been found to be quite cumbersome to implement in common design practice. In the PBPD method the needed work term $(E_e + E_p)$ is simply used as a means to calculate the required design base shear by establishing ties between the desired yield mechanism, design drift, force-displacement characteristics of the structure, and elastic input energy from the design ground motion.

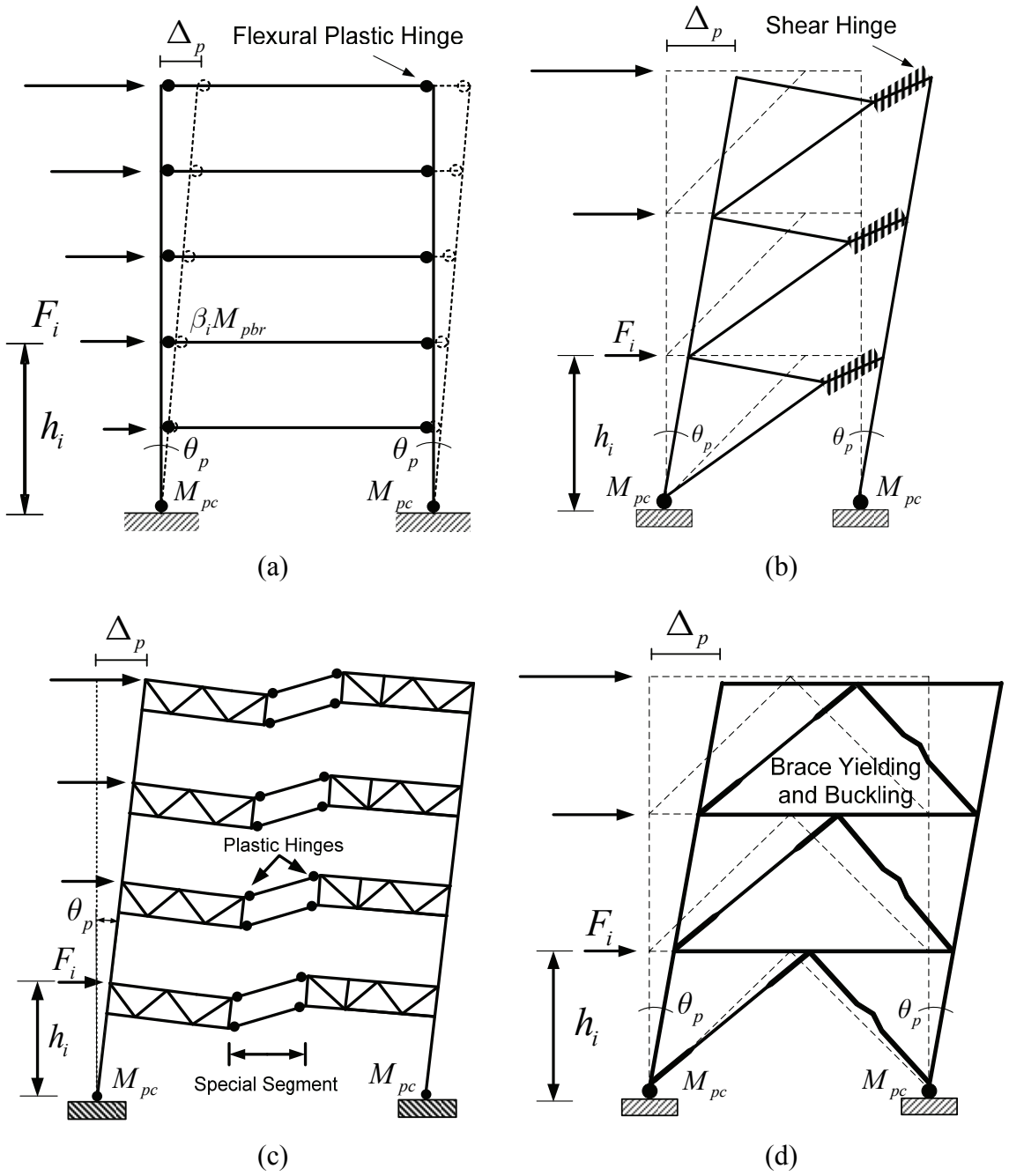

Figure 3.2. Desirable Yield Mechanisms of Typical Structural Systems: (a) Moment Frame; (b) Eccentrically Braced Frame; (c) Special Truss Moment Frame; and (d) Concentrically Braced Frame (Goel and Chao, 2008).

Thus, the work-energy equation can be written as:

$$\left(E_e + E_p\right) = \gamma E = \gamma\left(\tfrac{1}{2} M S_v^2\right) \tag{3.4}$$

where E_e and E_p are, respectively, the elastic and plastic components of the energy (work) needed to push the structure up to the target drift. S_v is the design spectral pseudo-velocity; and M is the total mass of the system. The energy modification factor, γ, depends on the structural ductility factor (μ_s) and the ductility reduction factor (R_μ). Figure 3.3 shows the relationship between the base shear (CW) and the corresponding drift (Δ) of the elastic and corresponding elastic-plastic SDOF systems.

Using the geometric relationship between the two areas representing work and energy in Figure 3.3, Equation (3.4) can be written as:

$$\frac{1}{2} C_y W \left(2\Delta_{\max} - \Delta_y\right) = \gamma\left(\frac{1}{2} C_{eu} W \Delta_{eu}\right) \tag{3.5}$$

Equation (3.5) can be reduced into the following form:

$$\gamma \frac{\Delta_{eu}}{\Delta_y} = \frac{\left(2\Delta_{\max} - \Delta_y\right)}{\Delta_{eu}} \tag{3.6}$$

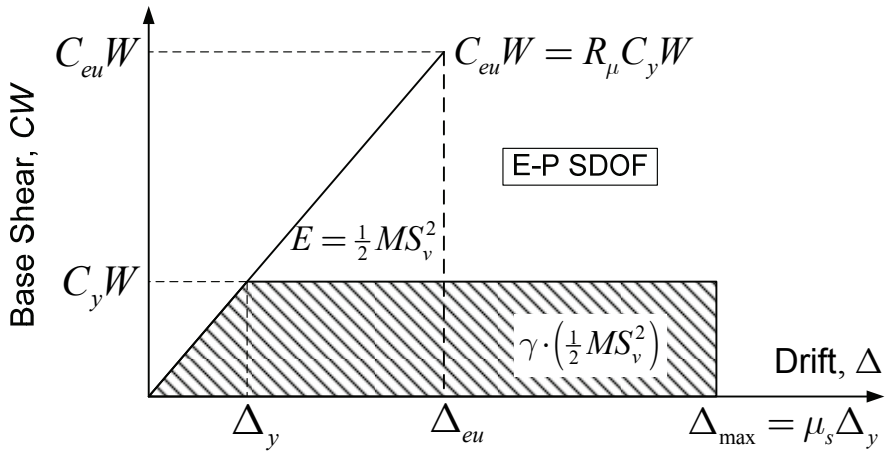

Figure 3.3. Structural Idealized Response and Energy (Work) Balance Concept for SDOF.

where Δ_{eu} and $\Delta_{\max}$ in Figure 3.3 are equal to $R_\mu \Delta_y$ and $\mu_s \Delta_y$, respectively. Substituting these terms into Equation (3.6), the expression for energy modification factor γ can be written as:

$$\gamma = \frac{2\mu_s - 1}{R_\mu^2} \tag{3.7}$$

where μ_s is the ductility factor equal to the design target drift divided by the yield drift ($\Delta_{\max}/\Delta_y$); R_μ is the ductility reduction factor equal to C_{eu}/C_y. It can be seen from Equation (3.7) that the energy modification factor γ is a function of the ductility reduction factor (R_μ) and the ductility factor (μ_s). The method by Newmark and Hall (1982) is used herein to relate the ductility reduction factor and the structural ductility factor for EP-SDOF as shown in Figure 3.4 and Table 3.1 (Miranda and Bertero, 1994; Lee and Goel, 2001). Plots of energy modification factor γ as obtained from Equation

(3.7) are shown in Figure 3.5. It should be mentioned that for this purpose any inelastic spectra for EP-SDOF systems can be used as preferred.

Table 3.1. Ductility Reduction Factor ($R_\mu = C_{eu}/C_y$) and its Corresponding Structural Period Range.

Period Range	Ductility Reduction Factor
$0 \le T < \frac{T_1}{10}$	$R_\mu = 1$
$\frac{T_1}{10} \le T < \frac{T_1}{4}$	$R_\mu = \sqrt{2\mu_s - 1} \cdot \left(\frac{T_1}{4T}\right)^{2.513 \cdot \log\left(\frac{1}{\sqrt{2\mu_s - 1}}\right)}$
$\frac{T_1}{4} \le T < T_1'$	$R_\mu = \sqrt{2\mu_s - 1}$
$T_1' \le T < T_1$	$R_\mu = \frac{T\mu_s}{T_1}$
$T_1 \le T$	$R_\mu = \mu_s$

Note: $T_1 = 0.57$ sec.; $T_1' = T_1 \cdot \left(\sqrt{2\mu_s - 1}/\mu_s\right)$ sec.

The elastic energy demand, E_e, can be determined from the elastic design pseudo-acceleration spectra which are typically given in the building codes. The design pseudo-acceleration based on the selected elastic design spectrum can be expressed as:

$$A = S_a \cdot g \tag{3.8}$$

where A is the design pseudo-acceleration, g is the acceleration due to gravity, and S_a is the spectral response acceleration. S_a can be further modified or increased to account for factors such as near-fault effect, redundancy consideration, or possible torsion in the

global structural system. Pending further research on these issues, guidance given in the current codes can be used.

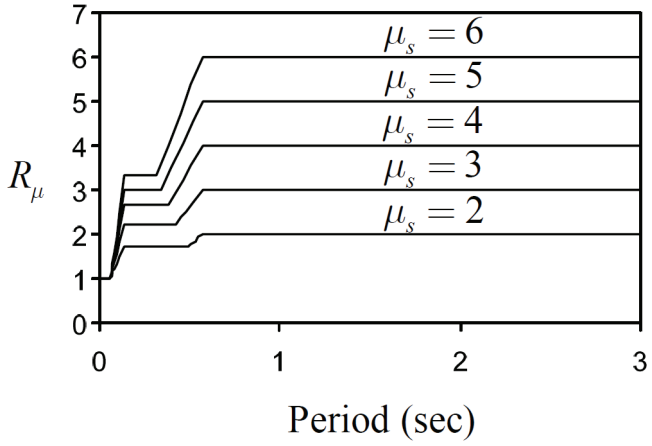

Figure 3.4. Idealized Inelastic Spectra by Newmark and Hall (1982) for EP-SDOF.

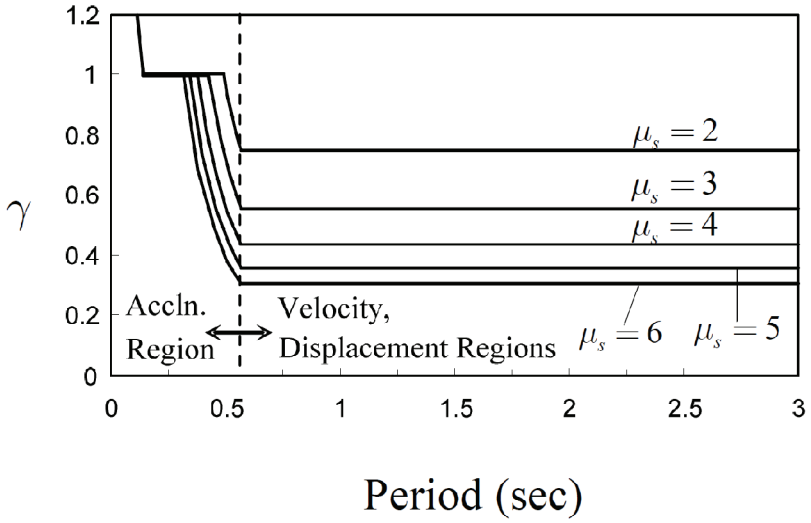

Figure 3.5. Energy Modification Factor, γ, versus Period.

The work-energy equation can be rewritten as:

$$\left(E_e + E_p\right) = \gamma\left(\frac{1}{2}MS_v^2\right) = \frac{1}{2}\gamma M\left(\frac{T}{2\pi}S_a g\right)^2 \tag{3.9}$$

Akiyama (1985) and other researchers have shown that the elastic vibrational energy, E_e, can be calculated by assuming that the entire structure can be reduced into an SDOF system, i.e.:

$$E_e = \frac{1}{2}M\left(\frac{T}{2\pi}\cdot\frac{V}{W}\cdot g\right)^2 \tag{3.10}$$

where V is the desired base shear at yield and W is the total seismic weight of the structure ($W=Mg$). Substituting Equation (3.10) into Equation (3.9) and rearranging the terms gives:

$$E_p = \frac{WT^2 g}{8\pi^2}\left(\gamma S_a^2 - \left(\frac{V}{W}\right)^2\right) \tag{3.11}$$

By using a pre-selected yield mechanism for a given structural system, as shown in Figure 3.2, and equating the plastic energy term E_p to the external work done by the design lateral forces gives:

$$E_p = \sum_{i=1}^{n} F_i h_i \theta_p \tag{3.12}$$

where θ_p is the global inelastic drift ratio of the structure (see Figure 3.2), which is the difference between the pre-selected design drift ratio (θ_u) and yield drift ratio (θ_y). The yield drift ratios of various structural systems have been initially considered to be fairly

constant for each type. For design purposes, yield drift ratios for MF, EBF, STMF, and CBF were assumed as shown in Table 3.2 (Lee and Goel, 2001; Chao and Goel, 2005; Chao and Goel, 2006a; Chao and Goel, 2006b). However, the assumption of constant yield drift ratio, although works well for MF systems due to their mainly shear mode of deformation, should be modified for braced structural systems as the flexural mode of deformation takes on increased importance in such systems with the increase in height. This issue, which leads to a varying yield drift ratio for braced systems, will be addressed in Chapter 5 in more details.

Table 3.2. Assumed Design Yield Drift Ratios.

Frame Type	MF	EBF	STMF	CBF
Yield Drift Ratio, θ_y (%)	1	0.5	0.75	0.3

Substituting Equations (3.1) and (3.11) into Equation (3.12), and solving for V/W gives:

$$\frac{V}{W} = \frac{-\alpha + \sqrt{\alpha^2 + 4\gamma S_a^2}}{2} \tag{3.13}$$

where V is the design base shear and α is a dimensionless parameter, which depends on the stiffness of the structure, the modal properties, and the design plastic drift level, and is given by:

$$\alpha = \left(\sum_{i=1}^{n} (\beta_i - \beta_{i+1}) h_i \right) \cdot \left(\frac{w_n h_n}{\sum_{j=1}^{n} w_j h_j} \right)^{0.75T^{-0.2}} \cdot \left(\frac{\theta_p 8\pi^2}{T^2 g} \right) \tag{3.14}$$

It should be noted that the required design base shear given by Equation (3.13) is related to the lateral force distribution (modal properties), the design plastic drift ratio, θ_p, and selected yield mechanism. Also note that in Equation (3.14), $\beta_{n+1} = 0$, when $i = n$.

It is noted that Equation (3.13) has the design target drift built into it, therefore the drift control is taken care of in the beginning of the design. Figure 3.6 shows the plots of the design base shears calculated from Equation (3.14) as a function of plastic drift ratios and period T for ten moment frames (2- to 20-story). The plastic drift ratios , θ_p, were selected as 0%, 0.5%, 1%, 1.5%, and 2% corresponding to assumed total target drifts of 1%, 1.5%, 2%, 2.5%, and 3%, respectively. It can be seen that, with other factors remaining unchanged, the design base shear increases as the target drift decreases. Figure 3.6 also shows how the design force is reduced from the elastic seismic force level depending upon the ductility and the period of the structure.

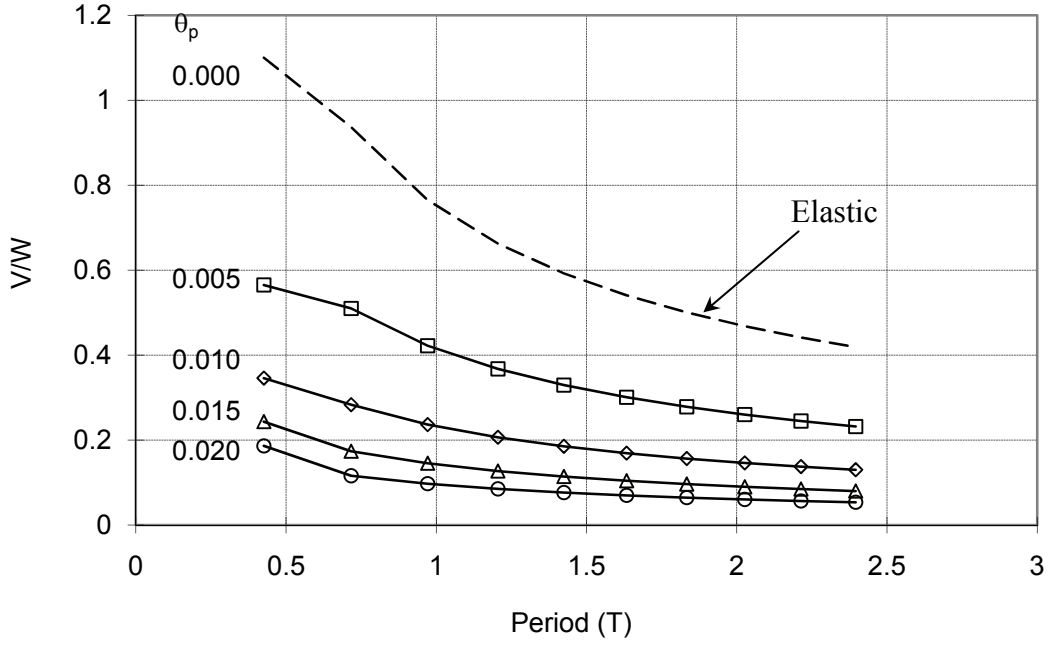

Figure 3.6. Relation between the PBPD Design Base Shear, Design Target Drift Ratio and Period (Lee and Goel, 2001).

The design base shear in Equation (3.13) was derived by assuming elastic-plastic hysteretic behavior of structural systems, such as steel MF, EBF, BRBF, or STMF. However, buckling of braces in concentrically braced frames (CBF) leads to "pinched" hysteretic loops. Therefore, using the same design base shear for a CBF would not be appropriate. A preliminary study based on a simple one-story one bay braced frame with pin-connected rigid beams and columns showed that the dissipated energy by CBF is approximately 35% of the energy dissipated by a corresponding frame with full elastic-plastic hysteretic loops, with both frames having equal strengths ($\eta = A_1 / A_2 = 0.35$ in Figure 3.7). Pending further study and considering that other structural members such as "gravity fames" will also resist earthquake forces, a slightly higher $\eta = 0.5$ is suggested

at this time for design purposes. However, caution should be exercised as this suggested value for η is based on one data point. Thus, the work-energy Equation (3.9) for CBF can be modified as (Chao and Goel, 2006b):

$$\left(\eta E_e + E_p\right) = \frac{1}{2}\gamma M\left(\frac{T}{2\pi}S_a g\right)^2 \tag{3.15}$$

The solution leads to the following equation:

$$\frac{V}{W} = \frac{-\alpha + \sqrt{\alpha^2 + 4\left(\gamma/\eta\right)S_a^2}}{2} \tag{3.16}$$

The above approach for modifying the design base shear can also be applied to other structural systems with degrading hysteretic behavior, such as reinforced concrete and masonry structures.

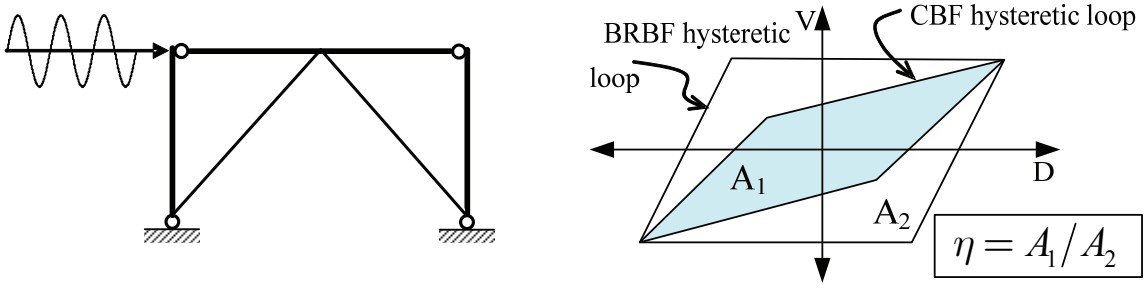

Figure 3.7. Typical Full EP and "Pinched" Hysteretic Loops.

It is noted that an alternative modified approach using the displacement amplification factor, C_2-factor, introduced in FEMA 356, is proposed in the current study

for base shear calculation of degrading structural systems such as CBF. More details can be found in Chapters 5 and 6.

In summary, the proposed method for determining the lateral design forces is based on basic principles of structural dynamics, while ensuring formation of selected yield mechanism and drift control simultaneously. The procedure accounts for inelastic behavior of a structure directly; hence there is no need for using response modification factor, R, occupancy importance factor, I, or displacement amplification factor (such as C_d), as are required in current practice and are largely based on engineering judgment.

It should also be noted that the design base shear in the proposed method as given by Equation (3.13) represents the ultimate yield force level (i.e., C_yW in Figure 3.3) at which complete mechanism is expected to form. In contrast, the code design base shear represents the required strength for use in design by elastic methods. This point is not made clear enough in the current design codes. For example, AISC Specifications (AISC, 2005b) permits design of some ductile structural systems such as MF by plastic method for the same factored design load combinations as used for elastic design. Thus, if one elects to use plastic method for code specified seismic design forces it can be quite unconservative, because part of the specified R factors includes overstrength due to structural redundancy, which is "used-up" in plastic design.

3.2.4 Design of Designated Yielding Members (DYMs)

The primary aim of using plastic design method is to provide adequate strength while ensuring formation of the desired yield mechanism. For moment frames, for instance, the plastic hinges may be confined to form only at the beam ends and column

bases. For other structural systems, inelastic deformation may be limited to shear links, special segments, braces, or coupling beams for EBF, STMF, CBF, or coupled wall systems, respectively. Previous studies have shown that it is desirable to have the distribution of structural strength along the building height follow the distribution of design story shears, *i.e.*, the shear distribution factor, β_i , which was obtained and calibrated by nonlinear dynamic time-history analysis results. This helps to distribute the yielding more evenly along the height, thereby, preventing yielding from concentrating at a few levels.

Only basic knowledge of plastic design is needed for design of members. For the designated yielding members (DYM) the required strength at each level can be determined by equating the external work to the internal work due to a small mechanism deformation, θ, as follows (see Figure 3.2, for one-bay frame):

$$\sum_{i=1}^{n} F_i h_i \theta = 2M_{pc}\theta + \sum_{i=1}^{n} \beta_i R_n \Theta_i \tag{3.17}$$

where Θ_i represents the deformation of the yielding members (flexural, shear, or axial deformation), which can be obtained from geometry of the yield mechanism as a function of θ . The term R_n represents the required plastic moment, shear force, or axial force of the yielding members at the top floor level and the only unknown variable in Equation (3.17). The required member strength (plastic capacity) at any level *i* can be determined by multiplying R_n by the shear distribution factor β_i at level *i*, namely, $\beta_i R_n$. M_{pc} is the assumed plastic moment of columns/walls at the base as shown in Figure 3.1. Note that

external work done by applicable gravity loads can also be included in Equation (3.17), if desired.

Equation (3.17) can be written for moment frames to obtain the required beam moment capacity at each level by plastic design approach (external work equals internal work and referring to Figure 3.2.a):

$$\sum_{i=1}^{n} F_i h_i \theta_p = 2M_{pc}\theta_p + \sum_{i=1}^{n} 2\left(\beta_i M_{pb}\right)\gamma_{pi} \tag{3.18}$$

where M_{pb} and $\beta_i M_{pb}$ are the required moment strengths at top floor level and level *i*, respectively. The rotation term can be obtained as $\gamma_{pi} = \left(L / L_i'\right)\theta_p$. It is noted that the external work done by a uniformly distributed gravity loading is zero due to the anti-symmetrical deformed shape of the beams (Figure 3.2.a). Therefore the required moment strength at level *i* is given by,

$$\beta_i M_{pb} = \beta_i \cdot \frac{\sum_{i=1}^{n} F_i h_i - 2M_{pc}}{2\sum_{i=1}^{n}\left(\beta_i \dfrac{L}{L_i'}\right)} \tag{3.19}$$

At this stage of the design process, one way to determine the required plastic moment of columns in the first story, M_{pc}, is to use the condition that no soft story mechanism would occur in the first story when a suitable factor (say 1.1) times the design lateral forces are applied on the frame (Leelataviwat et al., 1999), as shown in Figure 3.8. Assuming that plastic hinges form at the base and top of the first story columns, the corresponding work equation for a small mechanism deformation, θ , can be expressed as:

$$1.1V'h_1\theta = 4M_{pc}\theta \tag{3.20.a}$$

$$M_{pc} = \frac{1.1V'h_1}{4} \tag{3.20.b}$$

where V' is the base shear (for an equivalent one bay model), which may be taken as V divided by the number of bays; h_1 is the height of the first story; and the factor 1.1 accounts for overstrength above the design force. Equation (3.20.a) can be modified if the plastic hinges do not form in the columns at the base and the moment capacity at that location is smaller but known. By using Equations (3.17) through (3.20), the required member strength at floor level i , $\beta_i R_n$, can be determined, and the design can be performed by using applicable specifications (AISC or ACI-318).

It is noted that use of Equations (3.20) based on Figure 3.8 is conservative because it neglects the contribution from "gravity columns", which are generally continuous over the floors and provide additional lateral strength to the seismic resistant frames.

3.2.5 Design of Non-Designated Yielding Members (Non-DYMs)

The design of members that are intended to remain elastic, such as columns in a MF, columns and braces in an EBF, or truss members in an STMF, is performed based on capacity design approach. That is, these members should have design strength to resist the combination of factored gravity loads and maximum expected strength of the DYM accounting for reasonable strain-hardening and material overstrength.

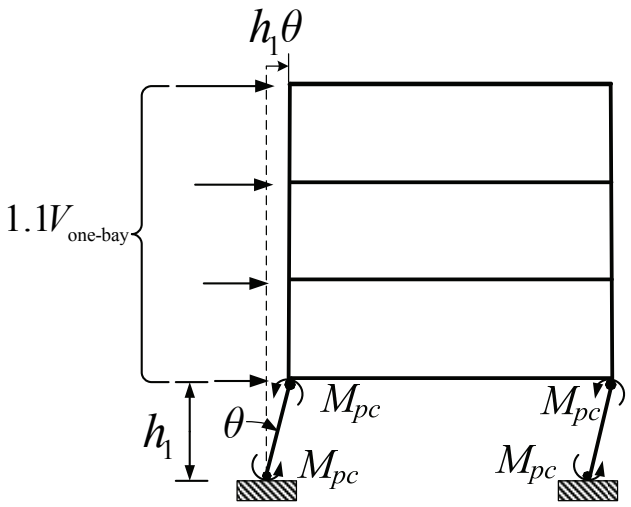

Figure 3.8. One-Bay Frame with Soft-Story Mechanism.

It has been mentioned by several investigators in the past that when a structure is subjected to seismic loading, especially in the inelastic state, large moments can occur in the columns, which can be quite different from those calculated by elastic analysis (Paulay and Priestley, 1992). Conventional design approaches usually do not accurately account for the maximum column moments and their locations (Bondy, 1996; Medina and Krawinkler, 2005). In fact, the column moments are quite often underestimated, because the columns are subjected to moments not only from those delivered from the beams or other members framing into the columns (conventional capacity design approach) but also from their own deformation (Bondy, 1996).

Considering the above mentioned shortcoming in the conventional design approach, a different method is employed in the proposed PBPD approach by considering the equilibrium of an entire "column tree" in the extreme limit state. For example, Figure

3.9 shows the free-body diagram of an exterior "column tree" of a moment frame (Figure 3.2a) when the frame reaches its target drift. In order to ensure the formation of intended strong-column weak-beam mechanism, columns must be designed for maximum expected forces by including gravity loads on beams and columns and by considering a reasonable extent of strain-hardening and material overstrength in the beam plastic hinges. The column at the base is also assumed to have reached its maximum capacity, M_{pc}.The moment at a strain-hardened beam plastic hinge can be obtained by multiplying its nominal plastic moment (M_{pb}) by an appropriate overstrength factor (ξ), which accounts for the effect of strain-hardening and material overstrength. At this stage, the required lateral forces (F_{iu}) acting on this free body may be assumed to maintain the distribution as given by Equations (3.1) through (3.3), and their magnitude can be easily obtained by using equilibrium of the free body. Then the column moments and shear force in each story are calculated by applying the expected beam end moments and lateral forces applied at each level (F_{iu}). Second order effects can be included by either using approximate amplification factors as given in design codes, or directly by considering the equilibrium of the "column-tree" in the limit deformed state.

In the case of MF, the sum of required balancing lateral forces, F_L, applied on the free-body of an exterior column tree can be obtained as (see Figure 3.9.a):

$$F_L = \frac{\sum_{i=1}^{n}\left(M_{pr}\right)_i + \sum_{i=1}^{n}\left(V_{SW}\right)_i \cdot \left(w + \frac{d_c}{2}\right)_i + M_{pc}}{\sum_{i=1}^{n}\alpha_i h_i} \tag{3.21}$$

where w is the width of shear plate and

$$\alpha_i = \frac{(\beta_i - \beta_{i+1})}{\sum_{i=1}^{n}(\beta_i - \beta_{i+1})} \quad \text{when } i = n,\ \beta_{n+1} = 0 \tag{3.22}$$

Equation (3.21) neglects the gravity load on the short length of the beam between the plastic hinge and the face of the column.

For the case of interior column tree, both directions of lateral forces lead to the same result; hence only the lateral forces acting to the left are shown in Figure 3.9.b. The sum of lateral forces, F_L, can be calculated as:

$$F_L = \frac{2 \cdot \sum_{i=1}^{n}\left(M_{pr}\right)_i + \sum_{i=1}^{n}\left[\left(V_{SW}\right)_i + \left(V'_{SW}\right)_i\right] \cdot \left(w + \frac{d_c}{2}\right)_i + 2M_{pc}}{\sum_{i=1}^{n}\alpha_i h_i} \tag{3.23}$$

The flowcharts in Figures 3.10 and 3.11 show the general PBPD procedure. Figure 3.10 shows the steps in determining the PBPD design base shear. Figure 3.11 shows the steps for design of DYMs and Non-DYMs.

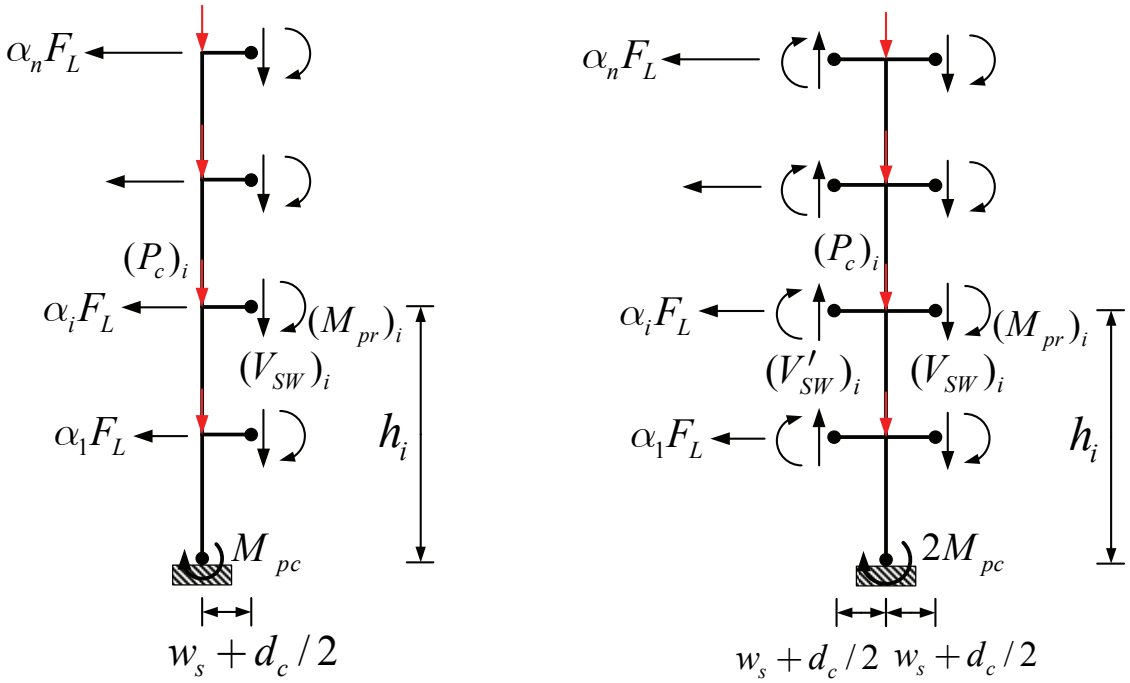

(a) (b)

Figure 3.9. (a) Free-Body Diagram of an Exterior Column Tree (Lateral Forces Acting to the Left); (b) Free-Body Diagram of an Interior Column Tree (Lateral Forces Acting to the Left).

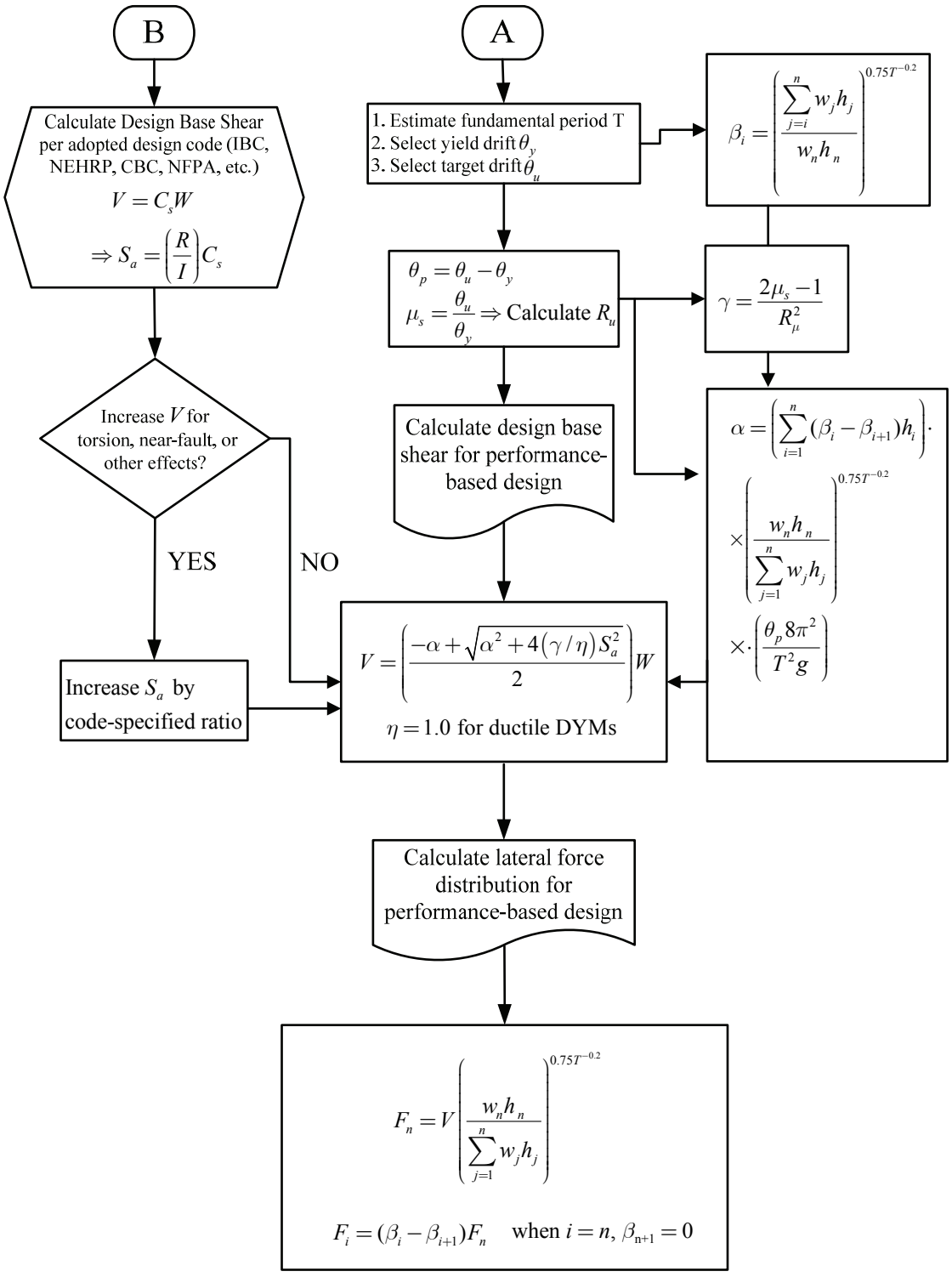

Figure 3.10. Performance-Based Plastic Design Flowchart: Determining Design Base Shear and Lateral Force Distribution.

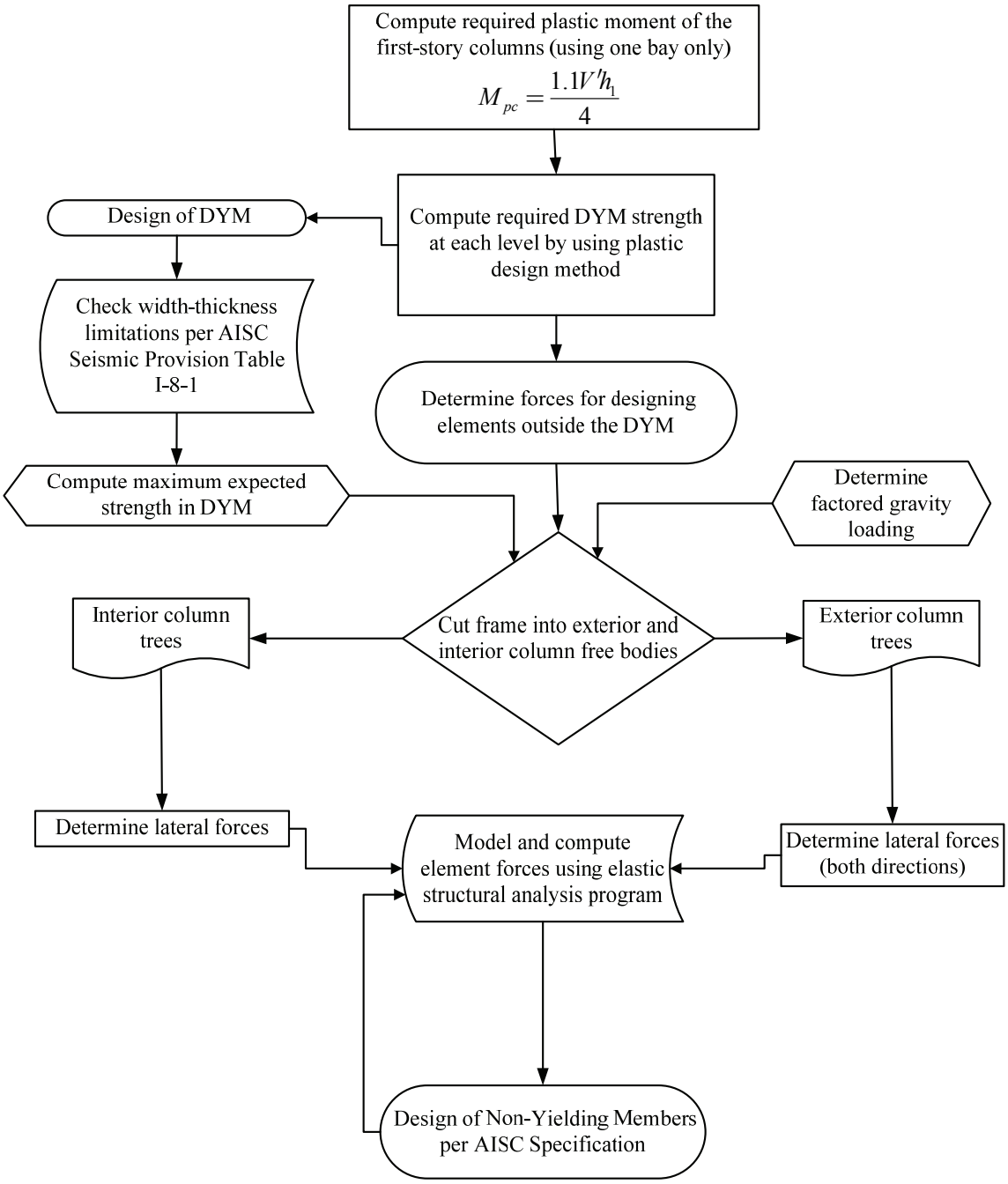

Figure 3.11. Performance-Based Plastic Design Flowchart: Element Design.

CHAPTER 4

SEISMIC PERFORMANCE EVALUATION OF CONCENTRICALLY BRACED FRAMES

4.1 General

Concentrically Braced Frames (CBFs) are considered to be quite efficient systems for steel structures that are commonly used to resist forces due to wind or earthquakes. This is mainly due to the fact that these systems provide complete truss action in order to transfer the lateral loads to the ground. During a moderate to severe earthquake, the bracing members and connections in such systems are expected to experience significant inelastic deformations in the post-buckling range (AISC, 2005a).

However, CBFs are generally considered less ductile seismic-resistant structures than other systems due to the buckling or fracture of the bracing members under large cyclic deformations. When designed by conventional elastic design methods, these structures can undergo excessive story drifts after buckling of bracing members. This can lead to early fractures of the bracing members, especially in those that popular rectangular tube sections (HSSs) are used for bracing members (Goel and Chao, 2008).

The research work led to the code adoption of provisions for ductile concentrically braced frames called Special Concentrically Braced Frames (SCBFs) (Goel, 1992a; AISC, 2005a). It has been expected that designing the braced systems by

using such provisions would result in stable and ductile behavior under major earthquake events.

The main objective in this chapter is to evaluate the performance and also the confidence levels against global collapse of the re-designed CBFs based on the PBPD approach and to compare them to those by Uriz and Mahin (2004) previously designed by the then current code (Sabelli, 2000). In this regard, the PBPD procedure for design of CBFs is briefly described in the following. Then, a summary of the reliability-based performance evaluation procedure developed as part of the FEMA/SAC Steel Project (FEMA, 2000b) is presented. The application of such procedure for CBFs is then discussed. Also, the results of applying this procedure on CBFs designed by Sabelli (2000), called hereafter NEHRP frames, are shown based on the study done by Uriz and Mahin (2004). Finally, the confidence level analysis results for the PBPD re-designed CBFs are presented and compared to those of the NEHRP frames.

4.2 Redesign of 3V and 6V CBFs by PBPD Approach

In a recent analytical study by Sabelli (2000), series of nonlinear dynamic analyses were carried out to assess the behavior of CBFs and Buckling Restraint Braced Frames (BRBFs) with different configurations. Two different heights of 3-story and 6-story for these frames were also considered. These frames were designed as SCBF according to the *1997 NEHRP Recommended Provisions for Seismic Regulations for New Buildings and Other Structures* (FEMA, 1997) and *1997 AISC Seismic Provisions* (AISC, 1997). The results showed that the Chevron type CBFs designed by such conventional

elastic design method can suffer severe damage or even collapse under design level ground motions (10% probability of exceedence in 50 years). Brace fracture was found to be a common feature in many of such dynamic analyses, especially those producing severe response. In those frames, the beams were designed based on the difference of nominal yield strength (P_y) and post-buckling strength of the braces ($0.3\phi_c P_{cr}$, assuming out-of-plane buckling). The material overstrength factor, R_y (the ratio of expected yield strength to specified minimum yield strength), was not specified for design of beams in the 1997 Provisions, which led to considerable yielding in the beams at the location of brace intersection under major earthquakes. As can be seen in the following, the frames were re-designed using the 1997 NEHRP spectra and the 2005 AISC Seismic Provisions (AISC, 2005a), where the beams are required to be designed based on the difference of expected yield strength ($R_y P_y$) and nominal post-buckling ($0.3P_{cr}$) of braces. The member sizes of 3V-NEHRP and 6V-NEHRP as well as frames are shown in Figures 4.11.a and 4.12.a, respectively. In the study by Goel and Chao (2008), these 3- and 6-story chevron type CBFs were re-designed following the recommended Performance-Based Plastic Design (PBPD) procedure. A summary of the PBPD procedure for CBFs is presented in the following sections. The final design sections based on the following procedure for 3V-PBPD and 6V-PBPD are shown in Figures 4.11.b and 4.12.b, respectively.

4.2.1 Design Base Shear

Since drift control is essential to achieving acceptable performance of CBFs, the design can be accomplished by using the PBPD methodology, which has been

successfully applied to moment frames, eccentrically braced frames, and special truss moment frames (Lee and Goel, 2001; Chao and Goel, 2006a; Chao and Goel, 2008). This design method uses pre-selected target drifts (θ_p in Figure 4.1) and yield mechanism as performance limit states. The design base shear is derived by using an energy (work) equation where the energy needed to push the structure up to the target drift is calculated as a fraction of elastic input energy which is obtained from the selected elastic design spectra (Figure 4.2). The resulting design base shear obtained from energy balance can be expressed as (Chao and Goel, 2006b):

$$\frac{V}{W} = \frac{-\alpha + \sqrt{\alpha^2 + 4(\gamma/\eta)S_a^2}}{2} \tag{4.1}$$

where V is the design base shear; W is the total seismic weight of the structure; α is a dimensionless parameter which depends on the natural period of the structure, the modal properties, and the intended drift level; C_e is the design pseudo-acceleration coefficient based on code design spectrum. The energy modification factor, γ, depends on the structural ductility factor ($\mu_s=\Delta_{max}/\Delta_y$) and the ductility reduction factor ($R_\mu=C_{eu}/C_y$), which is related to the natural period and can be determined as:

$$\gamma = \frac{2\mu_s - 1}{R_\mu^2} \tag{4.2}$$

The inelastic spectra proposed by Newmark and Hall (1982) as shown in Figure 4.3 (R_μ-μ_s-T relationship) were used to calculate γ from Equation (4.2). To account for the fact that buckling of braces in CBFs leads to "pinched" hysteretic response, a reduction

factor (η = *A1/A2* in Figure 4.4) is used in Equation (7.1) to express the energy dissipation ratio between a typical CBF and a frame with full elastic-plastic hysteretic loops (such as BRBF). Preliminary study suggests that $\eta = 0.5$ is reasonable for design purposes (Chao and Goel, 2006b). The two frames were re-designed by using Equation (7.1), along with the plastic design approach to detail the frame members to achieve the intended yield mechanism and behavior. The pre-selected target drift was 1.25% for 10%/50yrs hazard level.

4.2.2 Design of Bracing Members

Three criteria are used in PBPD approach for design of bracing members, as described in the following. These are strength, fracture life, and compactness criteria. From strength point of view, it is desirable to have the distribution of bracing member strength along the building height closely follow the distribution of design story shears to minimize the possibility of concentration of inelastic deformation in one or few stories. The braces are designed based on their ultimate state (plastic design), i.e., tension yielding and post-buckling, to resist the total design story shear, neglecting the contribution from columns (conservative). Thus,

$$\left(V_{\text{story shear}}\right)_i \le \left(\phi_t P_y + 0.5\phi_c P_{cr}\right)_i \cos\alpha_i \qquad (4.3)$$

or,

$$\frac{\left(V_{\text{story shear}}\right)_i}{0.9\cdot\cos\alpha_i} \le \left(P_y + 0.5P_{cr}\right)_i \qquad (4.4)$$

where $V_{story\ shear}$ is the story shear at level i for an equivalent one-bay frame; P_y is the nominal axial tensile strength of bracing members; P_{cr} is the nominal axial compressive strength of bracing members; $\phi_t = \phi_c = 0.9$ (AISC, 2005b); α is the angle of bracing members with the horizontal (see Figure 4.1). The design is carried out by assuming that both bracing members reach their ultimate inelastic strength. Note that the post-buckling strength is taken as $0.5P_{cr}$ for braces buckling in-plane. A post-buckling strength of $0.3P_{cr}$ should be used for braces buckling out-of-plane. It should also be noted that the effective length factor, K, is taken as 0.5 and 0.85 for the in-plane (K_x) and out-of-plane (K_y) directions, respectively (Lee and Goel, 1990). In order to ensure in-plane buckling, braces are selected such that $K_x L/r_x > K_y L/r_y$.

In order to prevent premature brace fractures, a fracture criterion for HSS braces is used in the PBPD approach for CBFs. The brace fracture life, N_f, is estimated by the following empirical equation, which was derived from test results of HSS braces under cycling loading (Tang and Goel, 1987):

$$N_f = \begin{cases} 262\dfrac{(b/d)(KL/r)}{\{(b-2t)/t\}^2} & \text{for } KL/r > 60 \\ 262\dfrac{(b/d)60}{\{(b-2t)/t\}^2} & \text{for } KL/r \le 60 \end{cases} \qquad (4.5)$$

where N_f is the fracture life representing the number of standard cycles, beyond which an HSS brace will fracture; d is the gross depth of the section; b is the gross width of the section ($b \ge d$); t is the wall thickness; $(b-2t)/t$ is clear width-thickness ratio of

compression flanges (Goel, 1992a; Shaback and Brown, 2003) ; KL/r is the slenderness ratio. A minimum N_f = 100 for HSS braces is suggested. Nonlinear dynamic analysis results have shown that the performance of CBFs is significantly enhanced (Chao and Goel, 2006b, and Goel and Chao, 2008) by using this criterion. It should be noted that current design practice does not consider the brace fracture life in an explicit manner.

For compactness criterion, the required compactness ratio specified by AISC *Seismic Provisions* (AISC, 2005a) is also checked for the braces. However, the compactness requirement is generally satisfied for HSS braces with a minimum N_f = 100. More information on design criteria for bracing members can be found in Goel and Chao (2008).

Built-up brace sections made of double HSS were used for the PBPD frames, as shown in Figure 4.5. This is an effective way to reduce width-thickness ratios without increasing the wall thickness of the sections (Lee and Goel, 1990). This technique utilizes simple gusset plate connections with direct welding between the gusset plate and double tubes, without the inconvenience of making the necessary slots at both ends of a single tube member for welded gusset plate connections. Such built-up double tube members generally also buckle in-plane, which can eliminate the possibility of damage to surrounding non-structural elements due to out-of-plane buckling of single tube section. In-plane buckling also simplifies the design of gusset plates because the plastic hinges will form in the brace instead of the gusset plates (three plastic hinges in brace). Tests carried out by Lee and Goel (1990) showed that double tube bracing members were able to dissipate more energy by sustaining more loading cycles when compared with single

tube members. The post-buckling strength is nearly half the initial buckling strength with in-plane buckling (fixed-end condition). Further, in order to avoid column plastic hinging due to presence of gusset plates (Figure 4.6), beam shear splice was used to prevent the beam moment transfer to column, as shown in Figure 4.5. Another advantage of using this scheme is that the connection can be shop-fabricated thereby enhancing the quality and reducing the field labor cost. More complete design details can be found elsewhere (*i.e.*, Goel and Chao, 2008).

4.2.3 Design of Non-Yielding Members

The design of non-yielding members, including beams and columns, is performed based on the capacity design approach, i.e., non-yielding members should have a design strength to resist the combination of factored gravity loads and the forces due to braces in their ultimate state.

Design of beams should follow the criteria given in AISC *Seismic Provisions* (AISC, 2005a). One important criterion is that in V-type or inverted-V (Chevron) bracing, the beams should be designed to support vertical and horizontal unbalanced forces resulting from the difference in the tension and compression brace forces after buckling. For this purpose, the tension and compression forces in the braces are assumed to be equal to $R_y F_y A_g$ and $0.3P_{cr}$, respectively. It should be noted though that the post-buckling strength of a brace is taken as $0.5P_{cr}$ for in-plane buckling (Figure 4.7). In addition, beams intersected by the braces should be designed assuming that no gravity loads are supported by the braces. A pin-supported beam model is used because shear

splices are used at the ends. The design of beams should follow the beam-column design requirements due to the presence of high axial forces. Lateral supports need to be provided at a minimum spacing of L_{pd}, in the vicinity of mid-span. The unbalanced loads resulting from the braces are (see Figure 4.7):

$$F_h = \left(R_y P_y + 0.5 P_{cr}\right)\cos\alpha \tag{4.6}$$

$$F_v = \left(R_y P_y - 0.5 P_{cr}\right)\sin\alpha \tag{4.7}$$

where F_h is the horizontal unbalanced force; R_y is the ratio of the expected yield strength to the specified minimum yield strength and specified as 1.4 for ASTM A500 Grade B HSS (AISC, 2005b); P_y is the nominal yield strength = $F_y A_g$, in which F_y = 46 ksi for the A500 Grade B tube section; P_{cr} is the nominal compressive strength = $F_{cr} A_g$. F_{cr} is the axial critical stress which is specified as (AISC, 2005b):

when $F_e \geq 0.44F_y$

$$F_{cr} = \left[0.658^{\frac{F_y}{F_e}}\right] F_y \tag{4.8}$$

when $F_e < 0.44F_y$

$$F_{cr} = 0.877F_e \tag{4.9}$$

$$\text{where, } F_e = \frac{\pi^2 E}{\left(KL/r\right)^2} \tag{4.10}$$

In the columns, axial forces result primarily from the gravity loads and vertical component of brace forces. Due to the presence of beam shear splices, little or no moment is transferred into the columns. Thus only axial loads are considered for column design, including the fixed base first story columns. Two limit states are considered for the design of columns:

1) Pre-buckling limit state

Prior to brace buckling, no unbalanced force occurs in the beam and the design axial force in a typical exterior column is (see Figure 4.8.a):

$$P_u = \left(P_{transverse}\right)_i + \left(P_{beam}\right)_i + \left(P_{cr}\sin\alpha\right)_{i+1} \qquad (4.11)$$

where $\left(P_{transverse}\right)_i$ is the tributary factored gravity load (1.2*DL*+0.5*LL*) on columns from the transverse direction at level *i*; $\left(P_{beam}\right)_i$ is the tributary factored gravity load from the beam at level *i* (= $\frac{1}{2}\left(w_u\right)_i L$); $\left(P_{cr}\right)_{i+1}$ is the buckling force of brace at *i+1* level. Similarly, for a typical interior column, the axial force demand is determined by (Figure 4.8.b):

$$P_u = \left(P_{transverse}\right)_i + \sum\left(P_{beam}\right)_i + \left(P_{cr}\sin\alpha\right)_{i+1} \qquad (4.12)$$

2) Post-buckling limit state

When a Chevron type CBF reaches its ultimate state, an unbalanced force is created in the beam (see Figure 4.7) and the axial force demand in a typical exterior column can be determined by (see Figure 4.9.a):

$$P_u = \left(P_{transverse}\right)_i + \left(P_{beam}\right)_i + \left(0.5P_{cr}\sin\alpha\right)_{i+1} + \frac{1}{2}F_v \qquad (4.13)$$

where $\left(P_{transverse}\right)_i$ is the tributary factored gravity load (1.2*DL*+0.5*LL*) from the transverse direction at level *i*; $\left(P_{beam}\right)_i$ is the tributary factored gravity load from beam at level *i* (= $\frac{1}{2}\left(w_u\right)_i L$); $0.5\left(P_{cr}\right)_{i+1}$ is the post-buckling force of brace at *i*+1 level; F_v is the vertical unbalanced force.

Similarly, the axial force demand for a typical interior column is (Figure 4.9.b):

$$P_u = \left(P_{transverse}\right)_i + \sum\left(P_{beam}\right)_i + \left(0.5P_{cr}\sin\alpha\right)_{i+1} + \frac{1}{2}F_v \qquad (4.14)$$

The design axial force demand is then determined by the governing pre-buckling or post-buckling limit state. It is noted that the above approach assumes that all braces reach their limit states simultaneously. This may be somewhat conservative for design of lower level columns, especially for high-rise buildings. In that case, the maximum probable axial force can be estimated by a more rational method, such as square root of the sum of squares method (SRSS, e.g. Redwood and Channagiri, 1991). Further research is needed on this issue of column design forces, especially in tall structures.

Column design is done by using Equations (4.8) to (4.10), with the effective length factor *K* = 1.0 (AISC, 2005b). Current AISC *Seismic Provisions* (AISC, 2005a) require that the compactness of columns in CBF meet the seismic width-thickness ratios given in the *Provisions* (e.g. $b/t \le 0.30\sqrt{E/F_y}$). This is supported by findings from previous studies (e.g. Sabelli et al., 2003), that columns in CBF can experience

significant inelastic rotations. However, in CBF designed by PBPD approach, brace fractures are practically eliminated (especially for 10% in 50 years earthquake motions) by keeping the interstory drifts well within carefully selected limits. In addition, moments transferred to the columns are minimized by using the beam shear splices. Therefore, columns in CBF design by PBPD are expected to experience only minor bending due to their continuity under dynamic analysis. Yielding at the column bases may occur under severe ground motions but is generally quite limited. Therefore, the above mentioned *b/t* limitation is used for the first-level column only; whereas the limitation of $0.38\sqrt{E/F_y}$ as specified in the AISC Specification (AISC, 2005b) is used for columns at all the other levels.

A summary of the above explained PBPD design steps for CBFs is given in the flowchart shown in Figure 4.10. These steps were followed in redesign of the 3- and 6-story CBF by PBPD method. The final design sections for PBPD frames are shown in Figures 4.11.b and 4.12.b, respectively.

4.3 Performance-Based Evaluation of CBFs

A reliability framework for seismic performance evaluation of Steel Moment-Resisting Frames (SMRFs) was developed as part of the FEMA/SAC Steel Project (FEMA, 2000b). In this approach, two main performance levels (immediate occupancy and collapse prevention) are considered under specified seismic hazards. The global and the local deformation demands (as obtained from analysis) are then compared with the deformation capacity of the structural system and structural elements, respectively

(FEMA, 2000b and Uriz, 2005). Basically, this procedure provides a simple method to estimate the confidence level of structures to meet the given performance level under specified seismic hazard (Yun et al., 2002). In other words, by considering such deformation demands and capacities in probabilistic terms with the assumption of lognormal probability distributions relative to uncertainty parameters (due to all uncertainties and randomness involved), an estimate of the confidence level to achieve the desired performance can be obtained in terms of the probability of the demand being less than the capacity.

Based on these, a demand and capacity factor design (DCFD), similar to the Load and Resistance Factor Design (LRFD), was adopted in FEMA/SAC Steel Project. This reliability-based quantitative approach involves evaluation of site-specific hazard, structural capacity, and structural demand, such that by having the hazard level and performance criteria the confidence level for the structure can be estimated. Hence, the main features in this approach are ground motion hazard curve, dynamic displacements, and displacement capacity. This procedure requires the calculation of a confidence parameter λ which can later be used to determine the confidence level associated with the assumed performance objective (Yun et al., 2002). The confidence parameter can be calculated as:

$$\lambda = \frac{\gamma \cdot \gamma_a \cdot D}{\phi \cdot C} \tag{4.15}$$

where

C = median estimate of the capacity of the structure, as indicated in FEMA351 (FEMA, 2000b).

D = median demand for the structure, obtained from structural analysis for a specified level of ground motion.

γ = demand variability factor that accounts for the variability inherent in the prediction of demand related to assumptions made in structural modeling and prediction of the character of ground shaking.

γ_a = analytical uncertainty factor that accounts for bias and uncertainty, inherent in the specific analytical procedure used to estimate demand as a function of ground shaking intensity.

ϕ = resistance factor that accounts for the uncertainty and variability inherent in the prediction of structural capacity as a function of ground shaking intensity.

λ = confidence parameter from which a level of confidence can be obtained.

Having calculated the confidence parameter, λ, by using Equation (4.15), the confidence level can be obtained from a table similar to Table 4.1 (Yun et al., 2002) or directly from the proper probability-based formulation. In this table, β_{UT} is the total uncertainty measure and k is the logarithmic slope of the hazard curve, both of which will be explained later in this chapter.

Uriz and Mahin (2004) used the performance-based earthquake evaluation (PBEE) framework originally developed for SMRFs in FEMA/SAC steel Project (FEMA, 2000b) to assess the performance of CBF and BRBF structures. In their study, the PBEE procedure was applied to four case study buildings; 3-story and 6-story

chevron CBFs, and 3-story and 6-story chevron BRBFs. All four frames were originally designed by Sabelli (2000) according to *1997 NEHRP provisions* (FEMA, 1997). In this chapter, only the performances of example CBFs are studied. Also, only the global collapse condition and collapse prevention (CP) performance level are considered. It should be noted, as was mentioned by Uriz and Mahin (2004), that due to lack of supporting experimental data, several significant assumptions are needed when using the PBEE procedure for CBFs. Many parameter values used are approximate for CBFs and as a result, the calculated values for confidence level are only approximate estimates and they may not be as accurate as they are for SMRFs. Nevertheless, they are reasonable enough for comparison purposes since the same parameters have been used for both NEHRP and PBPD designed CBFs.

A summary of the steps in calculating the confidence level with which a structure can achieve its intended performance objective, as outlined by FEMA 351 (FEMA, 2000b), can be given as follows:

1. The performance objective against which the structure should be evaluated is selected. This requires selection of the desired performance level, e.g. Collapse Prevention or Immediate Occupancy, and a desired probability that damage in a period of time will be worse than this performance level. Representative performance objectives may include:

- 2% probability of poorer performance than Collapse Prevention level in 50 years
- 50% probability of poorer performance than Immediate Occupancy level in 50 years.

2. Characteristic motion for the performance objective is determined. For probabilistic performance objectives, an average estimate of the ground shaking intensity at the probability of exceedance identified in the performance objective definition (Step 1) is determined. Ground shaking intensity is characterized by the parameter S_{aT1}, the 5% damped spectral response acceleration at the site for the fundamental period of response of the structure. NEHRP 1997 provides procedures for determining this parameter for any probability of exceedance in a 50-year period.

3. Structural demands for the characteristic earthquake ground motion are determined. A mathematical model is developed to represent the building structure. This model is then subjected to a structural analysis, using any of the methods mentioned in Chapter 3 of FEMA 351 (FEMA, 2000b). This analysis provides estimates of maximum interstory drift demand, maximum column axial compression force demand, and maximum column-splice axial tension force demand, for the ground motion selected in Step 2.

4. Median estimates of structural capacity are determined. Interstory drift capacity for the building frame, as a whole, may be estimated using the default values given in Chapter 3 of FEMA351 for regular structures. Alternatively, the detailed procedures of Section A.6 of FEMA351 (e.g. Incemental Dynamic Analysis or IDA) may be used.

5. A factored-demand-to-capacity ratio, λ is determined. The calculated estimates of demand D and capacity C are determined using Steps 3 and 4, respectively. The corresponding demand (γ) and resistance (ϕ) factors should be determined in accordance

with the applicable procedures. Then the confidence parameter λ can be obtained using Equation (4.15).

6. The confidence level is evaluated. The confidence level with regard to the ability of the structure to meet the performance objective should be the lowest value determined using the values of l as determined in accordance with Step 5 above and back-calculated from the equation:

$$\lambda = e^{-b\beta_{UT}(K_X - k\beta_{UT}/2)} \tag{4.16}$$

where:

b = a coefficient relating the incremental change in demand (drift, force, or deformation) to an incremental change in ground shaking intensity, at the hazard level of interest, typically taken as having a value of 1.0,

β_{UT} = an uncertainty measure equal to the vector sum of the logarithmic standard deviation of the variations in demand and capacity resulting from uncertainty,

k = the slope of the hazard curve, in ln-ln coordinates, at the hazard level of interest, i.e., the ratio of incremental change in S_{aT1} to incremental change in annual probability of exceedance,

K_X = standard Gaussian variate associated with probability x of not being exceeded as a function of number of standard deviations above or below the mean found in standard probability tables. Table 4.1 shows a solution for this equation, for various values of the parameters k, l, and β_{UT}.

The values of the parameter β_{UT} in Table 4.3 are used in Equation (4.16) to account for the uncertainties inherent in the estimation of demands and capacities.

Assuming that the amount of uncertainty introduced by each of the assumptions can be characterized, the parameter β_{UT} can be calculated using the equation:

$$\beta_{UT} = \sqrt{\sum_i \beta_{ui}^2} \tag{4.17}$$

where: β_{ui} represents the standard deviation of the natural logarithms of the variation in demand or capacity resulting from each of the various sources of uncertainty.

In the following sections, these steps are followed in order to obtain the confidence level of the four CBFs (3V-NEHRP, 3V-PBPD, 6V-NEHRP, and 6V-PBPD) against collapse prevention (CP) performance level under the seismic hazard level of 2% probability of exceedence in 50 years (2%/50yrs).

4.3.1 Determination of Site-Specific Hazard Parameters

In this study, seismic hazard parameters are assumed to be the same as those used in the FEMA/SAC for SMRF case studies (Yun et al., 2002) and the study on CBFs and BRBFs (Sabelli, 2000). Two basic hazard parameters are required for performance evaluation. These are: the intensity as the median 5%-damped linear spectral response acceleration, S_{aT1}, at the fundamental period of the building for the desired hazard level, and the logarithmic slope of the hazard curve, k, at the desired hazard level (FEMA, 2000b). In this study, the building is assumed to be located on firm soil in downtown Los Angeles, California and the seismic hazard parameters are based on the 1997 NEHRP Provisions (FEMA, 1997). Accordingly, twenty ground motions from FEMA/SAC database for the LA site and corresponding to a 2% probability of exceedance in 50 year

(hereafter called SAC LA ground motions) are used in dynamic analyses. These ground motions, which consist of LA21 to LA40, are taken from a larger database of representative ground motions developed by Somerville (1997).

The logarithmic slope k of the hazard curve at the desired hazard level is used to determine the resistance factors, demand factors and also the confidence levels. The hazard curve is a plot of probability of exceedance of a spectral amplitude versus the spectral amplitude for a given period, and is usually plotted on a log-log scale (FEMA, 2000b). In functional form it can be represented by the equation:

$$H_{si}(S_i) = k_0 S_i^{-k} \tag{4.18}$$

where:

$H_{Si}(S_i)$ = the probability of ground shaking having a spectral response acceleration greater than S_i,

k_0 = a constant, dependent on the seismicity of the individual site,

k = the logarithmic slope of the hazard curve, and k = 3 can be assumed for Alaska, California and the Pacific Northwest according to Table A.3 of FEMA 351.

4.3.2 Assessment of Structural Demand

The maximum story drift demands were obtained by performing nonlinear dynamic analysis for the suite of 20 SAC LA ground motion (2%/50yrs) which are LA21 to LA40. The analyses were carried out by using the SNAP-2DX program, which has the ability to model the brace behavior under large displacement reversals, as well as fracture

life of tubular braces (Rai et al., 1996). In addition, lump gravity columns were included in the model by using continuous leaning columns, which were linked to the braced frame through pin-ended rigid elements. Those gravity columns created significant *P-Δ* effect under large drifts. It is noted that, due to the presence of gusset plates, the beam ends at all levels (except for the top levels) of the NEHRP frames were modeled by assuming fixed-end condition. All beams and columns of the frame were modeled as beam-column elements. The same modeling technique was used in the study by Sabelli (2000) with the exception of P-Delta modeling. The seismic mass was assumed to be uniformly distributed when assigning such mass properties at the nodes of the braced frame model. The beam-to-column connections of the 3- and 6-story NEHRP frame (except for roof level) were modeled as moment resisting connections due to the presence of gusset plates. On the other hand, the beam-to-column connections at all levels of the 3- and 6-story PBPD frame were modeled as pin connections due to the introduction of beam splices (Figures 4.11 and 4.12). For comparison between performance of NEHRP and PBPD frames under the design level (10%/50yrs) as well as MCE level (2%/50yrs) ground motions the reader is referred to Goel and Chao (2008).

The maximum interstory drifts were considered to be a good indication of the global damage in CBFs. It is well related to the extent of plastic deformations in structural components (local level) as well as the global instability of the whole frame due to *P-Δ* effect. The peak interstory drifts at all stories for the four frames were obtained under each of the 20 SAC LA ground motions. As recommended by FEMA 351, a lognormal probability distribution was considered for these peak interstory drift values.

The median and standard deviation values were then obtained for these peak interstory drifts for all ground motions. The median value of these drift demands can be taken as the demand parameter D for use in Equation (4.15). The variability (uncertainty) of dynamic response for this hazard level is represented by the standard deviation of the natural logarithm of the peak drift demands (β_{DR}). Once the value of β_{DR} is determined, the demand variability factor, γ, is calculated from the Equation (4.19) as:

$$\gamma = e^{\frac{k}{2b}\beta_{D_R}^2} \tag{4.19}$$

where:

k = the logarithmic slope of the hazard curve (see section 4.3.1)

b = a coefficient that represents the amount that demand increases as a function of hazard. As mentioned by Uriz (2005), for flexible moment frames, this value is taken as *1.0*, but for stiffer braced frames with shorter periods a value larger than *1.0* might be expected based on the conservation of energy principle (Chopra 1995, Newmark and Hall, 1973).

As can be seen from Table 4.4Table 5.24, the median drift demand for 3-NEHRP is significantly larger than that of 3V-PBPD. The median drift of 3V-PBPD is about 22% of the 3V-NEHRP frame. In the case of 6-story CBFs, the median drift demand of 6V-NEHRP is about 30% larger than that of 6V-PBPD.

The demand uncertainty factor γ_a is based on uncertainties involved in the determination of the median demand, D. These uncertainties are mainly coming from the inaccuracies in the analytical modeling and procedure used in demand calculation. The

effect of such uncertainties in the recommended performance evaluation procedure can be captured by using an analysis uncertainty factor, γ_a, as given in Equation (4.20):

$$\gamma_a = C_B e^{\frac{k}{2b}\beta_{D_U}^2} \tag{4.20}$$

In this study, the same default values for γ_a recommended in FEMA 351 for SMRFs are used, although this assumption may be unconservative due to the larger scatter of the story drift results in CBFs compared to SMRFs. These analysis uncertainty values are shown in Table 4.2.

4.3.3 Determination of Drift Capacity

Incremental Dynamic Analysis (IDA) procedure developed by Vamvatsikos and Cornell (2002) aims at determining the global drift capacity of structures (FEMA, 2000b). This procedure was utilized in this study to obtain the drift capacities of the study frames. In this method, the maximum interstory drifts were obtained through nonlinear dynamic analyses under varying intensities of twenty 2%/50yrs SAC ground motions (FEMA, 2000b; Vamvatsikos and Cornell, 2002). Having the intensity (in terms of spectral acceleration, S_a) versus maximum story drift plot for each ground motion, the drift capacity for a particular ground motion can be estimated at the point where the slope of the curve falls below one-fifth of its initial slope. Additionally, as an upper bound, the drift capacities cannot be taken greater than 10%. Figure 4.13 and Figure 4.14 give the IDA results for the three- and six-story frames, respectively. The drift capacities are shown in these figures by hollow circles on each curve. The numerical values for global drift capacity C and the corresponding resistance factor ϕ are given in Table 4.4.

4.3.4 Confidence Level Assessment

After all the parameters needed in Equation (4-14) to calculate the confidence parameter λ are determined, the confidence level can be obtained for each frame. This can be done either by interpolating the appropriate values from Table 4.1, or by using the standard Gaussian variate K_X given by the following equation:

$$K_X = \frac{k\beta_{UT}}{2b} - \frac{\ln(\lambda)}{b\beta_{UT}} \tag{4.21}$$

Randomness and uncertainty parameters as well as resulting confidence levels are shown in Table 4.3 and 4.4, respectively. As can be seen, confidence level of the 3V-NEHRP frame against global collapse (<<1%) was dramatically improved when it was re-designed by the PBPD method (*i.e.*, 3V-PBPD frame). It is worth mentioning that the enhanced confidence level (>99.9%) is comparable to those of SMFs designed according to 1997 NEHRP provisions (Yun et al., 2002). It can also be seen that although the median drift capacities for the two three-story frames are somewhat close, the drift demand of the 3V-PBPD frame is only about 22% of the 3V-NEHRP frame. Table 4.4 also shows that, the confidence level for 6V-NEHRP frame (23.3%) is higher compared to the 3V-NEHRP frame, but is still much below the 90% satisfactory level suggested by FEMA 351 for SMFs. The confidence level of 86.2%, for the 6V-PBPD frame is also quite close to the desired 90% level.

4.4 Summary and Concluding Remarks

- Reliability-based evaluation by using the FEMA 351 procedure for SMFs, which accounts for randomness and uncertainty in the estimation of seismic demand and drift capacity, showed that steel concentrically braced frames (CBFs) designed by the performance-based plastic design (PBPD) method can have dramatically higher confidence levels against global collapse than those of SCBFs designed by current practice. Also, those confidence levels can be similar to the target confidence levels for SMFs in current practice, *i.e.*, 90% or above.

- Significant improvement in the confidence level (C. L.) can be seen for the 3V-PBPD compared to 3V-NEHRP. This C. L. is indeed comparable to those of MFs designed by 1997 NEHRP code (Yun et al., 2002). On the other hand, the 3V-NEHRP shows extremely low confidence level against global collapse. It can also be seen that although the median drift capacities for the two 3-story frames are somewhat close, they show quite different drift demands under 2/50 ground motions.

-The C.L. for 6V-NEHRP frame was somewhat better than that of the 3V-NEHRP frame, but was still much less than the 90% satisfactory level as suggested by FEMA 351. Significant difference can still be observed between the C.L.s of 6V-NEHRP and 6V-PBPD, with the latter having a confidence level quite close to 90%.

Table 4.1. Confidence Parameter λ, as a Function of Confidence Level, Hazard Parameter k, and Uncertainty β_{UT} (Yun et al., 2002).

Confidence	2%	5%	10%	20%	30%	40%	50%	60%	70%	80%	90%	95%	99%
						$\beta_{UT}=0.1$							
$k=1$	1.23	1.18	1.14	1.09	1.06	1.03	1.01	0.98	0.95	0.92	0.88	0.85	0.80
$k=2$	1.24	1.19	1.15	1.10	1.06	1.04	1.01	0.98	0.96	0.93	0.89	0.86	0.80
$k=3$	1.25	1.20	1.15	1.10	1.07	1.04	1.02	0.99	0.96	0.93	0.89	0.86	0.80
$k=4$	1.25	1.20	1.16	1.11	1.08	1.05	1.02	0.99	0.97	0.94	0.90	0.87	0.81
						$\beta_{UT}=0.2$							
$k=1$	1.54	1.42	1.32	1.21	1.13	1.07	1.02	0.97	0.92	0.86	0.79	0.73	0.64
$k=2$	1.57	1.45	1.34	1.23	1.16	1.09	1.04	0.99	0.94	0.88	0.81	0.75	0.65
$k=3$	1.60	1.48	1.37	1.26	1.18	1.12	1.06	1.01	0.96	0.90	0.82	0.76	0.67
$k=4$	1.63	1.51	1.40	1.28	1.20	1.14	1.08	1.03	0.98	0.92	0.84	0.78	0.68
						$\beta_{UT}=0.3$							
$k=1$	1.94	1.71	1.54	1.35	1.22	1.13	1.05	0.97	0.89	0.81	0.71	0.64	0.52
$k=2$	2.03	1.79	1.61	1.41	1.28	1.18	1.09	1.01	0.93	0.85	0.74	0.67	0.54
$k=3$	2.12	1.87	1.68	1.47	1.34	1.23	1.14	1.06	0.98	0.89	0.78	0.70	0.57
$k=4$	2.22	1.96	1.76	1.54	1.40	1.29	1.20	1.11	1.02	0.93	0.82	0.73	0.60
						$\beta_{UT}=0.4$							
$k=1$	2.46	2.09	1.81	1.52	1.34	1.20	1.08	0.98	0.88	0.77	0.65	0.56	0.43
$k=2$	2.67	2.27	1.96	1.64	1.45	1.30	1.17	1.06	0.95	0.84	0.70	0.61	0.46
$k=3$	2.89	2.45	2.12	1.78	1.57	1.41	1.27	1.15	1.03	0.91	0.76	0.66	0.50
$k=4$	3.13	2.66	2.30	1.93	1.70	1.52	1.38	1.24	1.12	0.98	0.82	0.71	0.54
						$\beta_{UT}=0.5$							
$k=1$	3.16	2.58	2.15	1.73	1.47	1.29	1.13	1.00	0.87	0.74	0.60	0.50	0.35
$k=2$	3.59	2.92	2.44	1.96	1.67	1.46	1.28	1.13	0.99	0.84	0.68	0.56	0.40
$k=3$	4.06	3.31	2.76	2.22	1.89	1.65	1.45	1.28	1.12	0.96	0.77	0.64	0.45
$k=4$	4.60	3.75	3.13	2.51	2.14	1.87	1.65	1.45	1.27	1.08	0.87	0.72	0.52
						$\beta_{UT}=0.6$							
$k=1$	4.11	3.21	2.58	1.98	1.64	1.39	1.20	1.03	0.87	0.72	0.55	0.45	0.30
$k=2$	4.91	3.85	3.09	2.37	1.96	1.67	1.43	1.23	1.05	0.87	0.66	0.53	0.35
$k=3$	5.88	4.60	3.70	2.84	2.35	2.00	1.72	1.47	1.25	1.04	0.80	0.64	0.42
$k=4$	7.04	5.51	4.43	3.40	2.81	2.39	2.05	1.76	1.50	1.24	0.95	0.77	0.51

Table 4.2. Analysis Uncertainty Parameters.

Study Frames	C_B	β_{DU}	γ_a
3V-NEHRP	1.0	0.15	1.03
3V-PBPD	1.0	0.15	1.03
6V-NEHRP	1.0	0.20	1.06
6V-PBPD	1.0	0.20	1.06

Table 4.3. Randomness and Uncertainty Parameters.

Frame	β_{RC}	ϕ_{RC}	β_{UC}	ϕ_{UC}	β_{RD}	β_{UT}
3V-NEHRP	0.537	0.649	0.15	0.967	0.890	0.30
3V-PBPD	0.394	0.793	0.15	0.967	0.545	0.30
6V-NEHRP	0.435	0.753	0.20	0.942	0.663	0.35
6V-PBPD	0.412	0.775	0.20	0.942	0.708	0.35

*β_{RC}: standard deviation of natural logs of drift capacities due to randomness
*β_{UC}: standard deviation of natural logs of drift capacities due to uncertainty
*β_{RD}: standard deviation of natural logs of drift demands due to randomness
*β_{UT}: vector sum of logarithmic standard deviations for both demand and capacity considering all sources of uncertainty

Table 4.4. Summary of Confidence Level Assessment for 3-Story and 6-Story CBFs.

Frame	Median Drift Capacity (from IDA) C	Capacity factor ϕ	Median Drift Demand D	Demand factors		Confidence Parameter $\lambda = \frac{\gamma \cdot \gamma_a \cdot D}{\phi \cdot C}$	Confidence Level (%)
				γ	γ_a		
3V-NEHRP	0.064	0.628	0.068	3.37	1.06	6.04	**<< 1%**
3V-PBPD	0.078	0.766	0.015	1.56	1.06	0.41	**> 99.9%**
6V-NEHRP	0.065	0.709	0.035	1.93	1.06	1.55	**23.3%**
6V-PBPD	0.100	0.730	0.027	2.12	1.06	0.82	**86.2%**

*ϕ: resistance factor that accounts for the randomness and uncertainty in estimation of structural capacity
*γ: demand uncertainty factor;
*γ_a: analysis uncertainty factor

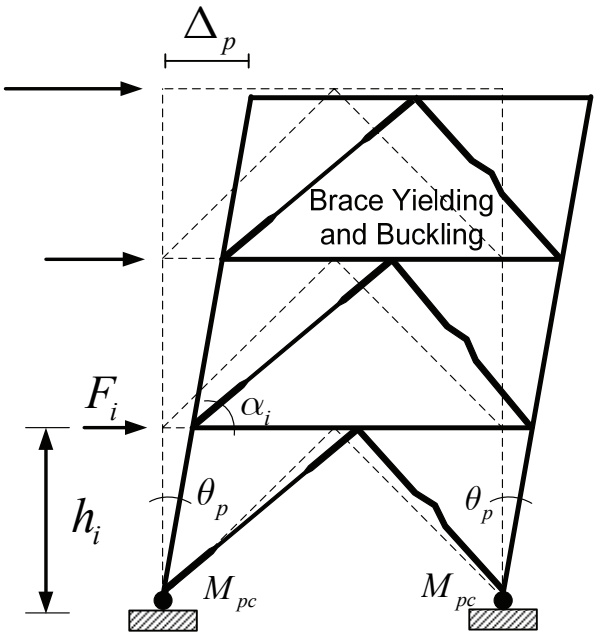

Figure 4.1. Target Yield Mechanism of CBF with Chevron Bracing.

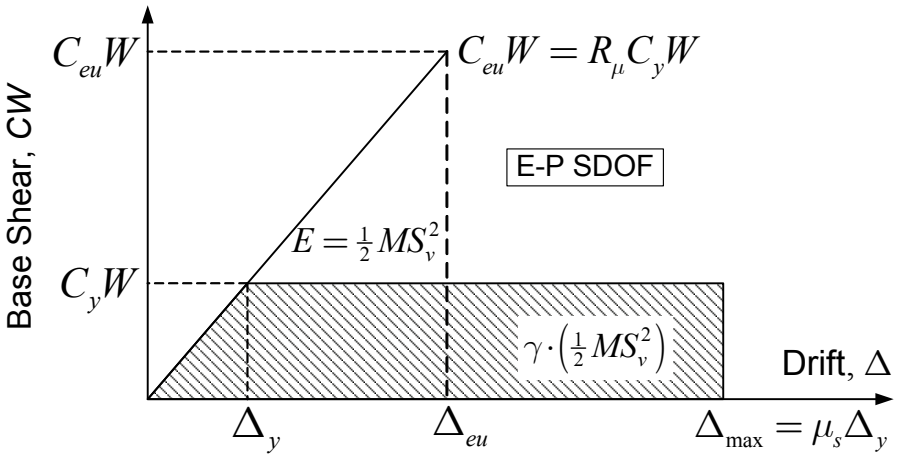

Figure 4.2. Energy Balance Concept.

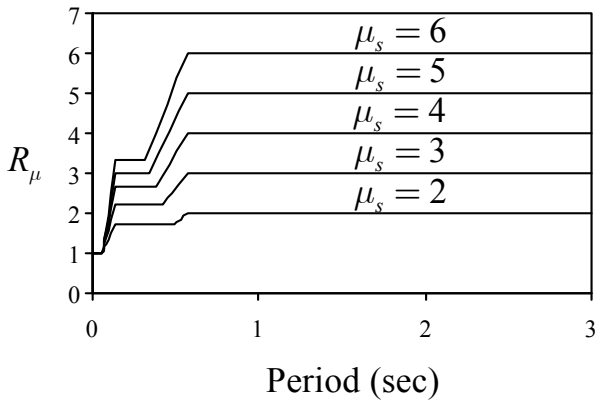

Figure 4.3. Inelastic Response Spectra by Newmark and Hall (1982).

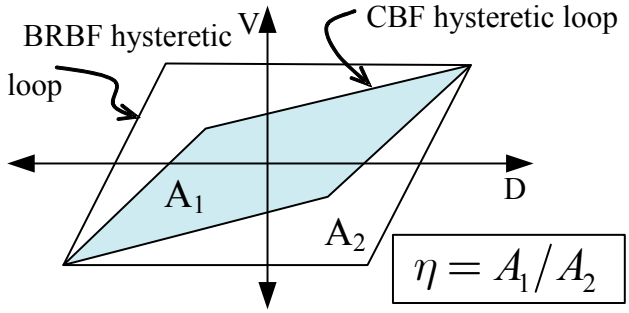

Figure 4.4. Energy Reduction Ratio, η.

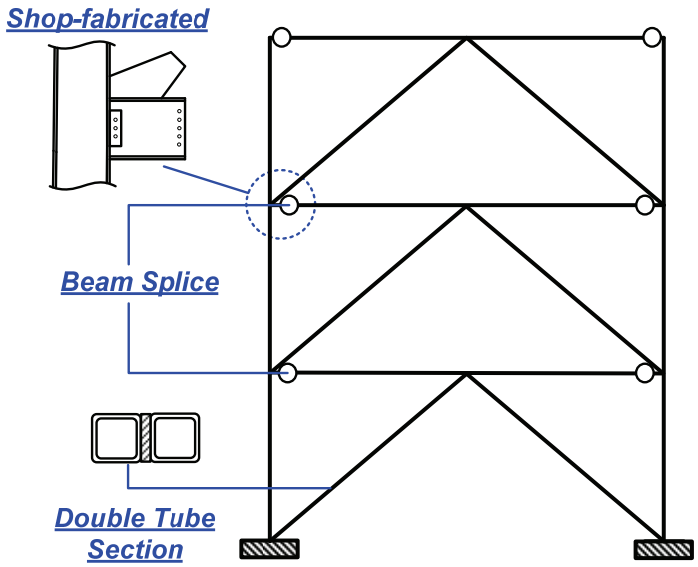

Figure 4.5. Recommended Connection Details for CBF.

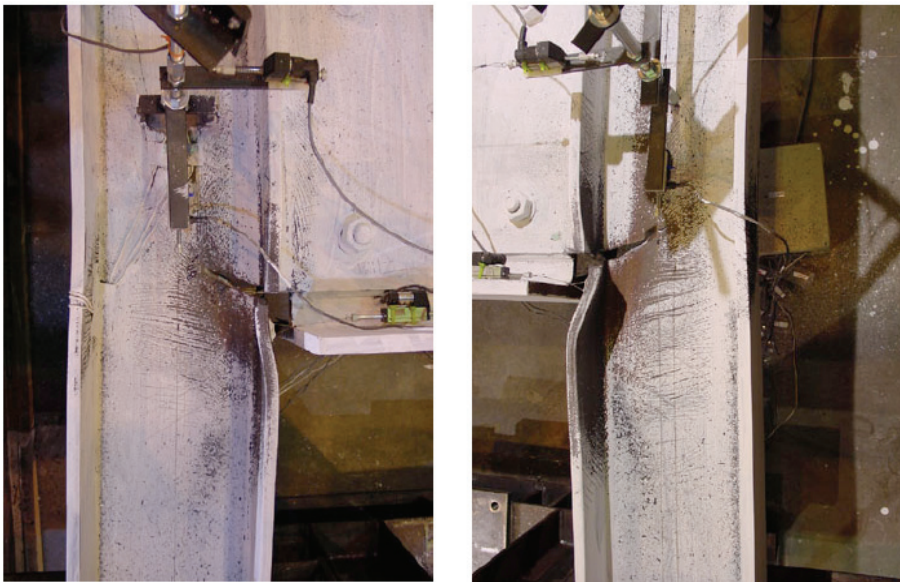

Figure 4.6. Fracture of Beam-to-Column Connection in a Two-Story CBF Specimen (Uriz, 2005).

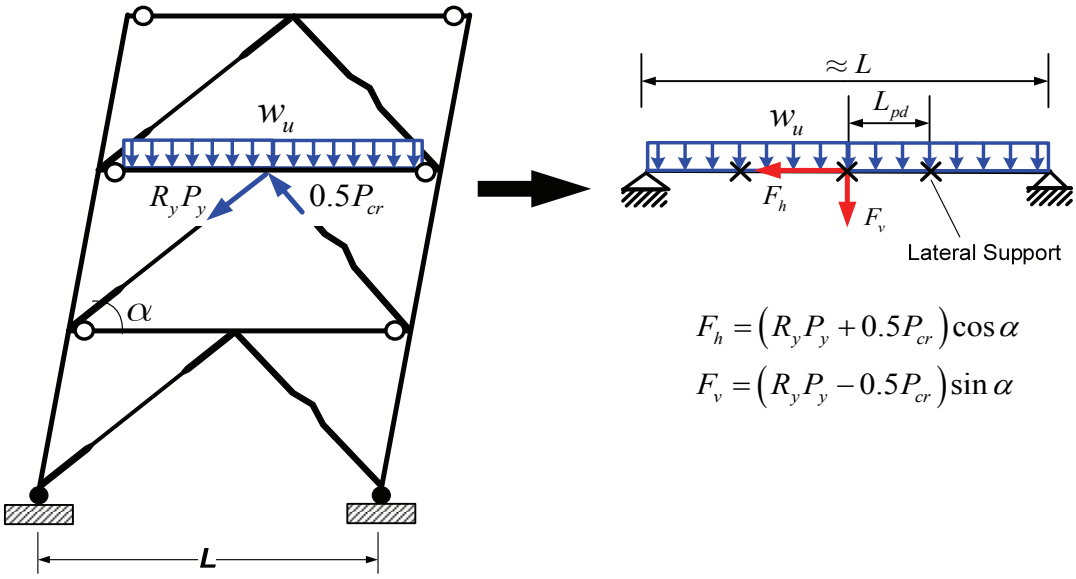

Figure 4.7. Beam Design Forces for a Chevron-Type CBF.

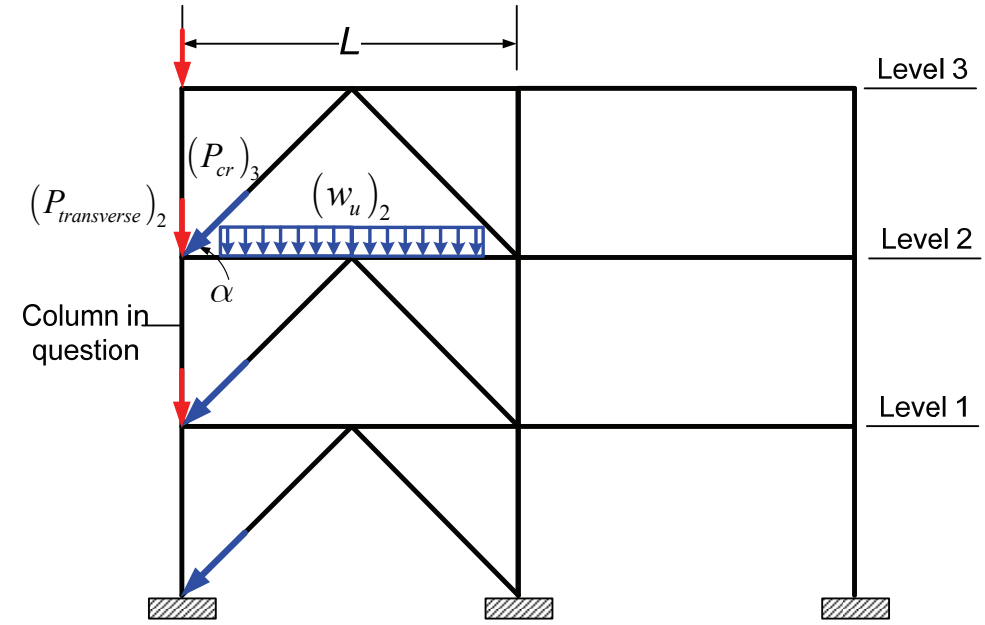

(a)

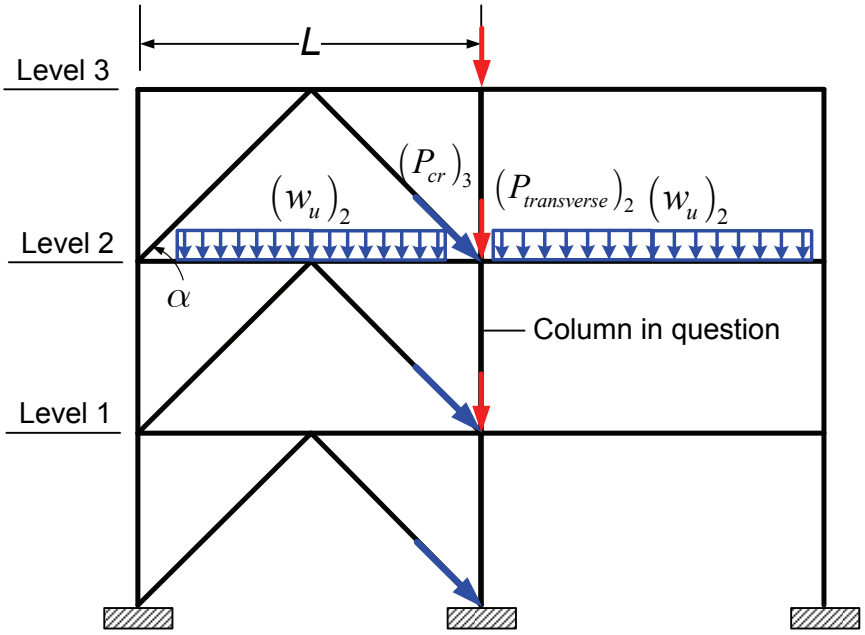

(b)

Figure 4.8. Axial Force Components for Brace Pre-Buckling Limit State: (a) Exterior Column; (b) Interior Column.

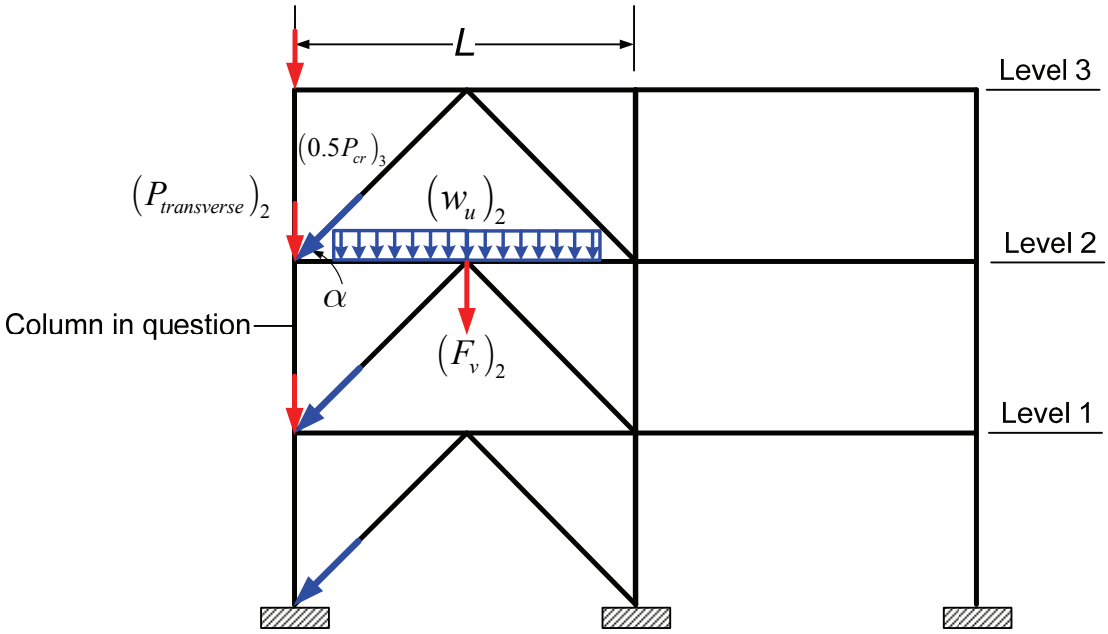

(a)

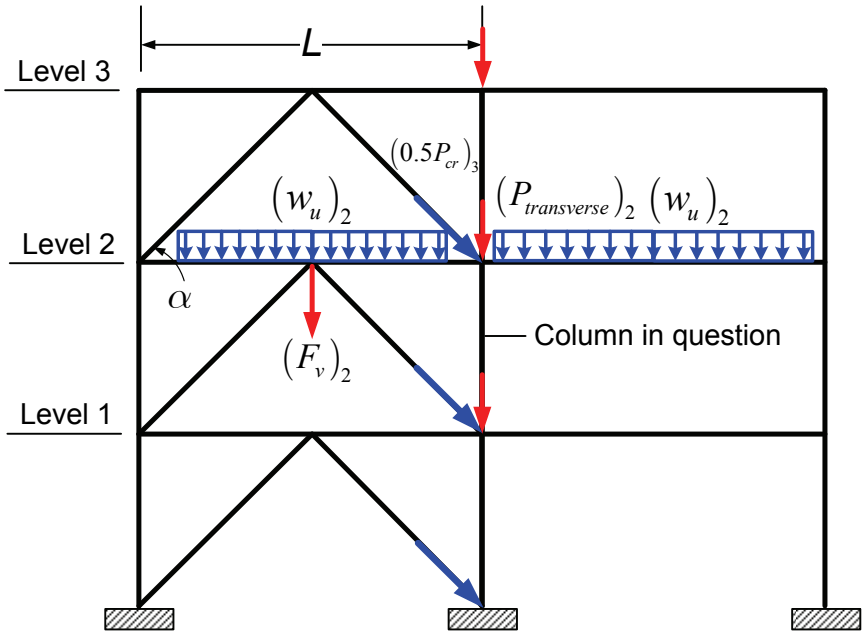

(b)

Figure 4.9. Axial Force Components for Brace Post-Buckling Limit State: (a) Exterior Column; (b) Interior Column.

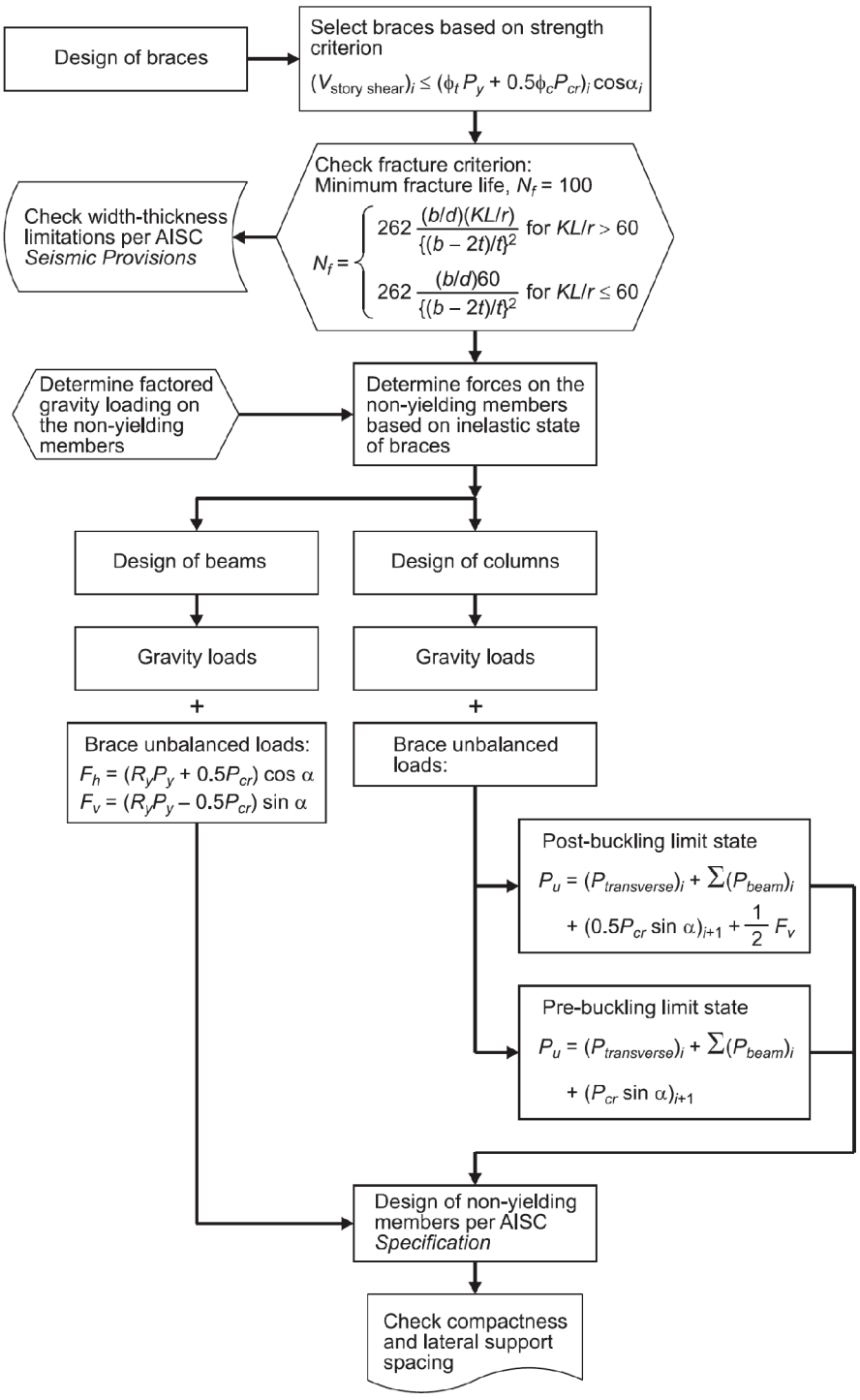

Figure 4.10. Performance-Based Plastic Design Flowchart for CBF: Element Design (Goel and Chao, 2008).

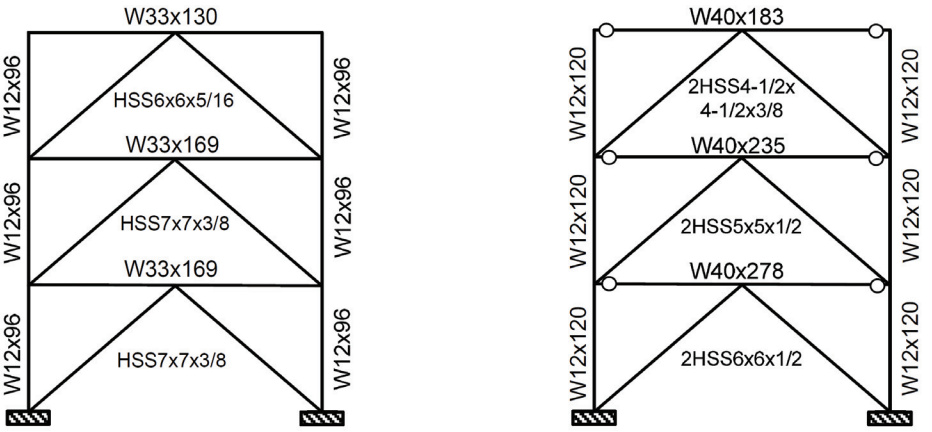

(a) (b)

Figure 4.11. Member Sections for the 3-story CBF Designed by (a) 3V-NEHRP; and (b) 3V-PBPD.

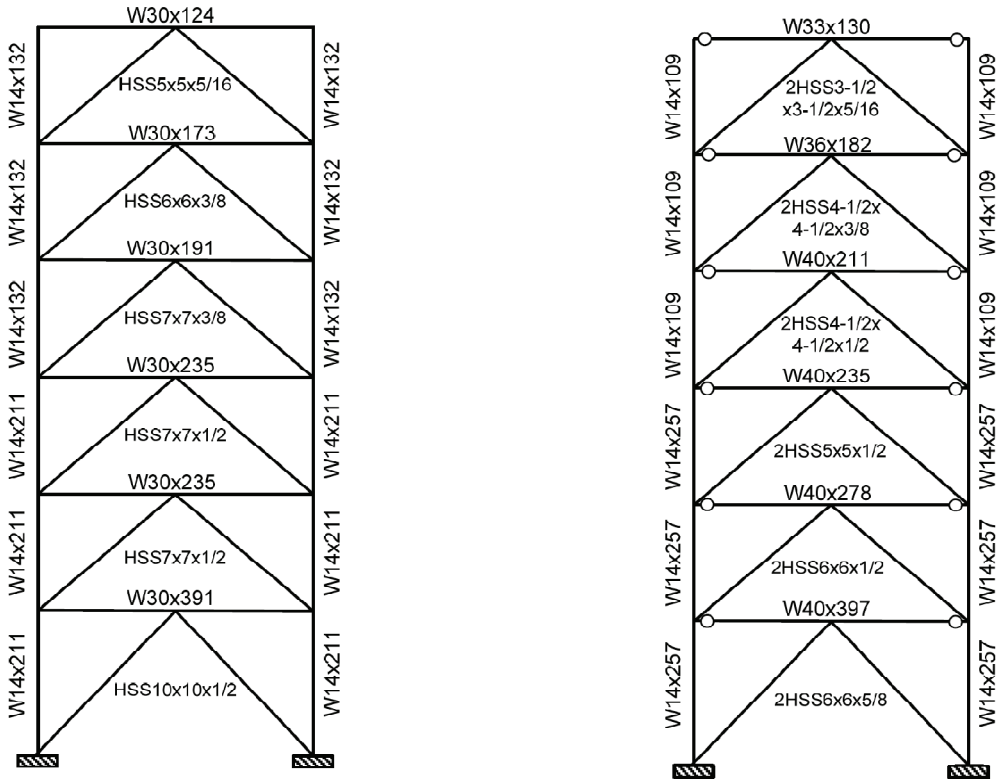

(a) (b)

Figure 4.12. Member Sections for the 6-Story CBF Designed by (a) 6V-NEHRP; and (b) 6V-PBPD.

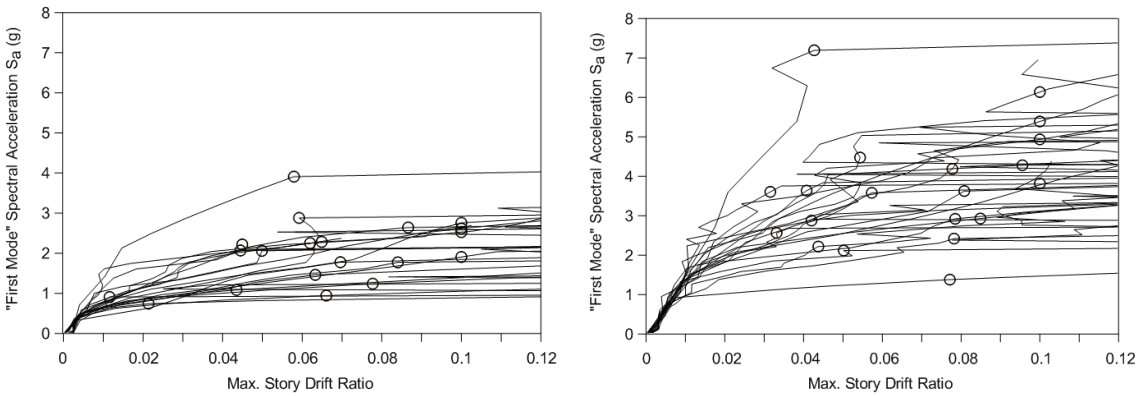

(a) (b)

Figure 4.13. IDA Curves for (a) 3V-NEHRP and (b) 3V-PBPD Frames under 2%/50yrs SAC Ground Motions.

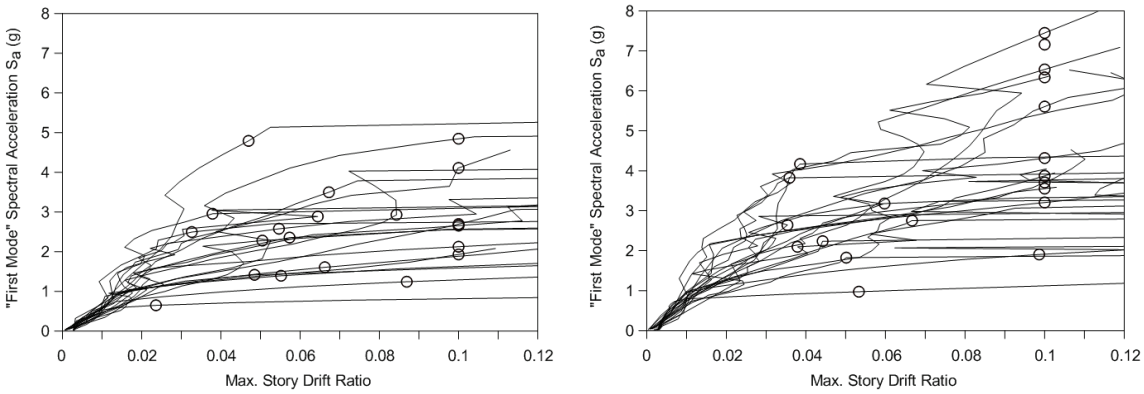

(a) (b)

Figure 4.14. IDA Curves for (a) 6V-NEHRP and (b) 6V-PBPD Frames under 2%/50yrs SAC Ground Motions.

CHAPTER 5

FURTHER DEVELOPMENT OF PBPD METHOD FOR CONCENTRICALLY BRACED FRAMES

5.1 General

The current PBPD procedure for design of CBFs was described in Chapter 4. The 3- and 6-story CBFs, originally designed by Sabelli (2001) based on NEHRP guidelines (1997), were re-designed by using the PBPD procedure explained in Chapter 4 (Goel and Chao, 2008). It was shown that the PBPD designed CBFs have much better performance under design level (2/3MCE) as well as MEC level ground motions compared to the NEHRP frames.

As part of the current PBPD procedure for CBFs, the beam-to-column connection detail was modified by using shear splice in the beam such that the large moments produced in the beams would not be transferred into the columns. However, since the shear splice has to be placed with an offset from the column face at least equal to the length of gusset plate over the beam flange, there are concerns that this eccentricity of the shear splice combined with the large shear force caused by the vertical component of the unbalanced force in chevron CBFs may produce large bending moments at the centerline of the column. A new configuration for the gusset plate connection is proposed in Section 5.2. The gusset plate in this configuration is only connected to the column such that the total unbalanced moment on the column would be reduced.

In Section 5.3, the current capacity design method for columns in CBFs based on the accumulative axial forces is evaluated by comparing the column moments from pushover and dynamic analyses. A more accurate design method for columns using pushover analysis is proposed.

An alternative method to account for pinched hysteretic behavior of CBFs in the PBPD approach is introduced in Section 5.4. This method is also applicable to other types of systems with degrading hysteretic behavior (Bayat, Chao, and Goel, 2010)

It is realized that the yield drift in slenderer braced frames such as CBFs, does not have a constant value due to the significant amount of flexural deformation caused by axial deformation of columns. Because of importance of having a good estimation of yield drift in PBPD method, a procedure is presented in Section 5.5 to analytically estimate the yield drift for slender braced frames.

Unlike MFs, a significant amount of the story drift in slender braced frames comes from the axial deformation of the columns. This is basically an elastic type of deformation which is not imposing additional deformation demand on bracing members as the main seismic components in braced frames. To address this issue, an approach is introduced in Section 5.6 in order to obtain the proper target drift for CBFs. In this method, an effective target drift is calculated based on the original definition of the target drift used in the work-energy equation in PBPD.

In Section 5.7, the suggested PBPD approach is utilized to design the 9-story SAC building by using CBFs as the lateral load resisting system. The performance of this design is then evaluated by using 10%/50yrs and 2%/50yrs SAC LA ground motions

(Somerville et al., 1997). Based on the observed maximum story drift profile along the height, the possibility of considering a different lateral load distribution in the PBPD procedure for CBFs is investigated. Using the new lateral load distribution, the provided strength and stiffness would be greater in upper stories which can be helpful in reducing the large story drifts observed under dynamic analyses. Extensive dynamic analyses were carried out to study the effect of varying lateral distribution on the performance of CBFs.

5.2 Proposed Gusset Plate Configuration

As part of the current PBPD procedure for CBF, the beam-to-column connection detail is modified by using shear splice in the beam such that the large moments produced in the beams would not transfer in to the columns (Chao and Goel, 2006b). However, since the shear splice has to be placed with an offset from the column face at least equal to the length of gusset plate over the beam flange, there are concerns that this eccentricity of the shear splice combined with the large shear force caused by the vertical component of the unbalanced force in chevron CBF may produce large bending moments at the centerline of the column. A new configuration for the gusset plate connection is presented in this section. The gusset plate in this configuration is only connected to the column such that the total unbalanced moment on the column can be reduced.

Figure 5.1.a shows the current detail for gusset plate connection, called connection Type I. The proposed configuration, called connection Type II, is shown in Figure 5.1.b. As can be seen in this figure, the gusset plate is only connected to the column. The top flange of the beam is coped in order to reduce the eccentricity between

the line of action of brace force and the intersection of beam and column. Although there is some eccentricity in the proposed connection (Type II), the total unbalanced moment transferred to the column is smaller in this configuration. This is due to the fact that the shear splice in this configuration is much closer to the column centerline. More importantly, the moments produced by the axial force in the brace and the one produced by the shear force at the shear splice act oppositely to each other. This would theoretically reduce the unbalanced moment on the column in a static type of analysis. Under dynamic analysis, other structural properties as well as ground motion properties would also affect the moments in columns. Since the columns are designed solely based on their accumulative axial force in the PBPD procedure, having lesser moment demand on columns would ensure their better performance and safety.

The analysis results for this proposed configuration are shown in the following section along with the results without considering and eccentricity to investigate the importance of the unbalanced transferred moments on the performance of the columns.

5.3 Capacity Design of Columns in CBFs

Previously, the CBF frames were modeled in SNAP-2DX program with pin-ended beams due to presence of shear splices. Since the shear splices are being placed beyond the gusset plate connection region, there is an eccentricity between the shear splice and the centerline of the column. Because of large vertical component of the

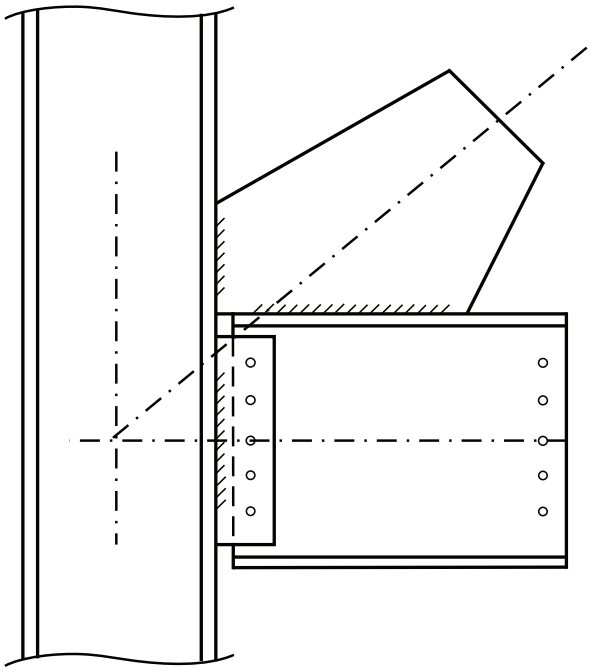

(a)

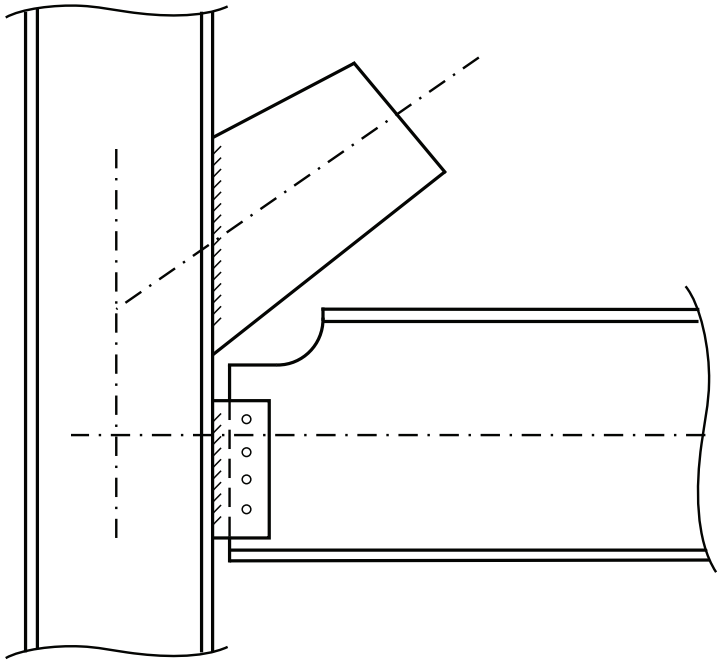

(b)

Figure 5.1. Gusset Plate Connection Configurations: (a) Type I; (b) Type II (proposed).

unbalanced force at the shear splice, the transferred moment to the column can be significant.

The purpose of this part of the study is to investigate how large such transferred moments can be, and whether or not they affect the overall design procedure for columns. Also, the possible effect of these moments on the performance of the structure will be studied. In addition, the behavior and performance of two alternative gusset plate connections to the beam-column joint are compared.

Table 5.1 shows the properties of the CBF models used in this section. The brace, beam, and column sections in all these models are similar to the PBPD designs (3V-PBPD and 6V-PBPD) described in Chapter 4. The models were analyzed by using the SNAP-2DX program.

Table 5.1. Description of the Studied CBF Models.

CBF Model	Design Method	Modeling of G.P./ Beam-Column Connection
3V-PBPD	PBPD	Type I connection, without Ecc. for shear splices
3V-PBPD01	PBPD	Type I conn., with Ecc. for shear splices (Ecc.=20 inches)
3V-PBPD02	PBPD	Type II connection , with G.P. connected to the column
6V-PBPD	PBPD	Type I connection, without Ecc. for shear splices
6V-PBPD01	PBPD	Type I conn., with Ecc. for shear splices (Ecc.=20 inches)
6V-PBPD02	PBPD	Type II connection, with G.P. connected to the column

As can be seen in Figure 5.2, modeling the eccentricity of the shear splice is resulting in larger column moments for both the design level earthquake LA01, as well as MCE level earthquake of LA27. As can be seen, considerable moments are transferred from beams to column due to the end eccentricities. Therefore, these eccentricities should be properly modeled in order to obtain more realistic moment demands in columns.

In terms of the overall performance, no significant change was observed by adding the eccentricities in the models (for both 3-story and 6-story models). Still no plastic hinge formed in the columns except at the base. For the models with eccentricity, plastic hinge rotation at the column base shows an increase of about 10-15% which is not significant.

Comparing the column moments for connections Type I and Type II, it is observed that for most of the stories these moments are somewhat larger in the Type II case (Figure 5.3 and Figure 5.5). On the other hand, the axial forces at the time of maximum moments are generally lower for Type II, and hence the available moment capacity is larger (Figure 5.4 and Figure 5.6).

It can also be seen from Figure 5.5.b Figure 5.6.b that for the 6-story CBF under 2/50 ground motion of LA38, the behavior of the Type I and Type II frames are practically the same (in terms of column axial forces and moments).

In summary, practically similar performances were seen for connections Type I and the proposed connection Type II under time-history analysis. However, connection Type II does not need an extra shear splice connection (like the one in Type I to reduce the transferred moment) and as a result can be considered to be a more cost-effective alternative. A more accurate design method for columns would be the one where moments obtained from pushover analysis of the frame are taken into account along with the axial forces in the design of columns. This method is investigated in the next sub section.

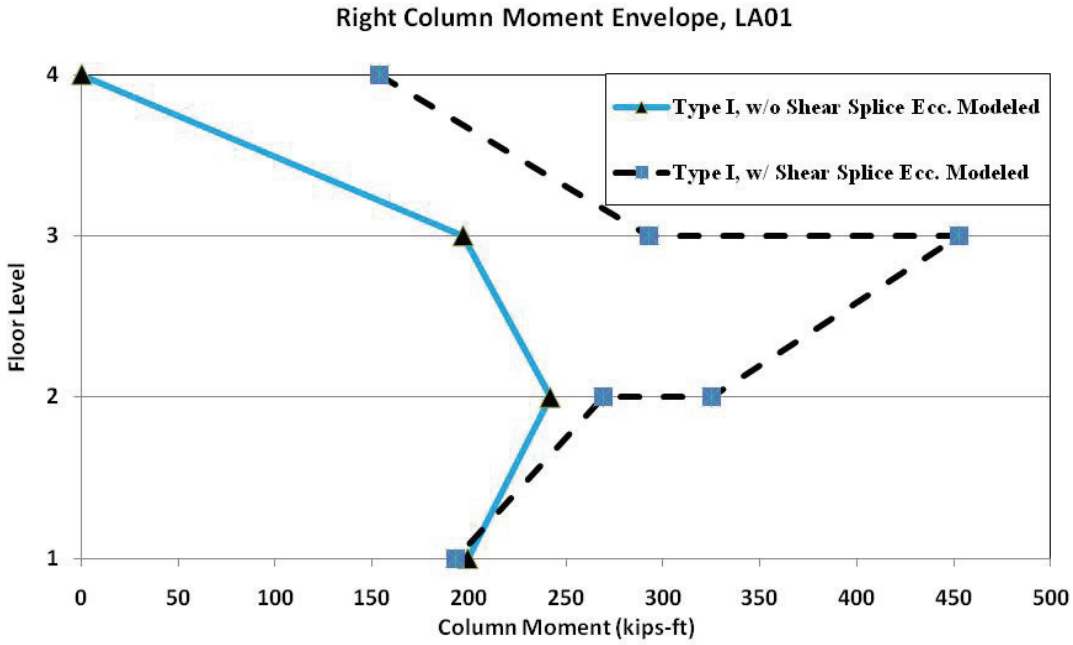

(a)

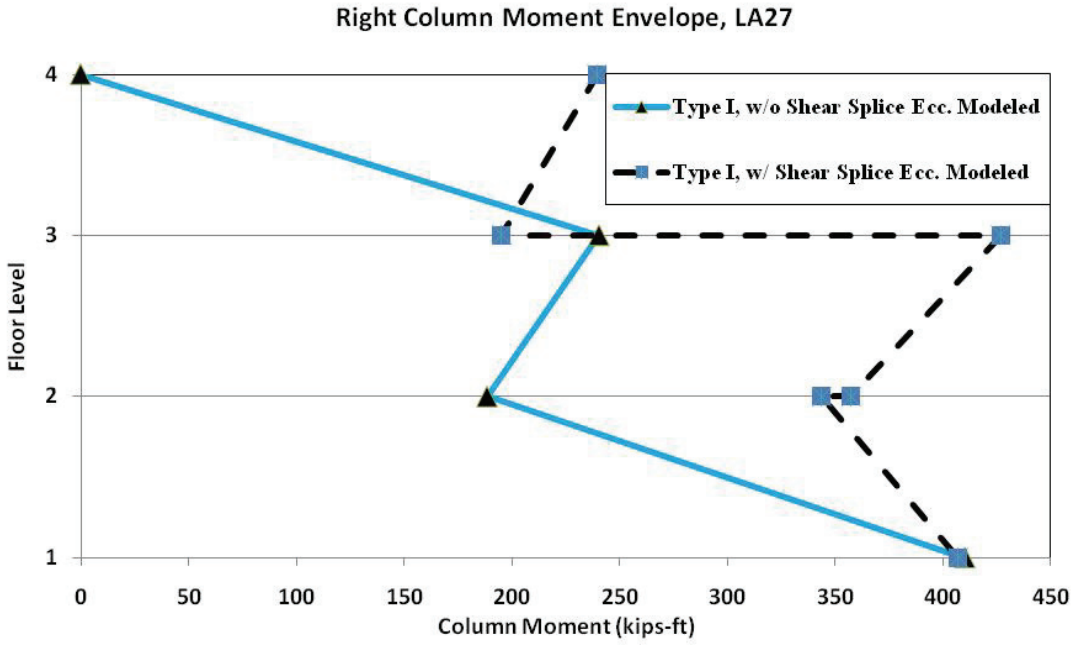

(b)

Figure 5.2. The Effect of Modeling Shear Splice Eccentricity on Column Bending Moments under: (a) LA01; and (b) LA27.

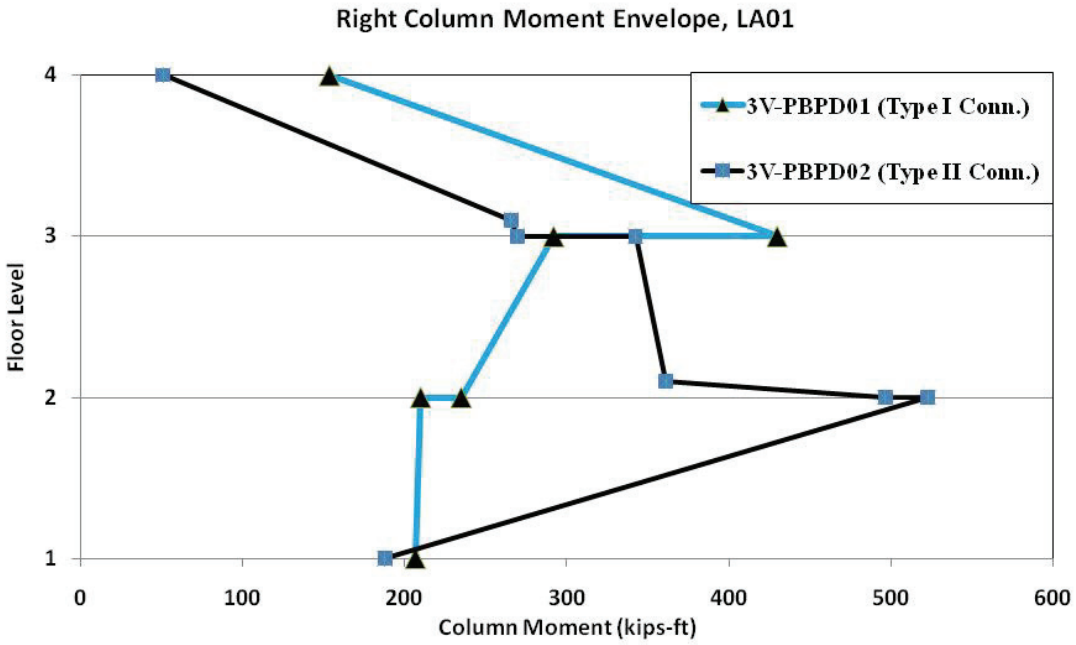

(a)

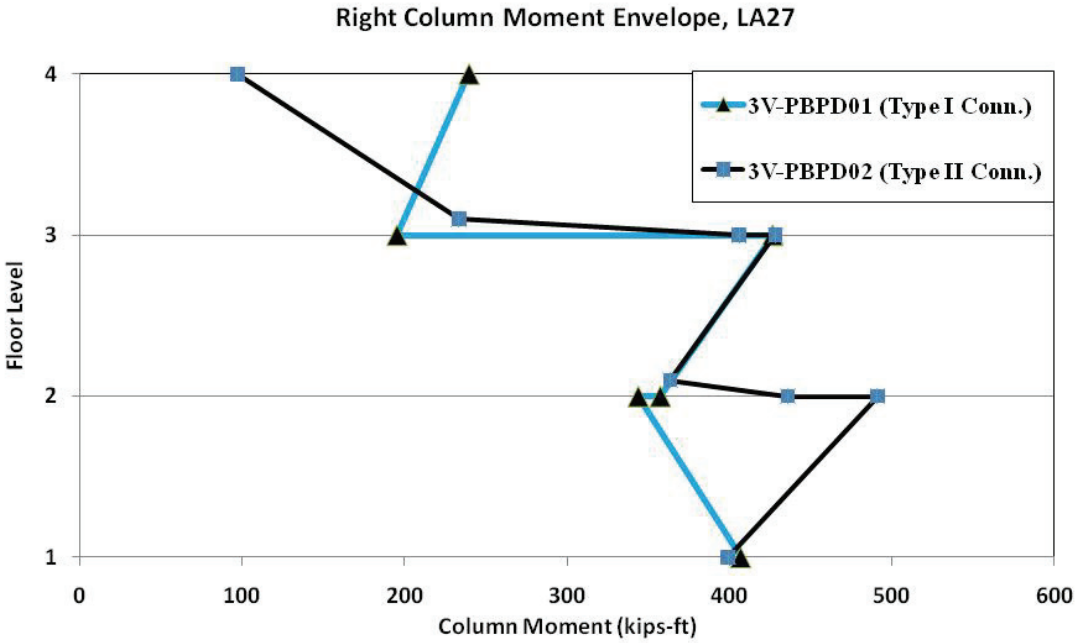

(b)

Figure 5.3. Right Column, Moment Envelops for Models 3V-PBPD01 (Type I) and 3V-PBPD02 (Type II) under: (a) LA01; and (b) LA27.

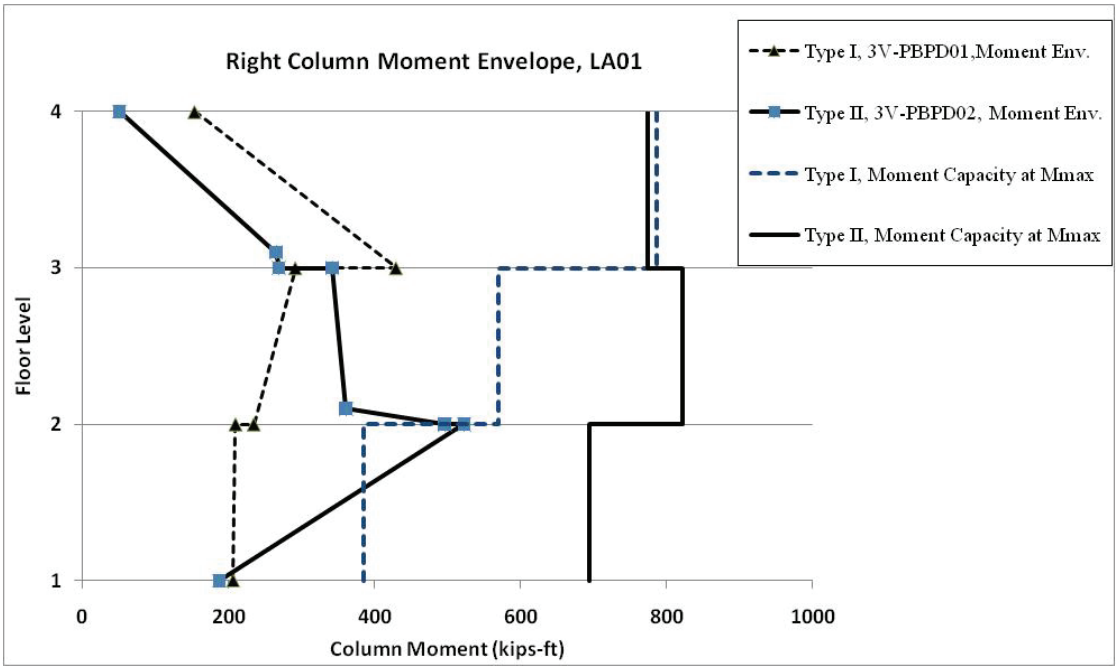

(a)

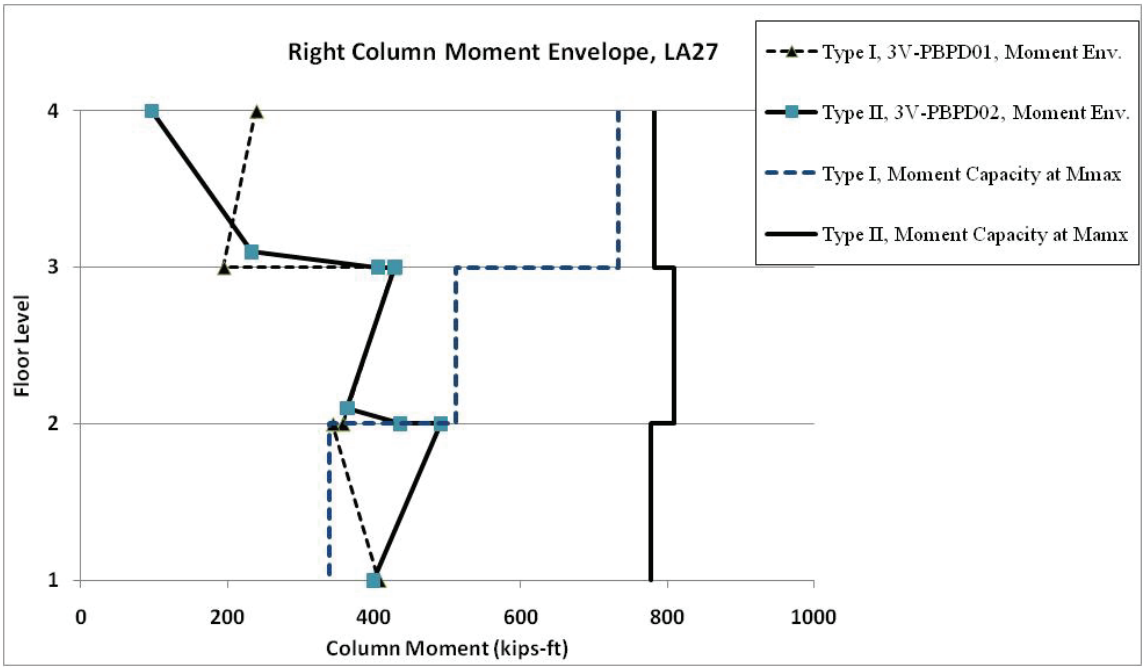

(b)

Figure 5.4. Column Moments for connection Type I and Type II in 3-Story CBF and Available Moment Capacities under: (a) LA01; and (b) LA27.

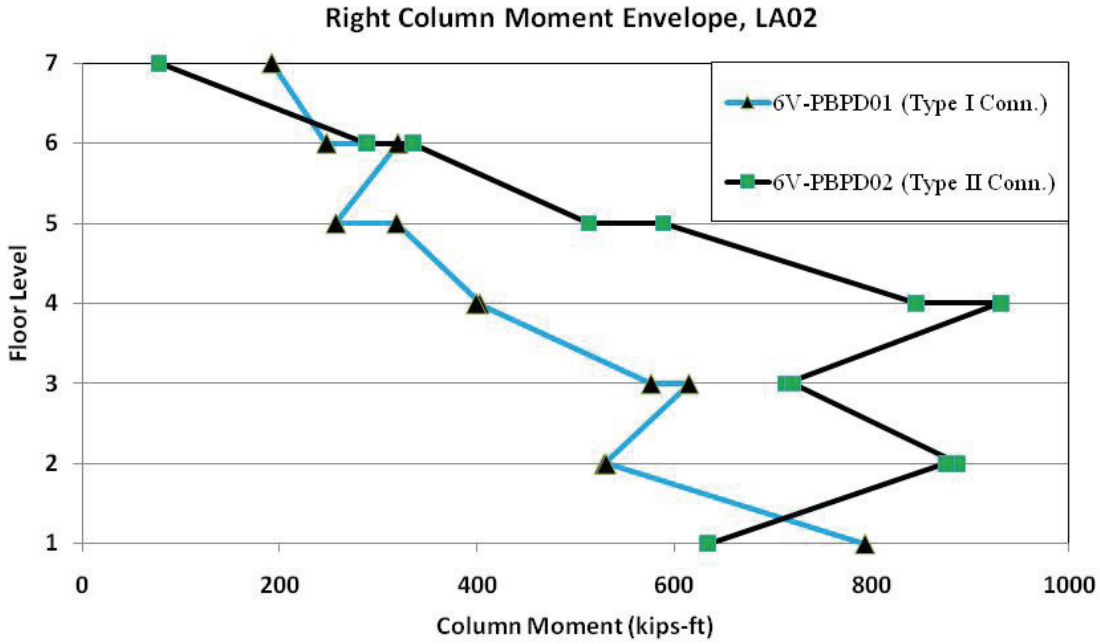

(a)

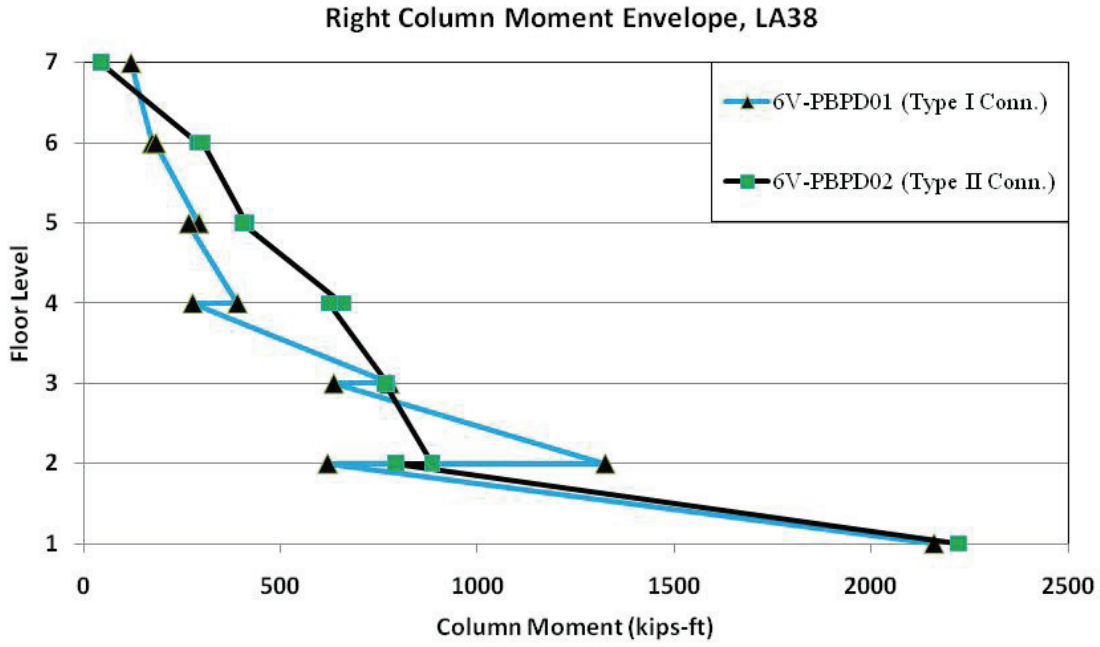

(b)

Figure 5.5. Right Column, Moment Envelops for Models 6V-PBPD01 (Type I) and 6V-PBPD02 (Type II) under: (a) LA02; and (b) LA38.

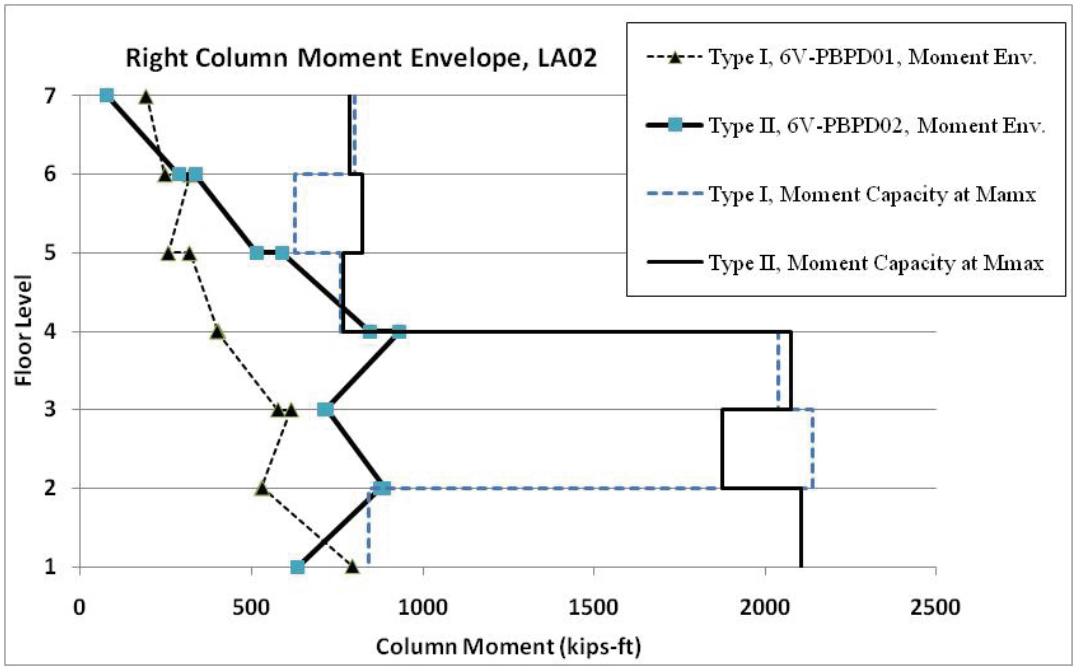

(a)

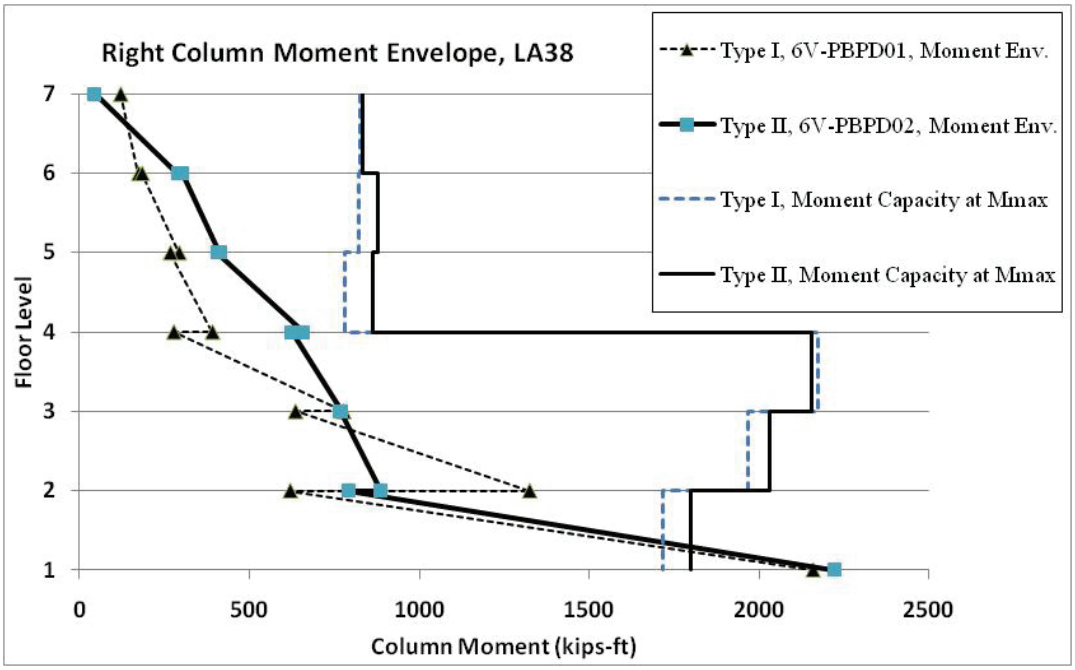

(b)

Figure 5.6. Column Moments for connection Type I and Type II in 6-Story CBF and Available Moment Capacities under: (a) LA02; and (b) LA38.

5.3.1 Re-Design of Columns in CBFs Based on Combined Axial Forces and Moments Obtained from Pushover Analysis (3-story and 6-story)

The design of columns in CBFs based on only cumulative axial forces has proven to be satisfactory under both 10/50 and 2/50 ground motions. The goal here is to introduce a more accurate design method for columns which takes the moments as well as axial forces into account. The results of pushover analysis for the case of Type II Connection are used for this purpose. For pushover analysis, the column is considered to be elastic except for a PMM plastic hinge modeled at the base of columns. The frames are then pushed to the DBE target drift of 1.25%. A typical target drift value of 1.75% was also selected for comparison purposes to MCE level results. The moments and axial forces obtained from these analyses are then used to redesign the columns of the 3V-PBPD and 6V-PBPD frames.

Table 5.2 to Table 5.4 show the column sections obtained by using the two design methods: 1) Considering cumulative axial forces from column tree; 2) considering combined axial and moments from pushover analysis. It can be seen from the Table 5.2, that by using pushover results for column design in 3-story CBF (i.e., combined axial force and moment) a section with the same weight but larger depth (W14x120) would be required. The additional moment capacity of W14x120 versus W12x120 can be quite beneficial in case larger than expected bending moments occur in the columns. It is seen from Table 5.3 and Table 5.4 that the effect of bending moments in column design becomes more important by the increase in the number of stories. For the 6-story frame, a W14x283 is required for the three lower stories if moments are considered in the design whereas W14x257 section was adequate considering only the cumulative axial forces.

Also, as shown in Figure 5.7 and Figure 5.8, the column moments at DBE target drift (1.25%) obtained from pushover analysis can be used with reasonable accuracy to account for column moments during the design. It should be noted that although the column moments obtained from pushover analysis are smaller than the ones under ground motions, they occur simultaneously with large axial forces under pushover analysis. As shown in the previous section, the maximum axial force and maximum moments are not occurring at the same time under time-history analysis.

Based on observation from this preliminary study, one may conclude that even by considering only axial forces in capacity design of columns, good performance can still be expected for the PBPD frame. Two main reasons that even with using only axial forces in design of columns, still a good performance can be achieved are:1) P_{max} and M_{max} in columns are not occurring at the same time; and 2) the axial force used in column design is based on the fact that all braces buckle and yield at the same time, which applies the largest possible axial demand on columns. But this does not generally occur during dynamic response; therefore the axial force demand is lower than the value used for design.

A practical conclusion is that since it is known that there would be some bending moments in columns due to unbalanced moments transferred to the column and also from the continuity of the column itself under dynamic analysis, it would be better to use a W-sections with larger depth (with almost the same weight) whenever possible, so that additional bending capacity can be provided.

In addition, based on the preliminary study in this section, designing columns in CBF by using the demands obtained from pushover analysis was seen to be a more accurate method. The accuracy of pushover method however decreases with the increase in the number of stories. A more comprehensive study on the subject can be done by comparing the demand ratios obtained from pushover to those from time-history analysis results.

Table 5.2. Column Design for 3-Story CBF.

Design Method	Pu (kips)	Mu (k-ft)	Design Section	Design Ratio
Cum. Axial Forces	1124	0	W12X120	0.848
Combined Axial and Moments	906	385	W14X120	1.05

Table 5.3. Column Design for 6-Story CBF (Lower Three Stories).

Design Method	Pu (kips)	Mu (k-ft)	Design Section	Design Ratio
Cum. Axial Forces	2464	0	W14X257	0.885
Combined Axial and Moments	1970	900	W14X283	1.01

Table 5.4. Column Design for 6-Story CBF (Top Three Stories).

Design Method	Pu (kips)	Mu (k-ft)	Design Section	Design Ratio
Cum. Axial Forces	811	0	W14X109	0.640
Combined Axial and Moments	640	196	W14X109	0.958

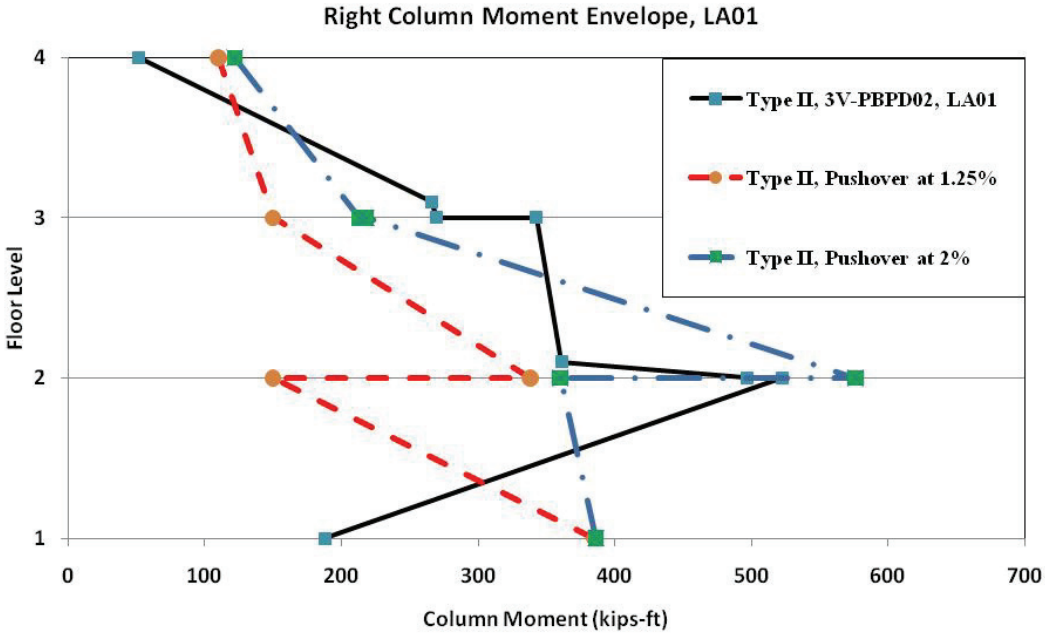

(a)

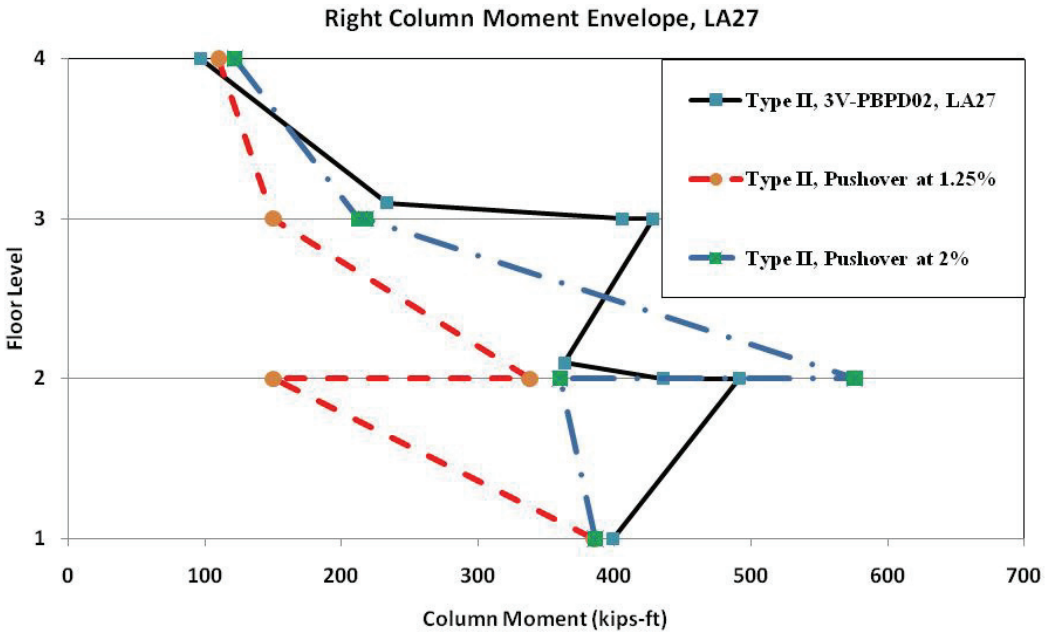

(b)

Figure 5.7. Column Moments for 3V-PBPD02: (a) Under LA01; and (b) Under LA27 Ground Motions.

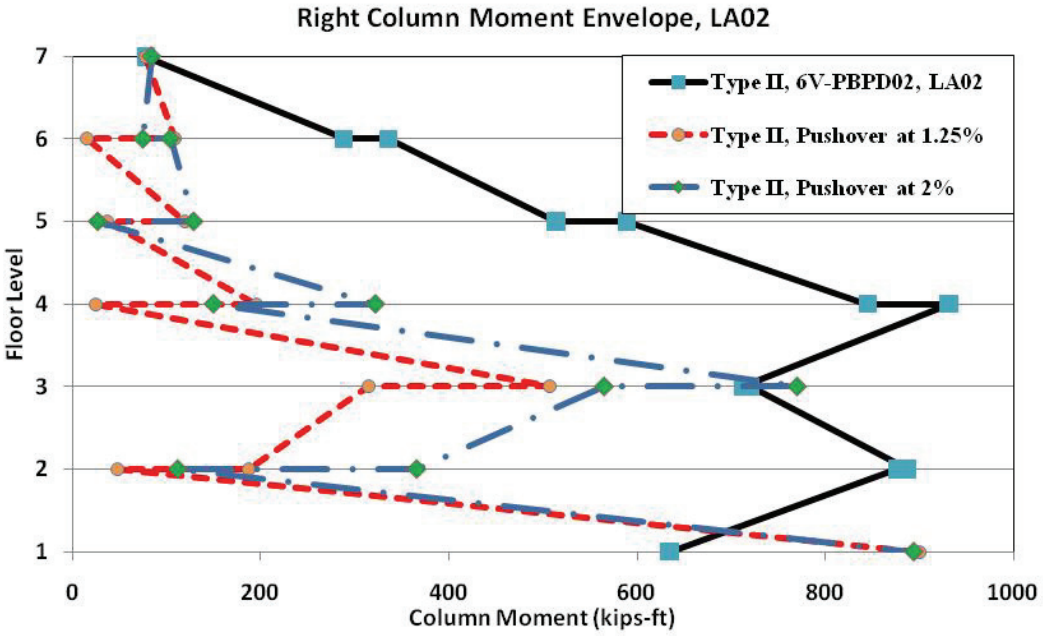

(a)

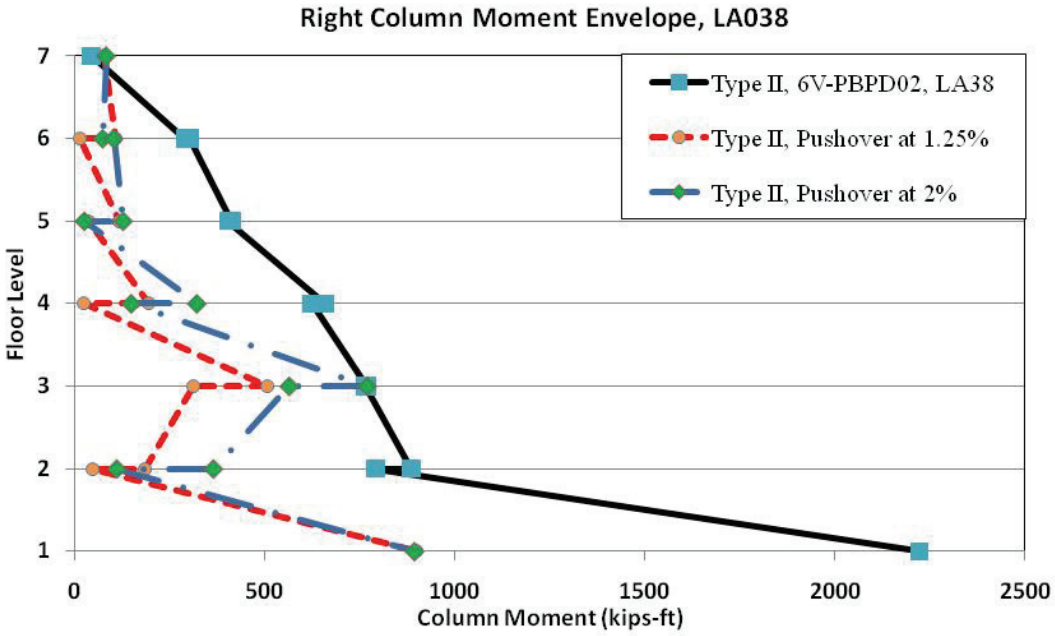

(b)

Figure 5.8. Column Moments for 6V-PBPD02: (a) Under LA02; and (b) Under LA38 Ground Motions.

5.4 λ -Factor Method to Account for Pinched Hysteretic Behavior

It is expected that the response of a degrading Single Degree Of Freedom (SDOF) will be different from that of an equivalent Elastic-Plastic (EP) system under the same earthquake ground motion. The degrading behavior, although normally caused by the behavior of components, can be expected in the system behavior as well. The degrading behavior can be Strength Degradation (STRD), Stiffness Degradation (SD), or pinched hysteretic behavior.

CBFs show somewhat pinched hysteretic behavior under cyclic as well as dynamic loadings due to buckling of the bracing members. Since the original PBPD approach was developed for MFs, and the strength and stiffness of the braces in CBFs decrease under cyclic compression, using the same design base shear as MFs would not be appropriate. In the current PBPD approach for CBFs, an energy modification factor, η, is used to account for pinched hysteretic behavior (Chao and Goel, 2006b and Goel and Chao, 2008). This approach is based on a preliminary study on one-story one-bay braced frame with pin-connected rigid beams and columns that showed the dissipated energy by CBF is approximately 35% of the energy dissipated by a corresponding frame with full EP hysteretic loops, with both frames having equal strength (Figure 3.7). A slightly higher η = 0.5 was suggested for design purposes. In this approach, the work-energy Equation (3-9) for a CBF can be modified as (Chao and Goel, 2006b):

$$\eta(E_e + E_p) = \frac{1}{2}\gamma M(\frac{T}{2\pi}S_a g)^2 \tag{5.1}$$

The solution of this equation leads to:

$$\frac{V}{W} = \frac{-\alpha + \sqrt{\alpha^2 + 4(\gamma/\eta)S_a^2}}{2} \tag{5.2}$$

By using the above energy modification factor, the design base shear for the system with pinched hysteretic behavior is increased with respect to the one for EPP system to compensate for the pinching effect.

In this approach, the energy modification factor η remains independent of the fundamental period. Figure 5.9 shows the ratio of the PBPD design base shear for the pinched system to that of the benchmark EPP system for different values of η. As shown in this figure, using the same η values, increase in the EPP design base shear is almost the same for short and long periods. It can also be seen that by using $\eta = 0.5$, the design base shear for the pinched system would be almost twice that of the EPP system.

On the other hand, several studies (e.g. Rahnama and Krawinkler, 1993, Gupta and Krawinkler, 1998, Gupta and Kunnath, 1998, Foutch and Shi, 1998, Medina and Krawinkler, 2004; Ruiz-Garcia and Miranda, 2005) have shown that, although pinching alone or in combination with stiffness degradation increases the peak displacement demands for short period SDOFs (periods less than 0.7 sec) but not for longer periods, as long as post-yield stiffness remains positive. It can be seen in Figure 5.10, taken from Ruiz-Garcia and Miranda (2005), that the mean displacement ratio of SD to EPP system is larger than 1.0 for short periods and can be taken practically equal to 1.0 for longer periods. The results in this figure are obtained for site Class D. Also, the ratio increases with increase in the *R* value. Larger *R* value corresponds to a weaker system. Therefore,

the significance of the effect of pinching (SD and STRD) on the overall performance of structures varies with the period.

An alternative approach, called λ-factor method, to take this variation into account for design of SD and pinched systems by the PBPD approach is presented herein.

In this approach, the target ductility (corresponding to the target drift) is directly modified to account for the SD, pinching, or other degradation effects. An effective ductility for the degrading system can be obtained by dividing the actual target ductility by a factor called the λ-factor. The λ-factor in general can be considered as the average ratio of the peak displacement of a degrading SDOF to that of an equivalent EPP SDOF under the same earthquake ground motion. Therefore, $\lambda = (\mu_{pinched}/\mu_{EPP})$.

CBFs show somewhat moderate pinching behavior due to buckling of bracing members. λ-R-T curves (with constant R-values) can be obtained by applying suitable sets of ground motion to pinched SDOFs with different periods and the corresponding equivalent EPP system as benchmark.

The procedure to obtain λ-R-T curves is as follows:

- Select the period for pinched SDOF, T. For this period to be achieved, mass can be taken equal to 1.0 and the stiffness k can be changed to get the desired T.
- Find the pseudo spectral acceleration at the selected period T for each ground motion in the set.
- Find maximum elastic base shear as $V_e = M \times S_a = 1.0 \times S_a = S_a$.

- Select the desired constant R value (e.g. $R=4$).
- Since the actual R value from dynamic analysis is $R = V_e/V_y$, in order to get constant R values under all ground motions in the set, either the V_y or the ground motion intensity should be adjusted. If V_y is taken as constant, then a proper scale factor should be applied to each ground motion such that $V_e = M \times S_a = 1.0 \times S_a = S_a = R \times V_y$.
- Find $\lambda = (\Delta_{pinched}/\Delta_{EPP})$.
- With the same R value, select a new period and repeat the above steps to obtain λ values.
- When the λ-R-T curve for an R value is obtained, select a different R value and follow the above procedure.

Alternatively and pending further study to obtain λ-R-T curves for pinched systems representing CBFs, the C_2 factor introduced in FEMA 356 (FEMA, 2000a) for SD systems can be used as an approximation. The coefficient C_2 is the modification factor to represent the effect of pinching, SD, and STRD on the peak displacement response according to FEMA 356. In FEMA 356, values of C_2 depend on the structural framing system and the structural performance levels. Those values, taken from Table 3-3 in FEMA 356, are also drawn in FEMA 440 (FEMA, 2005) and are shown in Figure 5.11.

These approximations for C_2 are obtained for systems with rather severe pinching behavior and also systems with STRD. For CBFs which have moderate pinching

behavior along with some strain hardening slightly different C_2 values are suggested in this study, as shown in Figure 5.12 and Figure 5.13.

The PBPD procedure to obtain the design base shear for such systems is as follows:

- *Estimate the fundamental period, T.*
- *Estimate the yield drift* θ_y .
- *Select the target drift* θ_u .
- *Find* $\mu_0=\theta_u/\theta_y$, *then calculate* R_{EPP} *from R-*μ*-T equation for EPP-SDOF (e.g. Newmark-Hall).*
- *Get* λ *from R-*μ*-T.*
- *Find the effective target ductility* $\mu_D= \mu_0/\lambda$.
- *Find R form R-*μ*-T equations for EPP-SDOF.*

After this step, the following steps are the same as presented in Chapter 3.

- *Calculate* γ *using Equation (3.7), as usual in PBPD.*
- *Find* α, *then calculate V/W.*

With modifications for Y.D. and T.D. in CBFs, the above procedure will be used in the next section of this chapter to obtain PBPD design base shear for CBFs with different heights. These design base shears will be also compared to the values obtained by using IBC code (see Figure 5.18). It can be seen from this figure that the PBPD design base shear is generally greater than the code value, especially for shorter periods. For longer periods (more than 0.7sec), the PBPD design base shear although still greater than the code value, but the difference is small.

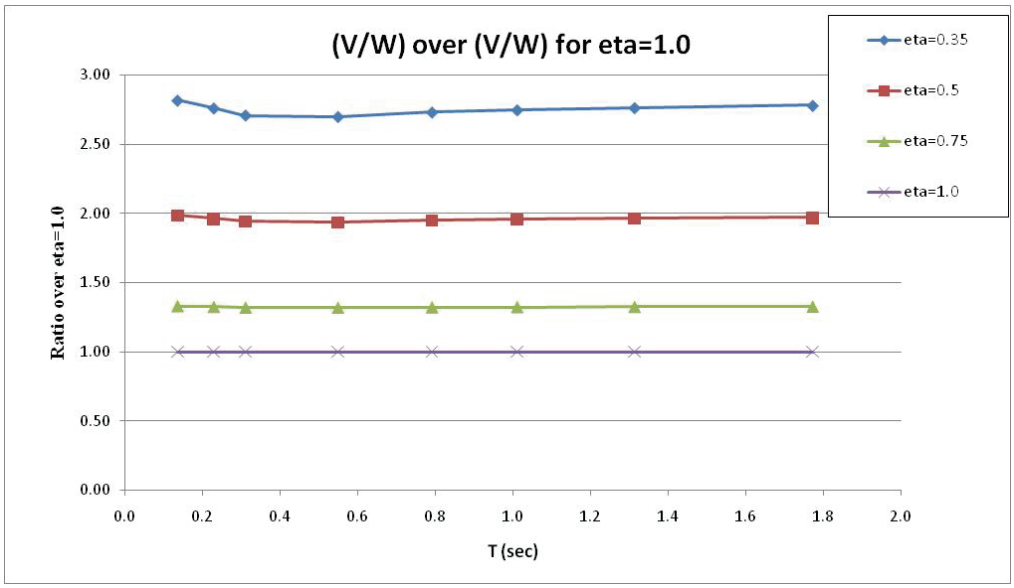

Figure 5.9. Ratio of the PBPD Calculated Design Base Shear for the Pinched System vs. The Benchmark EPP System.

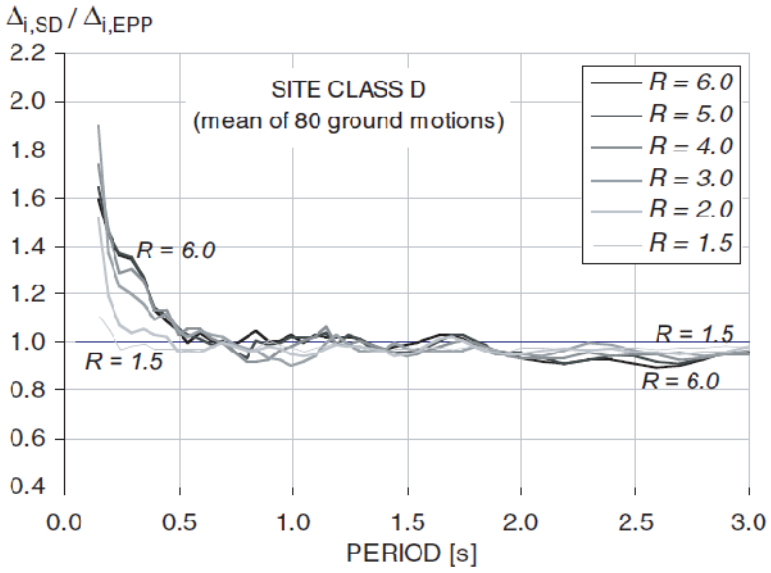

Figure 5.10. Mean Displacement Ratio of SD to EPP Models Computed with Ground Motions Recorded on Site Class D (from Ruiz-Garcia and Miranda, 2005).

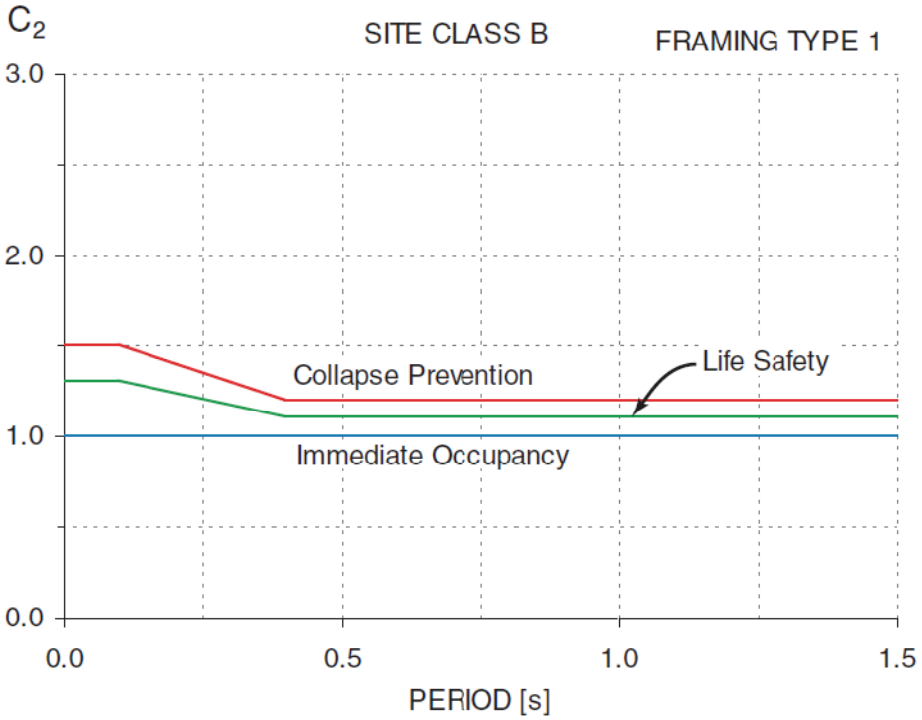

Figure 5.11. Variation of C_2 Factor According to FEMA440 (FEMA, 2005).

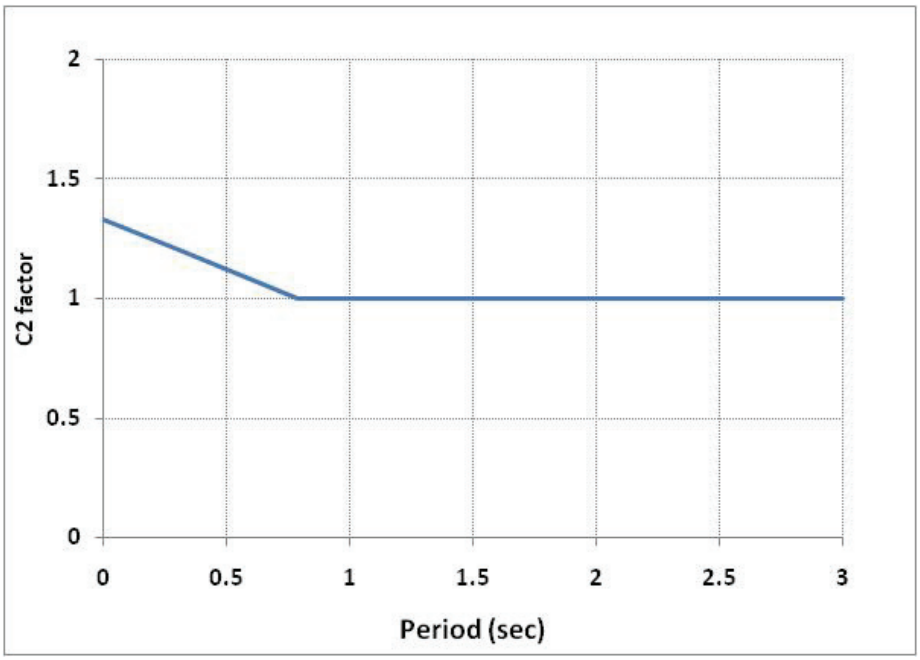

Figure 5.12. Preliminary Suggested C_2 Values (λ-Factor) for CBFs (used in Chapter 5).

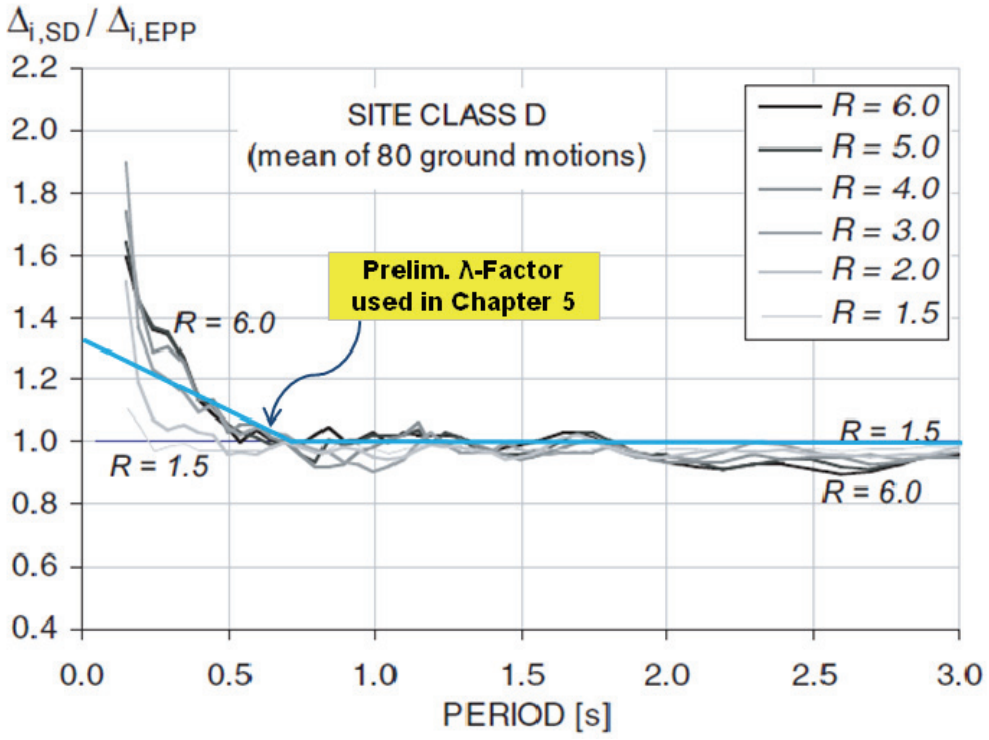

Figure 5.13. Suggested λ-Factor Values for CBF versus Mean Displacement Ratios Obtained by Ruiz-Garcia and Miranda (2005).

Table 5.5. Preliminary λ-Factor Values as Function of T (used only in Chapter 5)

$0 \le T \le 0.73$ sec	$T > 0.73$ sec
$\lambda = -0.48T + 1.35$	$\lambda = 1.00$

5.5 Yield Drift

Yield drift is one of the main parameters used in the PBPD method for calculation of the design base shear, as discussed in Chapter 3. The system target ductility demand will change with the yield drift. Therefore, having a good estimation of the yield drift is required in order to find the appropriate design base shear for a system that can meet the desired performance objectives. In general, the yield drift for SDOFs is defined at the intersection point of the two lines of the equivalent bi-linear pushover (capacity) curve. This definition has also been used in the PBPD method.

In case the yield drift obtained from pushover analysis turns out different from the initially assumed value, iterations would be necessary until reasonable convergence on this parameter is achieved.

It should be noted that in the PBPD method, it would be unconservative if a smaller than the actual value for yield drift is used in design base shear calculation. That is because a smaller yield drift would give a larger ductility ratio and therefore a smaller design base shear. The actual value for the yield drift can be obtained from pushover analysis under the same lateral force distribution used in design.

It has been observed in several studies that regular Moment Frames (MFs) show practically constant yield drift of about 1.0% regardless of their height or bay width (Lee and Goel, 2001; Goel and Chao, 2008). This is mainly due to the fact that in regular MFs, the contribution of stiffness of the beams is significantly larger than that of the columns, and also axial deformation of columns is negligible (Miranda and Akkar, 2006). On the other hand, it is known that the flexural type of deformation caused by axial deformation

of columns in slender braced frames (i.e. CBFs, BRBFs, EBFs, and SPSWs) results in significant change in the yield drift. For instance, it has been observed from the results of the study by Richard (2009) that the yield drift for BRBFs, CBFs, and EBFs significantly increases with the increase in the height of the frame. The yield drift for the 3-story frame is about 0.3%, whereas the yield drift for the 9-story and 18-story frames are approximately 0.5% and 1.1%, respectively (Figure 5.14).

A building structure can be considered as a vertical cantilever beam which has shear as well as flexural modes of deformation. Therefore, the lateral deflection of frames can be obtained by adding the deformations from the shear and flexural modes together. In order to obtain the shear deformation, one can assume the columns to be axially rigid (Figure 5.15.a). Therefore, there would be no axial deformation for columns in this mode which basically means that there is no flexural lateral deformation. In the flexural mode of deformation, the braces are considered to be axially rigid. Columns are axially flexible so their length can change. In this mode, plane sections remain plane and perpendicular to the fictitious neutral axis (similar to the assumption in the beam theory). The flexural mode of deformation is illustrated in Figure 5.15.b. As can be seen, the braced frame in this mode is deflecting similar to a cantilever beam. In a frame with dominant mode of shear deformation, the drifts at different stories are almost equal, whereas the total story drifts increase from bottom to top in a frame with dominant flexural deformation mode.

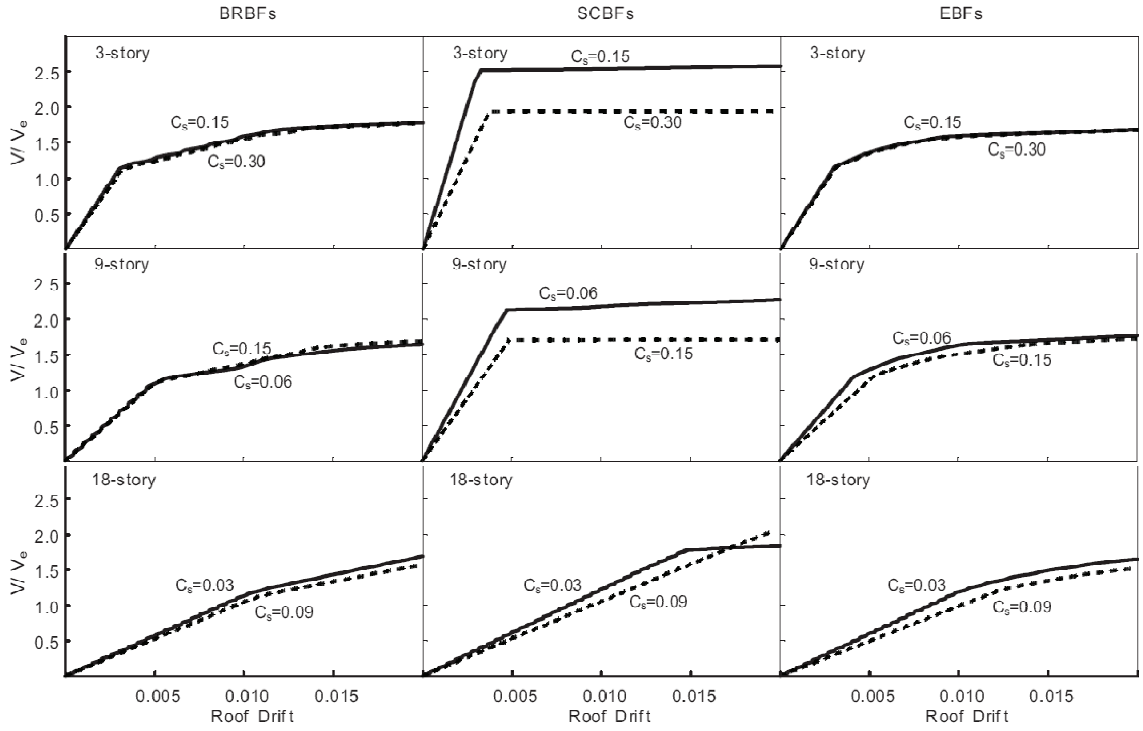

Figure 5.14. Pushover Analysis Results for different Braced Frames (from Richard, 2009).

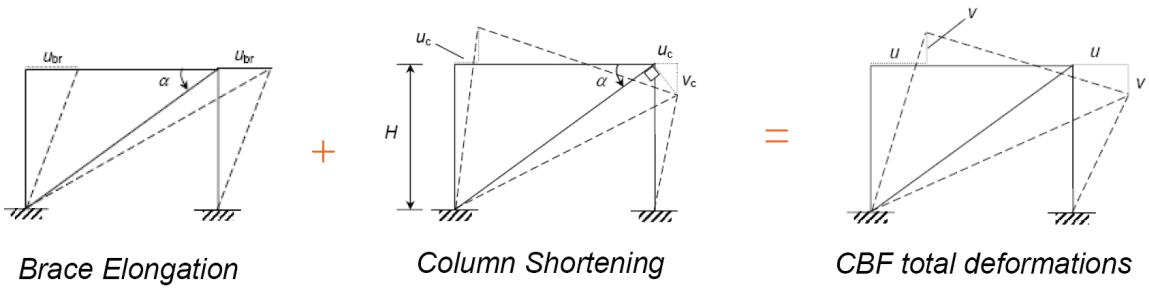

Figure 5.15. Different Components of Lateral Drift in a Braced Frame: (a) Shear Mode of Deformation; (b) Flexural Mode of Deformation; and (c) Total Deformations (from Calvi, M.J.N. Priestley, 2006 (presentation)).

There are several reasons for the fact that in a typical MF, the deflection due to the flexural mode of deformation is negligible (unless we have only a one bay MF). First of all, in a MF the lateral loads are mainly resisted by bending action in beams and columns as opposed to the axial action in braced and columns of a braced frame. As a result, the axial forces in columns of a MF are relatively smaller than those in a braced frame and thus the change in the length of the columns due to lateral loads would be smaller. The other reason is that there are usually several bays in a typical MF system which carry the lateral loads. The axial forces in the interior columns due to lateral loads are very small (negligible) and therefore there is no axial deformation in these columns. Exterior columns may have significant axial forces, but due to the presence of several bays, the moment arm against the overturning moment is large resulting in much smaller axial forces compared to braced frames with single bay. Also, for the beam lines to rigidly rotate in order to produce flexural deformation, they have to overcome the axial stiffness of the interior columns.

On the other hand, in braced systems like CBFs, there is usually a single bay resisting the lateral loads. Therefore, both columns are exterior and both carry significant axial forces (tension and compression). The two column lines are acting as the flanges of a cantilever beam. Therefore, the beams can rotate due to shortening of columns on one side and elongation on the other side resulting in the so called flexural deformation.

Therefore, the story drift in CBFs (and other braced systems) can be obtained by adding the shear and flexural components (Englekirk, 1994, Bertero et al, 1991):

$$\underset{Drift}{\Delta_{Story}} = \underset{Deformation}{\Delta_{Flexural}} + \underset{Deformation}{\Delta_{Shear}} = \Delta_f + \Delta_s \qquad (5.3)$$

It should be noted that since the objective here is to find the yield drift of the system, the deformations at the yield state of the system are considered. For a CBF, the shear component of deformation comes from axial deformation of the braces, and the flexural component is caused by axial deformation of the columns (Figure 5.15). For a one-story one-bay CBF (Figure 5.16), the shear component of the yield drift can be obtained as:

$$\begin{aligned}\Delta_{y,s} &= \delta_y / \cos\alpha = \delta_y \left(\frac{l_b}{L}\right) = \varepsilon_y l_b \left(\frac{l_b}{L}\right) = \varepsilon_y \, l_b^2 / L \\ &= \varepsilon_y / L \times \left((L)^2 + h^2\right)\end{aligned} \tag{5.4}$$

since $L \times \tan\alpha = h$, then:

$$\begin{aligned}\Delta_{y,s} &= \varepsilon_y / L \times (L)^2 \times (1 + \tan^2\alpha) \\ &= \varepsilon_y \times h \times (1 + \tan^2\alpha) / \tan\alpha\end{aligned} \tag{5.5}$$

therefore the shear component of the yield drift can be obtained as:

$$YD_{shear} = \frac{2\varepsilon_y}{\sin 2\alpha} \tag{5.6}$$

As can be seen from Equation (5.6), the yield drift due to shear deformations only depends on the yield strength of the braces and the geometry parameter α. For a regular CBF, the angle α is almost the same in all stories. Hence, somewhat equal story drift due to shear at the yield state can be expected for different stories in a multistory CBF.

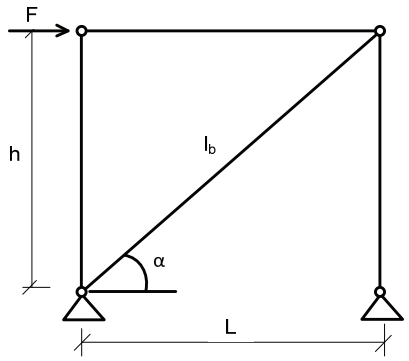

Figure 5.16. One-Story One-Bay CBF.

The flexural component of the story drift at yield state for the one-story one-bay CBF shown in Figure 5.16 can be obtained by considering the frame as a cantilever beam in which the two columns are acting as flanges in tension and compression. Then the flexural deformation of the frame can be obtained as follows:

$$\sigma = \frac{Mc}{I} \tag{5.7}$$

where σ is the average axial stress in columns due to the overturning moment, M, caused by the lateral loads. If the frame is assumed to behave like a beam, the moment of inertia, I can be estimated as:

$$I \simeq 2 \times A_c \times L^2 / 4 = \frac{A_c L^2}{2} \tag{5.8}$$

where A_c is the area of the column cross section and $c = L/2$. Therefore, the average strain in columns can be estimated as:

$$\varepsilon = \frac{\sigma}{E} = \frac{(Fh) \times L/2}{EA_c \times L^2/2} = \frac{Fh}{EA_c L} \tag{5.9}$$

where E is the modulus of elasticity. The vertical axial deformation of the columns can be obtained as:

$$\Delta_{vert} = \int_0^h \varepsilon dy = \frac{Fh^2}{EA_c L} \tag{5.10}$$

The horizontal drift due to this vertical deflection, which is basically the flexural component of the story drift, can be obtained as:

$$\Delta_{horiz} = \Delta_{vert} \times \frac{h}{L} = \frac{Fh^3}{A_c EL^2} \tag{5.11}$$

In order to obtain the horizontal deflection at any level in a multistory CBF due to flexural mode of deformation, the above approach can be followed. The vertical deflection can be calculated from Equation (5.12) by assuming an approximate constant average axial strain in columns, ε_{avg}. This axial strain should be only due to the lateral loads. Then, the horizontal deflections can be found by multiplying vertical deflections by h/L.

$$\Delta_{vert} = \int_0^h \varepsilon dy = \int_0^h \varepsilon_{avg} dy = \varepsilon_{avg} \times h \tag{5.12}$$

$$\Delta_{horiz} = \varepsilon_{avg} \times h \times \frac{h}{L} = \varepsilon_{avg} \times \frac{h^2}{L} \tag{5.13}$$

Thus, the flexural component of the yield drift can be estimated as:

$$YD_{flex} = \varepsilon_{avg} \times \frac{h}{L} \tag{5.14}$$

As can be seen from the above equation, the yield drift caused by flexural deformation depends on the height of the frame and also the bay width.

A reasonable estimate of the average axial strain in columns is needed for the yield drift calculation. First, it is assumed that about 20% of the axial capacity of columns is utilized by the gravity loads. Then, assuming that the column sections are the same for every three stories, axial force design ratios of 1.00, 0.75, and 0.50 can be assumed at mechanism for these columns. The bending moments in the columns are assumed to be negligible compared to the axial forces in these estimations. Since these design ratios are under combined gravity and lateral loading, the ratios utilized only by lateral loads are 0.80, 0.55, and 0.30. Hence, the average axial stress in these three columns due to the lateral loads would be *(0.80 + 0.55 + 0.30) / 3 = 0.55*. The column axial stress capacity can be estimated as:

$$\phi\sigma_{cr} \simeq (0.9)\times(0.85)\times\sigma_y \qquad (5.15)$$

where the approximation $F_{cr} \approx 0.85\ \sigma_y$ has been used. Therefore, the following estimate can be obtained for average axial stress in the columns:

$$\sigma_{avg} \simeq (0.55)\times\phi\sigma_{cr} = (0.55)\times(0.9)\times(0.85)\sigma_y = 0.42\sigma_y \qquad (5.16)$$

As a result, the following expressions can be derived for the yield drift due to flexural deformation:

$$\varepsilon_{avg} = 0.42\varepsilon_y \qquad (5.17)$$

and

$$YD_{flex} = \frac{\sigma_{avg}}{E} \times \frac{h}{L} = \frac{0.42\sigma_y}{E} \times \frac{h}{L} = \frac{0.42 \times 46}{29000} \times \frac{h}{L}$$
$$= 0.000761 \times \frac{h}{L} \tag{5.18}$$

The yield stress of 46 ksi for HSS sections was used to obtain the numerical values in the above equation.

It should be noted that in Chevron braced frames the effective *h* can be considered from the base to the bottom of top story (i.e. very small contribution of column axial deformation from the top story). Table 5.6 shows the calculated yield drift values for four CBFs of different heights. The geometrical information for theses frames is shown in Figure 5.17. The 6-story frame is assumed to have plan and elevation properties similar to the 9-story one frame. The effective height, h_{eff}, which is basically the total height minus the height of top story, is used in yield drift calculation. As can be seen, the calculated yield drifts are quite close to the ones obtained from a pushover analysis of the final designs shown in Figure 5.14. These yield drifts will be used in the following sections to calculate the design base shear for example CBF frames.

Table 5.6. Yield Drift for CBFs.

CBF Frame	h_{eff} (ft)	L (ft)	α	$Y.D._f$	$Y.D._s$	$Y.D._{total}$	Y.D. from pushover
3-Story (SAC)	25	30	40.9	0.055%	0.317%	0.37%	0.35-0.4%
6-Story (Guideline)	70	30	40.9	0.155%	0.317%	0.47%	0.48%
9-Story (SAC)	109	30	40.9	0.242%	0.317%	0.56%	0.5-0.6%
18-Story (SAC)	226	20	52.4	0.753%	0.328%	1.08%	1.1-1.4%

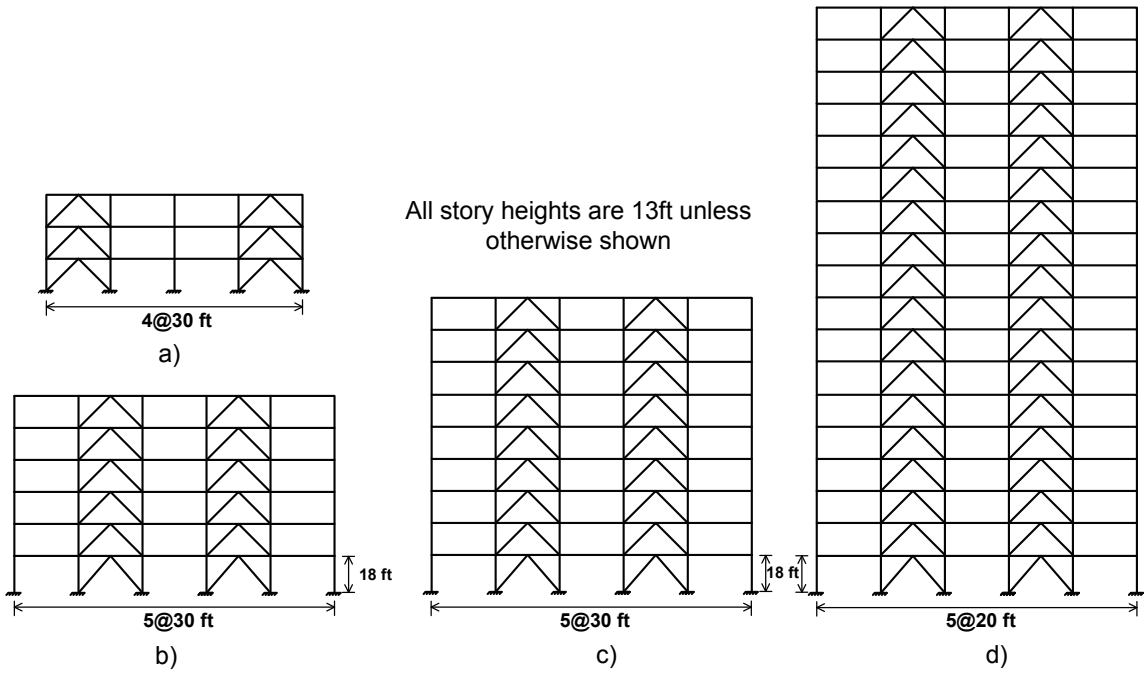

Figure 5.17. Plan and Elevation Views of CBF Buildings: (a) 3-Story; (b) 6-Story; (c) 9-Story; and (d) 18-Story.

5.6 Selection of Proper Target Drift for CBFs

In MFs, the roof drift can be considered as a good representative of story drifts since the shear mode of deformation governs the behavior. However, in braced frames (e.g. CBFs), the roof drift may not be an accurate estimation of the story drifts (especially as the height increases) due to the presence of flexural deformations.

In the previously studied 3-story and 6-story CBFs (Sabelli, 2000; Chao and Goel, 2006b; Chao, Bayat, and Geol, 2008; and Goel and Chao, 2008), the flexural deformations caused by axial deformation of columns were rather small compared to the shear deformations. This is the main reason that although such flexural deformations

were neglected in the PBPD design of 3-story and 6-story CBFs, the frames showed satisfactory performance under 2/3MCE and MCE ground motions. In those designs the Y.D. was assumed to be 0.3% and the T.D. was taken as 1.25%.

However, for taller CBFs, the flexural deformations become more significant and it would be unconservative to neglect their effect on the system Y.D. As explained in Section 5.5, the effect of flexural deformations on system Y.D. for CBFs increases with height. Such flexural deformations are also present in the T.D. A method is proposed in this section to find the proper T.D. for taller CBFs.

As was assumed in the yield drift derivation in the previous section, columns were considered to be axially rigid in order to obtain the shear deformations (Figure 5.15). On the other hand, braces should be considered axially rigid to obtain the flexural deformations (due to axial deformation of columns only).

Therefore, the length of the braces would remain unchanged while the flexural deformation takes place (i.e. no shear deformation). Hence, flexural deformations do not produce deformation (ductility) demand on braces.

This fact can be utilized in order to obtain the proper Target Drift (T.D.) for CBFs. For a given CBF the original T.D. of 1.25% (associated with shear deformation or deformation demand of braces) can be increased by the amount of the flexural component of the Y.D. The reason as mentioned above is that the flexural drift does not cause additional deformation demand on the braces.

For instance, the flexural component of Y.D. for the 18-story CBF is obtained to be 0.75% (Table 5.7). The adjusted T.D. for PBPD design of this frame would then be

$T.D._{adj}$ =1.25% + 0.75% = 2.00%. This means that when the roof drift of the frame under lateral loading reaches 2.0%, the story drifts due to brace deformation are approximately 1.25%. In other words, roof drift of 2.0% is approximately equivalent to 1.25% story drift caused by brace deformation.

The inelastic drift θ_p represents the amount of inelastic deformation demand on braces. By using the adjusted target drift $T.D._{adj}$, as explained above in PBPD procedure, the inelastic deformation, θ_p, would remain unchanged. The reason is that $\theta_p = \theta_u - \theta_y = T.D._{adj} - Y.D.$, and since the $T.D._{adj}$ already includes the term $Y.D._{flex}$ in it, this term would be eliminated and the inelastic drift would become $\theta_p = 1.25\% - Y.D._{shear}$, which is basically a constant value for CBFs with different heights.

The value of 1.25% for T.D. was considered suitable for DBE (10%/50yrs) hazard level (Goel and Chao, 2008). Based on the results from pseudo dynamic tests on full scale CBFs at NCREE (http://w3.ncree.org/), a story drift of 1.75% can be assumed for the shear target drift under MCE (2%/50yrs) hazard level. The NCREE tests showed that fracture in braces can start when the story drifts are about 2% under cyclic loading. The 0.25% was kept as the margin of safety.

The above procedure was then utilized to obtain the required PBPD design base shears for four different CBFs (Tables 5.7 and 5.8). These are the same frames as shown in Section 5.5 (Figure 5.17 and Table 5.6). Two different hazard levels are considered in these two tables to see which one would govern the design.

Table 5.7. PBPD Design Base Shear Under DBE (2/3MCE) Hazard Level.

CBF	h (total)	h_{eff}	L	α (deg)	YD_f (%)	YD_s (%)	YD_{total} (%)	TD	TD_{total}	C_2	PBPD V/W
	ft	for Y.D.	ft					(10/50)	(10/50)		
3-Story	39	26	30	40.9	0.06	0.32	0.37	1.25%	1.31%	1.2	**0.336**
6-Story	83	70	30	40.9	0.16	0.32	0.47	1.25%	1.41%	1.1	**0.281**
9-Story	122	109	30	40.9	0.24	0.32	0.56	1.25%	1.49%	1.0	**0.166**
18-Story	239	226	20	52.4	0.75	0.33	1.08	1.25%	2.00%	1.0	**0.111**

Table 5.8. PBPD Design Base Shear Under MCE Hazard Level.

CBF	h (total)	h_{eff}	L	α (deg)	YD_f (%)	YD_s (%)	YD_{total} (%)	TD	TD_{total}	C_2	PBPD V/W
	ft	for Y.D.	ft					(10/50)	(10/50)		
3-Story	39	26	30	40.9	0.06	0.32	0.37	1.75%	1.81%	1.2	**0.48**
6-Story	83	70	30	40.9	0.16	0.32	0.47	1.75%	1.91%	1.1	**0.322**
9-Story	122	109	30	40.9	0.24	0.32	0.56	1.75%	1.99%	1.0	**0.195**
18-Story	239	226	20	52.4	0.75	0.33	1.08	1.75%	2.50%	1.0	**0.141**

As can be seen from the design base shear values in these tables, the MCE hazard level base shear governs for all cases, and should therefore be used if a dual hazard level performance objective is expected.

In Figure 5.18, a comparison between the calculated PBPD design base shears and the ASCE 7-05 code (ASCE, 2005) values is shown. As can be seen, the DBE base shears are larger than the code values for short period, but almost the same for longer

periods. The MCE base shears are much larger than the code values for shorter periods and slightly larger for longer periods.

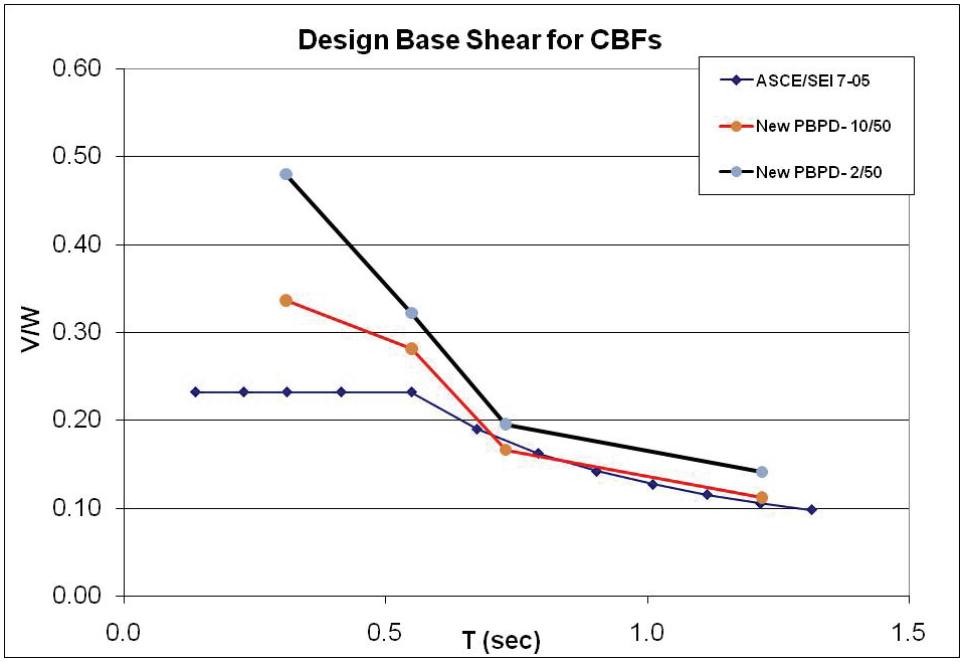

Figure 5.18. Comparing PBPD Design Base Shears with Current Code Values.

Table 5.9. Design Base Shear for CBFs Using Different PBPD Approaches.

CBF	New PBPD *V/W* (2/3 MCE)	New PBPD *V/W* (MCE)	Current PBPD (η=0.5) *V/W* (2/3 MCE)
3-Story	0.336	0.480	0.484
6-Story	0.281	0.322	0.338

It can also be seen from Table 5.9 that the *V/W* value for 3- and 6-story CBFs obtained by the proposed PBPD approach in this Chapter are quite close to the values previously obtained by using η = 0.5 as the energy modification factor. Therefore, there

was no need to redesign the 3-story and 6-story CBFs with the new design base shears, because the remaining steps of the PBPD procedure (after design base shear calculations) are essentially unchanged. This means that by using the proposed approach and including the MCE hazard level, the previous designs for 3- and 6-story CBF can be used.

It should be noted that in the energy modification approach the design base shear values would be quite large and over-estimated if MCE hazard level was also included.

In the following sections, the proposed PBPD procedure for CBFs will be applied to the 9-story SAC building (Figure 5.17) as an example of a mid-rise CBF structure.

5.7 PBPD Design of a Mid-Rise CBF (9-Story SAC Building)

The merits of the proposed approach to obtain the design base shear in the PBPD method become more evident when the method is applied to mid-rise to tall CBFs. This is due to the fact that the significance of the flexural deformations increases with the increase in the height of the frame.

In this section, the proposed approach will be used to obtain the required design base shear for CBF as the lateral load resisting system in the 9-story SAC building. The building was originally designed with perimeter MFs as the lateral load resisting system. Instead of the original MFs, four CBFs are used in this design in each direction to resist the lateral loads.

It should be noted that the main difference between the proposed PBPD approach and the current one is in calculation of the design base shear. The other PBPD steps after

the design base shear is determined are the same. Those design steps were explained in Chapter 4.

Plan view of the example 9-story structure is shown in Figure 5.19. The 9-story structure is 150 ft by 150 ft in plan, and 83 ft in height. The floor-to-floor heights are 18 ft for the first level and 13 ft for all the other levels. The bays are 30 ft on centers, in both directions, with five bays in each direction. The building's lateral force resisting system is comprised of two perimeter CBF bays in each direction. The interior frames of the structure consist of simple framing with composite floors. The details of the design weights of the building components can be found elsewhere (Sabelli, 2000).

As previously mentioned in Chapter 3, The calculation of the PBPD design base shear is also based on a lateral force distribution proposed by Chao, Goel, and Lee (2007), which can be expressed as $F_i = C'_{vi} V$, where:

$$C'_{vi} = (\beta_i - \beta_{i+1}) \left(w_n h_n \Big/ \sum_{j=1}^{n} w_j h_j \right)^{kT^{-0.2}} \tag{5.19}$$

and

$$\beta_i = V_i / V_n = \left(\sum_{j=1}^{n} w_j h_j \Big/ w_n h_n \right)^{kT^{-0.2}} \tag{5.20}$$

In the above equations, β_i represents the shear distribution factor at level i; V_i and Vn, respectively, are the story shear forces at level i and at the top (nth) level; w_j is the seismic weight at level j; h_j is the height of level j from the base; F_i is the lateral force at level i; and V is the total design base shear. The value of factor k in the exponent term was taken equal to 0.75.

The initial PBPD design of the 9-story CBF is performed in Section 5.7.1 using k = 0.75 as the lateral load distribution parameter. The performance of this design is then evaluated and recommendations for performance improvement are suggested. In the subsequent section, k = 0.50 is used as the lateral load distribution parameter in order to provide more strength and stiffness in the upper stories. This change in the lateral load distribution appears to enhance the performance of the frame, especially in the upper stories.

5.7.1 PBPD Design of 9-Story CBF Using k = 0.75 as The Lateral Load Distribution Parameter

Design parameters according to 1997 *NEHRP Provisions* (NEHRP/FEMA, 1997) for the 9-story CBF are listed in Table 5.10. A basic target drift (shear target drift) of 1.25% for 10%/50 year (2/3MCE) hazard, and 1.75% for 2%/50 year (MCE) hazard is selected. The elastic design spectral response acceleration, S_a, is calculated as:

$$S_a = C_s \cdot \left(\frac{R}{I}\right) = 0.175 \cdot \left(\frac{6}{1}\right) = 1.05 \tag{5.21}$$

The corresponding parameters are calculated and listed in Table 5.10 and Table 5.11. It can be seen that the MCE hazard level governs the design. The governing base shear is 3871 kips for the full structure (967.8 kips for one CBF). Design lateral force at each floor level is then calculated and given in Table 5.12.

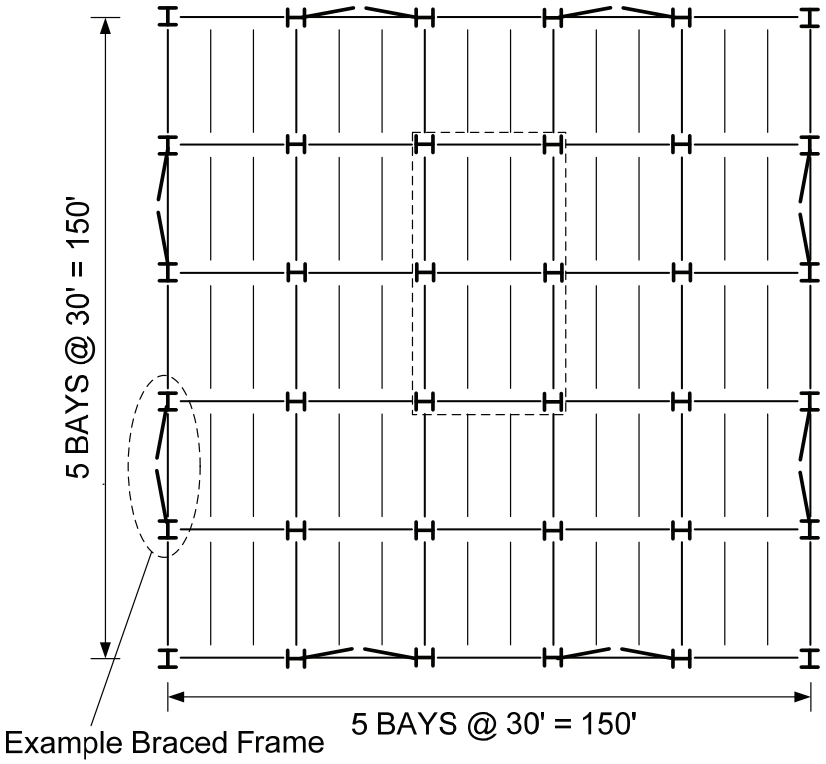

Figure 5.19. Plan View of 9-Story SAC Building.

Table 5.10. Design Parameters For the 9-Story CBF According to 1997 NEHRP.

Parameters	9-story CBF
MCE Short Period Spectral Response Acc., S_S	2.09 g
MCE One-Second Spectral Response Acc., S_1	1.155 g
Acceleration Site Coefficient, F_a	1.0
Velocity Site Coefficient, F_v	1.5
Short Period Design Spectral Response Acc., S_{DS}	1.393 g
One-Second Design Spectral Response Acc., S_{D1}	0.77 g
Site Class	D (Deep Stiff Soil)
Occupancy Importance Factor	*I = 1.0*
Seismic Design Category	D
Building Height	122 ft (above the base)
Approximate Building Period, T	0.734 sec.
Response Modification Factor	*R* = 6
Total Building Weight, W	19893 kips
Seismic Response Coefficient, $C_s = \frac{V}{W}$	0.175 g

Table 5.11. Design Parameters For the 9-Story CBF Based on PBPD Procedure ($k = 0.75$).

Parameters	10% in 50 year Hazard	2% in 50 year Hazard
S_a	1.049 g	1.574 g
T	0.734 sec.	0.734 sec.
k (Lat. Dist. Parameter)	0.75	0.75
Yield Drift, θ_y	0.56%	0.56%
$\theta_{y,flex}$	0.24%	0.24%
Basic Target Drift, θ_u	1.25%	1.75%
λ	1.0	1.0
Effective Target Drift, $\theta_{u,eff} = \theta_u + \theta_{y,flex}$	1.49%	1.99%
Inelastic Drift, $\theta_p = \theta_{u,eff} - \theta_y$	0.93%	1.43%
$\mu_s = \theta_{u,eff} / \theta_y$	2.66	3.55
R_μ	2.66	3.55
γ	0.610	0.484
α	3.88	3.96
η	1.0	1.0
V/W	0.166	0.195 (governs)
Design Base Shear V	3302 kips (for four CBFs)	3871 kips (for four CBFs)

Table 5.12. Lateral Force Distribution ($k = 0.75$).

Floor	F_i (kips)	F_i (kips)	Story Shear (kips)
	Full Structure	one CBF	one CBF
9	1095.7	273.9	273.9
8	677.8	169.4	443.4
7	544.9	136.2	579.6
6	445.8	111.5	691.1
5	362.2	90.5	781.6
4	287.2	71.8	853.4
3	217.5	54.4	907.8
2	151.3	37.8	945.6
1	88.7	22.2	967.8

The design of braces as the yielding members is performed based on the strength, fracture, and compactness criteria, as explained in Chapter 4. ASTM A500 Grade B tube sections (HSS) with 46 ksi nominal yield strength are used. The selected brace sections are built-up double tube sections and shown in Table 5.13. After design of braces, the non-yielding members, which are beams and columns, can be designed.

Table 5.13. Required Brace Strength and Selected Sections for 9-Story CBF ($k = 0.75$).

Floor	α	$Vi/0.9\cos(\alpha)$ kips	Brace Section	Strength $P_y+0.5P_{cr}$	Area in^2	F_{cr} ksi	$0.5P_{cr}$ kips	P_v kips	N_f
9	41	403	**2HSS3-1/2×3-1/2×5/16**	415	7.04	23.88	91.1	323.8	241
8	41	653	**2HSS4-1/2×4-1/2×3/8**	683	10.96	32.68	179.1	504.2	157
7	41	853	**2HSS4-1/2×4-1/2×1/2**	861	13.9	31.89	221.6	639.4	329
6	41	1017	**2HSS5×5×1/2**	996	13.76	34.45	271.5	723.0	224
5	41	1151	**2HSS6×6×1/2**	1266	19.48	37.95	369.6	896.1	132
4	41	1256	**2HSS6×6×1/2**	1266	19.48	37.95	369.6	896.1	132
3	41	1336	**2HSS6×6×5/8**	1483	23.4	34.72	406.2	1076.4	245
2	41	1392	**2HSS6×6×5/8**	1483	23.4	34.72	406.2	1076.4	245
1	50	1673	**2HSS7×7×5/8**	1815	28	37.67	527.4	1288.0	156

Table 5.14. Design of Beams ($k = 0.75$).

Floor	w_u (k/ft)	R_yP_y	$0.5P_{cr}$	F_h	F_v	P_u	M_u	Beam Section
9	0.95	453.4	91.1	410.9	237.7	205.5	1872.4	W33x130
8	1.13	705.8	179.1	667.9	345.6	333.9	2698.6	W36x182
7	1.13	895.2	221.6	842.9	441.9	421.4	3420.9	W40x211
6	1.13	1014.9	271.5	970.9	487.8	485.4	3765.1	W40x235
5	1.13	1254.5	369.6	1225.8	580.5	612.9	4460.8	W40x278
4	1.13	1254.5	369.6	1225.8	580.5	612.9	4460.8	W40x278
3	1.13	1507.0	406.2	1443.9	722.1	721.9	5522.9	W40x397
2	1.13	1507.0	406.2	1443.9	722.1	721.9	5522.9	W40x397
1	1.21	1803.2	527.4	1498.1	977.3	749.0	7444.4	W40x431

Table 5.15. Design of Columns ($k = 0.75$).

Floor	$P_{trans.}$	P_{beam}	$0.5P_{cr}Sin\ \alpha$	$0.5F_y$	P_u	P_u (cumulative)	Column Section
9	32.88	28.5	0	119	180	180	W14x109
8	37.56	33.9	60	173	304	484	W14x109
7	37.56	33.9	117	221	410	894	W14x109
6	37.56	33.9	145	244	461	1355	W14x211
5	37.56	33.9	178	290	540	1895	W14x211
4	37.56	33.9	243	290	604	2499	W14x211
3	37.56	33.9	243	361	675	3174	W14x426
2	37.56	33.9	267	361	699	3873	W14x426
1	37.56	36.3	267	489	829	4702	W14x426

Generally, capacity design approach is used for design of non-yielding members, which are columns and beams in CBFs. For columns, the post-buckling limit state of the braces governs the design.

Table 5.14 and Table 5.15 show the design parameters as well as the final design sections for beams and columns, respectively. Only cumulative axial forces are considered for design of columns. Column sections are changed after every three stories.

5.7.2 Evaluation of 9-story CBF designed by the lateral load distribution parameter k = 0.75

Nonlinear analyses were carried out by using the SNAP-2DX program, which has the ability to model brace behavior under large displacement reversals, as well as the fracture of braces with tubular sections (Rai et al., 1996). Gravity columns were included in the modeling by using a lumped continuous leaning column, connected to the braced

frame through rigid pin-ended links. *P-Δ* effect due to the gravity loads was also accounted for in the analysis. All beams and columns of the frame were modeled as beam-column elements.

Maximum story drifts under 2/3MCE and MCE level SAC ground motions are shown in Figure 5.20. Under the design level (2/3MCE) ground motion, although some ground motions induce somewhat large drifts in middle stories, the response is generally good and the median response is within the target drift limit except for the top story. However, under MCE level ground motions, both middle stories and also upper stories show quite large story drifts. In addition, brace fractures at lower and middle stories were observed under a couple of MCE ground motions. Further investigation showed that the main reason for brace fractures were large story drifts.

Large story drifts (and subsequent brace fractures) in lower and middle stories under MCE ground motions are mainly due to large velocity pulses in these records. However, large story drifts at upper stories are mainly due to the effect of higher modes on dynamic response and somewhat low strength/stiffness of these stories.

In order to reduce the upper story drifts, a smaller k value can be used. By doing this, larger forces are assigned at the upper stories which eventually make them stronger and stiffer. It should be noted that there is significant change in the story shears at lower stories by using a different k value, since all the upper story forces are added to the lower stories' shear. Basically, by using $k = 0.5$, larger portion of the design base shear is assigned at upper stories.

A recommendation was made for the improvement of the performance of this frame which is using $k = 0.50$ as the lateral load distribution parameters. By doing this, larger forces are assigned at the upper stories which eventually makes them stronger and stiffer. There would not be significant change in the story shears at lower stories.

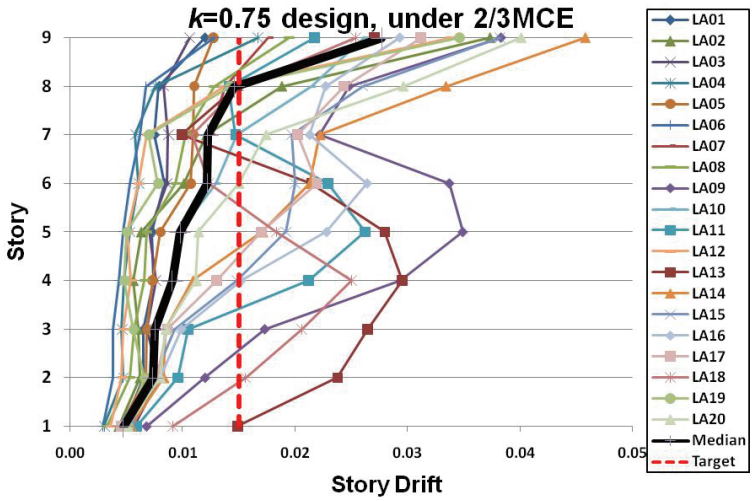

(a)

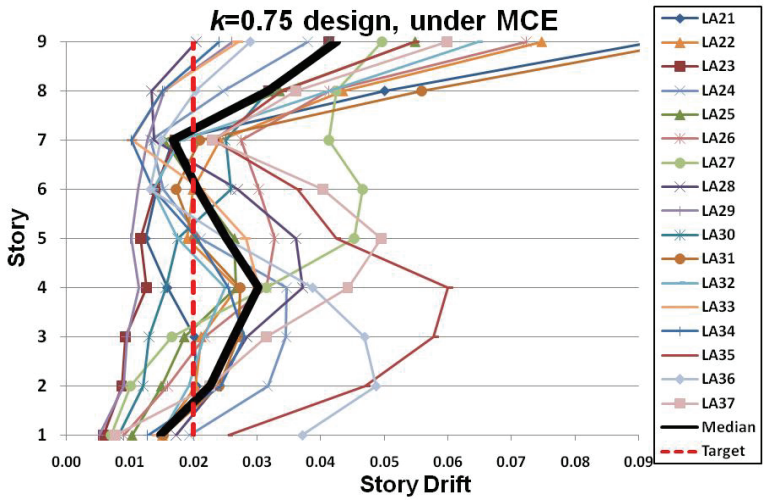

(b)

Figure 5.20. Story Drifts for 9V-PBPD Designed with k = 0.75 Under: (a) 2/3MCE; and (b) MCE Level SAC Ground Motions.

5.7.3 PBPD Design of 9-story CBF using k = 0.50 as the lateral load distribution parameter

The previous design steps are followed here as well except that $k = 0.50$ is used for the lateral force distribution. This is done to assign larger lateral forces at the upper levels in order to provide adequate strength and stiffness in those stories.

A preliminary study was done to compare the story shears obtained by using k = 0.75 and k = 0.50. The results are shown in Figure 5.21. As can be seen in part (a) of this figure, the story shears for k = 0.50 are larger in upper stories and somewhat smaller (less than 10%) in the lower stories. Figure 5.21.b compares the story shears better by showing the ratio of the story shears obtained with k = 0.50 to those with k = 0.75. As can be seen, with k = 0.50, the story shears in the top two stories are significantly greater than those with k = 0.75. In lower stories, the shears obtained by using k = 0.50 are slightly smaller (less than 10%) than the ones with k = 0.75. From the results shown in Figure 5.21, it is expected that the 9-story CBF designed by using k = 0.50 would show smaller drifts at upper levels.

The 9-story frame was then redesigned by using $k = 0.50$ for the lateral distribution parameter. The design parameters for base shear calculations are shown in Table 5.16. The MCE hazard level governs the design with $V/W = 0.180$. The frame showed dynamic instability (due to P-Delta effect) under a few SAC LA MCE ground motions. Therefore, it was decided to include P-Delta forces in the design of yielding members (braces).

These P-Delta forces can be estimated as horizontal forces in the fictitious rigid links connecting main frame to the lumped gravity column, assuming a linear deflected

shape at the target drift of 1.99%. These forces are shown in Table 5.17, along with the original lateral forces without the P-Delta forces. By adding these P-Delta forces, total design base shear was increased to *0.206W*. This value is closer to the *0.195W* obtained for design with $k = 0.75$. Therefore, a better and fair performance comparison can be made between the two frames by adding these approximate P-Delta forces.

The final sections for braces, beams and column are shown in Table 5.18, Table 5.19, and Table 5.20, respectively. As can be seen, the sizes of upper story braces were increased compared to the design with $k = 0.75$, but brace sizes for lower stories are the about the same. It should also be noted that the weight of the frame with $k = 0.5$ (designated as 9V-PBPD-A henceforth) is about 10% more than the frame with $k = 0.75$, which is mostly due to increase in the brace sizes and the supporting non-yielding members in the upper stories. However, this is only the comparison between the weights of seismic frames, not the entire structure including gravity frames.

As will be seen later in Chapter 6, P-Delta effects can be indirectly compensated for by modification of the λ-factor. Using the modified λ-factor in Chapter 6, the structure will have adequate design base shear from the beginning without the need to add approximate P-Delta forces as done herein.

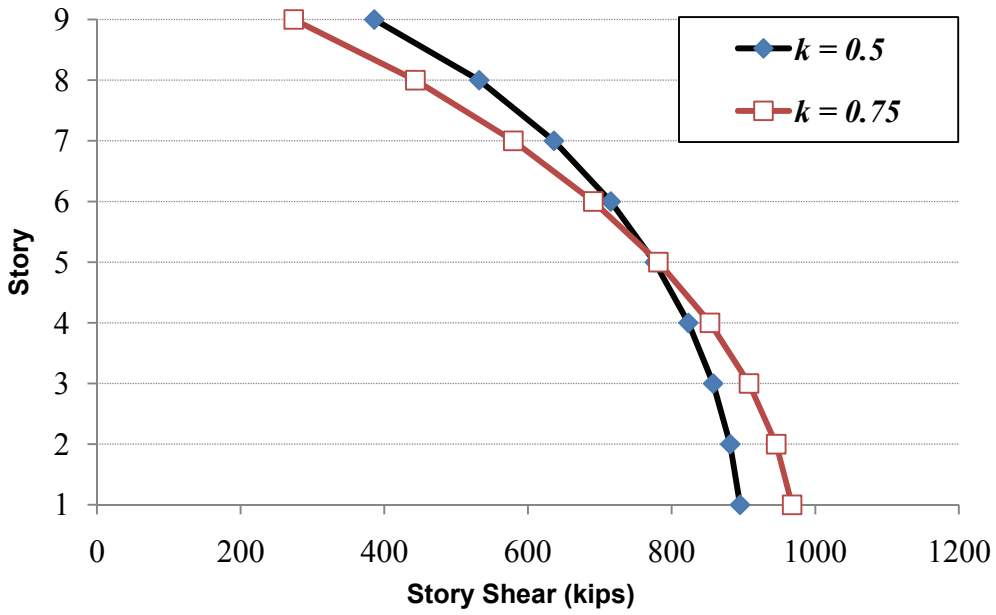

(a)

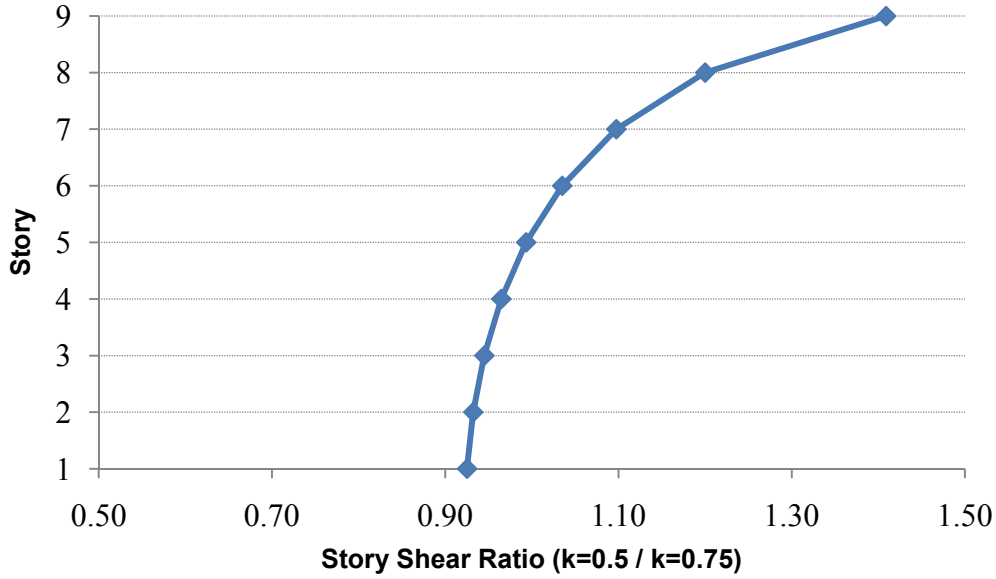

(b)

Figure 5.21. Comparison of the Story Shears with k = 0.50 and k = 0.75: (a) Story Shear Values; (b) Ratio of Story Shears.

Table 5.16. Design Parameters for the 9-Story CBF Based on PBPD Procedure (*k = 0.50*): 9V-PBPD-A.

Parameters	10% in 50 year Hazard	2% in 50 year Hazard
S_a	1.049 g	1.574 g
T	0.734 sec.	0.734 sec.
k (Lat. Dist. Parameter)	0.50	0.50
Yield Drift, θ_y	0.56%	0.56%
$\theta_{y,flex}$	0.24%	0.24%
Basic Target Drift, θ_u	1.25%	1.75%
λ	1.0	1.0
Effective Target Drift, $\theta_{u,eff} = \theta_u + \theta_{y,flex}$	1.49%	1.99%
Inelastic Drift, $\theta_p = \theta_{u,eff} - \theta_y$	0.93%	1.43%
$\mu_s = \theta_{u,eff} / \theta_y$	2.66	3.55
R_μ	2.66	3.55
γ	0.610	0.484
α	4.209	6.472
η	1.0	1.0
V/W	0.154	0.180 (governs)
Design Base Shear V	3063 kips (for four CBFs)	3581 kips (for four CBFs)

Table 5.17. Lateral Force Distribution ($k = 0.50$) : 9V-PBPD-A.

Floor	F_i (kips)	F_i (kips)	Story Shear (kips)	P-Delta Lateral Forces (kips)	Story Shear- w/ P-Delta (kips)
	Full Structure	one CBF	one CBF	at T.D.= 1.99%	one CBF
9	1543.8	386.0	386.0	15.0	400.9
8	584.4	146.1	532.1	14.9	561.9
7	416.2	104.1	636.1	14.9	680.8
6	316.5	79.1	715.3	14.9	774.8
5	244.7	61.2	776.5	14.9	850.8
4	187.4	46.8	823.3	14.9	912.5
3	138.5	34.6	857.9	14.9	962.0
2	94.7	23.7	881.6	14.9	1000.5
1	54.9	13.7	895.3	15.0	1029.2

Table 5.18. Required Brace Strength and Selected Sections for 9-Story CBF ($k = 0.50$) : 9V-PBPD-A.

Floor	***α***	***Vi/0.9cos(α)* kips**	**Brace Section**	**Strength $P_y+0.5P_{cr}$**	**Area in^2**	***F_{cr} ksi***	***$0.5P_{cr}$ kips***	***P_v kips***	***N_f***
9	41	590	**2HSS4-1/2×4-1/2×3/8**	683	10.96	32.68	179.1	504.2	157
8	41	827	**2HSS4-1/2×4-1/2×1/2**	861	13.9	31.89	221.6	639.4	329
7	41	1002	**2HSS5×5×1/2**	996	13.76	34.45	271.5	723.0	224
6	41	1141	**2HSS6×6×1/2**	1266	19.48	37.95	369.6	896.1	132
5	41	1253	**2HSS6×6×1/2**	1266	19.48	37.95	369.6	896.1	132
4	41	1343	**2HSS6×6×5/8**	1483	23.4	34.72	406.2	1076.4	245
3	41	1416	**2HSS6×6×5/8**	1483	23.4	34.72	406.2	1076.4	245
2	41	1473	**2HSS6×6×5/8**	1483	23.4	34.72	406.2	1076.4	245
1	50	1779	**2HSS7×7×5/8**	1815	28	37.67	527.4	1288.0	156

Table 5.19. Design of Beams (*k = 0.50*): 9V-PBPD-A.

Floor	w_u (k/ft)	R_yP_y	$0.5P_{cr}$	F_h	F_v	P_u	M_u	Beam Section
9	0.95	703.8	179.1	667.9	343.6	333.9	2681.6	**W36x182**
8	1.13	893.2	221.6	842.9	441.9	421.4	3420.9	**W40x211**
7	1.13	1014.9	271.5	970.9	487.8	483.4	3763.1	**W40x235**
6	1.13	1254.5	369.6	1223.8	580.5	612.9	4460.8	**W40x278**
5	1.13	1254.5	369.6	1223.8	580.5	612.9	4460.8	**W40x278**
4	1.13	1507.0	406.2	1443.9	722.1	721.9	5522.9	**W40x397**
3	1.13	1507.0	406.2	1443.9	722.1	721.9	5522.9	**W40x397**
2	1.13	1507.0	406.2	1443.9	722.1	721.9	5522.9	**W40x397**
1	1.21	1803.2	527.4	1498.1	977.3	749.0	7444.4	**W40x431**

Table 5.20. Design of Columns (*k = 0.50*): 9V-PBPD-A.

Floor	$P_{trans.}$	P_{beam}	$0.5P_{cr}Sin\ \alpha$	$0.5F_v$	P_u	P_u *(cumulative)*	Column Section
9	32.88	28.5	0	173	234	234	**W14x109**
8	37.56	33.9	117	221	410	644	**W14x109**
7	37.56	33.9	145	244	461	1105	**W14x109**
6	37.56	33.9	178	290	540	1645	**W14x257**
5	37.56	33.9	243	290	604	2249	**W14x257**
4	37.56	33.9	243	361	675	2924	**W14x257**
3	37.56	33.9	267	361	699	3623	**W14x455**
2	37.56	33.9	267	361	699	4322	**W14x455**
1	37.56	36.3	267	489	829	5151	**W14x455**

5.7.4 Evaluation of 9-Story CBF Designed By the Lateral Load Distribution Parameter $k = 0.50$

As was done before for 3-story and 6-story frames earlier in this chapter, nonlinear analyses were carried out by using the SNAP-2DX program. The same modeling techniques were used. The results for maximum story drifts under 2/3MCE and MCE level SAC ground motions are shown in Figure 5.22.

It can be seen that by using $k = 0.50$, the upper story drifts become quite smaller compared to the case of $k = 0.75$. In addition, the story drift profile matches much better with the target drift limit in the case of $k = 0.50$ and also tends to be more uniform along the height.

Under the design level (2/3MCE) ground motions, the response is generally good and the median response is well within the target drift limit. This is consistent with the fact that the MCE level governed the design, therefore it is expected that the story drifts under MCE level ground motions are closer to the drift limit. Under a couple of MCE ground motions, lower stories show large drifts. In addition, brace fracture at lower and middle stories occurred under a couple of MCE ground motions.

Figure 5.23 show comparison between story drift response under different ground motions for the two designs; one with $k = 0.75$ and the other with $k = 0.50$. Also, the median story drifts under the two sets of SAC LA ground motions (2/3MCE and MCE) for the two designs are shown in Figure 5.24. From these figures, it is evident that by using $k = 0.50$ much smaller story drifts in the upper stories and more uniform story drift profile can be expected.

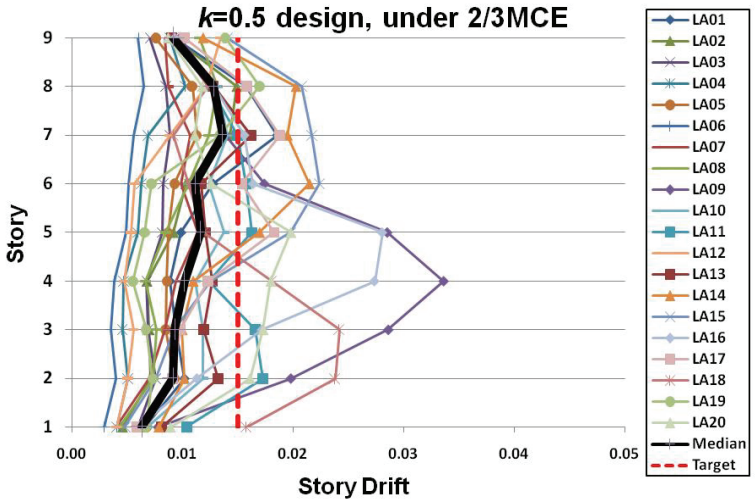

(a)

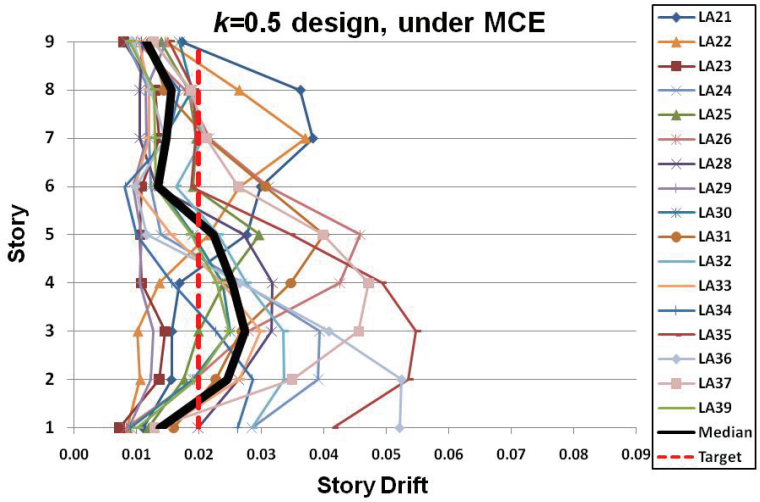

(b)

Figure 5.22. Story Drifts for 9V-PBPD Designed with k = 0.50 Under: (a) 2/3MCE; and (b) MCE Level SAC Ground Motions.

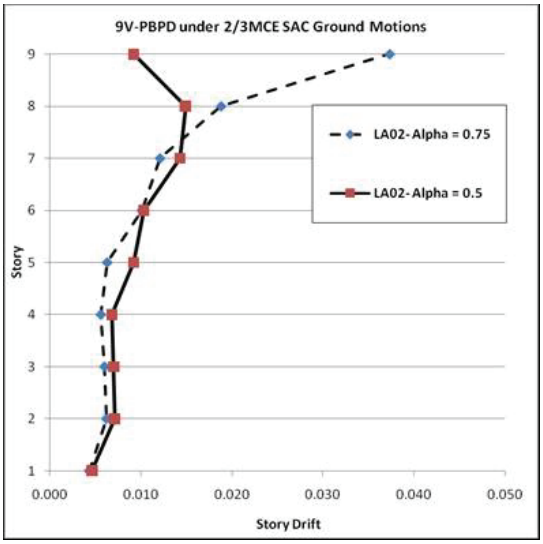

(a)

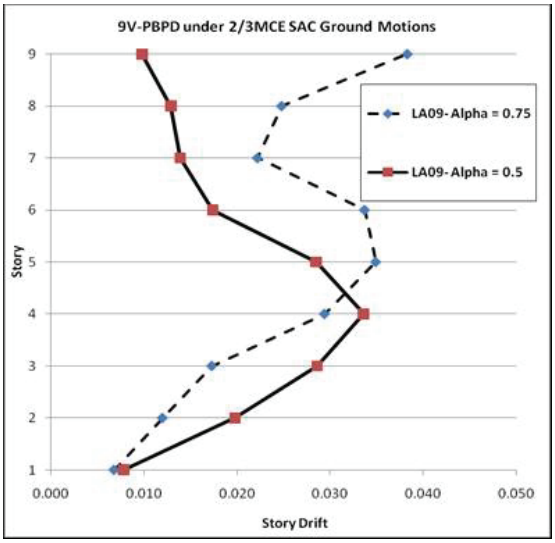

(b)

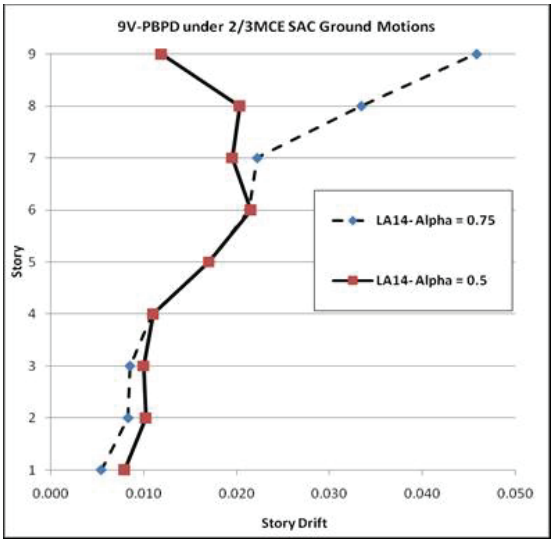

(c)

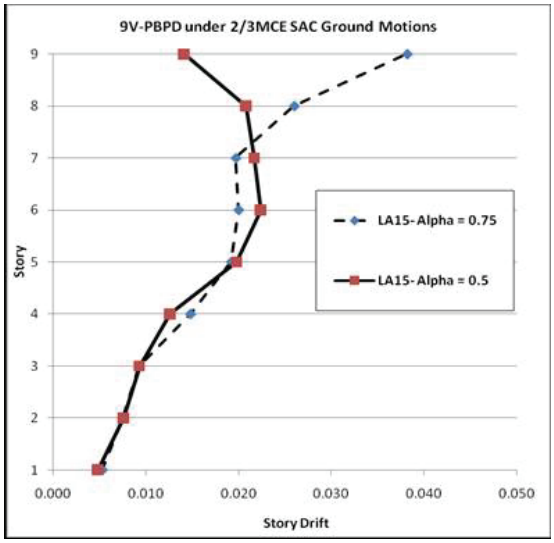

(d)

Figure 5.23. Comparison of the Story Drift Profile for Design with $k = 0.50$ vs. $k = 0.75$ under: (a) LA02; (b) LA09; (c) LA14; and (d) LA15 Ground Motions.

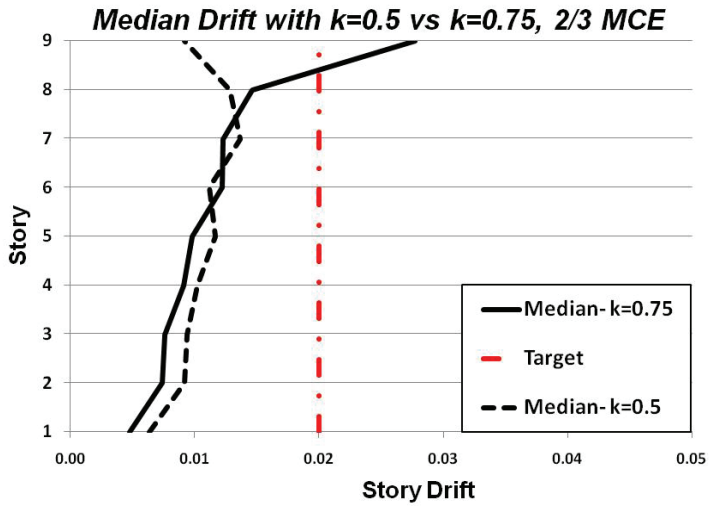

(a)

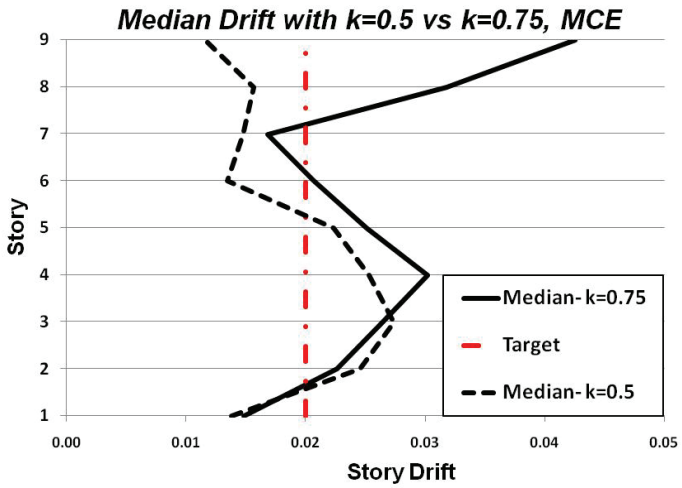

(b)

Figure 5.24. Comparison of the Median Story Drifts for 9-Story CBF under SAC LA Ground Motions: (a) under 2/3 MCE; and (b) under MCE Hazard Level.

5.8 Performance Comparison between Beam Shear Splice vs. Conventional Connection

As was discussed in Section 4.2 (Chapter 4), beam shear splices are recommended for CBF in order to minimize moment transfer into the columns (Figure 4.5). For analysis purposes such shear splices can be modeled as pin connections at the beam ends. On the other hand, the conventional gusset plate detail provides considerable flexural constraint in the beam-to-column connection region. Therefore, the conventional beam-to-column connections need to be treated as rigid connections with moment transfer capability.

In this section, the effect of recommended beam shear splice detail, i.e., moment release, on the seismic performance of the 9V-PBPD-A frame is studied. Two models of the 9V-PBPD-A frame are considered. One, which is the original model, has beam shear splices at the ends of the beams (9V-PBPD-A-Pin), while the other model has the usual gusset plate connection (9V-PBPD-A-Rigid). Hence, the only difference between these two frames is their beam-to-column connection detail. The two models were subjected to the DBE and MCE SAC ground motion records for LA site.

Figure 5.25 and Figure 5.26 show the analysis results of these two frames under the LA01 record which is a DBE ground motion. No brace fractures were observed and the maximum story drifts are quite similar. However, several plastic hinges formed in the columns of the frame with rigid connections (9V-PBPD-A-Rigid). Column plastic hinges (PH) rotations are more significant in 5th, 6th, and 7th stories as shown in Figure 5.26.a. Formation of the column plastic hinges is due to large moments transferred from beam to columns when conventional gusset plate connections are used (see Figure 4.6).

Figure 5.27 to Figure 5.29 show the results of dynamic analysis of the two frames under LA21 (MCE) ground motion. As can be seen in Figure 5.27, significant column plastic hinging occurred as the largest pulse of the LA21 ground motion hit the 9V-PBPD-Rigid frame. The column plastic hinge rotations are most significant in stories 5 to 8. In addition, several brace fractures occurred in the 9V-PBPD-A-Rigid frame. On the other hand, very little column plastic hinge formation can be seen in 9V-PBPD-A-Pin frame. Also, one brace fractured, albeit near the end of the ground motion (Figure 5.27.a). It should be noted that the residual drifts are also larger for 9V-PBPD-A-Rigid frame as shown in Figure 5.29.

The performance under another MCE level ground motion record, LA36, is shown in Figure 5.30 and Figure 5.31. As was the case for other ground motions, significant column plastic hinging and larger residual story drifts can be observed for the 9V-PBPD-A-Rigid frame. The plastic hinge rotations of columns are quite large in the first two stories and also some beam plastic hinges can be seen, Figure 5.31.a.

It is worth mentioning that although the maximum 2nd story drifts under LA36 are about the same for both frame models, i.e., 5.25% for Pin model and 4.85% for Rigid model (Figure 5.30.b), the 9V-PBPD-A-Pin frame was able to accommodate such deformation without formation of column plastic hinges. But, such deformation caused undesirable plastic hinges in the columns of 9V-PBPD-A-Rigid frame. This shows that the frame with pin connections has more deformation capacity or ductility.

It should be noted that although the story drifts were much larger in the case of LA36 compared to LA21, no brace fracture was seen under LA36 for either frame. This

can be attributed to shorter duration of the LA36 ground motion (see Table 5.21), which resulted in less low-cycle fatigue in the braces.

Figure 5.32 to Figure 5.34 show the story drifts under the two sets of DBE and MCE level SAC LA ground motions. The median drifts are shown in Figure 5.34. As can be seen, the median drifts under DBE ground motions (LA01-LA20) are quite close for the two frames. Under MCE ground motions (LA21-LA40) the 9V-PBPD-A-Pin frame shows larger story drifts in the lower stories except for the 1st story. Although the median drifts are somewhat larger for the Pin model, there is much less plastic hinging in the columns, which again indicates larger deformation capacity and hence larger ductility of the 9V-PBPD-A-Pin frame.

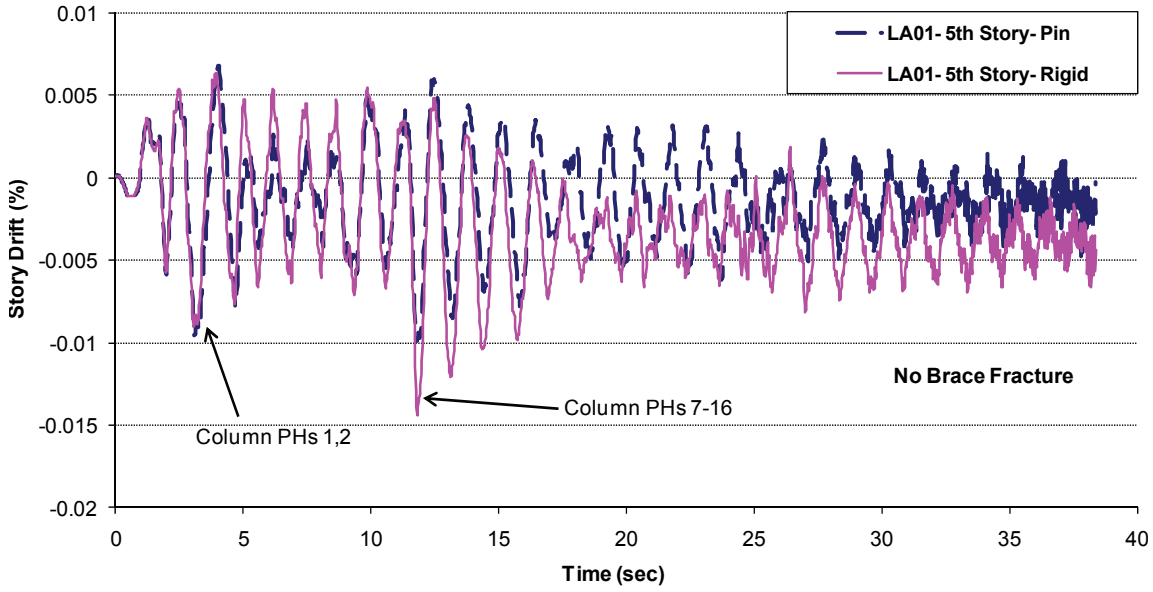

(a)

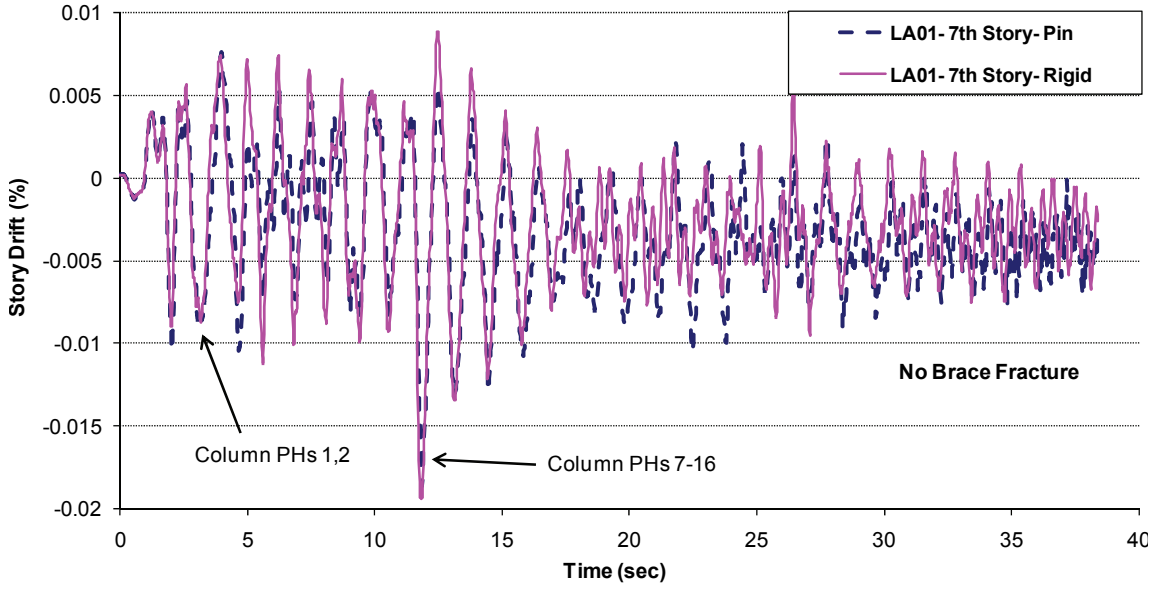

(b)

Figure 5.25. Story Drift vs. Time under LA01 for 9V-PBPD-A-Pin and 9V-PBPD-A-Rigid for: (a) 5th Story; and (b) 7th Story.

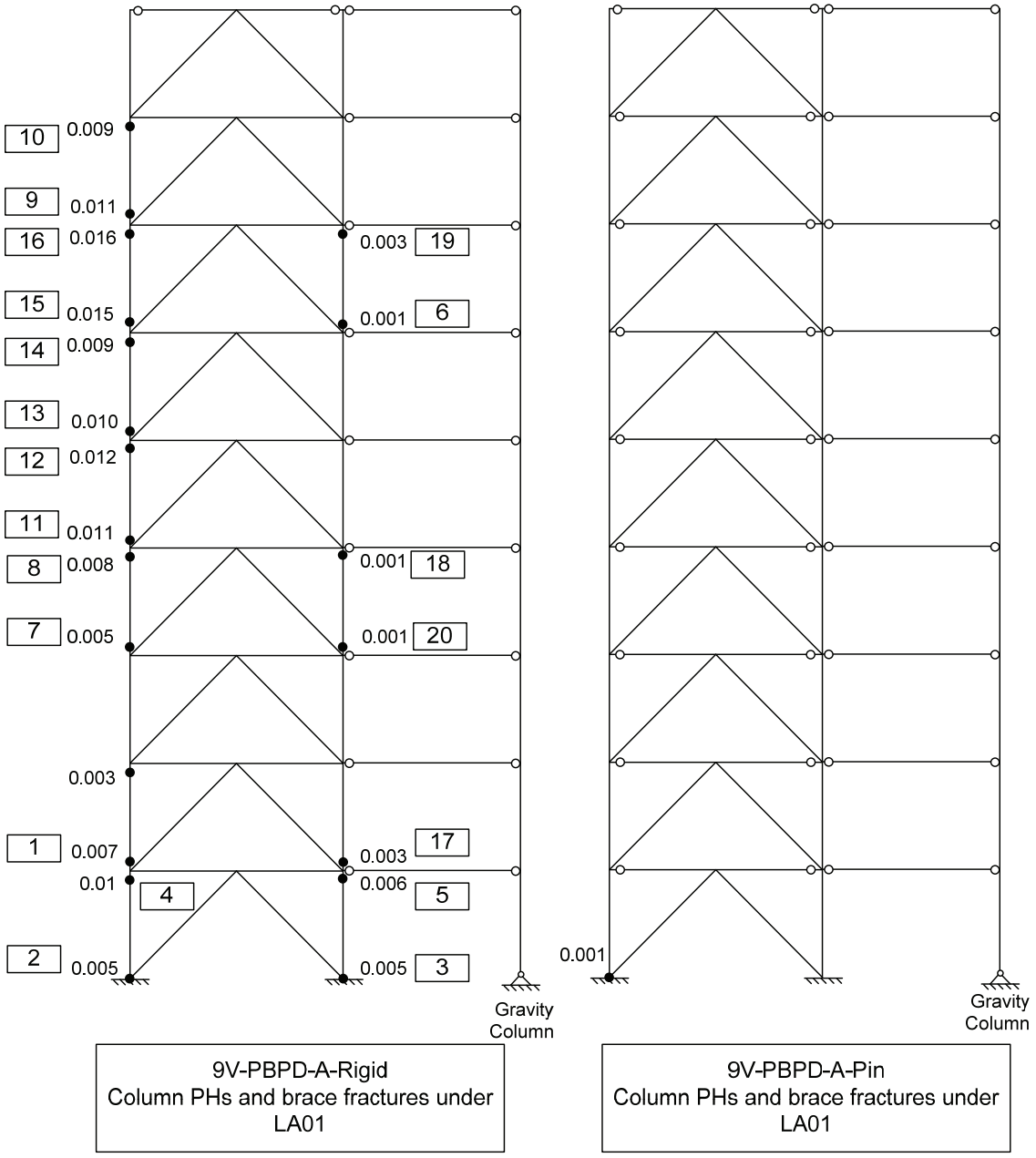

(a) (b)

Figure 5.26. Column PHs and No Brace Fractures under LA01 for: (a) 9V-PBPD-A-Pin; and (b) 9V-PBPD-A-Rigid Frames.

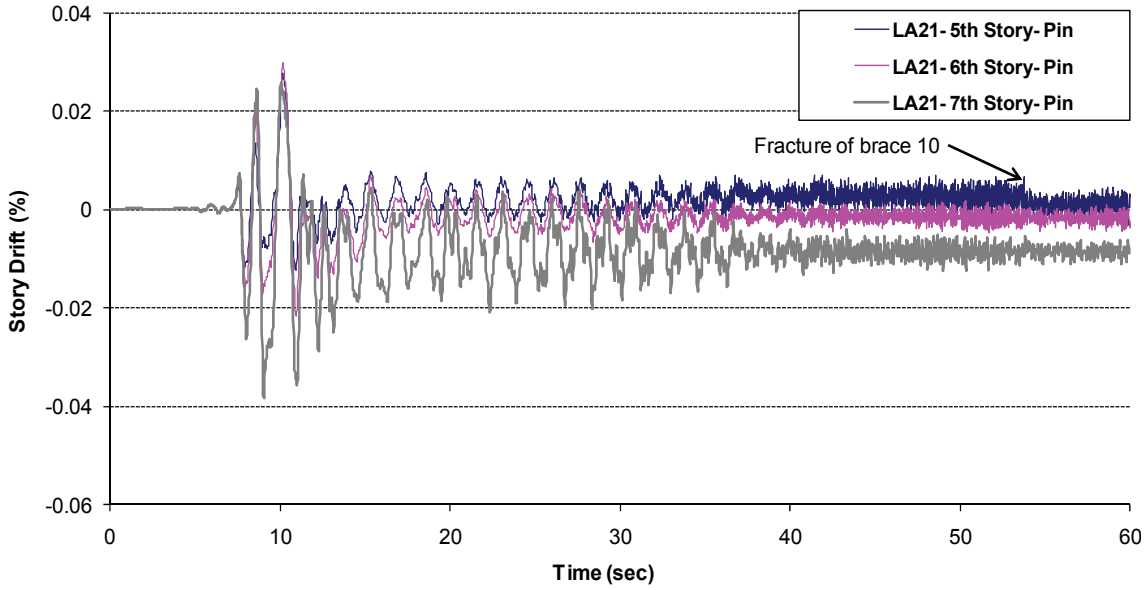

(a)

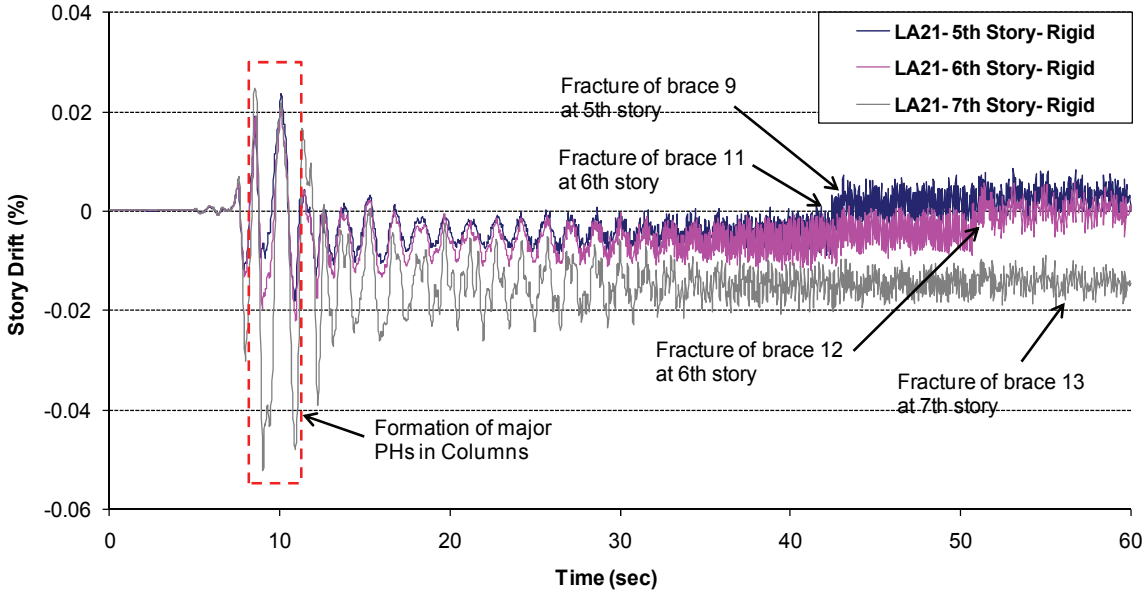

(b)

Figure 5.27. Sequence of Brace Fractures and PH Formation under LA21 for: (a) 9V-PBPD-A-Pin; and (b) 9V-PBPD-A-Rigid Frame.

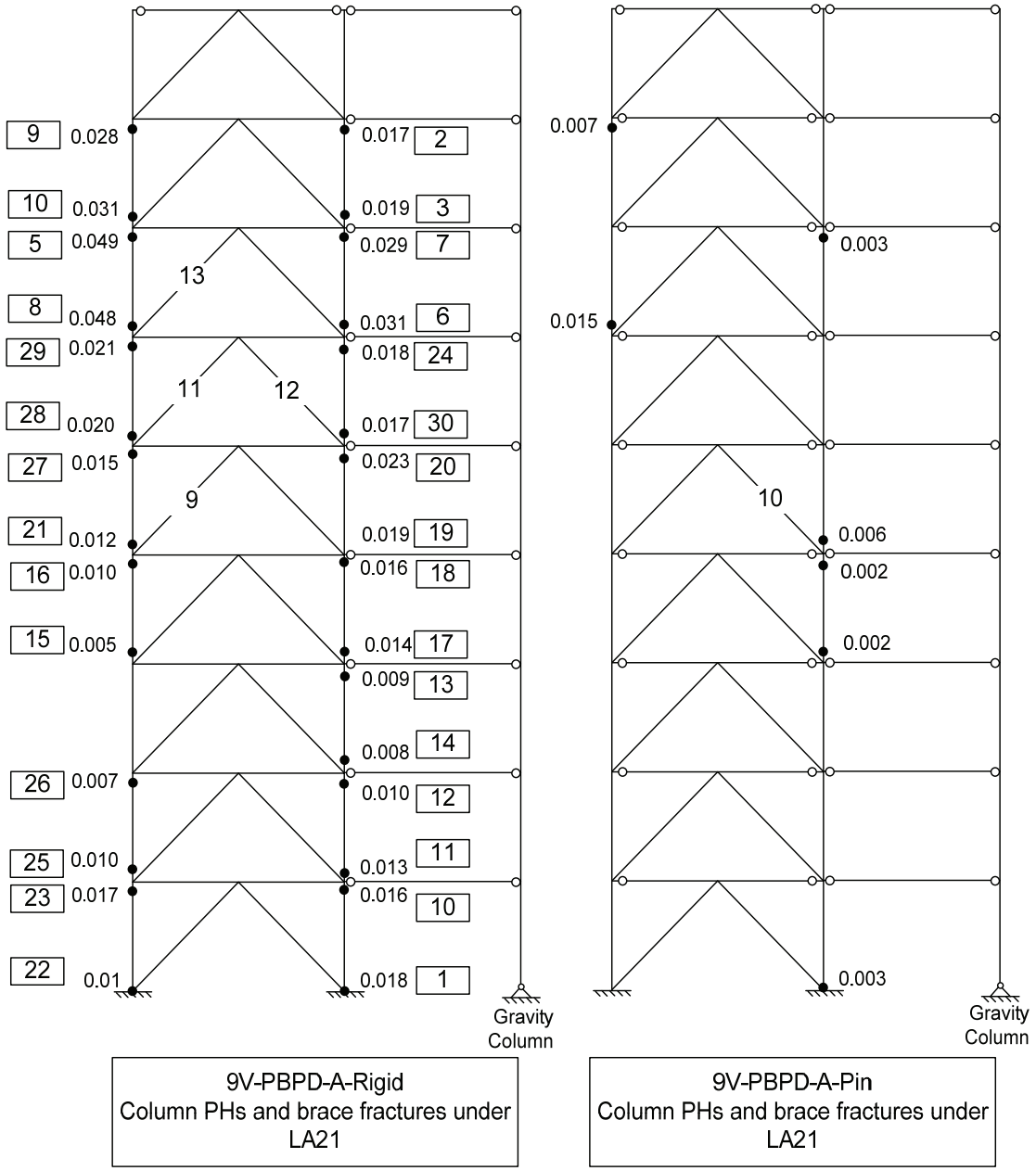

(a) (b)

Figure 5.28. Column PHs and Brace Fractures under LA21 for: (a) 9V-PBPD-A-Pin; and (b) 9V-PBPD-A-Rigid Frames.

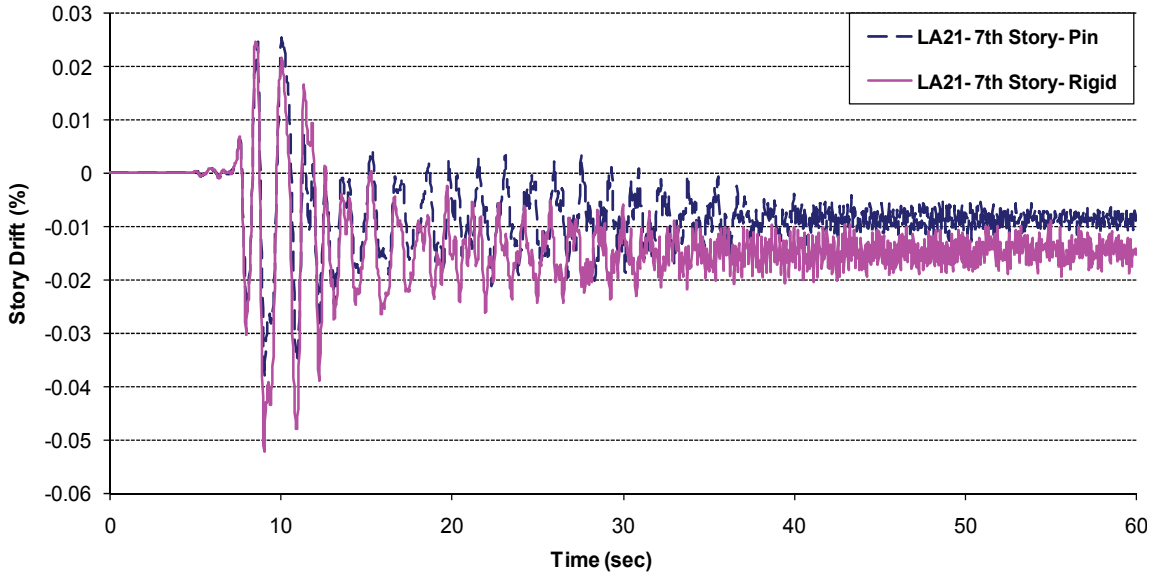

Figure 5.29. Larger Residual Drift for Model with Rigid Connections under LA21.

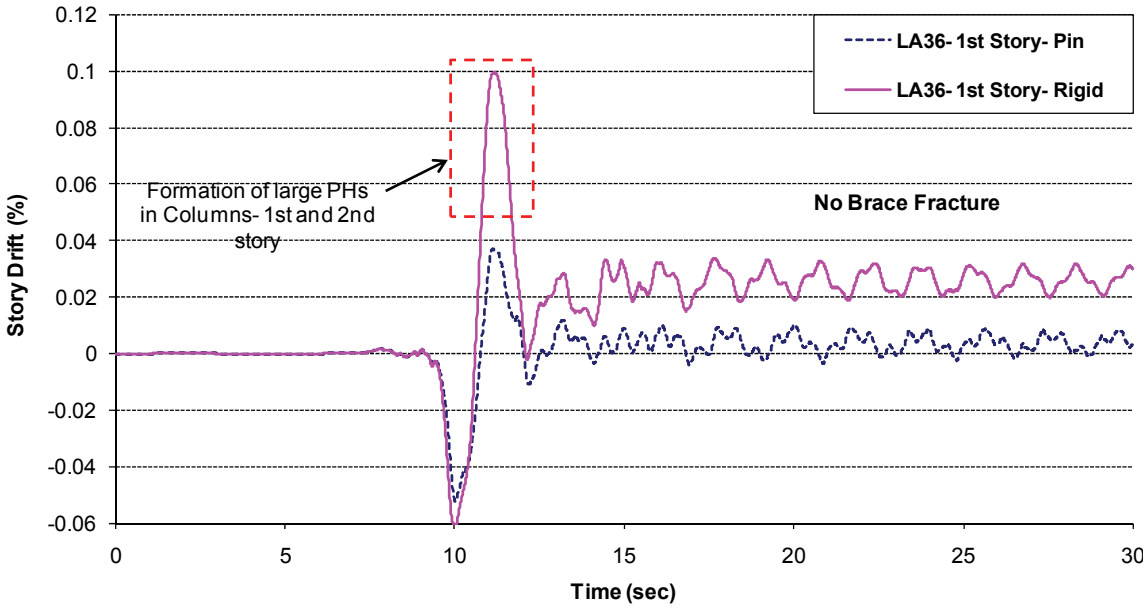

(a)

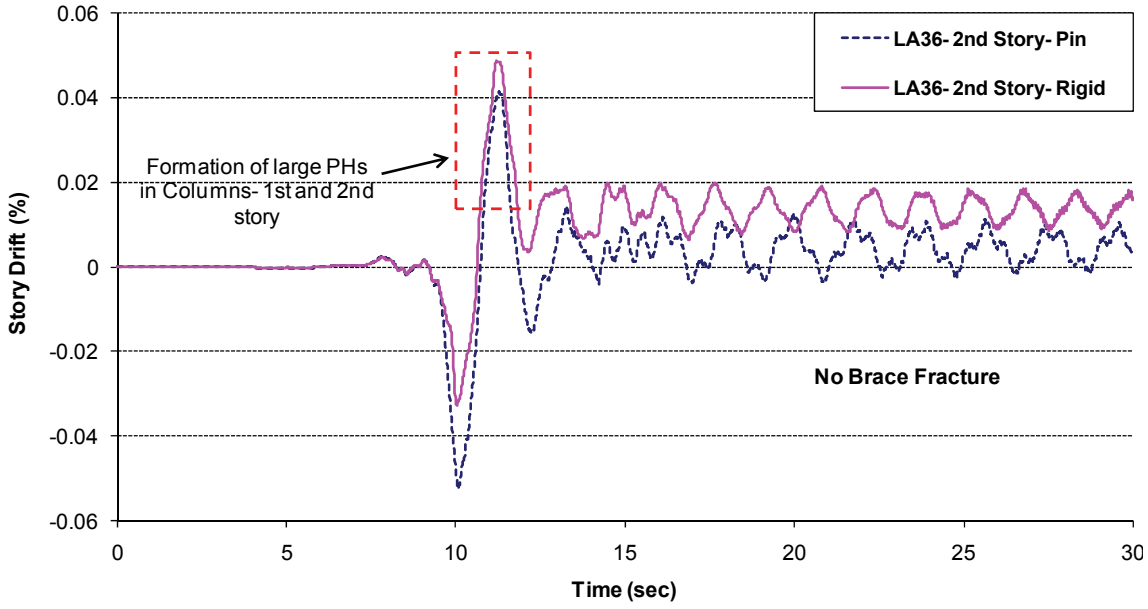

(b)

Figure 5.30. Significant Column PH Formation and Larger Residual Drift under LA36 for 9V-PBPD-A-Rigid Frame.

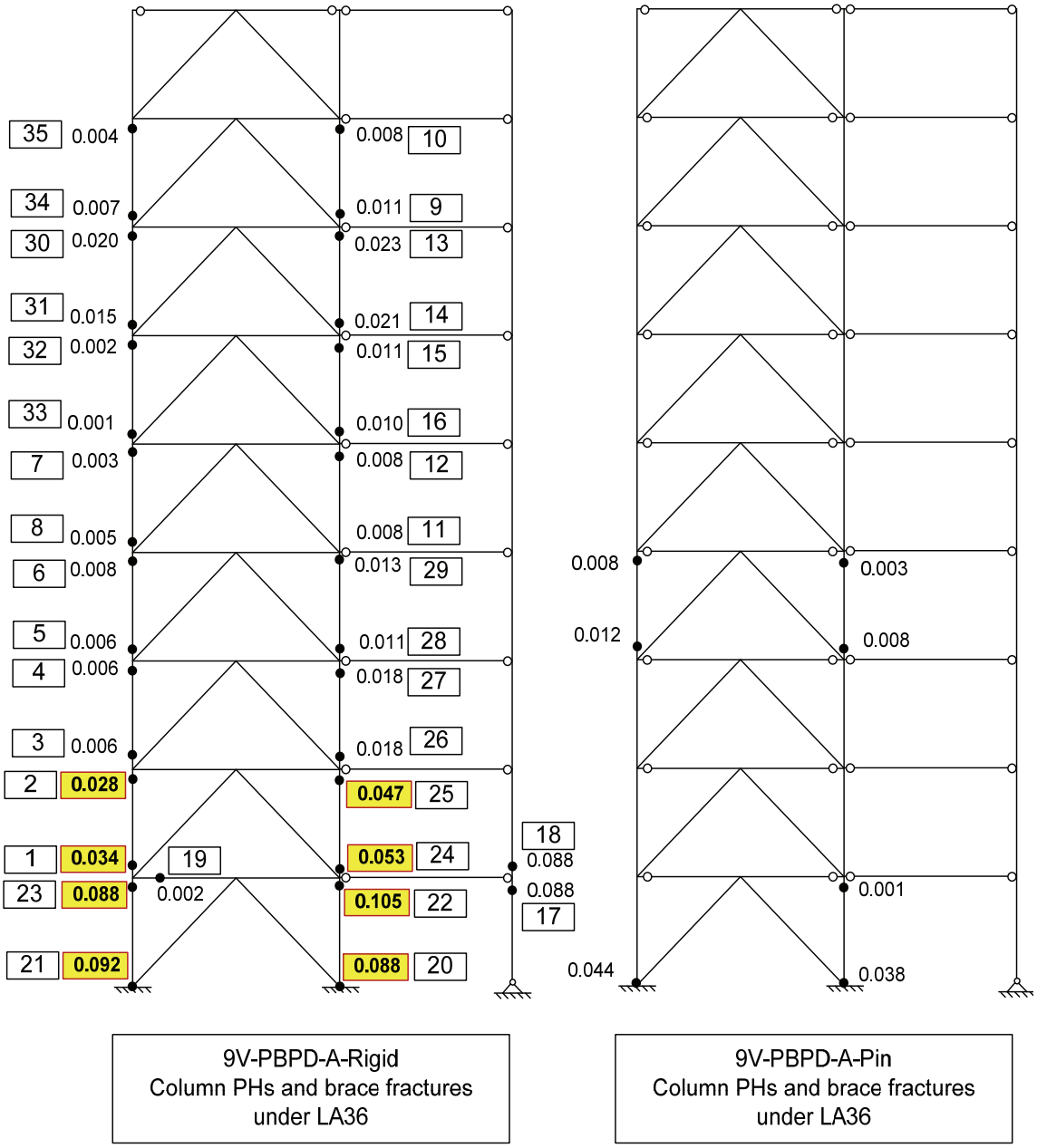

(a) (b)

Figure 5.31. Column PHs under LA36 for: (a) 9V-PBPD-A-Pin; and (b) 9V-PBPD-A-Rigid.

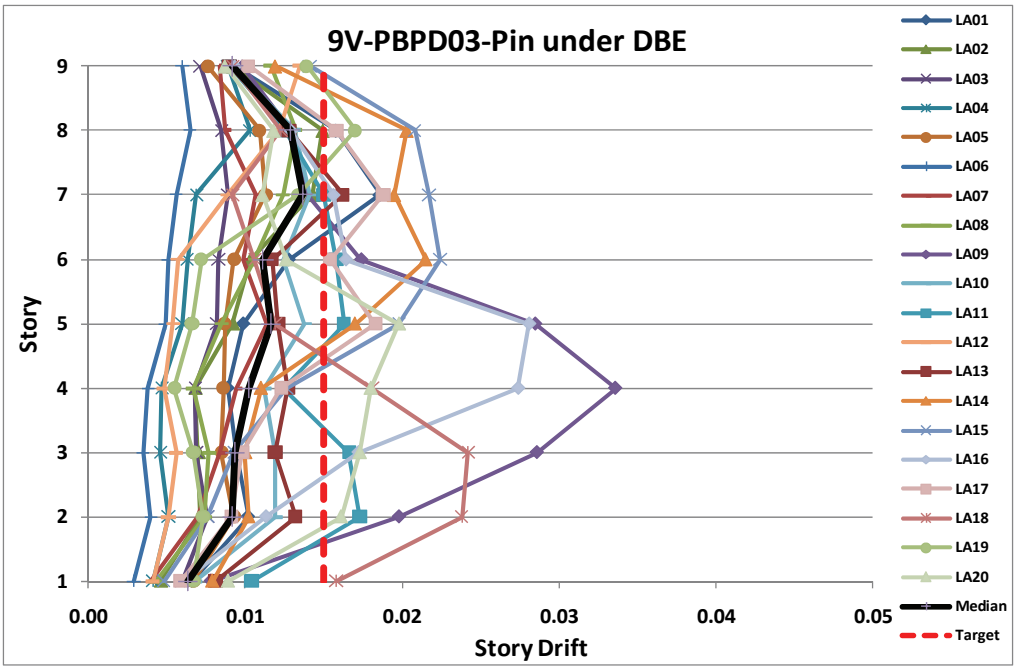

(a)

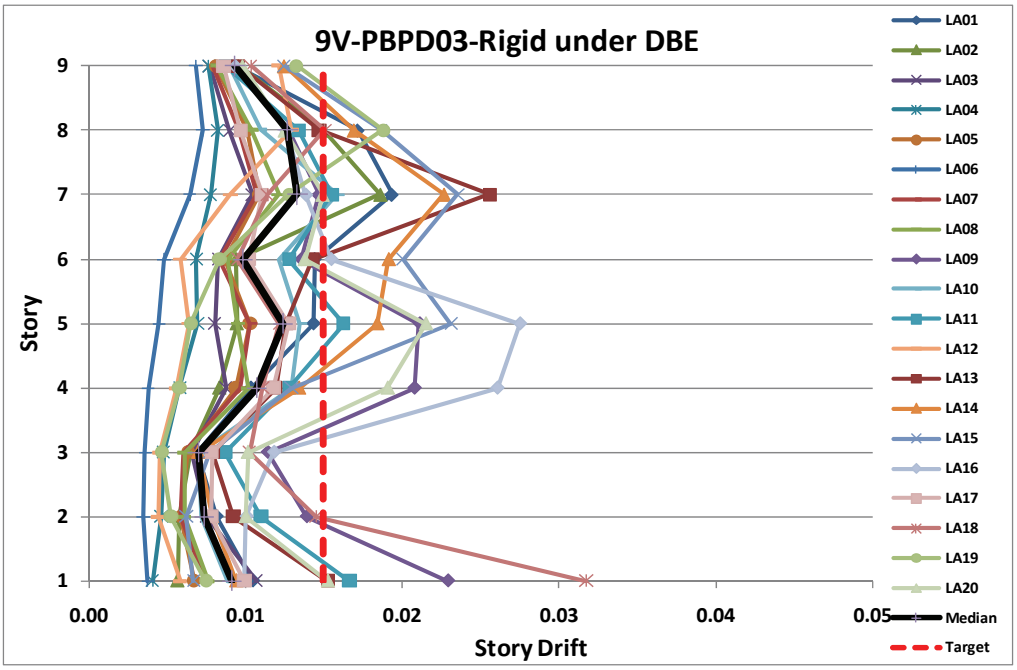

(b)

Figure 5.32. Pin and Rigid Models under SAC LA 2/3MCE Ground Motions.

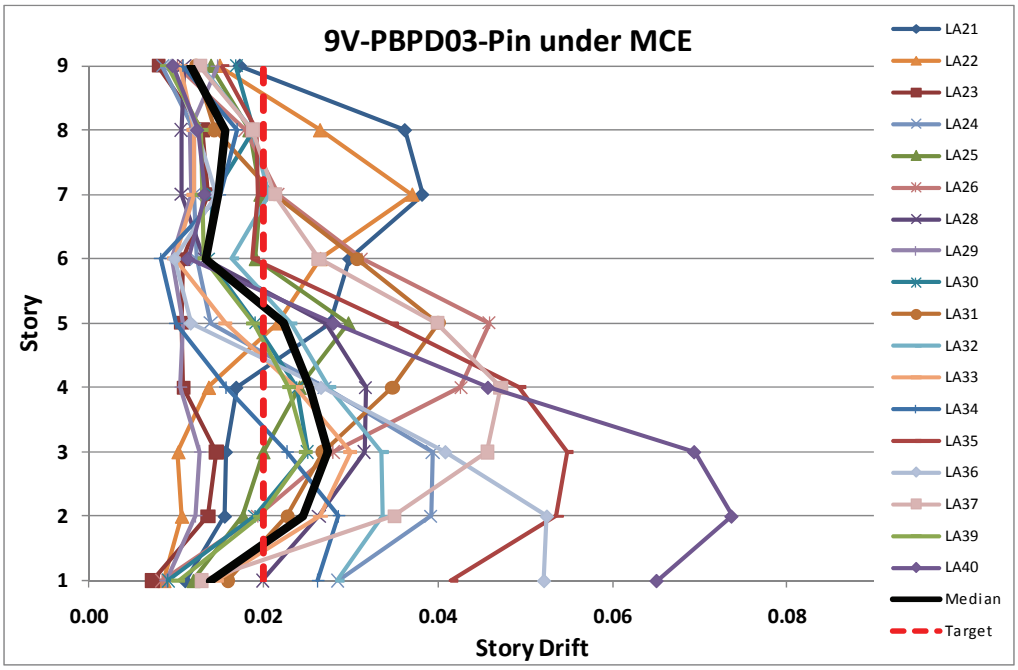

(a)

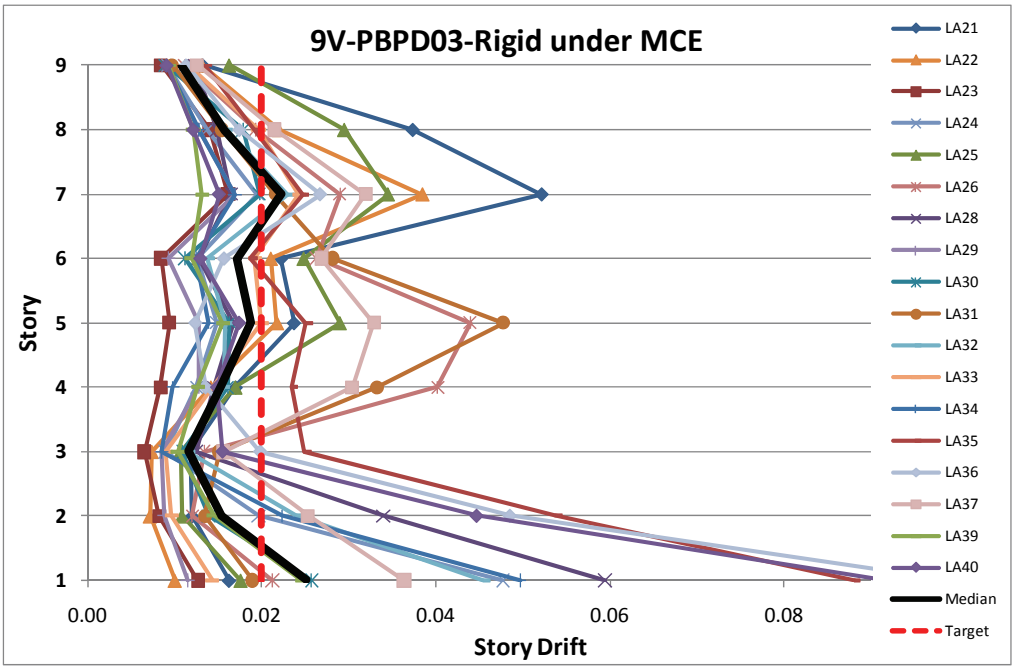

(b)

Figure 5.33. Pin and Rigid Models under SAC LA MCE Ground Motions.

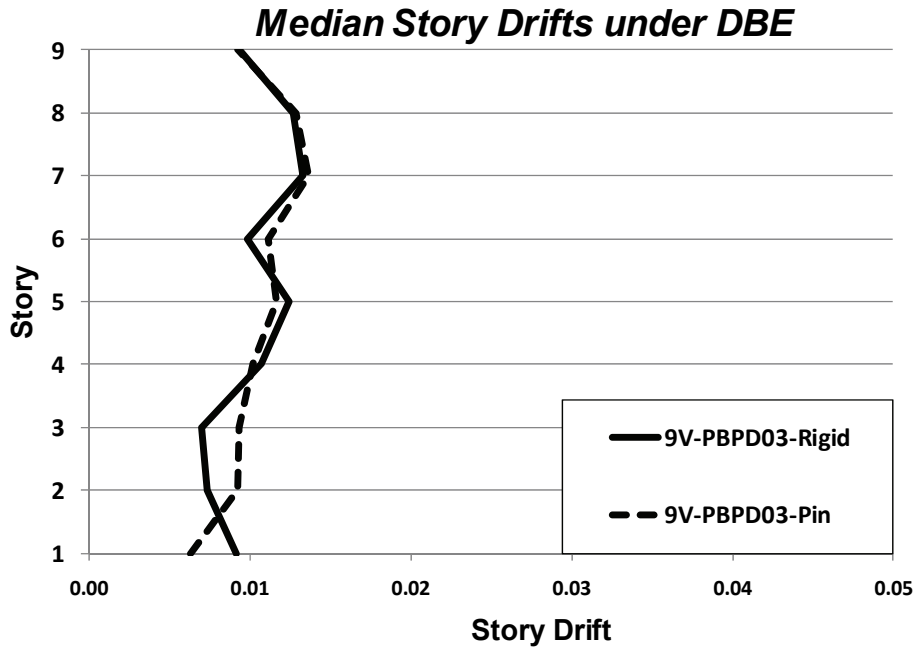

(a)

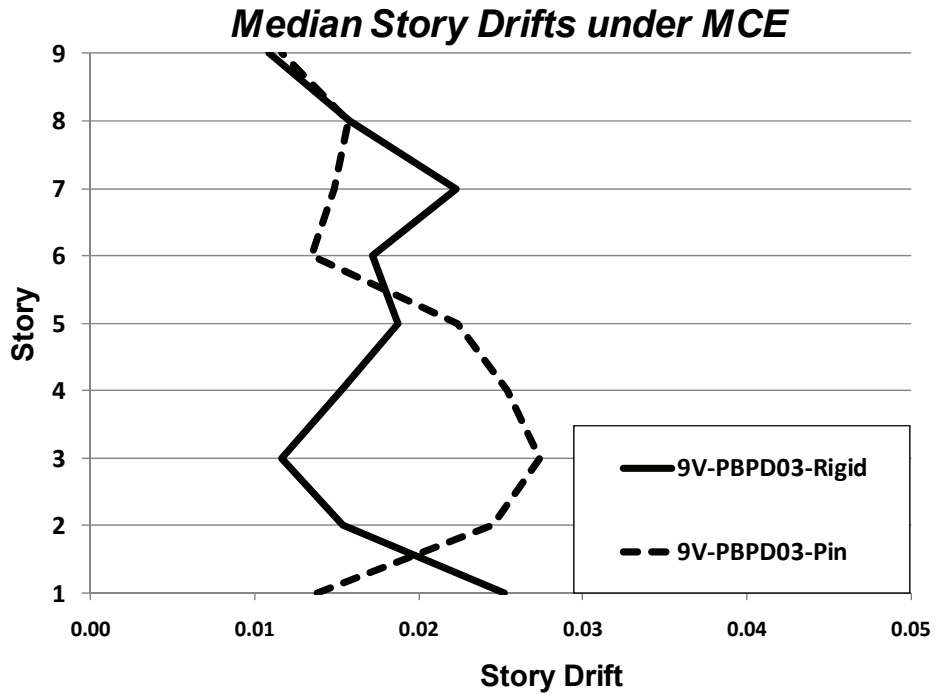

(b)

Figure 5.34. Story Drift Values under 2/3MCE and MCE Hazard Levels.

Table 5.21. Comparison of LA21 and LA36 Ground Motion Parameters.

Ground Motions	Duration (sec)	PGA
LA21- 1995 Kobe	59.98	1.282g
LA36- Elysian Park (simulated)	29.99	1.101g

5.9 Evaluation of Confidence Level of 9V-PBPD-A Against Collapse

In this section, the FEMA 351 (FEMA, 2000b) performance evaluation procedure explained in Chapter 4 is applied to 9-story model of 9V-PBPD-A in order to obtain its confidence level against collapse. The procedure and ground motions used are identical to those of Chapter 4. The IDA analyses were carried out using SNAP-2DX program. P-Delta effects in dynamic analyses were considered by modeling a lumped gravity column rigidly connected to the braced frame.

The analysis uncertainty parameters for the 9-story frame were considered similar to the 6-story frame, as shown in Table 5.22 and Table 5.23. It should be noted that the values previously obtained for 3 and 6-story frames in Chapter 4 are shown in these tables again for comparison purposes. Figure 5.35 shows the IDA curves for the 9V-PBPD-A frame under LA21 to LA40 ground motions. Table 5.24 shows summary of confidence level evaluation results. It can be the confidence level for 9V-PBPD-A frame is about 52% is not quite satisfactory when compared to the superior confidence levels of 3V-PBPD and 6V-PBPD frames. This low confidence level can be attributed to relatively

smaller median drift capacity as well as larger median drift demand for the 9-story PBPD frame, as shown in Table 5.24. Larger drift demands in the 9-story are partly caused by the presence of larger P-Delta effects. This issue is addressed in Chapter 6 and proper modifications are suggested to improve the confidence level of the 9-story CBF, to about the level of 6V-PBPD.

Table 5.22. Analysis Uncertainty Parameters.

Study Frames	C_B	β_{DU}	γ_a
3V-NEHRP	1.0	0.15	1.03
3V-PBPD	1.0	0.15	1.03
6V-NEHRP	1.0	0.20	1.06
6V-PBPD	1.0	0.20	1.06
9V-PBPD-A	1.0	0.20	1.06

Table 5.23. Randomness and Uncertainty Parameters.

Frame	β_{RC}	ϕ_{RC}	β_{UC}	ϕ_{UC}	β_{RD}	β_{UT}
3V-NEHRP	0.537	0.649	0.15	0.967	0.890	0.30
3V-PBPD	0.394	0.793	0.15	0.967	0.545	0.30
6V-NEHRP	0.435	0.753	0.20	0.942	0.663	0.35
6V-PBPD	0.412	0.775	0.20	0.942	0.708	0.35
9V-PBPD-A	0.309	0.866	0.20	0.942	0.515	0.35

*β_{RC}: standard deviation of natural logs of drift capacities due to randomness
*β_{UC}: standard deviation of natural logs of drift capacities due to uncertainty
*β_{RD}: standard deviation of natural logs of drift demands due to randomness
*β_{UT}: vector sum of logarithmic standard deviations for both demand and capacity considering all sources of uncertainty

Table 5.24. Summary of Confidence Level Assessment for 3, 6, and 9-Story CBFs.

Frame	Median Drift Capacity (from IDA) C	Capacity factor ϕ	Median Drift Demand D	Demand factors		Confidence Parameter $\lambda = \frac{\gamma \cdot \gamma_a \cdot D}{\phi \cdot C}$	Confidence Level (%)
				γ	γ_a		
3V-NEHRP	0.064	0.628	0.068	3.37	1.06	6.04	**<< 1%**
3V-PBPD	0.078	0.766	0.015	1.56	1.06	0.41	**> 99.9%**
6V-NEHRP	0.065	0.709	0.035	1.93	1.06	1.55	**23.3%**
6V-PBPD	0.100	0.730	0.027	2.12	1.06	0.82	**86.2%**
9V-PBPD-A	0.062	0.816	0.0376	1.49	1.06	1.180	**52.1%**

*ϕ: resistance factor that accounts for the randomness and uncertainty in estimation of structural capacity
*γ: demand uncertainty factor
*γ_a: analysis uncertainty factor

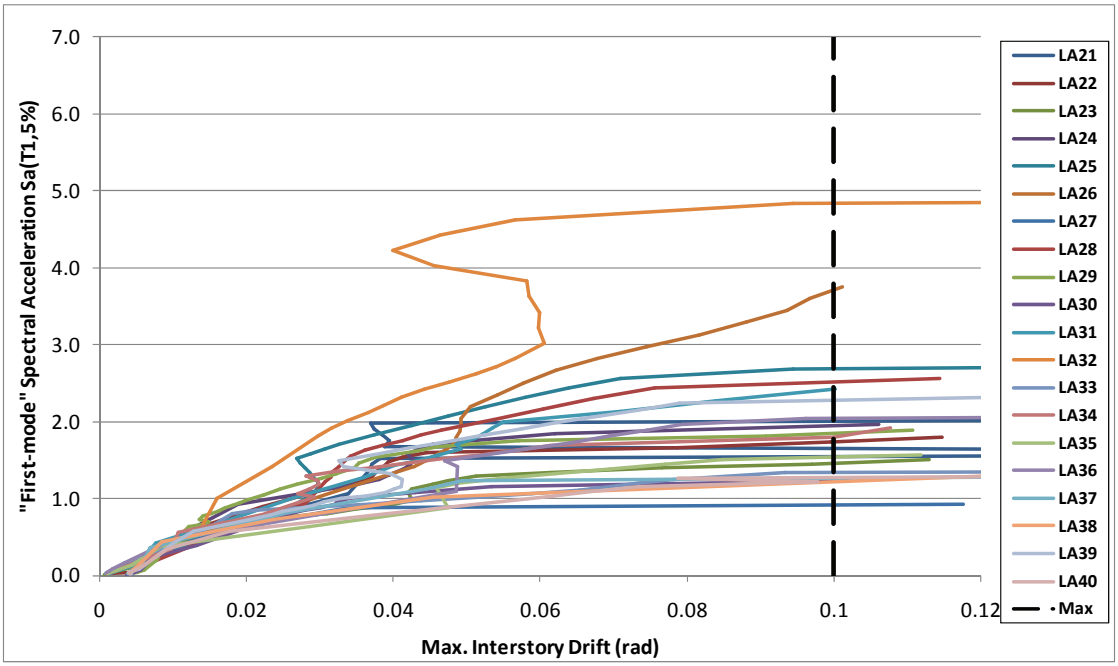

Figure 5.35. IDA Curves for 9V-PBPD-A Frames under 2%/50yrs SAC Ground Motions.

CHAPTER 6

CONFIDENCE LEVEL ENHANCEMENT OF THE 9-STORY CBF DESIGNED BY PBPD METHOD

6.1 Introduction

As was presented in Chapter 5, somewhat low confidence level (C.L.) of 52% against collapse was obtained for the 9V-PBPD-A frame designed by the procedure described in Sections 5.4 to 5.6, even though the story drifts where within drift limits under design level ground motions. It should also be noted that the C.L. for the 3- and 6-story PBPD frames were excellent with values of 99.9% and 86%, respectively (see Table 4.4).

The main objective in this chapter is to further improve the C.L. of the 9-story CBF (as a representative of mid-rise CBF systems) against collapse. Modifications to improve the C.L. are suggested. These include modification in the PBPD design base shear (DBS) calculation for taller CBF by revising the λ-factor, and considering alternate brace configuration of two story X-pattern (Split-X). Also, the effect of increasing the brace fracture life, N_f, on the C.L. is studied (Bayat, Goel, and Chao, 2010).

In general, the main design objectives in the calculation of the required PBPD design base shear are: 1) not exceeding the targeted story drifts under design level ground motions; 2) minimizing potential for collapse under MCE ground motions; 3) achieving satisfactory C.L. against collapse.

Lower C.L. observed for 9V-PBPD-A (compared to 3V-PBPD and 6V-PBPD) is believed mainly to be due to somewhat low value of DBS used in the design. Therefore, the main focus in this chapter is to suggest way to calculate suitable value of DBS that would result in improved C.L. against collapse. In addition, the effect of using Split-X configuration, as well as that of increased N_f on the C.L. are investigated.

6.2 New λ-Factor

The λ-factor approach was introduced in Chapter 5, for calculation of design base shear in the PBPD procedure for CBF structures. In this method, the effective target drift is obtained by dividing actual target drift by an appropriate value of λ-factor. This effective target drift is then used along with the modified yield drift (adjusted for column axial deformations) to obtain the effective ductility of the equivalent Elastic-Plastic SDOF system. The PBPD design base shear is then obtained by using this effective ductility.

As was also mentioned in Chapter 5, the estimation for λ-factor in that chapter was an initial attempt. By careful assessment of the parameters involved in the DBS calculation, and also based on observations on the seismic performance and confidence level of the 9V-PBPD-A frame, it was realized that the estimation of λ-factor, as used in Chapter 5 (Figure 5.13), can be improved in order to enhance the seismic response of longer period taller CBFs.

The P-Delta effect was not directly accounted for in DBS calculation. In the case of 9V-PBPD-A, the P-Delta forces were later added for the design of braces in order to

indirectly capture this second order effect. An alternate method to account for the P-Delta effects can be through suitable modification of the λ-factor, in a way that reflects this effect. By following such approach, enhanced response can be achieved through calculation of appropriate design base shear from the very beginning of the design process.

Therefore, a new and slightly different estimation of λ-factor is proposed here. Figure 6.1 shows this new λ-factor along with the one previously used in Chapter 5. As can be seen, the main difference between the two is for periods larger than 0.7 second which corresponds to mid to high-rise CBF systems. Table 6.1 shows the values of the new λ-factor as a function of T.

Also as can be seen in Figures 6.1 to 6.3, the λ-factor value for periods longer than 1.0 sec is selected to be 1.10 in order to compensate for the P-Delta effect. As a result, it is expected that the new λ-factor would affect mainly the design of mid-rise to high-rise CBF systems.

Figure 6.2 shows comparison between the new λ-factor and the suggested C_2 values from FEMA 356 (2000a). As can be seen, the new λ-factor gets closer to the values suggested for Collapse Prevention by FEMA 356 in the range of mid-rise CBFs (T= 0.5 ~ 0.75 second) and comes closer to the values suggested for Life Safety for longer periods. However, such comparison may not be quite fair since the new λ-factor accounts for P-Delta effects, potential brace fractures, as well as pinched hysteretic behavior, whereas the C_2 factor of FEMA 356 accounts for the latter only.

As shown in Figure 6.3, the new λ-factor does not exactly follow the mean of displacement ratio for the set of ground motions for stiffness degrading (SD) systems. The reasons are: 1) The mean was obtained for SDOF systems; 2) It does not include the effect of brace fractures; 3) It does not capture P-Delta effect for longer period frames. However, the proposed λ values in general follow the trend of the mean ratios.

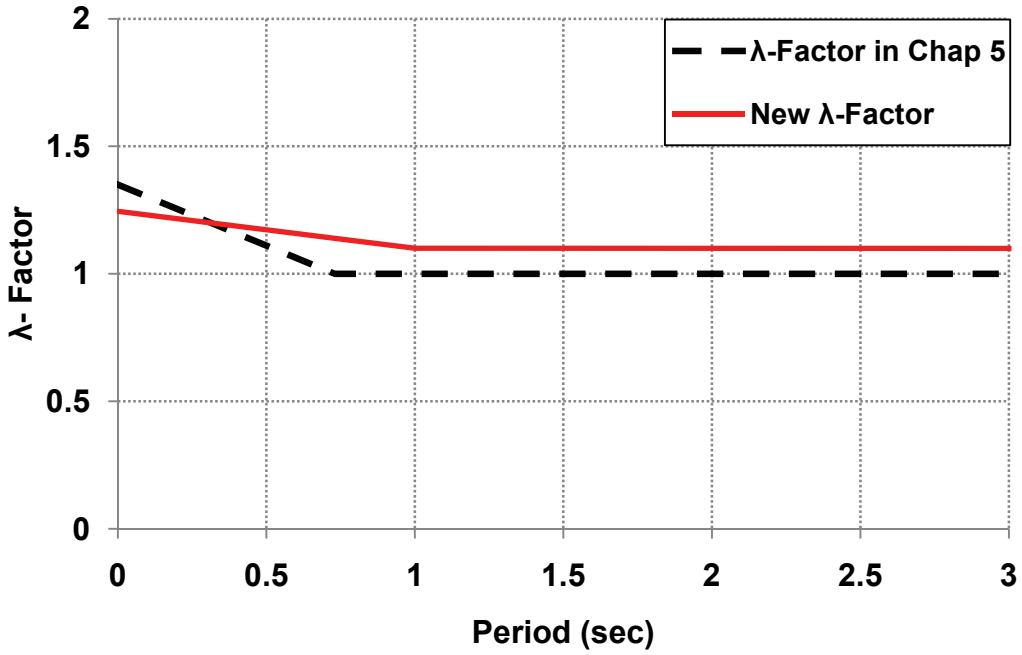

Figure 6.1. New λ-Factor versus λ-Factor used in Chapter 5.

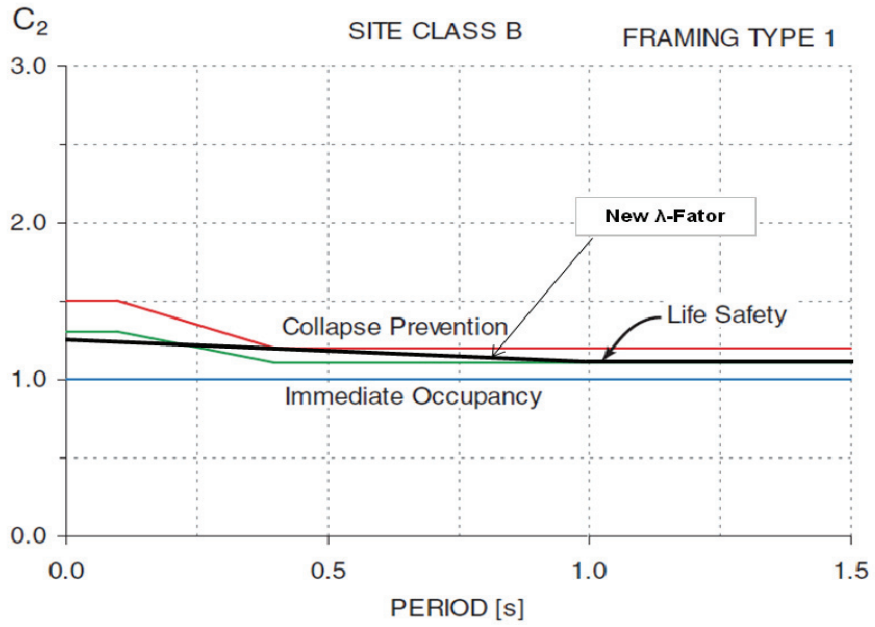

Figure 6.2. Comparison of the New λ-Factor with C_2 values in FEMA 356 (2000).

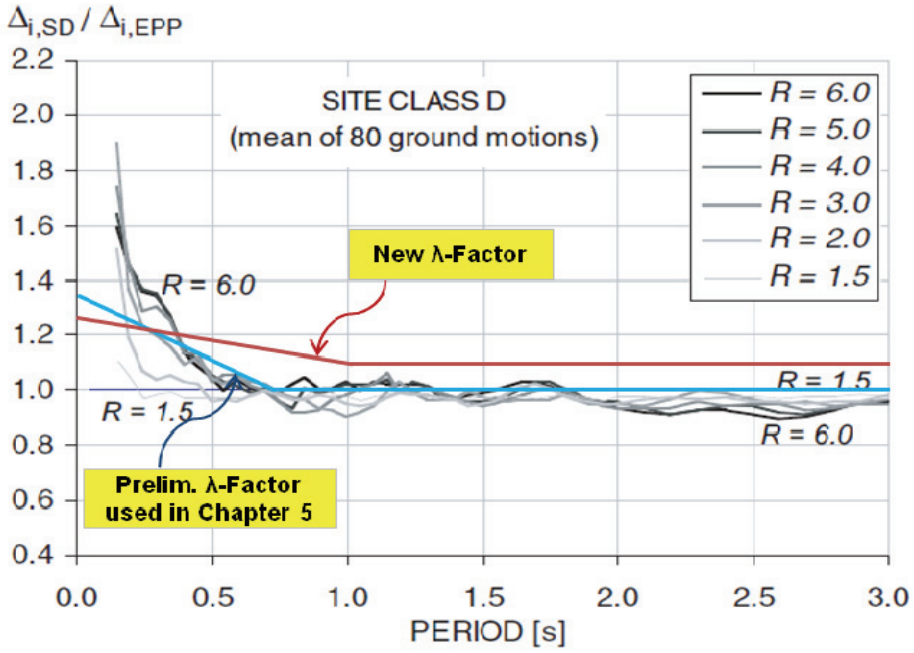

Figure 6.3. New λ-Factor Values for CBF versus Mean Displacement Ratios Obtained by Ruiz-Garcia and Miranda (2005).

Table 6.1. New λ-Factor Values as Function of T.

$0 \le T \le 1.0$ sec	$T > 1.0$ sec
$\lambda = -0.145T + 1.245$	$\lambda = 1.10$

Calculated *V/W* values by using the new λ-factor are shown and compared with the previous values from Chapter 5 in Figure 6.4 and Tables 6.2 and 6.3. As shown, the percentage increase in the DBS using new λ-factor versus λ-factor in Chapter 5 increases with the period. Considering the case of $k = 0.5$, the DBS for 3-story frame is almost the same with the new λ-factor. DBS increases by 14% for 6-story frame, 32% for 9-story frame, and 25% for 18-story frame.

It should also be mentioned that the DBS for 3 and 6-story frames are almost similar to the previous values obtained in Goel and Chao (2008).

The Advantages of using this new λ-factor include:

a) Achieving real dual hazard level design for DBE and MCE, meaning for example DBS for DBE level would result in a structure that would satisfy the DBE performance requirements, i.e., targeted drifts, very limited or no brace fracture.

b) When MCE level governs the DBS, that value should be used to satisfy the performance objectives selected for both levels. That has also been found to result in enhanced C.L. against collapse. If one chooses to only satisfy the DBE level requirements, design can be based on DBE base shear alone.

c) Any value of the *k* factor (for lateral force distribution) between 0.5 and 0.75 can be used. However, it is recommended that for taller frames smaller value be used, which results in smaller drifts in the upper stories.

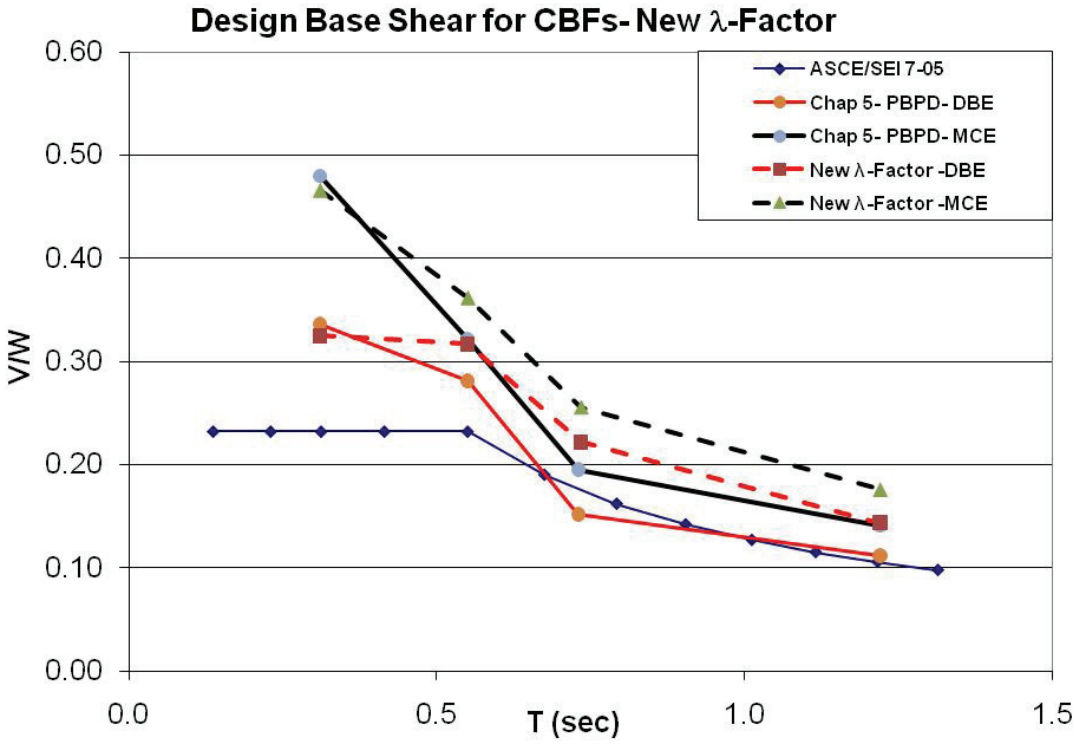

Figure 6.4. Comparison of Design Base Shear from PBPD versus ASCE/SEI 7-05 (values obtained using *k = 0.75*).

Table 6.2. PBPD Design Base Shear using *k = 0.75*.

Frame	Period T (sec)	λ-factor in Chap 3		New λ-factor		$(V/W)_{New\ \lambda} / (V/W)_{\lambda\ in\ Chap\ 3}$
		DBE	MCE	DBE	MCE	
3V	0.31	0.336	0.480	0.325	0.466	0.97
6V	0.55	0.281	0.322	0.317	0.362	1.12
9V	0.734	0.166	0.195	0.222	0.256	1.31
18V	1.22	0.111	0.141	0.144	0.176	1.25

Table 6.3. PBPD Design Base Shear using $k = 0.50$.

Frame	Period T (sec)	λ-factor in Chap 3		New λ-factor		$(V/W)_{New\ \lambda} / (V/W)_{\lambda\ in\ Chap\ 3}$
		DBE	MCE	DBE	MCE	
3V	0.31	0.311	0.447	0.305	0.438	0.98
6V	0.55	0.260	0.298	0.296	0.337	1.13
9V	0.734	0.154	0.180	0.206	0.237	1.32
18V	1.22	0.103	0.130	0.134	0.163	1.25

6.3 Re-Design of the 9-Story CBF (9V-PBPD-B)

The 9-story SAC building with Chevron CBF as described in Chapter 5 is redesigned in this section. The main differences of this design compared with the previous design in Chapter 5 are: (1) Modified DBS is used here by using the new λ-factor; (2) Six braced bays in each direction are used in this design instead of four bays in the 9V-PBPD-A, Figure 6.5.

Value of $k = 0.5$ was used for the lateral distribution parameter. As can be seen from Table 6.3, the MCE design base shear governs the design. Hence, $V/W = 0.237$ for the MCE hazard was used for the design. Lateral design forces, selected sections for the braces, beams and columns along with the fracture life of braces are given in Tables 6.4, 6.5, and 6.6, respectively.

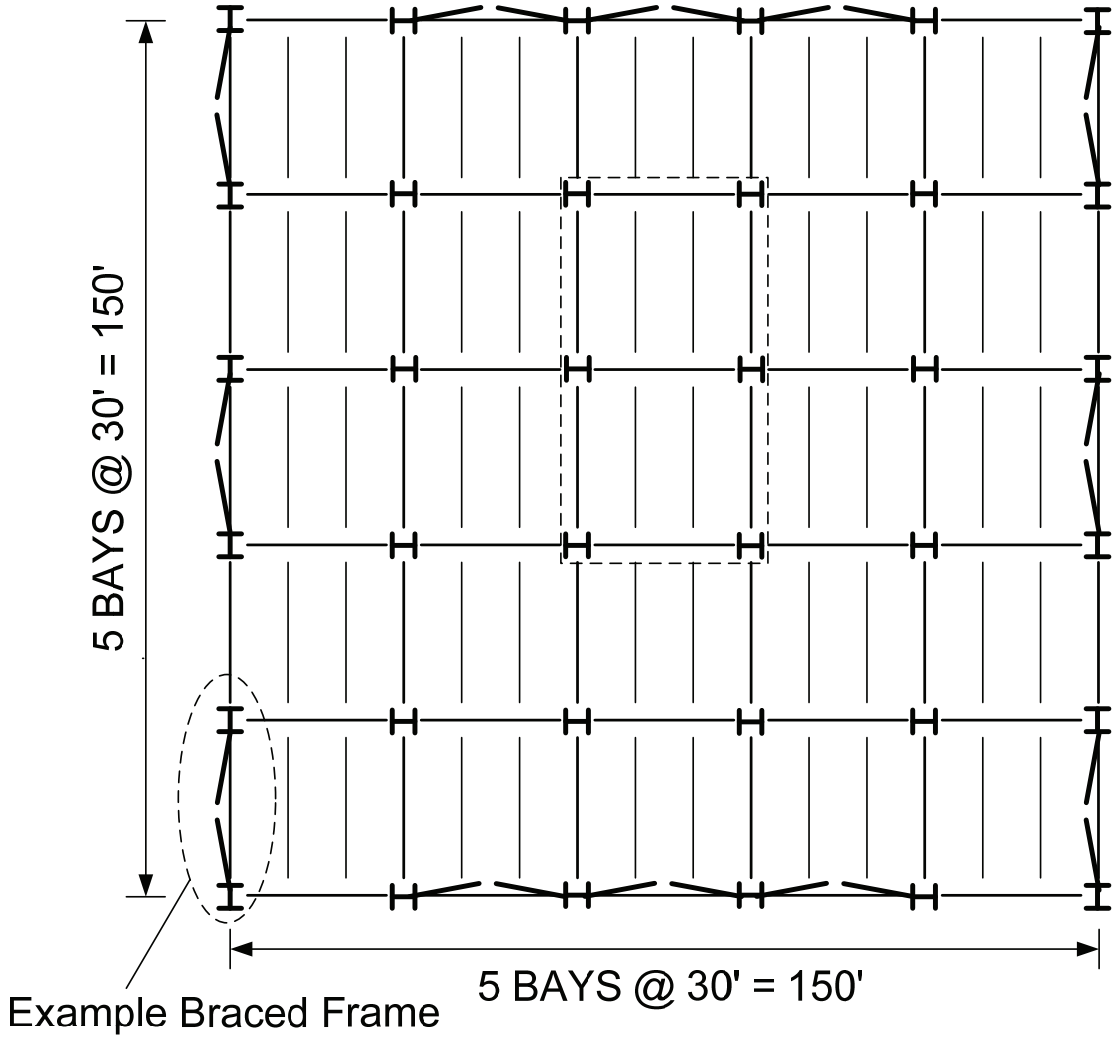

Figure 6.5. Plan View of 9-Story SAC Building: 9V-PBPD-B Design.

Table 6.4. Lateral Force Distribution ($k = 0.50$) for 9V-PBPD-B.

Floor	F_i (kips)	F_i (kips)	Story Shear (kips)
	Full Structure	one CBF	one CBF
9	1356.9	339.2	339.2
8	513.7	128.4	467.6
7	365.8	91.5	559.1
6	278.2	69.6	628.6
5	215.1	53.8	682.4
4	164.7	41.2	723.6
3	121.7	30.4	754.0
2	83.2	20.8	774.8
1	48.3	12.1	786.9

Table 6.5. Required Brace Strength and Selected Sections for 9V-PBPD-B.

Floor	***α***	***Vi/0.9cos(α)*** **kips**	**Brace Section**	**Strength** $P_y+0.5P_{cr}$	**Area** in^2	F_{cr} ***ksi***	$0.5P_{cr}$ ***kips***	P_y ***kips***	N_f
9	41	499	**2HSS4×4×5/16**	500	8.2	29.93	122.7	377.2	152
8	41	688	**2HSS4-1/2x4-1/2x3/8**	683	10.96	32.67	179.0	504.2	157
7	41	823	**2HSS4-1/2x4-1/2x1/2**	861	13.9	31.83	221.2	639.4	329
6	41	926	**2HSS5×5×1/2**	997	15.76	34.49	271.8	725.0	224
5	41	1005	**2HSS5×5×1/2**	997	15.76	34.49	271.8	725.0	224
4	41	1065	**2HSS6×6×1/2**	1266	19.48	37.97	369.8	896.1	132
3	41	1110	**2HSS6×6×1/2**	1266	19.48	37.97	369.8	896.1	132
2	41	1141	**2HSS6×6×1/2**	1266	19.48	37.97	369.8	896.1	132
1	50	1360	**2HSS6×6×5/8**	1482	23.4	34.68	405.8	1076.4	245

Table 6.6. Design of Beams for 9V-PBPD-B.

Floor	w_u (k/ft)	R_yP_y	$0.5P_{cr}$	F_h	F_v	P_u	M_u	Beam Section
9	0.95	528.1	122.7	491.2	265.9	245.6	1785.2	**W36x135**
8	1.13	705.8	179.0	667.8	345.6	333.9	2310.0	**W40x167**
7	1.13	895.2	221.2	842.6	442.1	421.3	2925.4	**W40x199**
6	1.13	1014.9	271.8	971.1	487.6	485.5	3215.1	**W40x215**
5	1.13	1014.9	271.8	971.1	487.6	485.5	3215.1	**W40x215**
4	1.13	1254.5	369.8	1225.9	580.4	612.9	3807.0	**W40x249**
3	1.13	1254.5	369.8	1225.9	580.4	612.9	3807.0	**W40x249**
2	1.13	1254.5	369.8	1225.9	580.4	612.9	3807.0	**W40x249**
1	1.21	1507.0	405.8	1229.5	843.5	614.7	5492.0	**W40x324**

Table 6.7. Design of Columns for 9V-PBPD-B.

Floor	$P_{trans.}$	P_{beam}	$0.5P_{cr}Sin\ \alpha$	$0.5F_v$	P_u	P_u *(cumulative)*	Column Section
9	32.88	28.5	0	133	194	194	**W14x109**
8	37.56	33.9	81	173	325	519	**W14x109**
7	37.56	33.9	117	221	410	929	**W14x109**
6	37.56	33.9	145	244	460	1390	**W14x211**
5	37.56	33.9	178	244	494	1883	**W14x211**
4	37.56	33.9	178	290	540	2423	**W14x211**
3	37.56	33.9	243	290	604	3027	**W14x398**
2	37.56	33.9	243	290	604	3632	**W14x398**
1	37.56	36.3	243	422	738	4370	**W14x398**

6.4 Design of the 9-Story CBF with Split-X Configuration (9X-PBPD-B)

In this section, the effect of using Split-X brace configuration on seismic performance and also C.L. of the 9-story CBF is investigated. Other design assumptions such as pin ended beams, fixed base, and use of double HSS for braces are the same as before.

The design parameters are kept the same for this configuration as for chevron braced frame in the previous section. Therefore, the same MCE design base shear of $V/W=0.237$ applies and is used for this design as well. The same bracing members are used since the story shears are the same as the chevron configuration. However, much smaller unbalanced force on the beams, and therefore much lighter beam sections (more reasonable design) are obtained for the Split-X frame. Column sections remain about the same as in the Chevron design. The free-body diagrams used for capacity design of beams and columns are shown in Figure 6.6. Expected yield forces, R_yP_y, and post-buckling strength of braces, $0.5P_{cr}$, are considered in tension and compression, respectively, to obtain the design forces for beams and columns. P_L and P_R represent lateral forces due to other sources, such as frame action, inertia forces, etc. Those forces were assumed to be zero when designing beam case B. The same assumption was used for columns and only axial forces due to truss action were used for the design.

Important design parameters of different 9-story PBPD frames studied herein are given in Table 6.8.

Beam and column sections for the design with Split-X configuration, 9X-PBPD-B, are shown in Tables 6.9 and 6.10, respectively. It can be seen that the beams in two

different designs for Split-X configuration are significantly lighter than those of Chevron configuration. The column sections are almost the same, except in the 4th story where the Split-X design needed W14x398 based on capacity design requirements. The difference between 9X-PBPD-B and 9X-PBPD-B1 is just in their beam sizes, as will be discussed later in this section.

Generally, the performance of 9X-PBPD-B was found to be somewhat more stable than the Chevron design under MCE ground motions (e.g. 9V-PBPD-B frame showed dynamic instability under LA21 but 9X-PBPD-B frame did not.

The Split-X configuration (9X-PBPD-B frame) mainly involves axial behavior of all members, but the Chevron frame has significant flexural component, especially in the beams after buckling of the compression braces. That is why large beam sizes are needed in the Chevron frame.

As mentioned earlier, beams sizes in the Split-X configuration are considerably smaller compared to the Chevron configuration, making the Split-X frame lighter in weight. However, local inelastic activity, such as large beam plastic hinge rotation, was observed in the response of the 9X-PBPD-B frame, especially under MCE ground motions. Further investigation showed that it was due to small axial design forces for the beams. Nevertheless, local inelastic activity in the beams did not have much effect on the global behavior of the frame.

Larger beam sizes with higher strength and stiffness are needed to prevent or minimize such local inelastic activity. As shown in Table 6.9, W18x175 beam sections were used in the revised design at all floor levels except at the roof level (W36x135), and

the 1st floor beam which is W24x176 (due to larger vertical unbalanced forces). Use of those beam sizes successfully eliminated the local inelastic activity. The 9X-PBPD-B1 design was used for further evaluation. As shown in Table 6.10, the column sections are almost similar for the Chevron and Split-X configurations.

Larger unbalance forces on the beams than those obtained by capacity design considering free-body diagrams of Figure 6.6 were observed in the results from time history analyses. These unbalanced forces could cause plastic hinges at the mid-span of the beams in case B. However, formation of these plastic hinges did not affect the global drift response of the structure, as also observed by Lacerte and Tremblay (2006).

The results also imply that the assumed initial ultimate force pattern for capacity design of beams was unconservative. However, it should be mentioned that floor slabs, when present, do provide significant contribution to resist in-plane beam forces. Such contribution was neglected in this study. Final beam sections for the 9X-PBPD-B1 frame was done through some trial and error. More representative estimate of beam design forces in the Split-X configuration of CBF warrants further study.

Table 6.8. Different Designs/Models used for 9-story PBPD CBF.

9-Story CBF Designs	DBS	Brace Configuration	N_f	Notes
9V-PBPD-A*	Based on λ-factor in Chapter 3	Chevron	regular	
9V-PBPD-B	Based on New λ-factor	Chevron	regular	
9V-PBPD-B-Nf	Based on New λ-factor	Chevron	increased	Same as 9V-PBPD-B, only with increased N_f
9X-PBPD-B	Based on New λ-factor	Split-X	regular	Small beam sizes, showed local instability in beams (Table 6.9)
9X-PBPD-B1	Based on New λ-factor	Split-X	regular	Modified: only beam sized increased to W18x175 (Table 6.9)
9X-PBPD-B1-Nf	Based on New λ-factor	Split-X	increased	Same as 9V-PBPD-B, only with increased N_f

* Suffix A at the end of model designation indicates that design base shear is obtained by using the preliminary λ-factor in Chapter 5, whereas suffix B indicates that the design base shear is obtained using new λ-factor suggested in Chapter 6.

Table 6.9. Beam Sections for Different Designs.

Floor Level	Beam Sections		
	9V-PBPD-B	9X-PBPD-B	9X-PBPD-B1
Roof	W36x135	W36x135	W36x135
8	W40x167	W18x65	W18x175
7	W40x199	W27x84	W18x175
6	W40x215	W18x65	W18x175
5	W40x215	W18x65	W18x175
4	W40x249	W18x65	W18x175
3	W40x249	W18x65	W18x175
2	W40x249	W18x65	W18x175
1	W40x324	W24x176	W24x176

Table 6.10. Column Sections for Different Designs.

Story	Column Sections		
	9V-PBPD-B	**9X-PBPD-B**	**9X-PBPD-B1**
9	W14x109	W14x109	W14x109
8	W14x109	W14x109	W14x109
7	W14x109	W14x109	W14x109
6	W14x211	W14x211	W14x211
5	W14x211	W14x211	W14x211
4	W14x211	W14x398	W14x398
3	W14x398	W14x398	W14x398
2	W14x398	W14x398	W14x398
1	W14x398	W14x398	W14x398

Table 6.11. Different Fracture Life, N_f, Values Used.

9-story CBF Model / Story	9V-PBPD-B 9X-PBPD-B1 (regular N_f)	9V-PBPD-B-Nf 9X-PBPD-B1-Nf (increased N_f)
9	152	237
8	157	237
7	329	329
6	224	224
5	224	224
4	132	227
3	132	227
2	132	227
1	245	245

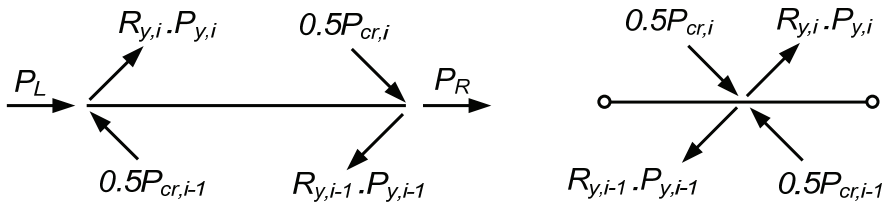

a) b)

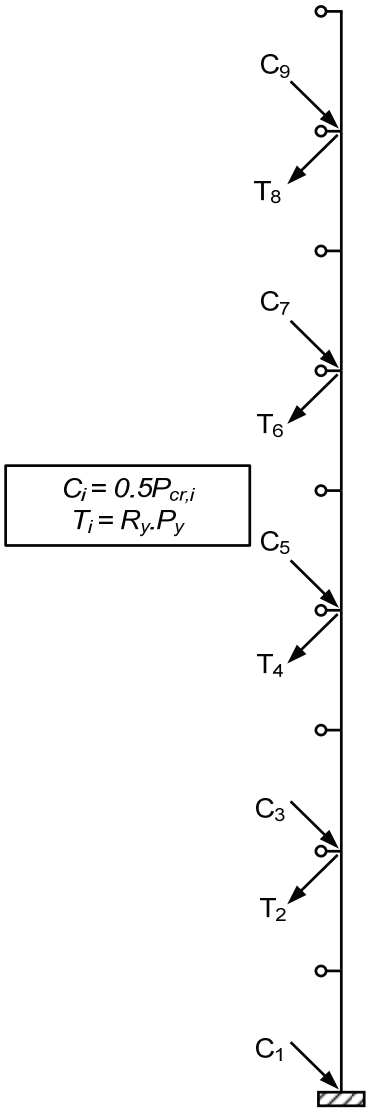

(c)

Figure 6.6. Capacity Design of Beams and Column in Split-X Configuration: (a) Beam, Case A; (b) Beam, Case B; and (c) Column Tree.

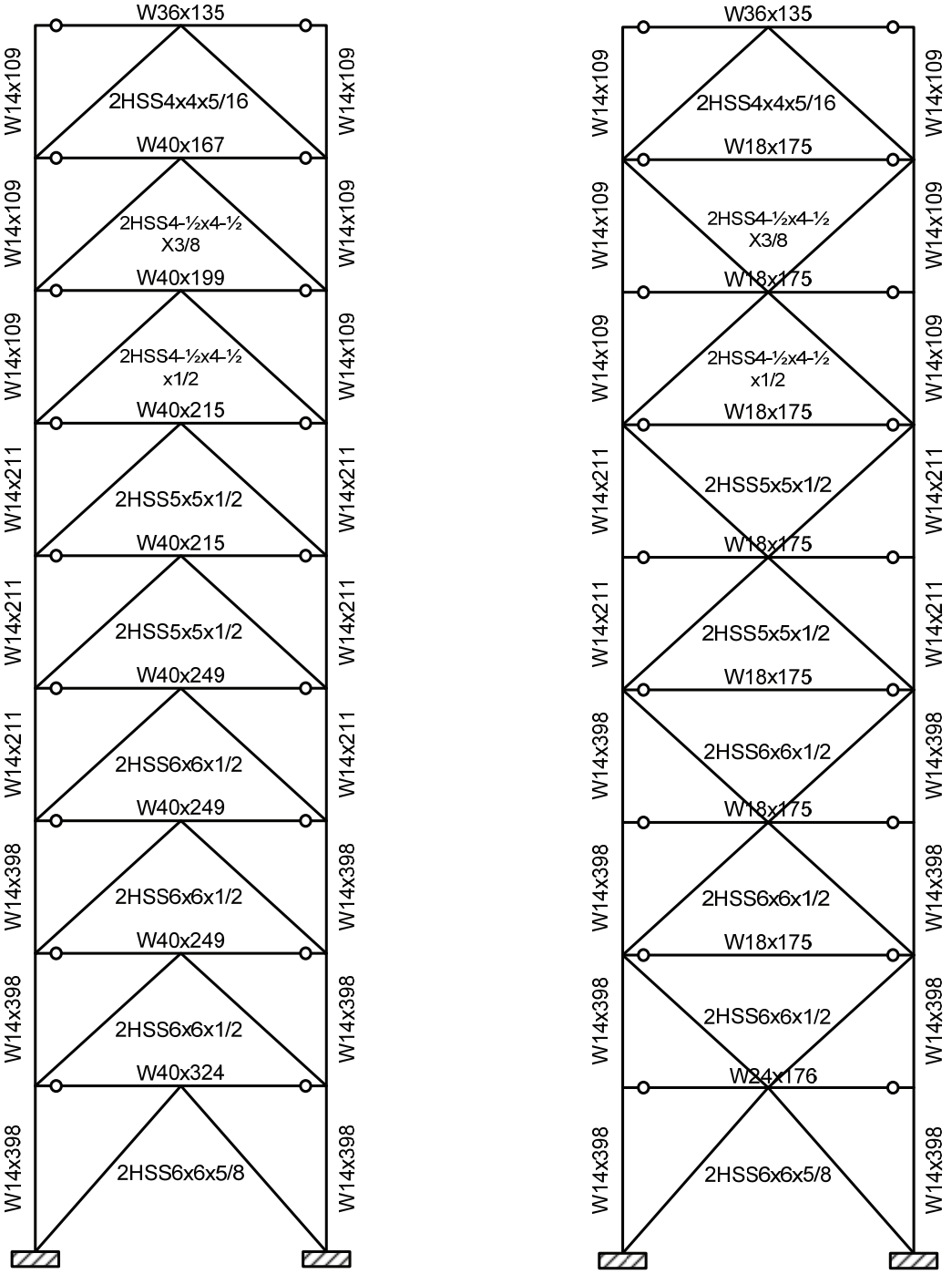

Figure 6.7. Member Sections for 9-Story CBF Designed by PBPD: (a) Chevron Configuration; and (b) Split-X Configuration.

6.5 Evaluation of Seismic Performance

In this section, performance of the 9V-PBPD-B and 9X-PBPD-B1 frames (designed by using the new λ-factor) under DBE and MCE level SAC LA ground motions is evaluated. In addition, the confidence level of these frames are calculated and compared with that of the previous design in Chapter 5.

SNAP-2DX software was used as was done in Chapter 4 and 5. The same modeling assumptions used for 9V-PBPD-A were also made for these frames, which include consideration of gravity and P-Delta column as well as beam-end releases and eccentricities.

In Section 6.5.1 the time-history response and maximum story drifts of the new Chevron and Split-X braced frames are shown. The confidence levels against collapse of these new frames are then evaluated by using the FEMA 351 (2000b) procedure in Section 6.5.2.

To evaluate the effect of increasing the fracture life, N_f, on dynamic response as well as confidence level, the N_f values for 9V-PBPD-B and 9X-PBPD-B1 were increased to the levels greater than 200 for all brace sections. The corresponding models are called 9V-PBPD-B-Nf and 9X-PBPD-B1-Nf, respectively. The results with increased values of N_f are discussed in Section 6.5.3.

6.5.1 Performance Comparison of 9V-PBPD-B and 9X-PBPD-B1 vs. 9V-PBPD-A

Maximum story drifts under SAC LA ground motions for the redesigned 9V-PBPD-B and 9X-PBPD-B1 frames based on the new λ-factor are shown in Figures 6.8 and 6.9, respectively, for DBE and MCE ground motions.

The median drift values can also be seen in Figure 6.10. The median story drifts under DBE level are close to each other for all three frames, with 9V-PBPD-B and 9X-PBPD-B1 showing smaller drifts at upper levels. The median drifts fall well within the target drift limit used in the design. The 9V-PBPD-B and 9X-PBPD-B1 frames show smaller median drifts, especially at lower levels. This shows that the increase in design base shear resulted in lower drift demands for these designs under MCE ground motions. Also, 9X-PBPD-B1 frame shows somewhat more uniform distribution over the height.

The number of brace fractures were almost the same for all three models (9V-PBPD-A, 9V-PBPD-B, and 9X-PBPD-B1) under both DBE and MCE ground motions. However, models with increased N_f, 9V-PBPD-B-Nf and 9X-PBPD-B1-Nf, showed much less and also delayed brace fractures compared to their corresponding models with original N_f values. Therefore, the increase in design base shear did not have much effect on brace fractures. Such fractures, however, could be prevented by using a minimum N_f of 200 for taller CBF structures, instead of 100 as used earlier in Chapter 4.

The ground motions under which each design showed collapse are shown in Table 6.12. As can be seen, the Split-X configuration shows more stable behavior. In addition, the 9V-PBPD-B model designed by using the new λ-factor shows somewhat more stable

response compared with 9V-PBPD-A frame designed in Chapter 5 based on original λ-factor.

It can be seen that the collapse of 9V-PBPD-B was due to brace fracture since this model did not show collapse when N_f was increased. However, under LA38, the increase in N_f value did not affect the time at which the collapses occurred, indicating that the collapses were not caused by brace fractures.

Figure 6.11 shows the 3rd story drift time-history response of 9V-PBPD-B frame under LA28. Such response can be considered as the typical response of the 9-story frames designed by PBPD under those ground motions that cause some brace fractures. Due to near-field nature of the MCE level SAC LA ground motions, most of the earthquake energy is transferred to the frames through large velocity pulses in a rather short time interval in the early stages of the record. Maximum story drifts of PBPD 9-story frames occur mostly under such velocity pulses, except for 9V-PBPD-B model under LA21 which showed collapse due to extensive brace fracture (Figure 6.12.a). Brace fractures, which are due to low-cycle fatigue, occurred at later stages of the ground motion. As a result, even for ground motions under which some brace fractures were observed, the maximum story drifts under MCE ground motions had occurred before the fracture of braces started.

Figure 6.12.a shows the exception to the trend mentioned above. In this case, the peak story drift occurred at about 10 seconds past the start of the ground motion. However, at about t = 45 seconds, the frame became unstable due to excessive brace fractures and eventually collapsed after formation of soft stories.

Figure 6.12.b shows the 4th story drift versus time for the same frame as in Figure 6.12.a, but with increased N_f values in stories 2,3,4, and 5 (model 9V-PBPD-B-Nf). As can be seen, this model survived under LA21 even though there were brace fractures. The increase in N_f delayed fracture of braces 7 and 8 for about 7 seconds, which was enough in this case for the structure to survive the earthquake.

Figure 6.13 shows 4th story drift versus time response of the Split-X configuration model 9X-PBPD-B1 (with original N_f values) under LA21. As shown, only minor brace fractures occurred at the end of the ground motion.

Table 6.12. Collapse Cases under Time History Analyses.

Model	**9V-PBPD-A**	**9V-PBPD-B**	**9V-PBPD-B-Nf**	**9X-PBPD-B1**	**9X-PBPD-B1-Nf**
Ground Motions caused Collapse	LA27 (t=46.8sec) LA38 (t=12.7sec)	LA21 (t=51.3sec) LA38 (t=36.7sec)	LA38 (t=36.7sec)	LA38 (t=50.2sec)	LA38 (t=50.2sec)

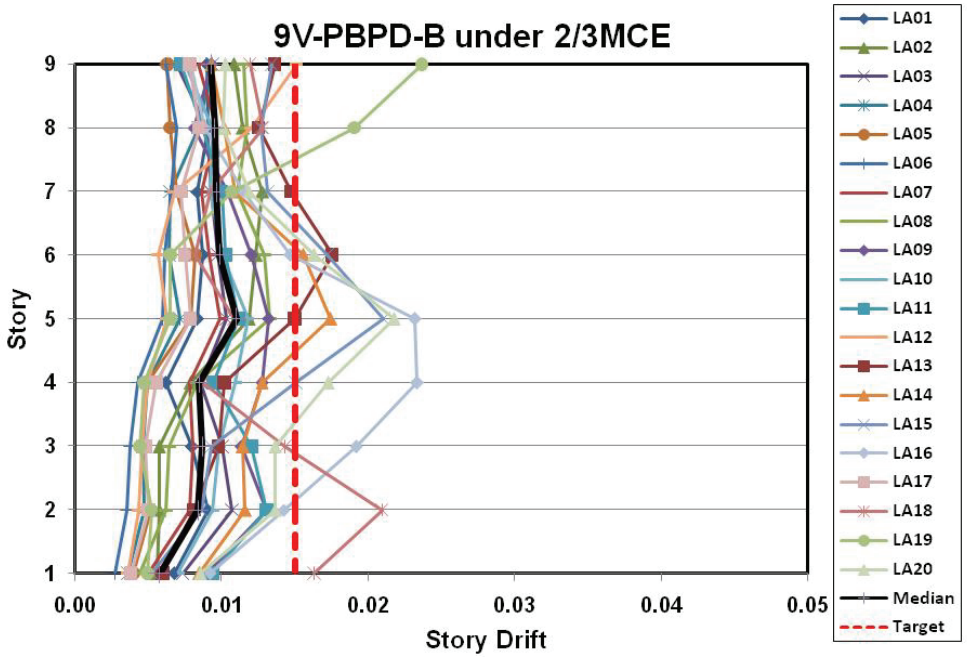

(a)

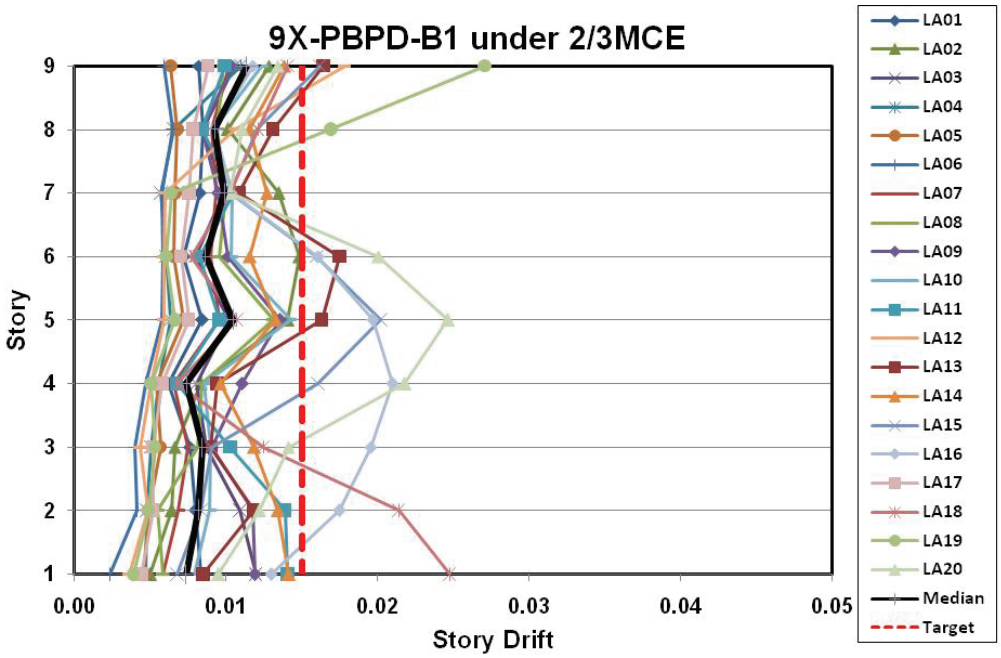

(b)

Figure 6.8. Maximum Story Drifts under SAC DBE Ground Motions: (a) 9V-PBPD-B; and (b) 9X-PBPD-B1.

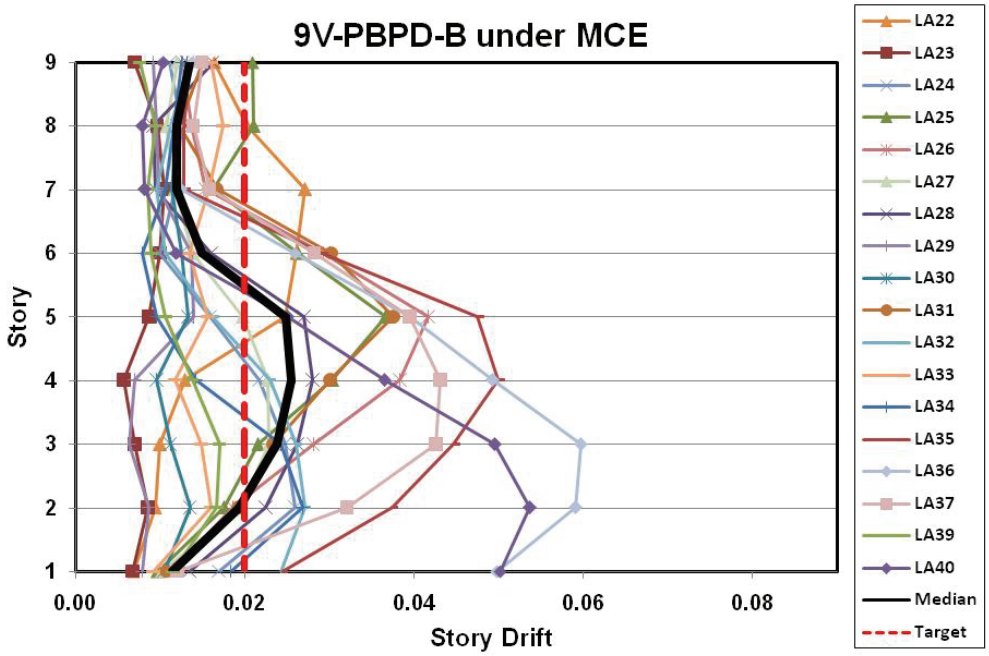

(a)

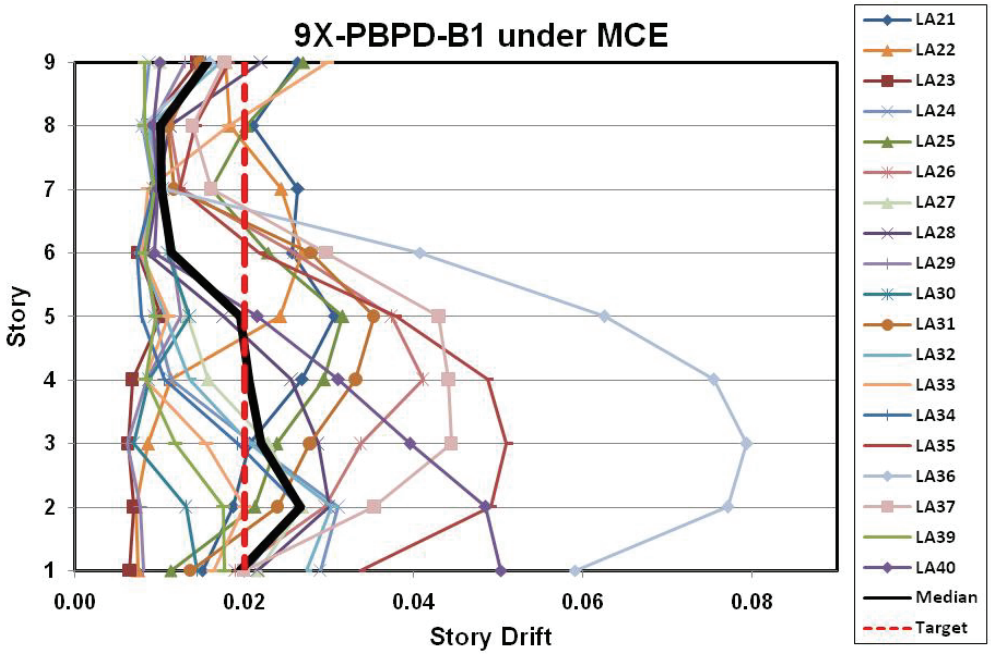

(b)

Figure 6.9. Story Drifts under SAC MCE Ground Motions: (a) 9V-PBPD-B; and (b) 9X-PBPD-B1.

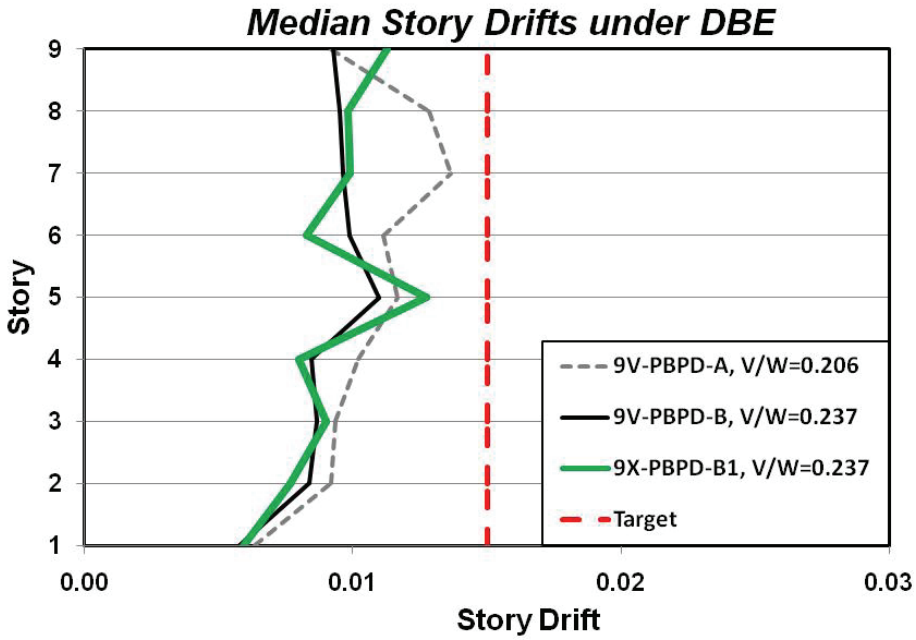

(a)

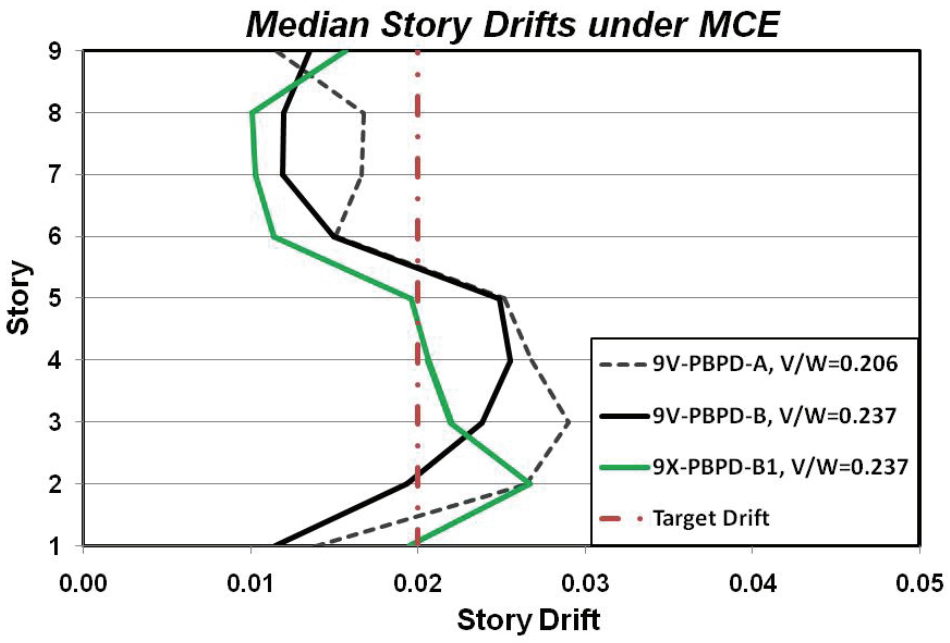

(b)

Figure 6.10. Median Story Drifts for Different Designs under: (a) DBE; and (b) MCE Ground Motions.

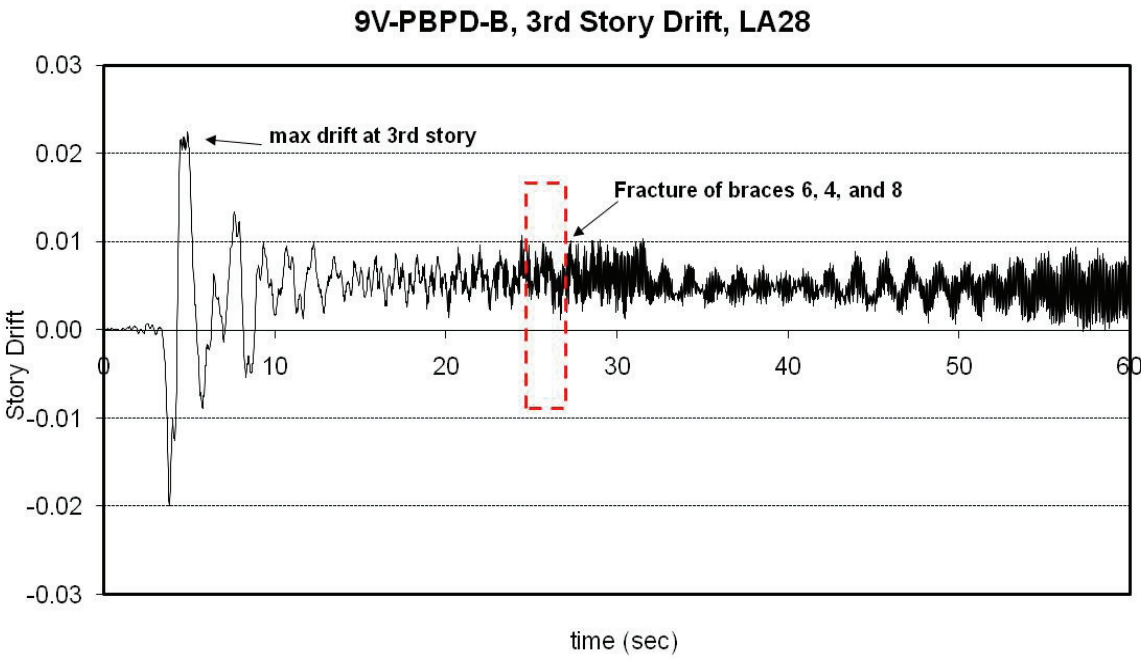

Figure 6.11. Story Drift vs. Time for 3rd Story and Brace Fractures for 9V-PBPD-B under LA28.

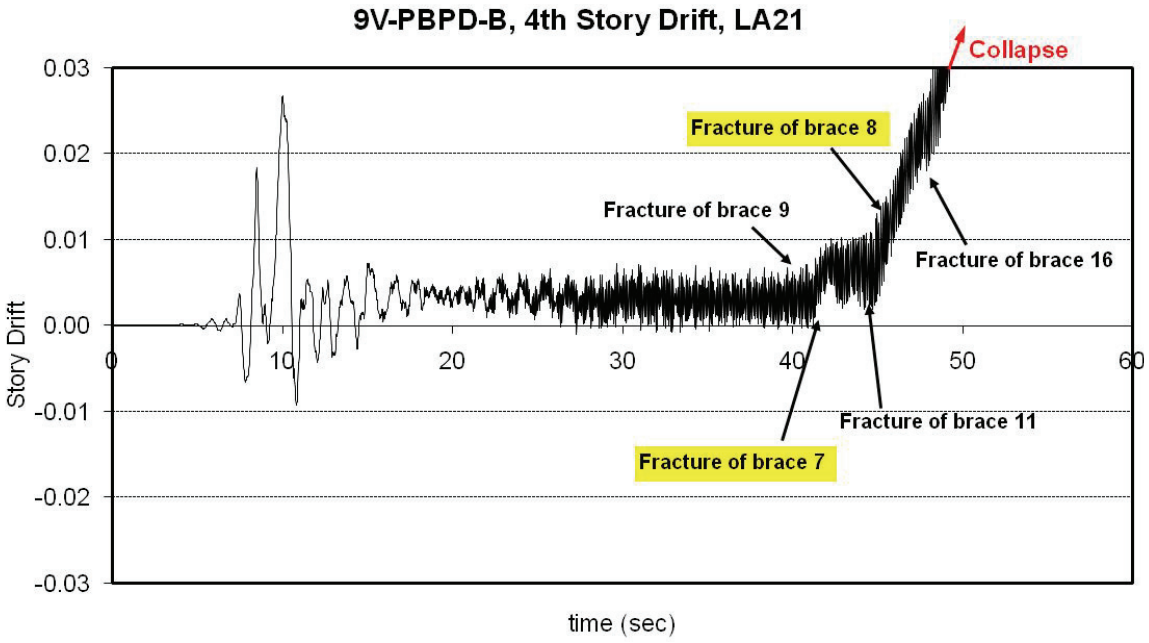

(a)

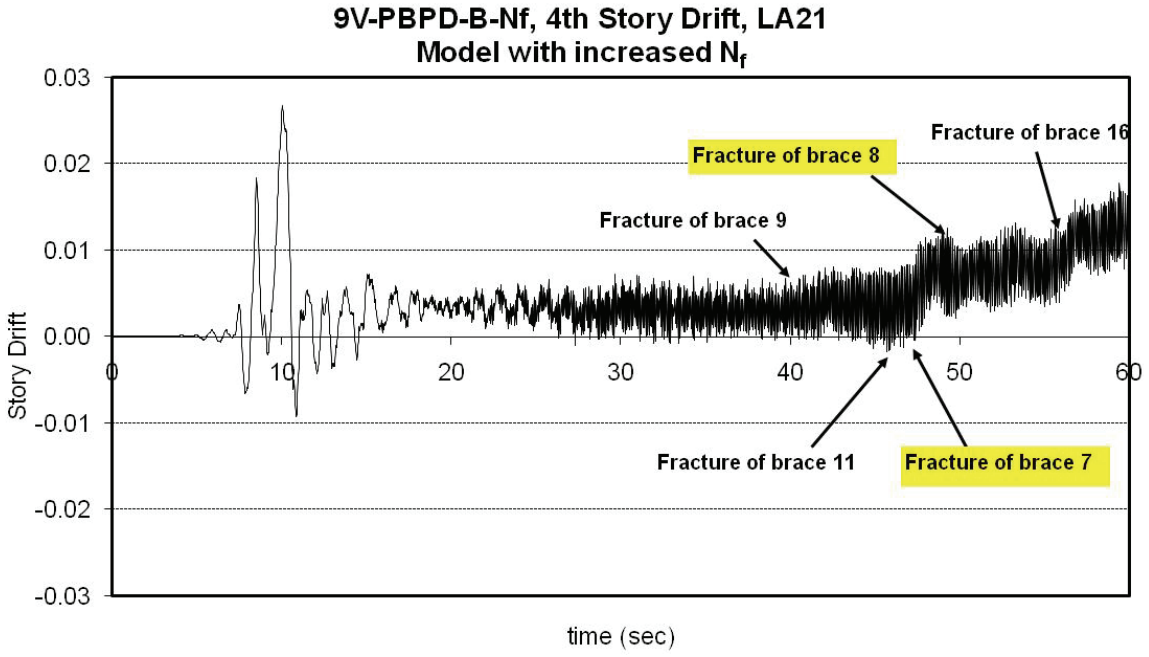

(b)

Figure 6.12. 4th Story Drift vs. Time under LA21: (a) 9V-PBPD-B; (b) 9V-PBPD-Nf.

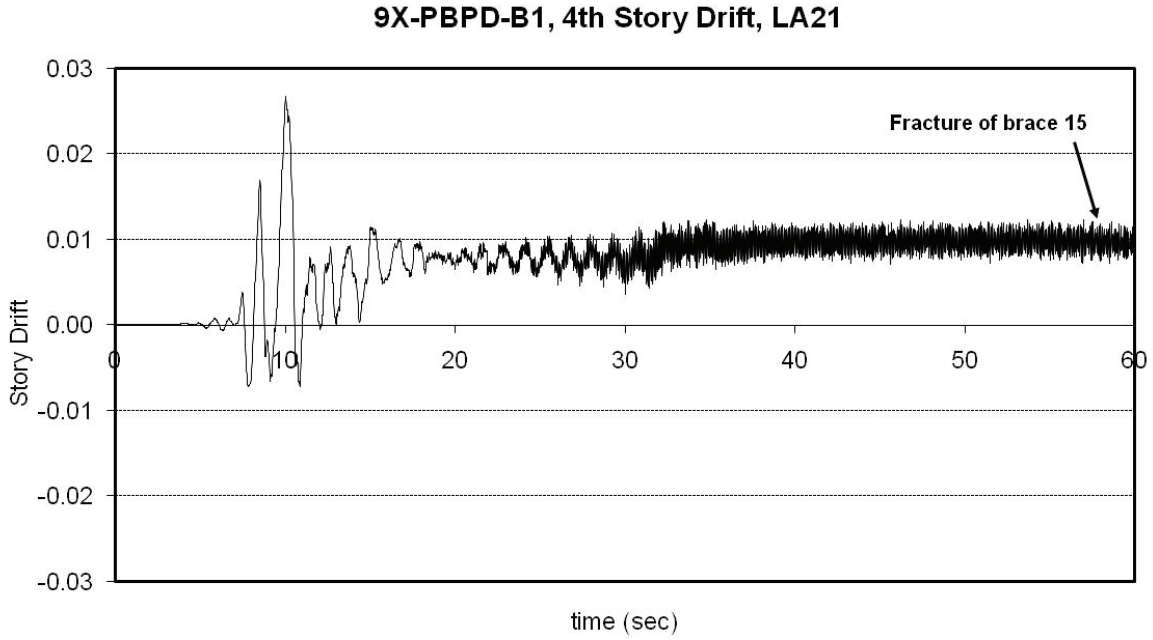

Figure 6.13. 4th Story Drift vs. Time under LA21: 9X-PBPD-B1.

6.5.2 Confidence Level Evaluation of 9V-PBPD-B and 9X-PBPD-B1 Frames

The confidence levels of the 9V-PBPD-B and 9X-PBPD-B1 frames were evaluated by following the FEMA 351 (2000b) procedure as described in Chapter 4. Tables 6.12 to 6.14 show the parameters used in confidence level evaluation. Figure 6.14 shows the IDA curves for these two designs under MCE set of SAC LA ground motions. It can be seen from Table 6.14 that the new designed frames show improvement in confidence level against collapse. The confidence level for 9V-PBPD-B came out to be 68.6% versus 52.1% of the original 9V-PBPD-A frame (Chapter 5). This 16.5% increase in the confidence level comes mainly from the increase in the design base shear using new λ-factor.

It can also be seen that the brace configuration has significant effect on the confidence level. The 9X-PBPD-B1 frame has same brace sections as 9V-PBPD-B, but

only with different configuration. The confidence level of the Split-X frame is about 10% better than the corresponding Chevron frame (77.4% versus 68.6%). This was mainly due to smaller scatter in drift demand for the Split-X frame under MCE ground motions. It should be noted that the beams sizes in the Split-X frame are considerably smaller compared to those of Chevron frame, but still the Split-X design shows better confidence level.

6.5.3 The Effect of Increasing N_f on the Confidence Level

It was seen that the brace fractures (e.g., under LA21 ground motion) led to instability or quite large story drifts. Thus far, main focus of the study presented in this chapter was on evaluation of the effect of increasing the design base shear on the seismic performance of the 9-story frames. In this section, an increased level of N_f for 9V-PBPD-B and 9X-PBPD-B1 designs is considered in order to minimize the adverse effects of lower N_f on the performance and confidence level of these frames. This can be achieved by increasing N_f to values more than 200 (for braces with N_f smaller than 200) without any change in other properties of the model. The increased values of N_f are shown in Table 6.11 which shows increase in stories 2, 3, 4, 8, and 9. Such increases in fracture life for hollow structural sections can be achieved by various methods as mentioned in section C13.2d of AISC Seismic Provisions (AISC, 2005a). Filling with plain concrete can be used as an effective way of reducing the severity of local buckling and delay fractures hollow tubular braces (Liu and Goel, 1988; Lee and Goel, 1987). Goel and Lee (1992) developed an empirical equation to estimate the effective width-to-thickness ratio of concrete-filled HSS braces. As another method, longitudinal stiffeners such as rib

plates or small angle sections in a hat configuration can be used on tube walls (Liu and Goel, 1987).

Therefore, the N_f values for braces in 9V-PBPD-B and 9X-PBPD-B1 frames were increased to over 200 (stories 2, 3, 4, 8, 9). As shown in Table 6.8, these new models are designated 9V-PBPD-B-Nf and 9X-PBPD-B1-Nf, respectively. The time-history response as well as confidence level analysis were carried out for these frame models as well.

The maximum story drifts for the models with increased N_f were found to be essentially the same as the models with regular N_f, except for 9V-PBPD-B model under LA21 ground motions. 9V-PBPD-B frame collapsed under LA21, but the increased N_f model 9V-PBPD-B-Nf survived without collapse with about 3.4% maximum story drift. For other ground motions, the maximum story drifts did not change with increase in N_f. However, brace fractures were delayed by about 4 to 14 seconds (depending on ground motion), and in some cases the fractures were totally eliminated in the increased N_f models.

The parameters used in calculation of confidence level against collapse are shown in Tables 6.13 and 6.14. The final values for confidence level against collapse are shown in Table 6.15. Also, Figure 6.15 shows the IDA curves for these two models under MCE set of SAC LA ground motions. As can be seen, the increase in N_f value increases the confidence level of 9V-PBPD-B by about 11% from 68.6% to 79.4%. The main reason for this increase was that 9V-PBPD-B-Nf model showed smaller scatter in drift demand compared to 9V-PBPD, even though the two models had the same median drift demand.

For the Split-X configuration, both the drift demand and its scatter essentially remained unchanged with increase in N_f. However, 9X-PBPD-B1-Nf model showed slightly larger drift capacity which resulted in somewhat higher confidence level. As can be seen from Table 6.15, confidence level increased 5.3% (from 77.4% to 82.7%) by increasing N_f to values more than 200 for the Split-X configuration.

6.6 Summary and Conclusions

The main objective of the study presented in this chapter was to improve the confidence level (C.L.) for the 9-story CBF against collapse. Several modifications were proposed. The first modification was in the design base shear (DBS) calculation. A slightly larger λ-factor was suggested for mid to high-rise CBF frames to offset the detrimental effect of P-Delta overturning forces in the calculation of DBS.

The effect of using Split-X (two story X bracing) configuration on seismic performance and C.L. of CBF was also studied. In addition, the effect of increasing brace fracture life, N_f, on seismic performance and C.L. was evaluated.

The main conclusions from the results presented in this chapter are:

1- Higher values of design base shear (DBS) for 9-story (and taller) CBF were obtained using the proposed new λ-factor in PBPD method. This new λ-factor results in larger design base shear for mid to high-rise CBF structures.

2- The 9-story Chevron CBF design based on the new DBS showed smaller story drifts under both DBE (10%/50 yrs) and MCE (2%/50 yrs) ground motions compared to the 9V-PBPD-A frame designed in Chapter 5.

3- Higher levels of confidence level (C.L.) against collapse were obtained using the new DBS for Chevron configuration. The C.L. of 52% obtained in Chapter 5 for 9V-PBPD-A increased to 68.6% by using the new DBS in 9V-PBPD-B.

4- Improvement was seen in C.L. of the Chevron frame designed by using increased N_f (of more than 200) for fracture life of the braces. This increase in N_f resulted in increase of C.L. of the 9-stoy Chevron CBF from 68.6% to 79.4% (about 11%).

5- It was shown that C.L. of 9-story CBF improved by only changing the brace configuration to Split-X. The C.L. increased from 68.6% to 77.4% (about 10%) by using Split-X instead of Chevron configuration. The same brace sections were used. However, much lighter beams are needed in the Split-X configuration. The C.L. obtained for the Split-X design with original N_f values was almost equal to that of Chevron design with increased N_f.

6- Increasing the design base shear did not have much effect on drift capacity of the 9-story CBF frames obtained from IDA. However, larger design base shear resulted in lower drift demands with reduced scatter under MCE ground motions which basically translates into higher confidence level.

7- Increase in design base shear based on the new λ-factor was seen to be the main factor in reducing the story drifts under MCE level ground motions. Better controlled drift demands resulted in higher confidence level.

8- Increase in N_f value (brace fracture life factor) did not have significant effect on drift response under MCE level SAC LA ground motions since the maximum story drifts generally occur at the early stages for such near-field ground motions.

Table 6.13. Analysis Uncertainty Parameters.

Study Frames	C_B	β_{DU}	γ_a
3V-NEHRP	1.0	0.15	1.03
3V-PBPD	1.0	0.15	1.03
6V-NEHRP	1.0	0.20	1.06
6V-PBPD	1.0	0.20	1.06
9V-PBPD	1.0	0.20	1.06

Table 6.14. Randomness and Uncertainty Parameters.

Frame	β_{RC}	ϕ_{RC}	β_{UC}	ϕ_{UC}	β_{RD}	β_{UT}
3V-NEHRP	0.537	0.649	0.15	0.967	0.890	0.30
3V-PBPD	0.394	0.793	0.15	0.967	0.545	0.30
6V-NEHRP	0.435	0.753	0.20	0.942	0.663	0.35
6V-PBPD	0.412	0.775	0.20	0.942	0.708	0.35
9V-PBPD-A	0.309	0.867	0.20	0.942	0.515	0.35
9V-PBPD-B	0.266	0.899	0.20	0.942	0.622	0.35
9V-PBPD-B-Nf	0.258	0.905	0.20	0.942	0.559	0.35
9X-PBPD12-B1	0.226	0.927	0.20	0.942	0.522	0.35
9X-PBPD12-B1-Nf	0.225	0.927	0.20	0.942	0.498	0.35

*β_{RC}: standard deviation of natural logs of drift capacities due to randomness
*β_{UC}: standard deviation of natural logs of drift capacities due to uncertainty
*β_{RD}: standard deviation of natural logs of drift demands due to randomness
*β_{UT}: vector sum of logarithmic standard deviations for both demand and capacity considering all sources of uncertainty

Table 6.15. Summary of Confidence Level Assessment for 3-Story, 6-Story, and 9-Story CBFs.

Frame	Median Drift Capacity (from IDA), C	Capacity factor, ϕ^*	Median Drift Demand, D	Demand factors		Confidence Parameter $\lambda = \frac{\gamma \cdot \gamma_a \cdot D}{\phi \cdot C}$	Confidence Level (%)
				γ^*	$\gamma_a{}^*$		
3V-NEHRP	0.064	0.628	0.068	3.37	1.06	6.04	<< 1%
3V-PBPD	0.078	0.766	0.015	1.56	1.06	0.41	> 99.9%
6V-NEHRP	0.065	0.709	0.035	1.93	1.06	1.55	23.3%
6V-PBPD	0.100	0.730	0.027	2.12	1.06	0.82	86.2%
9V-PBPD -A	0.062	0.816	0.0376	1.49	1.06	1.180	52.1%
9V-PBPD -B	0.061	0.847	0.0276	1.79	1.06	1.015	68.6%
9V-PBPD-B-Nf	0.061	0.852	0.0276	1.60	1.06	0.902	79.4%
9X-PBPD-B1	0.0604	0.873	0.0305	1.51	1.06	0.924	77.4%
9X-PBPD-B1- Nf	0.0646	0.873	0.0305	1.51	1.06	0.832	82.7%

* ϕ : resistance factor that accounts for the randomness and uncertainty in estimation of structural capacity

*γ: demand uncertainty factor;

*γ_a: analysis uncertainty factor

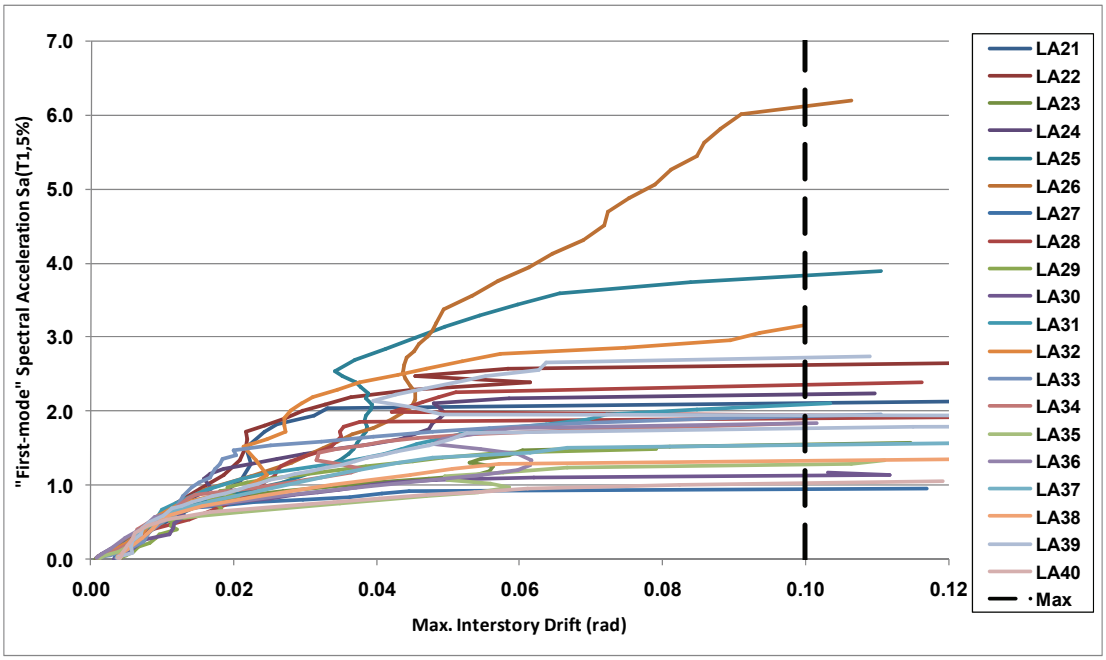

(a)

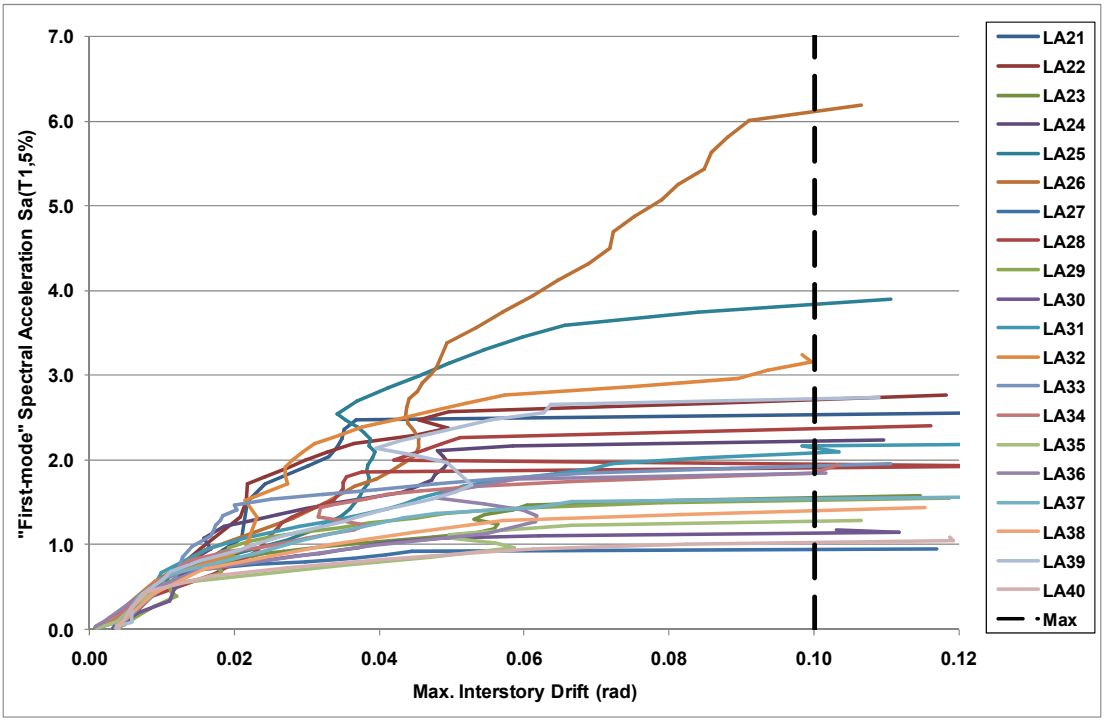

(b)

Figure 6.14. IDA Plots for: (a) 9V-PBPD-B-Nf; and (b) 9V-PBPD-B.

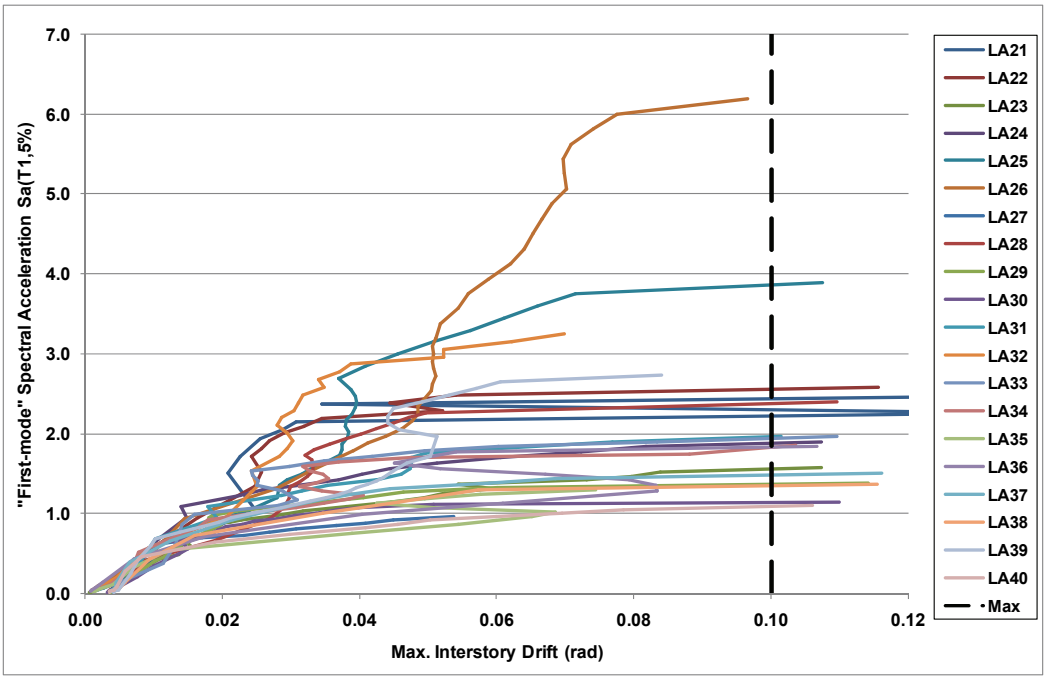

(a)

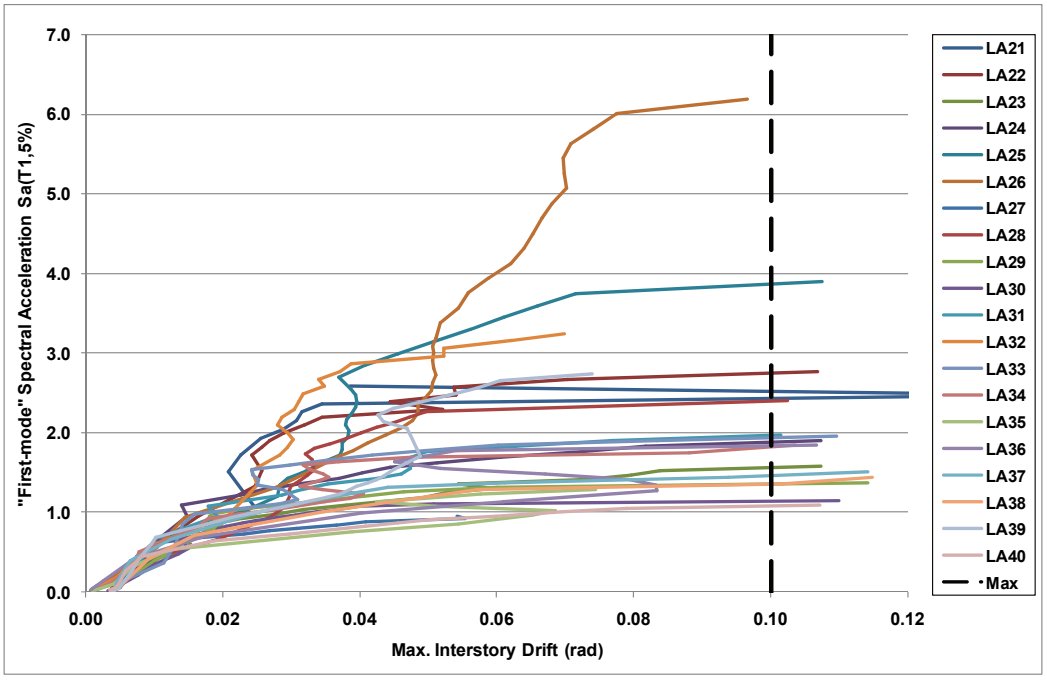

(b)

Figure 6.15. IDA Plots for: (a) 9X-PBPD-B1-Nf; and (b) 9X-PBPD-B1.

CHAPTER 7

APPLICATION OF PBPD METHOD TO TALL MOMENT FRAMES

7.1 General

The PBPD method has been successfully applied to design of low-rise structures up to 10 stories (Goel and Chao, 2008). The current PBPD procedure for design of columns in steel MF systems, although works very well for low-rise frames, but results in over-design of columns for mid to high-rise frames. The method has been applied to design of 20-story MF structures (Lee and Goel, 2001), resulting in frames that satisfied both the target drift and yield mechanism design performance criteria. However, the column design moments obtained by using the current column tree analysis were quite conservative.

The main focus of research presented in this chapter is on the column design procedure in the PBPD method for tall moment frames.

Current method of designing columns as Non-Designated Yielding Members (Non-DYM) in MF structures is reviewed and modifications are proposed in order for the final design to better match with the targeted performance. Two main issues are addressed: (1) Calculation of base column plastic moment, M_{pc}, to guard against formation of soft-story mechanism and also to achieve a more representative column design moment profile over the height of the structure, and (2) P-Delta effect.

In Section 7.2, the current method of calculating the base column plastic moment, M_{pc}, is presented and then the modifications are proposed in order to calculate this moment accounting for all possible sources of overstrength such that a the formation of soft story can be prevented with improved confidence.

In section 7.3, the current method of accounting for P-Delta effects in column design by using column tree analysis along with two proposed methods are evaluated to determine as to which method is more suitable to be used for column design in tall moment frames. These modifications are then applied to redesign the 20-story SAC LA building by the PBPD method in Section 7.4. The performance of the original SAC frame and the PBPD frame under nonlinear static and dynamic analyses are compared in Section 7.5.

7.2 Calculation of Base Column Plastic Moment

Previously application of PBPD method for design of taller moment frames has lead to somewhat overdesign of columns (Lee and Goel, 2001). This was due to quite conservative column moments obtained from the current column tree analysis method. Therefore, the column tree analysis procedure was re-evaluated and improved upon. As mentioned in Chapter 3, the plastic moment of columns at base, M_{pc} , can be obtained by using the following equation (Goel and Chao, 2008):

$$M_{pc} = \frac{1.10 V h_1}{4} \tag{7.1}$$

where V is the base shear for equivalent one bay model. The 1.10 factor was considered as margin factor to account for possible overloading due to strain hardening and uncertainty in material strength in order to prevent formation of soft-story mechanism (Leelataviwat, 1998). However, some other factors can also potentially cause the base shear in the designed frame to be greater than the design base shear. In order to have better confidence that the soft story mechanism is prevented under the ultimate lateral forces, those factors should also be accounted for in the calculation of M_{pc}.

The influencing factors include: (1) design resistance factor for beams ($\varphi = 0.9$), yield overstrength for beams ($R_y = 1.1$), strain hardening of beams (1.1), and also an average oversize factor when selecting design sections for beams (1.1). Taking these factors into account, and also considering a 10% margin of safety, a resultant factor of $(1/0.9)\times(1.1)\times(1.1)\times(1.1) = 1.48$ would be needed. Therefore, a value of 1.50 is used in the modified equation, Figure 7.1:

$$M_{pc} = \frac{1.50 V h_1}{4} \tag{7.2}$$

Another issue with using Equation (7.1) is that the moment at the top of first story columns generally comes out greater than the moment at the base (M_{pc}), making the design moment larger moment than M_{pc}. This issue can also be resolved by using the modified equation for M_{pc}, because by considering all possible sources of overstrength in the calculation of M_{pc} and corresponding lateral forces the moment at the top of first story columns will be smaller or equal to M_{pc}. In other words, by using Equation (7.2) for M_{pc} calculation, the maximum moment in the first story columns will occur at the base. This

has been verified in column tree analysis of 10 and 20-story frames. Figures 7.2 and 7.3 show the column moments obtained by column tree analysis for 10-story and 20-story SAC moment frames, respectively, using the current and the modified equations for M_{pc}. It should be noted that the column moments shown in Figures 7.2 and 7.3 were obtained directly from the column tree analysis without considering any P-Delta effect. As can be seen from these figures, the maximum moment in the first story occurs at the base when using the modified equation. In addition, it can be seen that using the current equation for M_{pc} leads to substantially larger design moments, especially in lower and middle stories. Therefore, by using the modified equation, the column moments can be reduced. In addition, the column moment profile becomes more reasonable with the maximum column moment in the first story occurring at the base instead of at the top. And, as was noted in formulation of the modified equation, this larger value of M_{pc} can prevent the formation of soft-story mechanism with higher level of confidence.

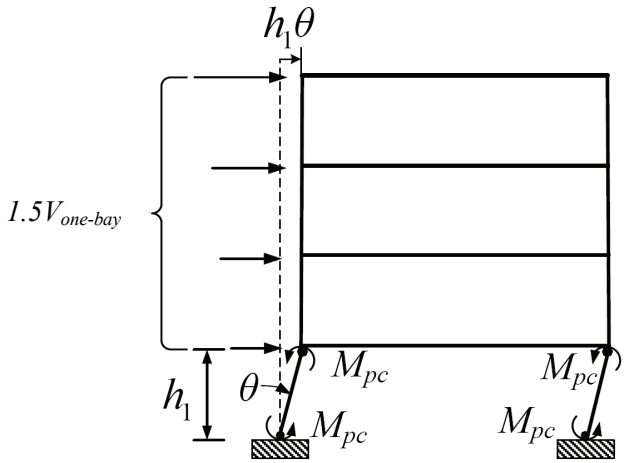

Figure 7.1. One Bay Frame with Soft-Story Mechanism.

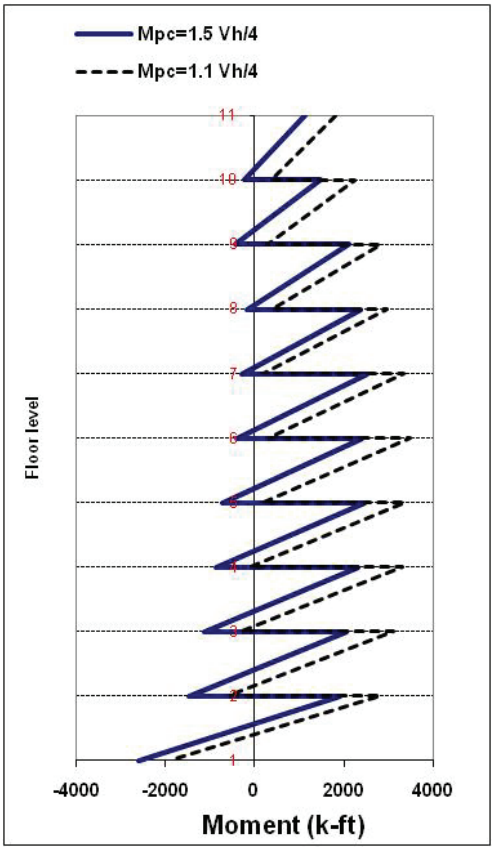

Figure 7.2. Comparing Column Design Moments of an Exterior Column for a 10-Story 2-Bay Moment Frame using Different Equations for M_{pc}.

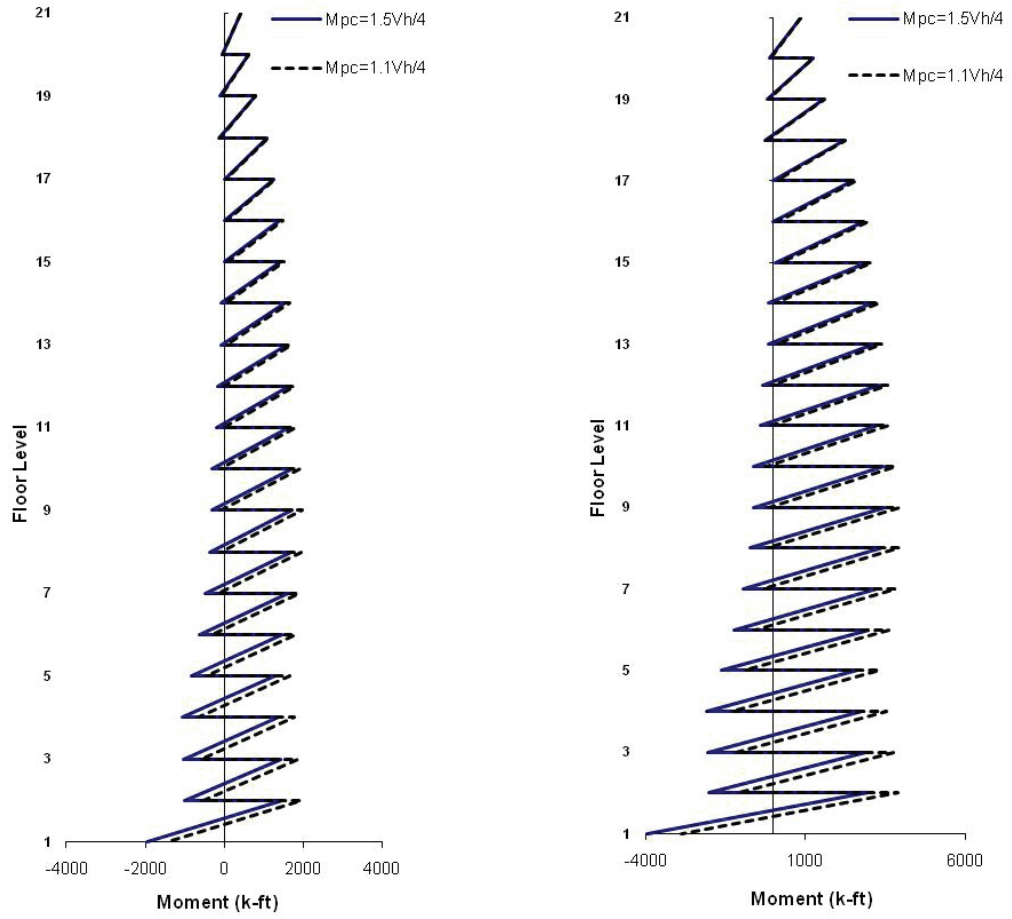

(a) (b)

Figure 7.3. Comparing Column Design Moments of an Exterior Column for 20-Story SAC Moment Frame using Different Equations for M_{pc}: (a) Exterior Column; and (b) Interior Column.

7.3 Consideration of P-Delta Effect in Design of Columns (Non-DYM)

It is commonly agreed that in order to achieve a desirable performance of structures during earthquakes, columns should remain elastic (except at the base). The current practice involves iterative design-evaluation procedures with the possibility of not converging to a proper design. To overcome this difficulty, "column-tree analysis" was introduced as part of PBPD framework (Leelataviwat, Goel, and Stojadinovic, 1999) so that more realistic column design moments can be obtained. In this method, column design moments are obtained by considering the equilibrium of the entire column tree as part of the yield mechanism in the design limit state. Figure 7.4 shows the free-body diagram of exterior column-tree of a moment frame at target drift.

An important factor that amplifies the moments in design of columns is P-Delta effect, which needs to be accounted for in the design process. Several methods are currently used for this purpose. The most common methods include: (1) Amplification of first-order analysis moments by B_1 and B_2 factors; and (2) Direct second-order analysis by using appropriate structural analysis programs (AISC, 2005a).

Thus far, the B_2-factor method has been used in the PBPD procedure (Lee and Goel, 2001, and Goel and Chao, 2008). In this method, column tree moments are amplified by the B_2-factor. This method along with two other methods are studied herein. By comparing the results of these different procedures as applied to the 20-story SAC frame, more suitable method to be used for PBPD design of tall frames can be selected. The three methods, including the two proposed methods and the current B_2-factor method, are discussed in the following sections.

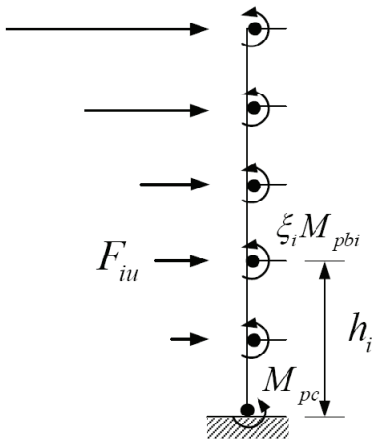

Figure 7.4. Free Body Diagram of an Exterior Column.

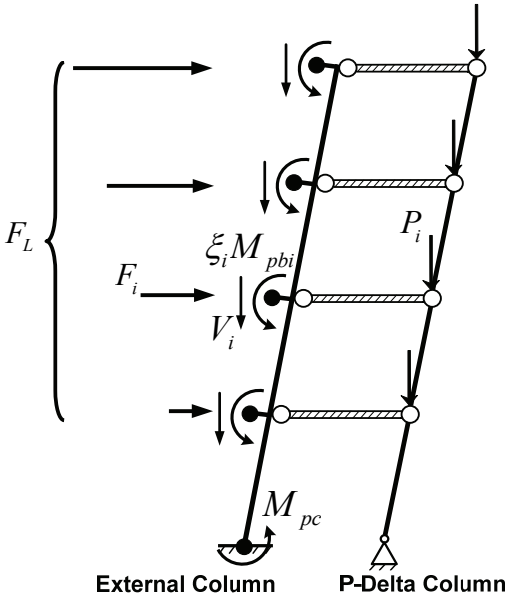

Figure 7.5. Column Tree with Gravity Column in "Direct P-Delta" Method.

7.3.1 B_2-Factor Method

The B_2-factor method was originally developed to be applied to the column moments obtained by elastic analysis. Earlier, this method has been used to amplify the

column moments obtained from column tree analysis (Lee and Goel, 2001; Goel and Chao, 2008). Therefore, the validity of applying this amplification factor on the column moments obtained from a limit state type of analysis (e.g. column tree method) needs to be verified.

The other issue that needs to be considered about B_2-factor is that its value becomes quite large in lower stories of taller frames which may lead to conservative design of those columns. Hence, the application of B_2-factor method needs to be evaluated for tall moment frames.

Two methods are proposed herein to account for the P-Delta effects by considering the structure at its ultimate state.

7.3.2 Direct P-Delta Method in Column Tree Analysis

In this method, which can be considered a more direct way of considering P-Delta effect as compared with the B_2-factor method, the column tree is considered in an assumed deflected shape at target drift and the gravity loads are applied on a lumped gravity column (Figure 7.5). A linear deflected shape is assumed herein. The gravity column is connected to the column tree by means of rigid pin-ended beams. The rigid beams are basically transferring the horizontal forces caused by the second order effect at each level. At this point, equilibrium of the column tree is formulated to obtain lateral forces, F_L, and the resulting column moments, axial and shear forces are calculated.

7.3.3 Pushover Analysis Method

In this method, a non-linear static pushover analysis of the entire frame is carried out up to the target drift by applying design lateral force distribution. The DYMs are modeled to behave inelastically, while the Non-DYM are modeled (or "forced") to behave elastically. P-Delta effect is captured by applying the floor gravity loads on "gravity columns" which can be lumped into one, if desired.

Since the column sizes are needed for modeling purposes, the column moments and axial forces obtained by a first order column tree analysis are used for preliminary column design. Nonlinear pushover and also dynamic time-history analyses were carried out using Perform-3D software (CSI, 2007) to evaluate which method is more suitable for design purposes.

The column design moments for the exterior column of a 10-story 2-bay and the interior column of the 20-story SAC LA frame, using different methods as presented above, are shown in Figures 7.6 and 7.8, respectively. Figures 7.6.a and 7.8.a show the column moments obtained from the first order column tree analysis for the 10-story and 20-story frames. In Figure 7.6.b and 7.8.b, the amplified moments by using direct P-Delta and B_2-factor method are shown. Figures 7.6.c and 7.8.c show the column design moments obtained by the pushover analysis method for these frames. Figures 7.7 and 7.9.b show the moment amplification with respect to the first order column tree moments by three different methods. As can be seen from these figures, while the column moments obtained from pushover analysis are significantly smaller than the ones obtained from column tree analysis without P-Delta, the amplified moments by the B_2-factor and the

Direct P-Delta method are quite close, except that B_2-factor method leads to relatively heavier columns in the lower stories and Direct P-Delta method leads to somewhat heavier columns in mid and top stories.

Dynamic time-history analysis results were used to determine which of the proposed methods is more suitable for use in PBPD method in order to account for the P-Delta effect. As can be seen in Figure 7.10, the column tree analysis results amplified by B_2-factor give the most appropriate design moments for columns in all stories, while also being slightly conservative. This can also be confirmed by comparing the performances of the frames designed by these three methods under dynamic analysis. The envelope of column design moments obtained from pushover analysis are also shown in the Figure 7.10. As can be seen, except for the first story, pushover method underestimates the required column moments, which in turn leads to rather weak and flexible structure. Also, having insufficient column strength/stiffness in the upper stories by using results of pushover analysis can lead to undesirable performance under dynamic analysis due to higher mode effects, especially for mid to high-rise structures. Furthermore, although pushover analysis is considered to be an important tool giving insight about the behavior under lateral forces, deformation demands, and ultimate strength of the structures, Figures 7.6 to 7.10 show that it is unable to predict the actual column moment demands in taller frames under dynamic analysis.

One main reason the pushover method underestimates the column moments of the 20-story frame, is the height of this structure, which causes the deflected shape under pushover at 2% target roof drift to be different from the assumed linear shape in column

tree analysis (Figure 7.16 to 7.18). This different deflected shape causes the story drifts to be small at mid to top levels and consequently keeps the beams at these levels from reaching their full capacity. Therefore, the transferred moments from beam to column at these floors are reduced. This can explain why column moments from pushover analysis are significantly smaller than the column tree analysis results for mid to upper stories.

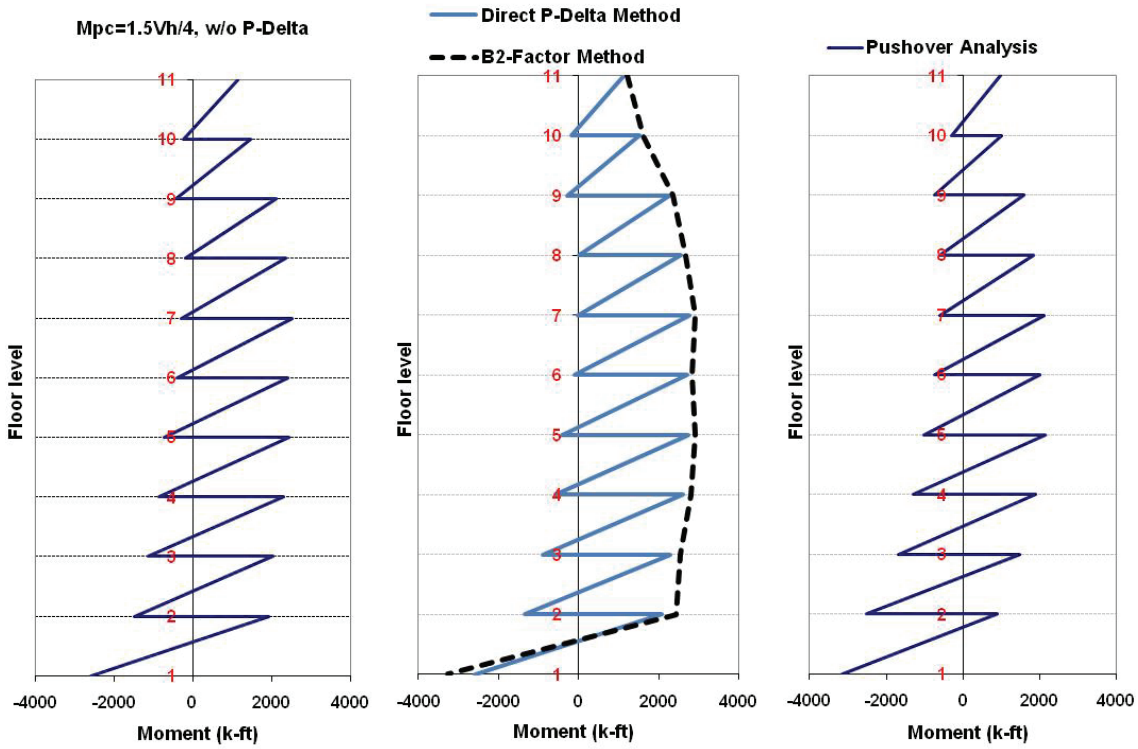

(a) (b) (c)

Figure 7.6. Column Moments in an Exterior Column of 10-Story 2-Bay Frame; (a) Column Tree Moments without P-Delta; (b) Column Tree Moments Amplified by Direct P-Delta Method and B_2-Factor Method; (c) Column Moments from Pushover Analysis.

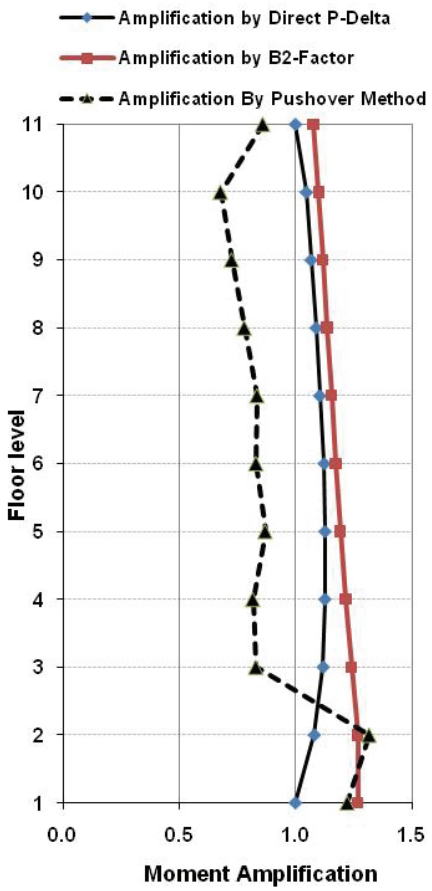

Figure 7.7. P-Delta Amplification by Three Different Methods.

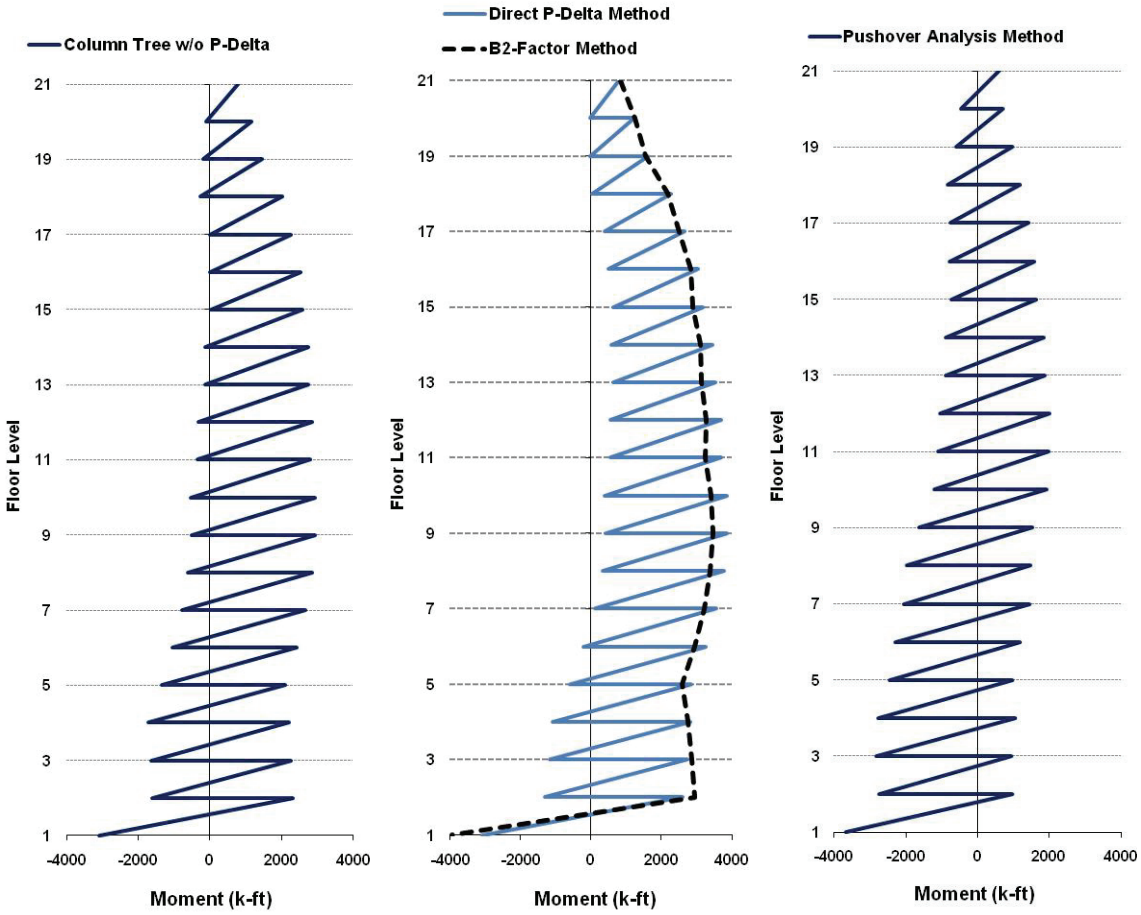

(a) (b) (c)

Figure 7.8. Column Moments in an Exterior Column of 20-Story SAC Frame; (a) Column Tree Moments without P-Delta; (b) Column Tree Moments Amplified by Direct P-Delta Method and B_2-Factor Method; (c) Column Moments from Pushover Analysis.

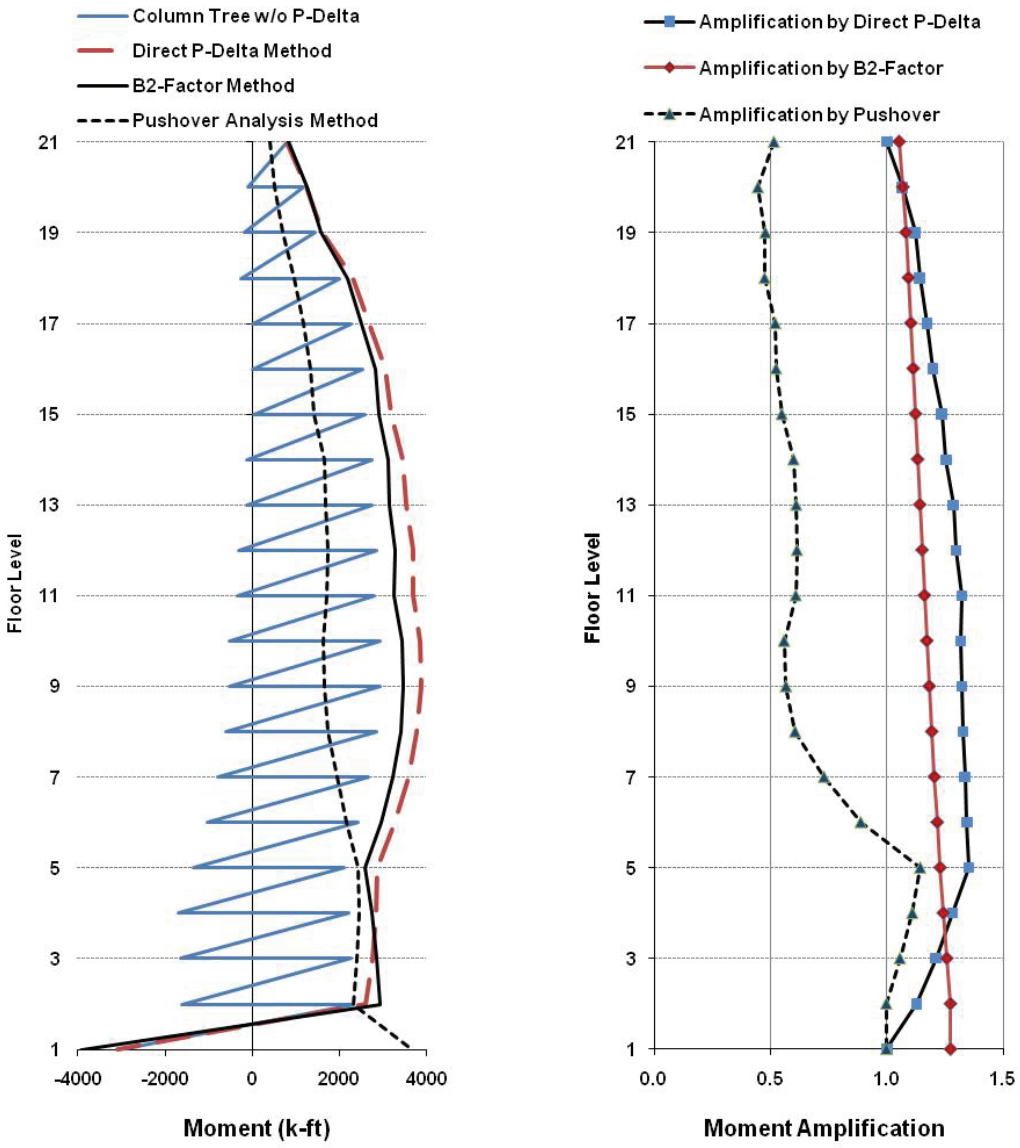

(a) (b)

Figure 7.9. (a) Comparing the Design Column Moments Obtained by Each Method; (b) P-Delta Amplification by Three Different Methods.

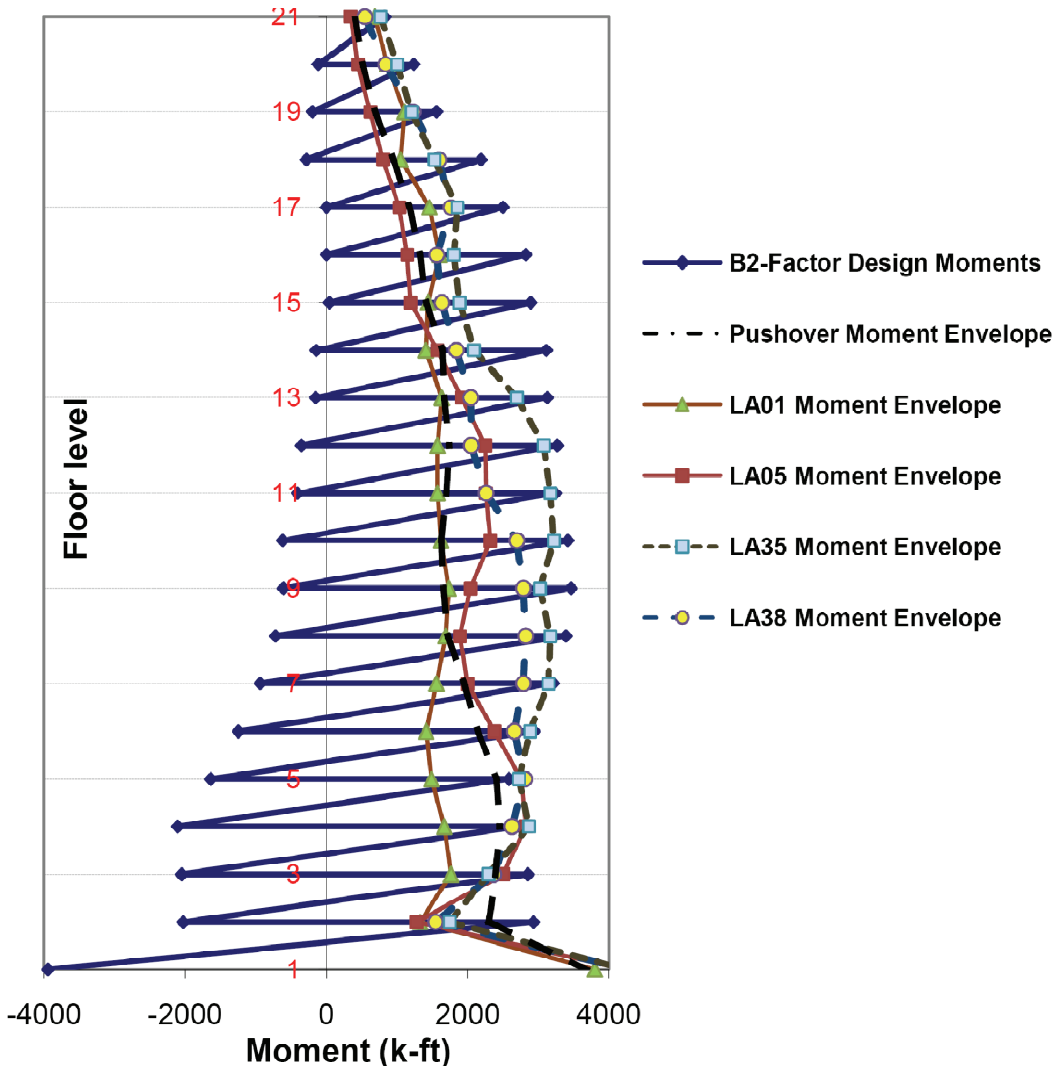

Figure 7.10. Comparison of Interior Column Moments from Inelastic Dynamic Analyses with Different Design Methods.

7.4 Design Example: Re-Design of 20-Story SAC LA Frame

The above mentioned modifications are more beneficial for design of tall moment frames, in which the importance of factors such as column design, participation of higher modes, and the P-Delta effect increase. The LA 20-story structure, originally designed as part of the SAC Steel Research Program (Gupta and Krawinkler 1999; Lee and Goel, 2001), was re-designed by PBPD method with the above modifications for column design. To be consistent with the original design, the same building code (UBC, 1994) was used for PBPD method as well. The target yield mechanism is similar to the one shown in Figure 3.2.a with the beam plastic hinges assumed at 6 inches from the column face. PBPD lateral force distribution (Chao et al., 2007) was used to distribute the base shear over the height of the structure. The beams were designed as full sections assuming ductile unreinforced flange connections with the columns. The differences in the original frame designed by the then current practice and the re-designed one by PBPD method will be discussed in regard to member sizes and computed responses under inelastic pushover as well as time-history analyses.

7.4.1 Building Geometry and General Design Parameters

The framing plan and elevation of the NS perimeter moment frame are shown in Figures 7.11 and 7.12, respectively. Since the original SAC frame was designed based on UBC 1994, for comparison purposes same loading and design criteria were used for redesign of the frame by PBPD method. The gravity loads are given in the following (Gupta and Krawinkler, 1999) and seismic weights are shown in Table 7.1 (where the valued are for one seismic frame).

- Floor dead load for weight calculations: 96 psf
- Floor dead load for mass calculations: 86 psf
- Roof dead load excluding penthouse: 83 psf
- Penthouse dead load: 116 psf
- Reduced live load per floor and for roof: 20 psf

  Cladding and parapet loads are based on the surface area of the structures.

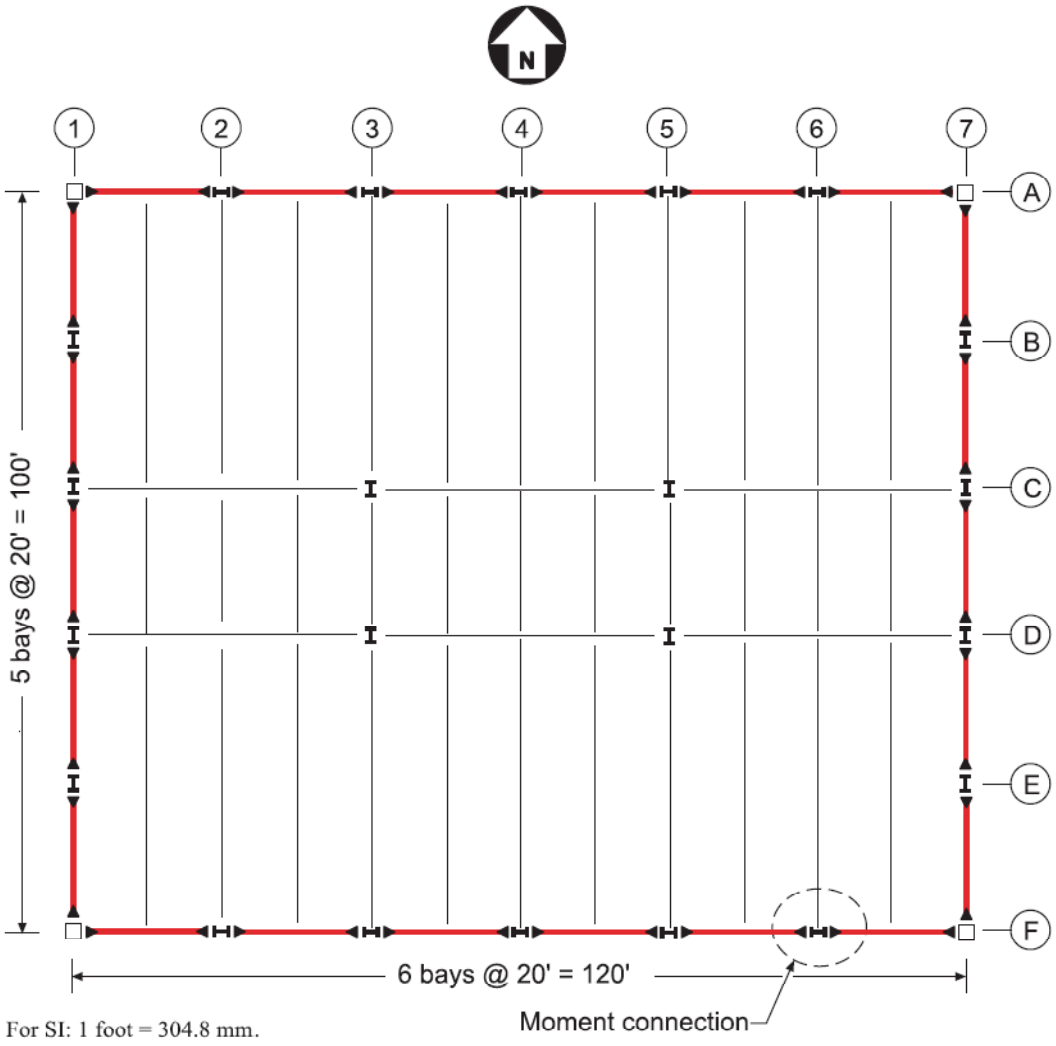

Figure 7.11. Typical Floor Plan of the LA 20-Story SAC Building.

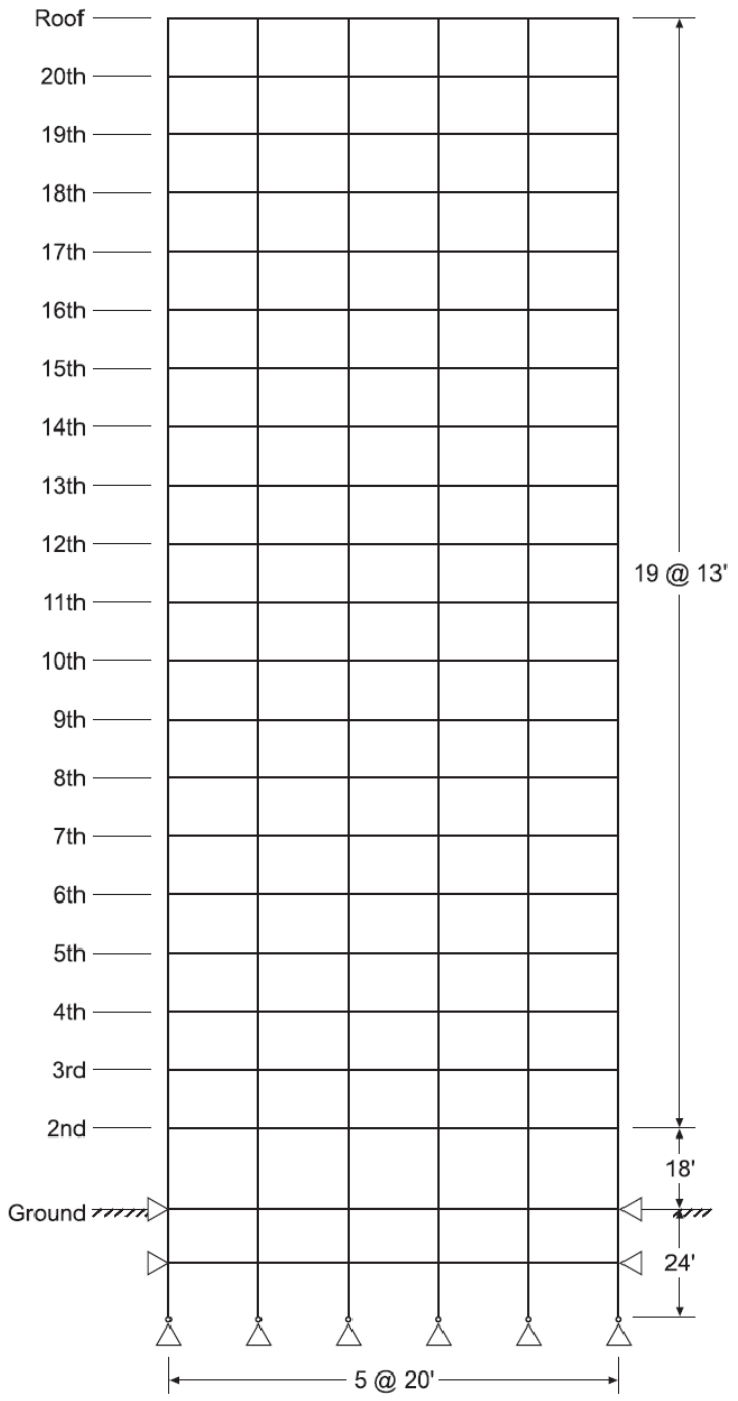

Figure 7.12. Elevation View of the Perimeter Moment Frame in the N-S Direction.

Table 7.1. Floor Seismic Weights.

Floor	Weight (kips)
Roof	645.0
Floor 20 to Floor 3	608.0
Floor 2	622.0

Table 7.2. Design Parameters Based on the 1994 UBC.

Parameter	Value
Occupancy Category	Standard
Soil Profile Type	S_2
Importance Factor	1.0
R_w	12
Building Height	265 ft
T	2.299 sec.
Importance Factor	1.0
Maximum Drift Ratio	2%

7.4.2 Design Base Shear and Lateral Force Distribution

The target yield mechanism was the same as shown in Figure 3.2.a with beam plastic hinges assumed at 6 inches from the column face. The design lateral force distribution as calculated by using Equation (3.1) to (3.3) is shown in Table 7.3.

According to UBC (1994), the elastic base shear coefficient, S_a, is given as:

$$S_a = ZIC \tag{7.3}$$

where, Z is the seismic zone factor, I is the occupancy importance factor and C is the seismic coefficient to be calculated as follows:

$$C = (0.075R_w) < 1.25S/T^{2/3} < 2.75 \quad (7.4)$$

With $R_w = 12$ for SMF, $S = 1.2$ for S_2 soil type, and $T = 2.299$ *sec.*, the value of C turns out to be *0.9*. For $Z = 0.4$ and $I = 1.0$, the value of $S_a = 0.36$.

The design base shear was determined for two level performance criteria: 1) a 2% maximum story drift ratio (θ_u) for a ground motion hazard with 10% probability of exceedance in 50 years (10/50 and 2/3MCE); 2) a 3% maximum story drift ratio (θ_u) for 2/50 event (MCE). A yield drift ratio (θ_y) of 1.0 % was used, which is typical for steel moment frames. The calculated values of all significant design parameters are listed in Table 8-4, and it is seen that the design base shear for the first hazard level (2/3) MCE governs the design.

Table 7.3. Lateral Force Distribution Calculation for PBPD Frame.

Floor	h_j (ft.)	w_j (kips)	$w_j h_j$ (k-ft)	$\sum w_j h_j$ (k-ft)	β_i	$\beta_i - \beta_{i+1}$	$(\beta_i - \beta_{i+1}) \cdot h_i$	F_i * (kips)	Story Shear V_i (kips)
Roof	265	645	170925	170925	1.000	1.000	265.00	263.4	263.4
20	252	608	153216	324141	1.501	0.501	126.34	132.1	395.5
19	239	608	145312	469453	1.899	0.398	95.14	104.9	500.3
18	226	608	137408	606861	2.236	0.336	76.00	88.6	588.9
17	213	608	129504	736365	2.528	0.292	62.23	77.0	665.9
16	200	608	121600	857965	2.785	0.258	51.52	67.9	733.7
15	187	608	113696	971661	3.015	0.229	42.83	60.3	794.1
14	174	608	105792	1077453	3.219	0.204	35.58	53.9	847.9
13	161	608	97888	1175341	3.402	0.183	29.42	48.1	896.1
12	148	608	89984	1265325	3.565	0.163	24.14	43.0	939.0
11	135	608	82080	1347405	3.710	0.145	19.59	38.2	977.3
10	122	608	74176	1421581	3.838	0.128	15.67	33.8	1011.1
9	109	608	66272	1487853	3.951	0.113	12.28	29.7	1040.8
8	96	608	58368	1546221	4.049	0.098	9.38	25.7	1066.5
7	83	608	50464	1596685	4.132	0.083	6.92	22.0	1088.5
6	70	608	42560	1639245	4.202	0.070	4.87	18.3	1106.8
5	57	608	34656	1673901	4.258	0.056	3.20	14.8	1121.6
4	44	608	26752	1700653	4.301	0.043	1.90	11.3	1133.0
3	31	608	18848	1719501	4.331	0.030	0.94	8.0	1140.9
2	18	622	11196	1730697	4.349	0.018	0.32	4.7	1145.6
SUM		12211	1730697		66.272	4.349	883.28	1145.6	

*Note: For one moment frames in N-S direction

Table 7.4. Design Parameters for PBPD Frame.

Design Parameters	10% in 50 years Hazard (2/3MCE)	2% in 50 years Hazard (MCE)
S_a	0.36 g	0.54 g
T	2.299 sec.	2.299 sec.
Yield Drift Ratio θ_y	1.0%	1.0%
Target Drift Ratio θ_u	2%	3%
Inelastic Drift Ratio $\theta_p = \theta_u - \theta_y$	1%	2%
$\mu_s = \theta_u / \theta_y$	2.0	3
R_μ	2.0	3
γ	0.75	0.438
α	0.942	1.884
V/W	0.094	0.082
Design Base Shear V *	1146 kips (governs)	1006 kips

7.4.3 Design of Beams

The beams were designed as full sections assuming ductile unreinforced flange connections with the columns (such as Slotted Web connections). The distance of the plastic hinges from the face of the columns was assumed as 6". The plastic moment of the columns at the base in one-bay model was calculated by using the modified Equation (7.2):

$$M_{pc} = 1.5V'h_1/4 = 1.5\times(1146/5)\times 18/4 = 1547.1\ k\text{-}ft \tag{7.5}$$

The required beam strength at each floor level, $\beta_i M_{pb}$, was calculated by using Equation (3.19). The distance between centers of plastic hinges, L_i', is determined by

assuming that a 6 in. shear plate and W24 column sections are used at all levels. That is, $L_i' = L - (d_c + w_s) \times 2 = 20 \times 12 - (12" + 6") \times 2 = 204"$ = 17 ft. = 0.85L. The design parameters for the beams are given in Table 7.5, and the final design sections in Table 7.6 and 7.7.

Table 7.5. Design Parameters for Beams.

Floor	$F_i / 5$ (kips)	$F_i h_i / 5$ (k-ft)	$\beta_i M_{pb} = M_u$ (k-ft)	$M_n = \frac{M_u}{\phi}$ * (k-ft)	Z ** (required) (in^3)
Roof	50.2	13249	265	295	71
20	25.1	6338	398	443	106
19	20.0	4773	504	560	134
18	16.9	3813	593	659	158
17	14.7	3122	671	745	179
16	12.9	2585	739	821	197
15	11.5	2149	800	889	213
14	10.3	1785	854	949	228
13	9.2	1476	902	1003	241
12	8.2	1211	946	1051	252
11	7.3	983	984	1094	262
10	6.4	786	1018	1131	272
9	5.7	616	1048	1165	279
8	4.9	471	1074	1193	286
7	4.2	347	1096	1218	292
6	3.5	244	1115	1238	297
5	2.8	161	1130	1255	301
4	2.2	95	1141	1268	304
3	1.5	47	1149	1277	306
2	0.9	16	1154	1282	308

*Note: Lateral force for one-bay
*Note: φ=0.9
*Note: $M=ZF_y$; $F_y=50$ ksi (A992 Grade 50)

Table 7.6. Beam Design Results for PBPD Frame.

Floor	Design Section	Z (in^3)	Compactness*	ϕZF_y (k-ft)	M_u (k-ft)
Roof	**W16X40**	73	O.K.	274	265
20	**W21X50**	110	O.K.	413	398
19	**W21X62**	144	O.K.	540	504
18	**W21X68**	160	O.K.	600	593
17	**W24X76**	200	O.K.	750	671
16	**W24X76**	200	O.K.	750	739
15	**W24X84**	224	O.K.	840	800
14	**W24X84**	224	O.K.	840	854
13	**W24X94**	254	O.K.	953	902
12	**W24X94**	254	O.K.	953	946
11	**W27X94**	278	O.K.	1043	984
10	**W27X94**	278	O.K.	1043	1018
9	**W27X94**	278	O.K.	1043	1048
8	**W27X102**	305	O.K.	1144	1074
7	**W27X102**	305	O.K.	1144	1096
6	**W27X102**	305	O.K.	1144	1115
5	**W27X102**	305	O.K.	1144	1130
4	**W27X102**	305	O.K.	1144	1141
3	**W27X102**	305	O.K.	1144	1149
2	**W27X102**	305	O.K.	1144	1154

*Note: In accordance with AISC Seismic Design Manual

Table 7.7. Beam Design Results for PBPD Frame.

Floor	Design Section	C_{pr}	M_{pr} (k-ft)	w_g (kip/ft)	V_{SW} (kips)	V'_{SW} (kips)	$\phi V_n \geq V_{SW}$ (kips)
Roof	**W16X40**	1.00	335	0	39	39	146
20	**W21X50**	1.05	529	0	62	62	237
19	**W21X62**	1.05	693	0	82	82	252
18	**W21X68**	1.05	770	0	91	91	273
17	**W24X76**	1.05	963	0	113	113	316
16	**W24X76**	1.05	963	0	113	113	316
15	**W24X84**	1.05	1078	0	127	127	340
14	**W24X84**	1.05	1078	0	127	127	340
13	**W24X94**	1.05	1222	0	144	144	376
12	**W24X94**	1.05	1222	0	144	144	376
11	**W27X94**	1.05	1338	0	157	157	396
10	**W27X94**	1.05	1338	0	157	157	396
9	**W27X94**	1.05	1338	0	157	157	396
8	**W27X102**	1.05	1468	0	173	173	419
7	**W27X102**	1.05	1468	0	173	173	419
6	**W27X102**	1.05	1468	0	173	173	419
5	**W27X102**	1.05	1468	0	173	173	419
4	**W27X102**	1.05	1468	0	173	173	419
3	**W27X102**	1.05	1468	0	173	173	419
2	**W27X102**	1.05	1468	0	173	173	419

*Note: In accordance with AISC Seismic Design Manual Table 1-2.

7.4.4 Design of Columns

The design of columns was done by using the concept of column tree. The column trees for the 4-story MF were shown in Figure 3.9, where the terms $\alpha_i F_L$, $(V_{SW})_i$, $(M_{pr})_i$, and $(P_c)_i$ are treated as applied loads. Similar column trees were constructed for this 20-story frame as well. The sum of required balancing lateral forces for the exterior and interior column trees were obtained by using Equations (3.21) and (3.23), respectively. For the exterior column tree F_L came out as 141.3 kips and that for the interior column tree as 282.6 kips. Design parameters for the columns are listed in Table 7.8, and Table 7.9 gives the required strength of the columns. It should be mentioned that the gravity loads on the exterior as well as interior columns were ignored because of rather small tributary areas for this example frame in the N-S direction (See Figure 7.11). The design end moments for the columns as amplified by B_2-factors are shown in Figure 7.33. The B_2-factor method was selected because it works slightly better than the direct P-Delta method for design of lower story columns as indicated by the results presented in Section 7.3.

Doubler plates of 0.5 in. thickness were needed for top four stories, but only for interior columns. Final column sections are shown in Table 7.10. Also shown in Table 7.10 are member sections used in the original SAC frame. The material weights for one PBPD frame and the SAC frame are shown in Table 7.11.

Table 7.8. Parameters for Column Design of PBPD Frame.

			Exterior Column		Interior Column		
Floor	α_i	$\alpha_i h_i$	$\alpha_i F_L$ (kips)	Column Shear (kips)	$\alpha_i F_L$ (kips)	Column Shear (kips)	Floor Weight On Gravity Column (kips)
Roof	0.230	60.93	34.5	34.5	69.0	69.0	720
20	0.115	29.05	17.3	51.8	34.6	103.5	679
19	0.092	21.87	13.7	65.5	27.4	131.0	679
18	0.077	17.48	11.6	77.1	23.2	154.2	679
17	0.067	14.31	10.1	87.2	20.1	174.3	679
16	0.059	11.85	8.9	96.0	17.8	192.1	679
15	0.053	9.85	7.9	103.9	15.8	207.9	679
14	0.047	8.18	7.0	111.0	14.1	222.0	679
13	0.042	6.76	6.3	117.3	12.6	234.6	679
12	0.038	5.55	5.6	122.9	11.2	245.8	679
11	0.033	4.51	5.0	127.9	10.0	255.8	679
10	0.030	3.60	4.4	132.3	8.9	264.7	679
9	0.026	2.82	3.9	136.2	7.8	272.4	679
8	0.022	2.16	3.4	139.6	6.7	279.2	679
7	0.019	1.59	2.9	142.5	5.8	284.9	679
6	0.016	1.12	2.4	144.9	4.8	289.7	679
5	0.013	0.74	1.9	146.8	3.9	293.6	679
4	0.010	0.44	1.5	148.3	3.0	296.6	679
3	0.007	0.22	1.0	149.3	2.1	298.7	679
2	0.004	0.07	0.6	149.9	1.2	299.9	694
Sum	1.000	203.09	149.9		299.9		

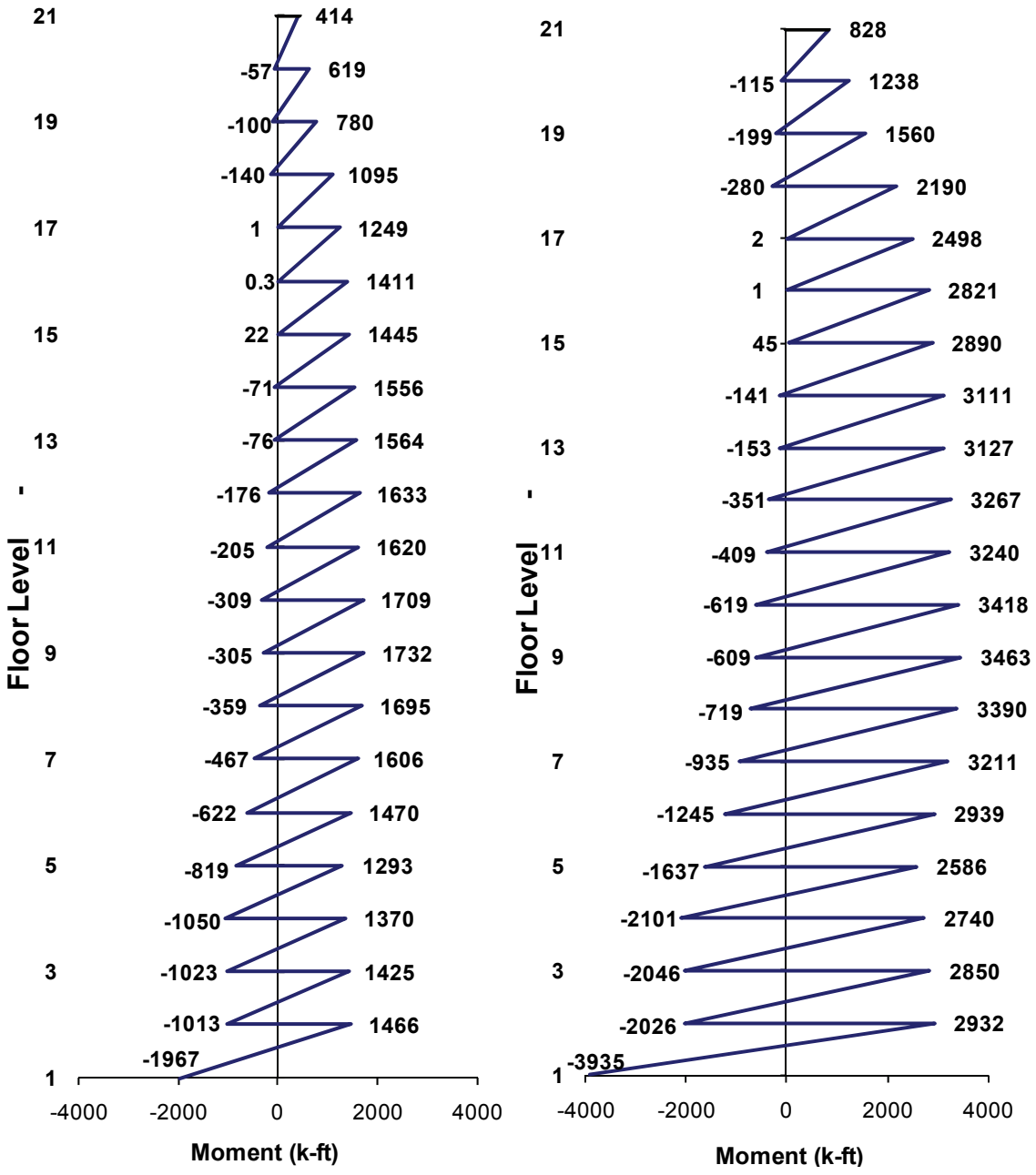

Figure 7.13. Amplified Design Moments for: (a) Exterior Column; (b) Interior Column.

Table 7.9. Required Strength for Columns of PBPD Frame.

Floor	Exterior Column		Interior Column
	Moment, M_u (k-ft)	Axial Force , P_u (kips)	Moment, M_u (k-ft)
Roof	414.0	39.4	827.9
20	618.9	102.8	1237.8
19	780.2	184.3	1560.3
18	1095.1	297.5	2190.2
17	1249.1	410.8	2498.2
16	1410.7	537.6	2821.3
15	1445.0	664.4	2890.1
14	1555.7	808.2	3111.3
13	1563.5	952.0	3126.9
12	1633.4	1109.4	3266.8
11	1619.8	1266.8	3239.5
10	1708.8	1439.5	3417.6
9	1731.7	1612.2	3463.3
8	1695.2	1784.9	3390.3
7	1605.7	1957.6	3211.4
6	1469.6	2130.3	2939.2
5	1292.9	2302.9	2585.9
4	1370.0	2498.8	2739.9
3	1425.2	2694.7	2850.4
2	-1967.3	2890.6	-3934.6

Table 7.10. Member Sections for PBPD Frame and SAC Frame.

	PBPD Frame			SAC Frame		
Floor	Beams	Ext. Columns	Int. Columns	Beams	Ext. Columns	Int. Columns
Roof	W16X40	W24X68	W24X117	W21X50	H15X15X0.5	W24X84
20	W21X50	W24X68	W24X117	W24X62	H15X15X0.5	W24X84
19	W21X62	W24X104	W24X176	W27X84	H15X15X0.75	W24X117
18	W21X68	W24X104	W24X176	W27X84	H15X15X0.75	W24X117
17	W24X76	W24X162	W24X250	W30X99	H15X15X0.75	W24X131
16	W24X76	W24X162	W24X250	W30X99	H15X15X0.75	W24X131
15	W24X84	W24X162	W24X250	W30X99	H15X15X0.75	W24X131
14	W24X84	W24X207	W24X279	W30X99	H15X15X1.0	W24X192
13	W24X94	W24X207	W24X279	W30X99	H15X15X1.0	W24X192
12	W24X94	W24X207	W24X279	W30X99	H15X15X1.0	W24X192
11	W27X94	W24X250	W24X279	W30X108	H15X15X1.0	W24X229
10	W27X94	W24X250	W24X279	W30X108	H15X15X1.0	W24X229
9	W27X94	W24X250	W24X279	W30X108	H15X15X1.0	W24X229
8	W27X102	W24X306	W24X306	W30X108	H15X15X1.0	W24X229
7	W27X102	W24X306	W24X306	W30X108	H15X15X1.0	W24X229
6	W27X102	W24X306	W24X306	W30X108	H15X15X1.0	W24X229
5	W27X102	W24X335	W24X306	W30X99	H15X15X1.25	W24X331
4	W27X102	W24X335	W24X306	W30X99	H15X15X1.25	W24X331
3	W27X102	W24X335	W24X306	W30X99	H15X15X1.25	W24X331
2	W27X102	W24X408	W24X335	W30X99	H15X15X2.0	W24X331

Table 7.11. Material Weight for One Moment Frame (5 Bays).

Weight Calculation	PBPD (kips)	Original SAC (kips)	PBPD/SAC
Beams	178.4	191.8	0.93
Columns	398.0	318.9	1.25
Total	576.4	510.7	1.13

7.5 Verification by Nonlinear Analysis

Nonlinear static (pushover) and dynamic (time-history) analyses were carried out by using the Perform-3D computer program (CSI, 2007). The analytical model is shown in Figure 7.14 which also includes a lumped "gravity column" associated with one frame which allows consideration of *P-Δ* effect as well as its contribution to the response of the total structure. In addition, panel zone deformation and degradation of moment-rotation behavior of plastic hinges were also included in the analysis.

Figure 7.15 shows base shear versus roof drift plot of the two frames from the pushover analysis results. It can be noticed that the PBPD frame has somewhat greater ultimate strength than the SAC frame. The design base shears for the two frames are also shown in the figure. It is noted that the design base shear for SAC frame is significantly smaller than its ultimate strength. That is because for steel moment frames the design is generally governed by drift. For both frames sharp decrease in strength after reaching the ultimate strength is especially notable. This is clearly because of the prominent role of *P-Δ* effect in tall frames as compared with shorter structures. Figures 7.16, 7.17, and 7.18

show plots of deformed shapes and plastic hinge formations in the two frames. As targeted in the design, absence of plastic hinges in columns of the PBPD frame (except at the base) can be noticed, Figure 7.18. In contrast, significant plastic hinging in the columns in the lower stories is observed (Figure 7.17) which also shows up in the differences in deformed shape of the two frames, i.e., concentration of drift in the lower stories of the SAC frame (Figure 7.16).

Nonlinear dynamic (time history) analyses were then carried out on the two frames by using nine 10/50 and ten 2/50 SAC ground motions (Somerville et al., 1997). The maximum and mean story drifts for the two frames due to 10/50 ground motions are shown in Figures 7.19 and 7.20, respectively, and the location of plastic hinges and magnitude of plastic rotations in Figures 7.21 and 7.22. Similar response results due to ten 2/50 ground motions are plotted in Figures 7.23, 7.24, 7.25, and 7.26. Although there is significant scatter in the distribution of maximum story drifts of both frames, the mean values of maximum story drifts under 2/50 ground motions are somewhat more uniformly distributed along the height of the PBPD frame. More importantly though, even under 2/50 ground motions there is no plastic hinging in the columns of the PBPD frame except at the base as intended in design, Figure 7.26. In contrast, significant plastic hinging was observed in the lower story columns of the SAC frame which resulted in much larger residual story drifts as compared with PBPD frame under LA38 ground motion as shown in Figure 7.27. The results for 2/50 ground motions as discussed above do not include responses due to LA30, LA35, and LA36 records. Those responses were found to be more severe, resulting in larger story drifts for the PBPD frame, but in complete collapse

of the SAC frame, as evidenced in Figure 7.28 for LA35 ground motion. The progression of collapse started at t=13.62 seconds, when the sway mechanism of the lower 5 stories formed with plastic hinges at the base and top of the fifth-story columns (see Figure 7.29).

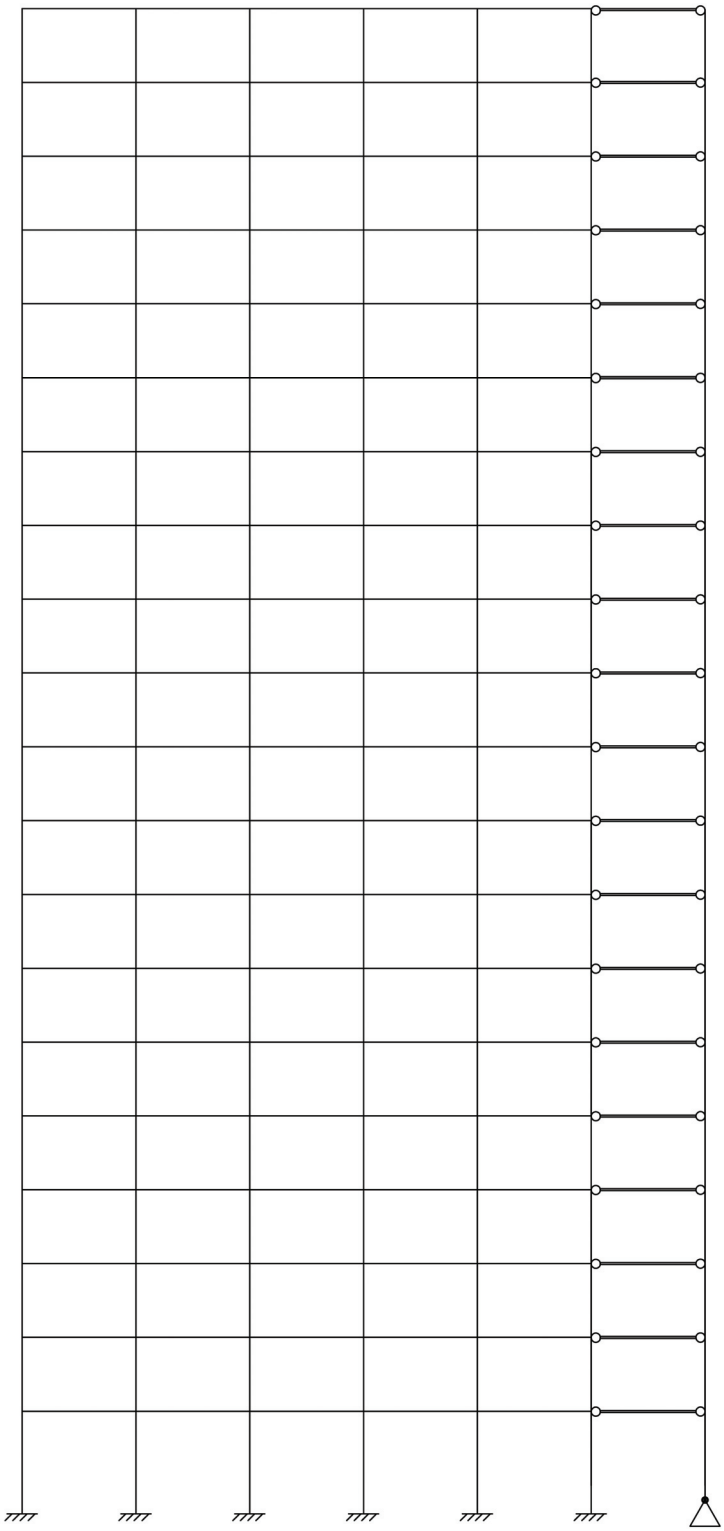

Figure 7.14. The Structural Model Used in Performance Evaluation.

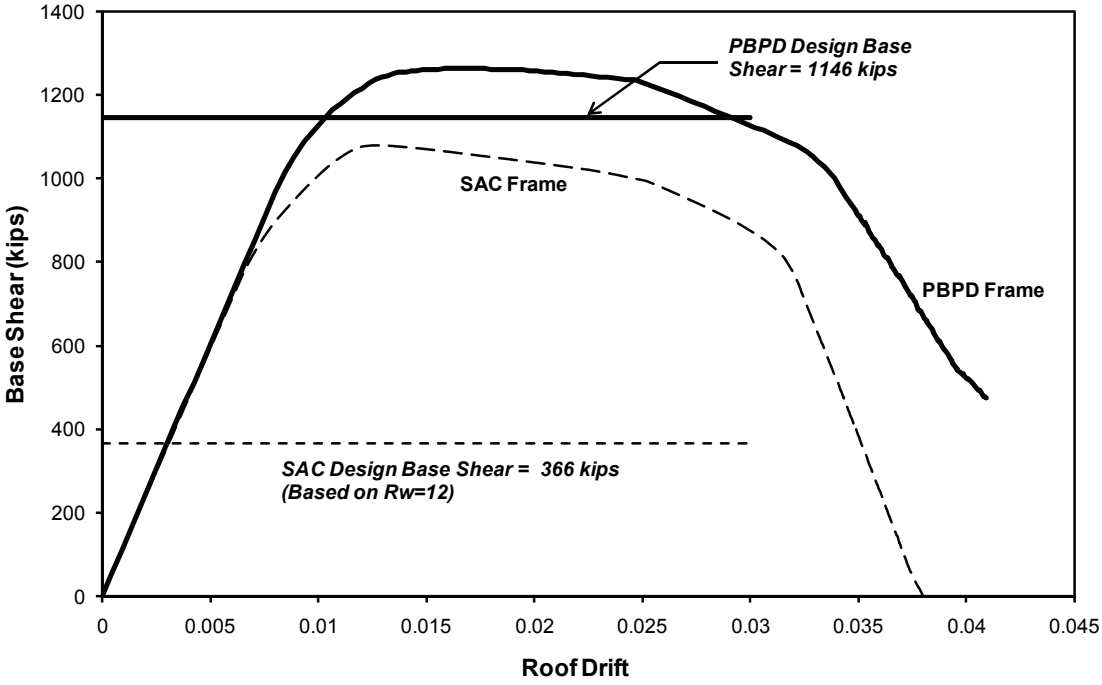

Figure 7.15. Comparison Between Pushover Curves of PBPD Frame and SAC Frame.

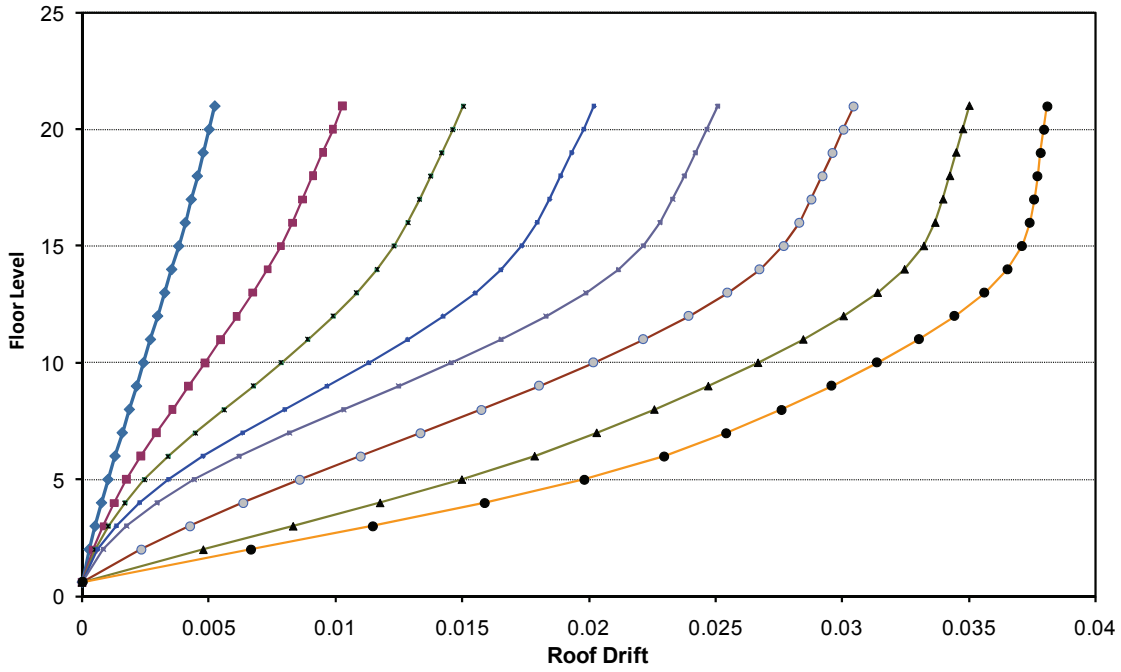

(a)

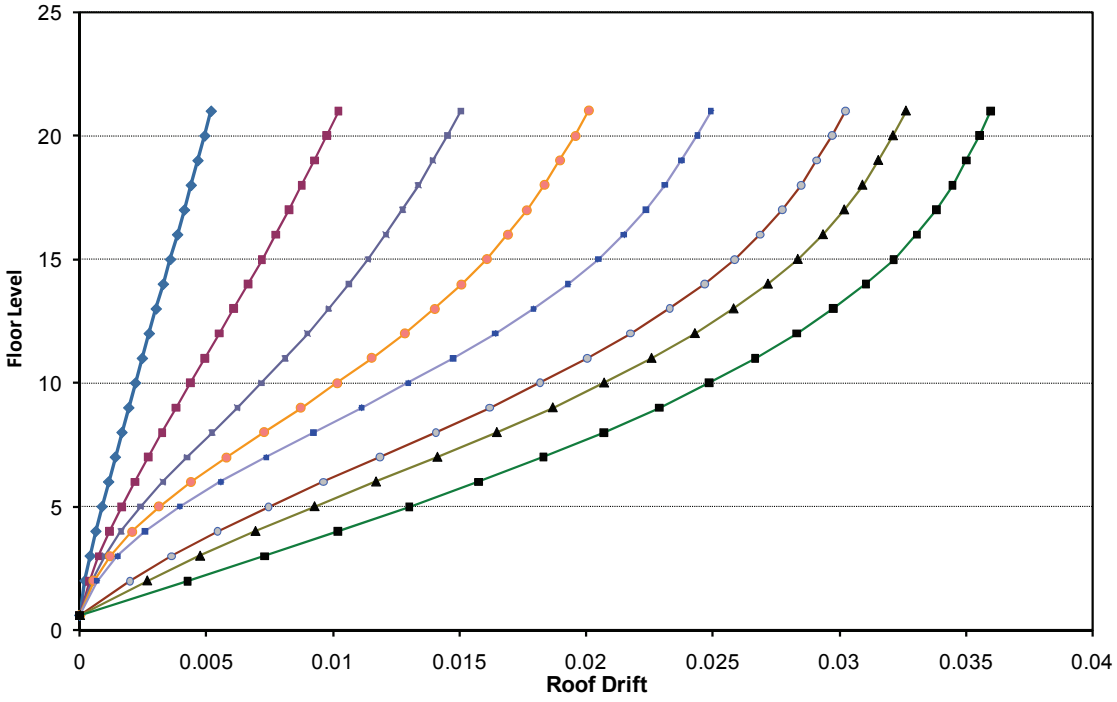

(b)

Figure 7.16. Frame Deformed Shapes under Pushover Analysis at Different Roof Drifts: (a) SAC Frame; (b) PBPD Frame.

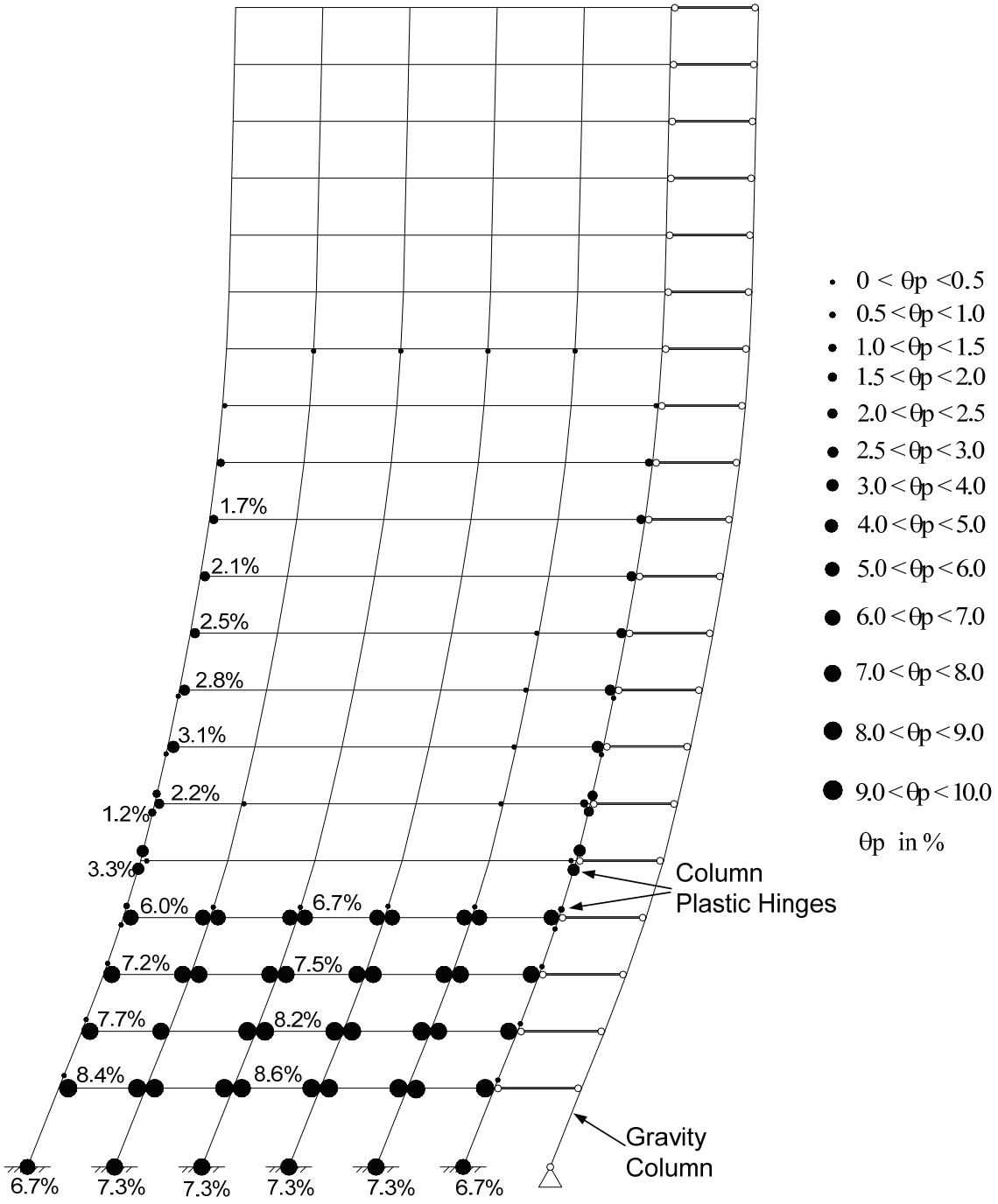

Figure 7.17. Plastic Hinge Rotations for SAC Frame under Pushover at 3.5% Roof Drift.

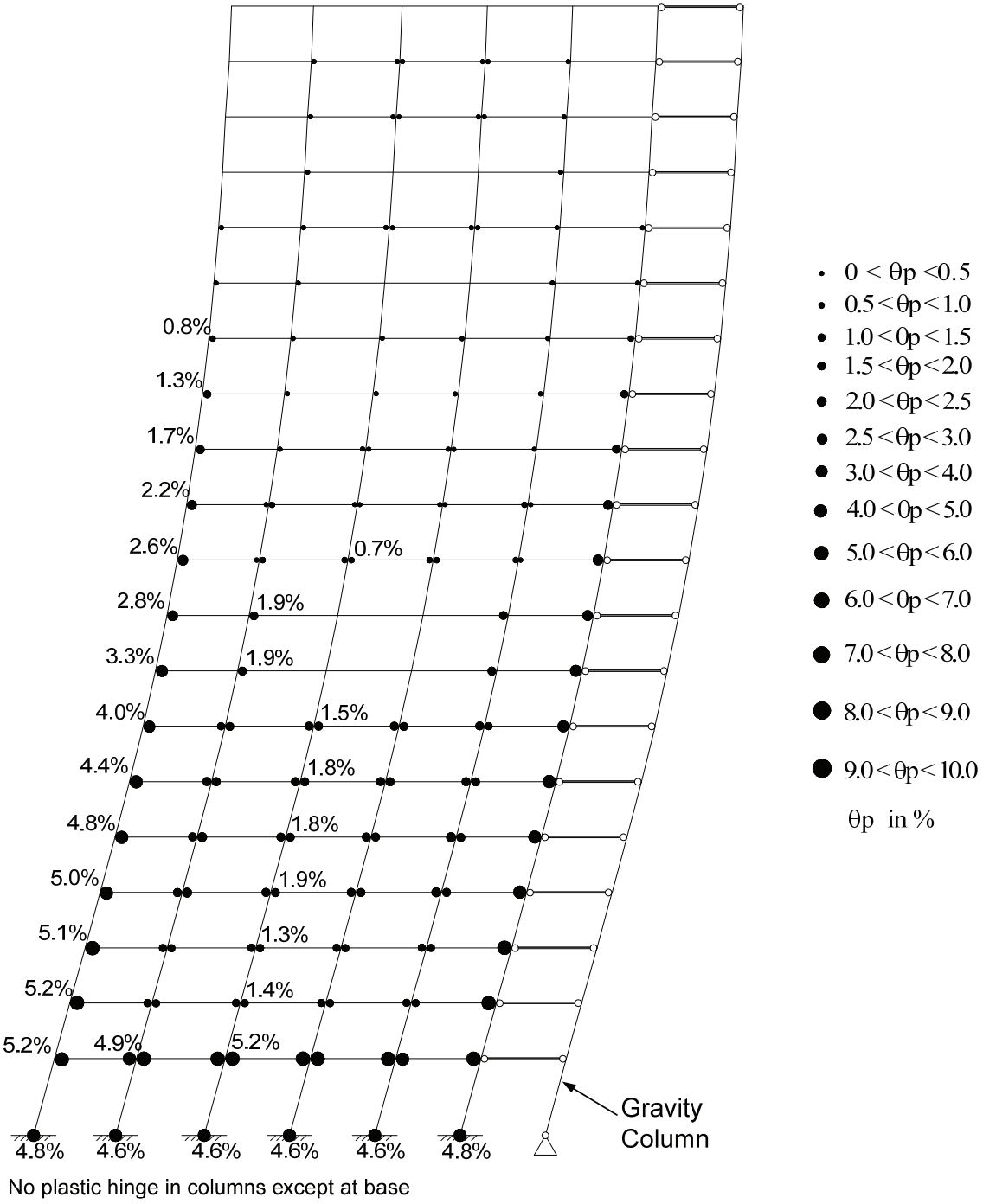

Figure 7.18. Plastic Hinge Rotations for PBPD Frame under Pushover at 3.5% Roof Drift.

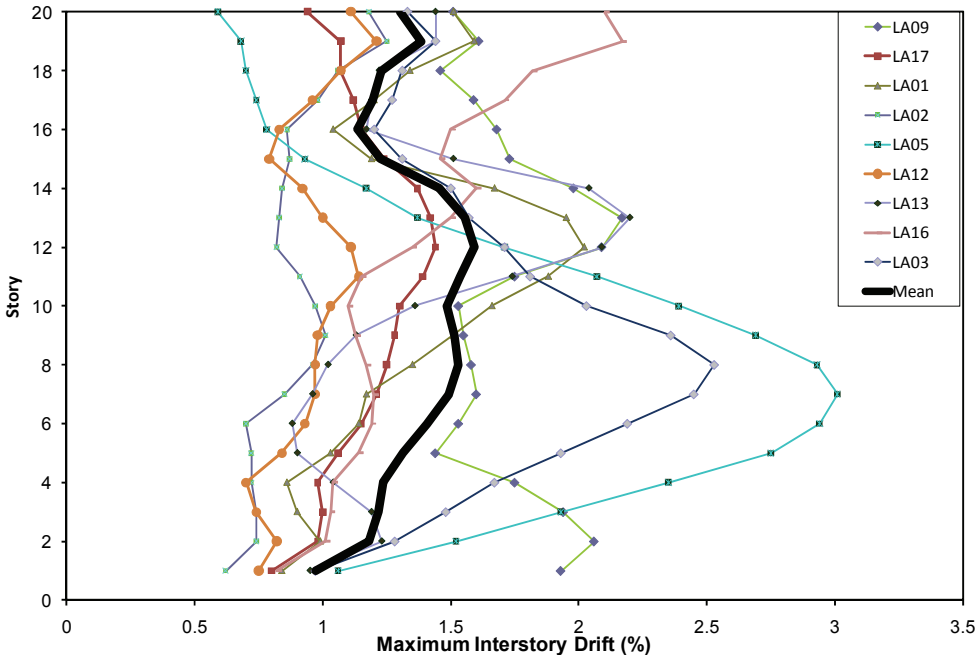

(a)

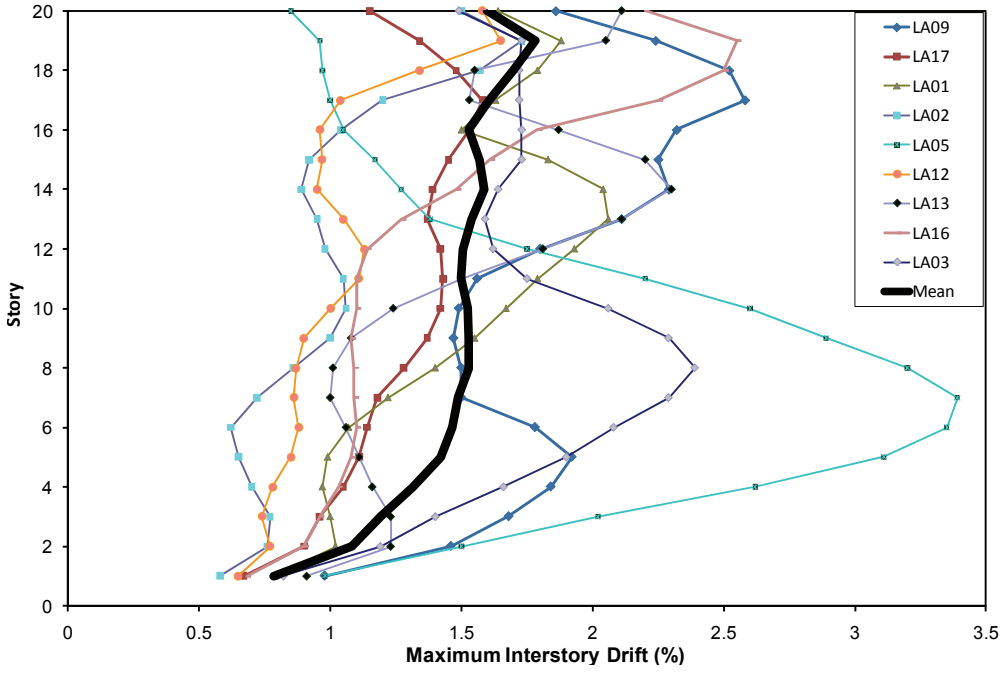

(b)

Figure 7.19. Maximum Interstory Drifts due to 10/50 Ground Motions: (a) SAC Frame; (b) PBPD Frame.

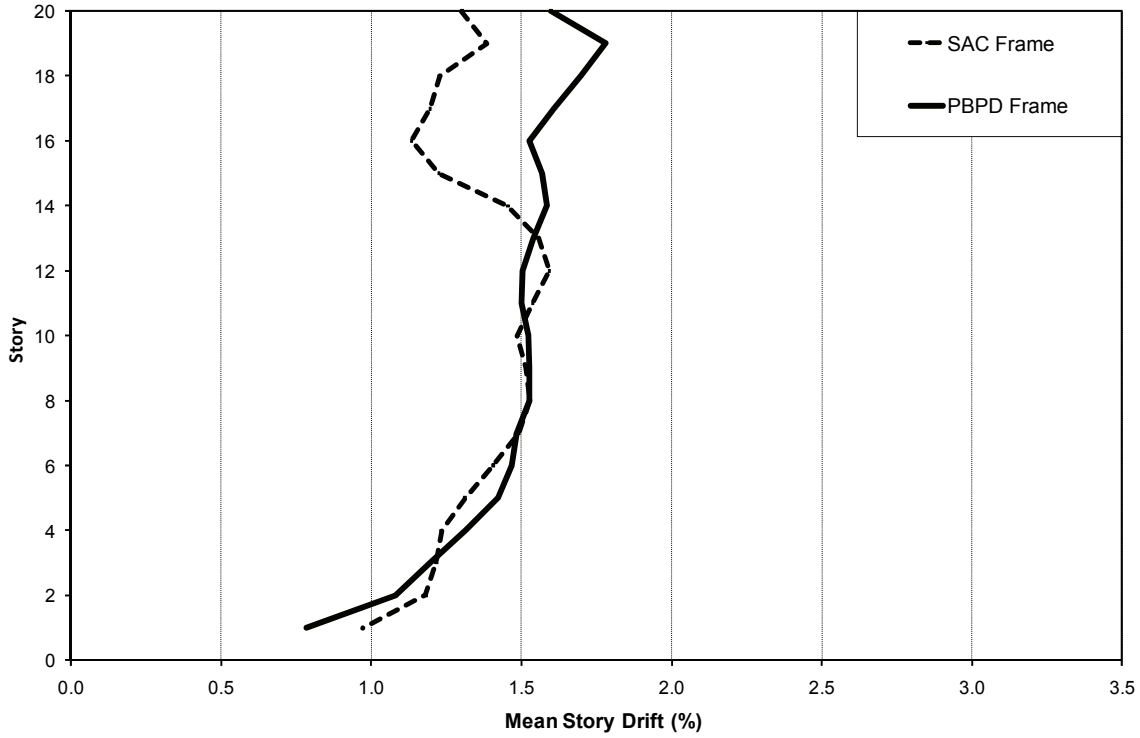

Figure 7.20. Mean Story Drifts due to 10/50 Ground Motions.

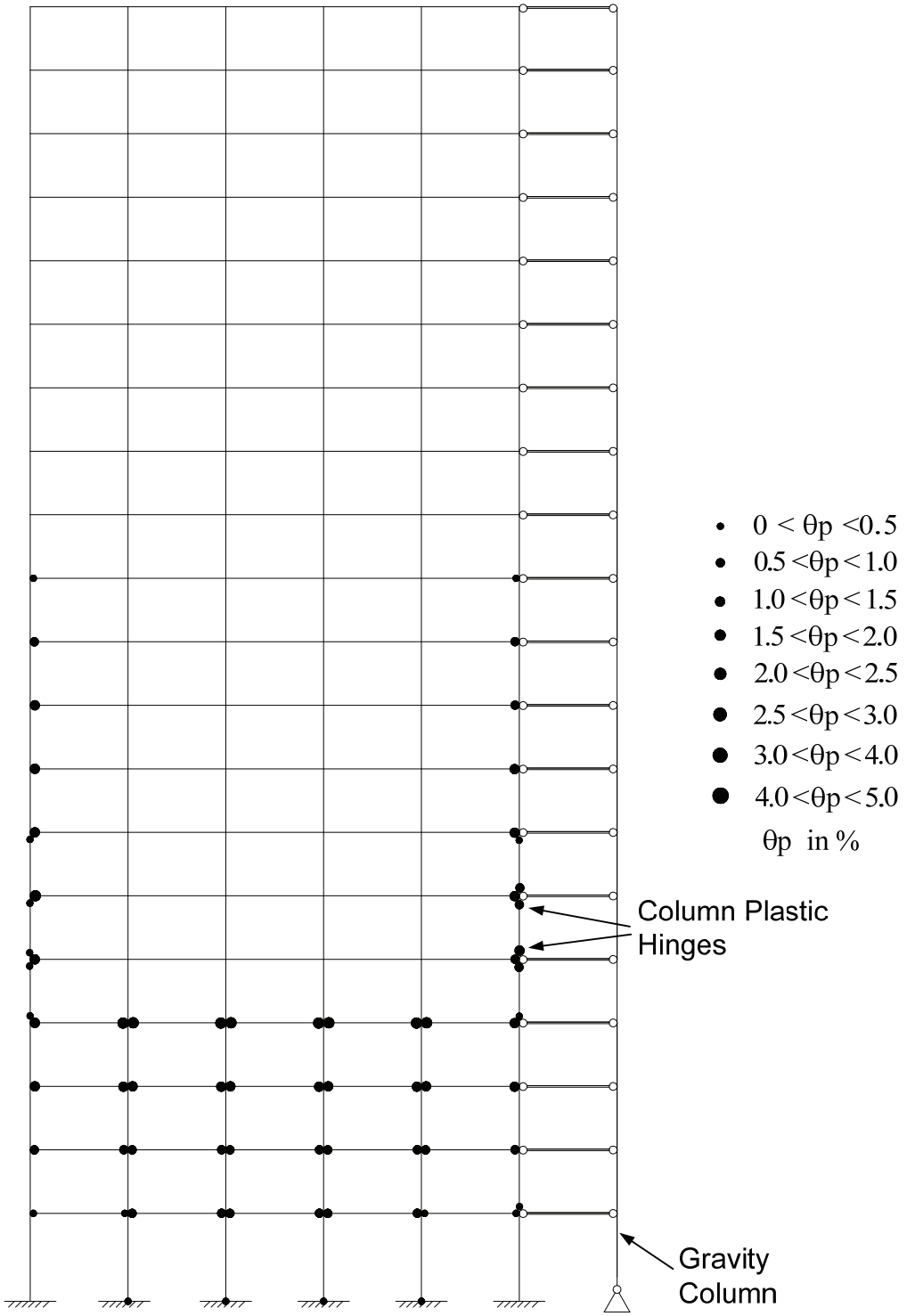

Figure 7.21. Plastic Hinge Locations for SAC Frame under LA05 Ground Motion.

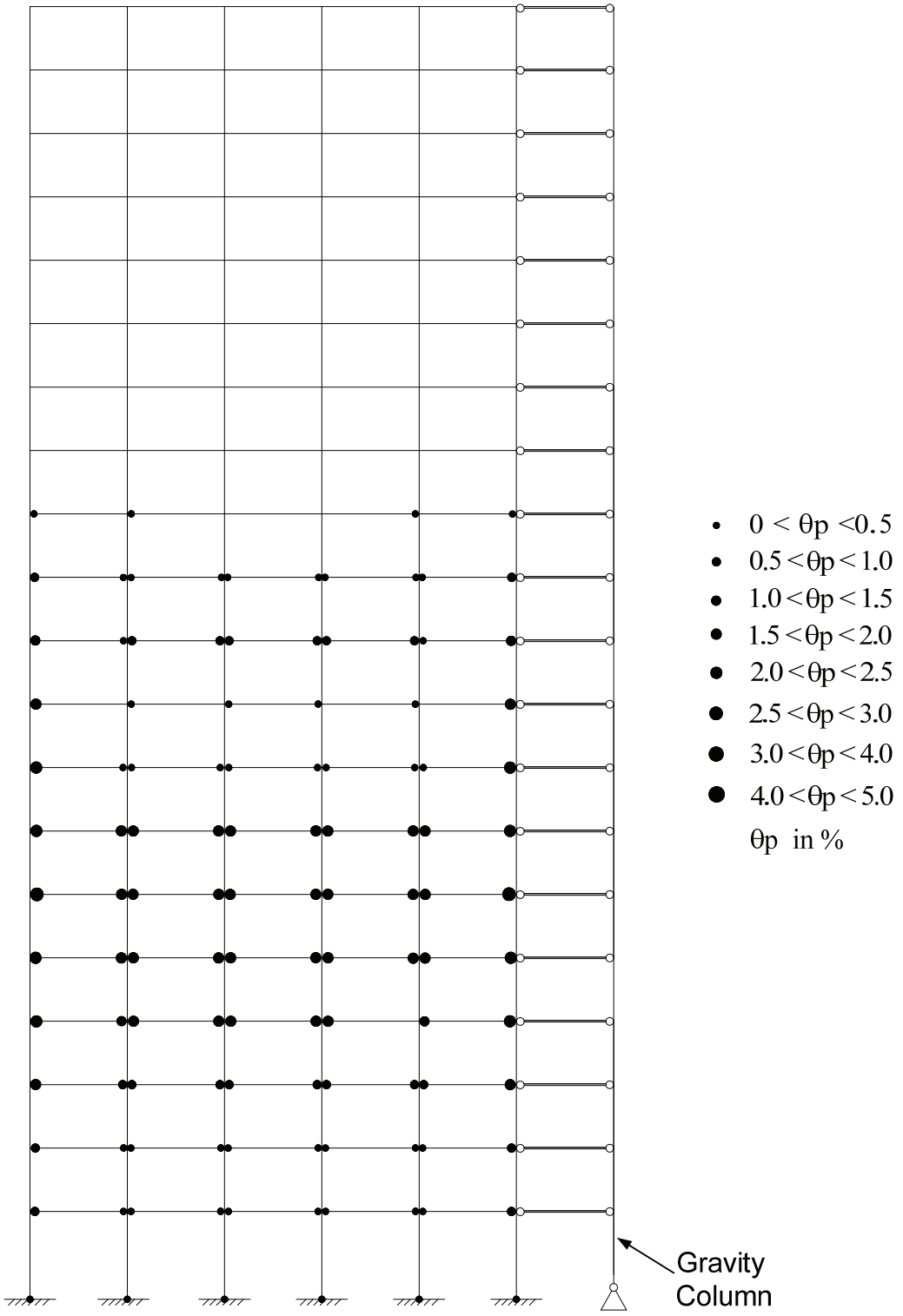

Figure 7.22. Plastic Hinge Locations for PBPD Frame under LA05 Ground Motion.

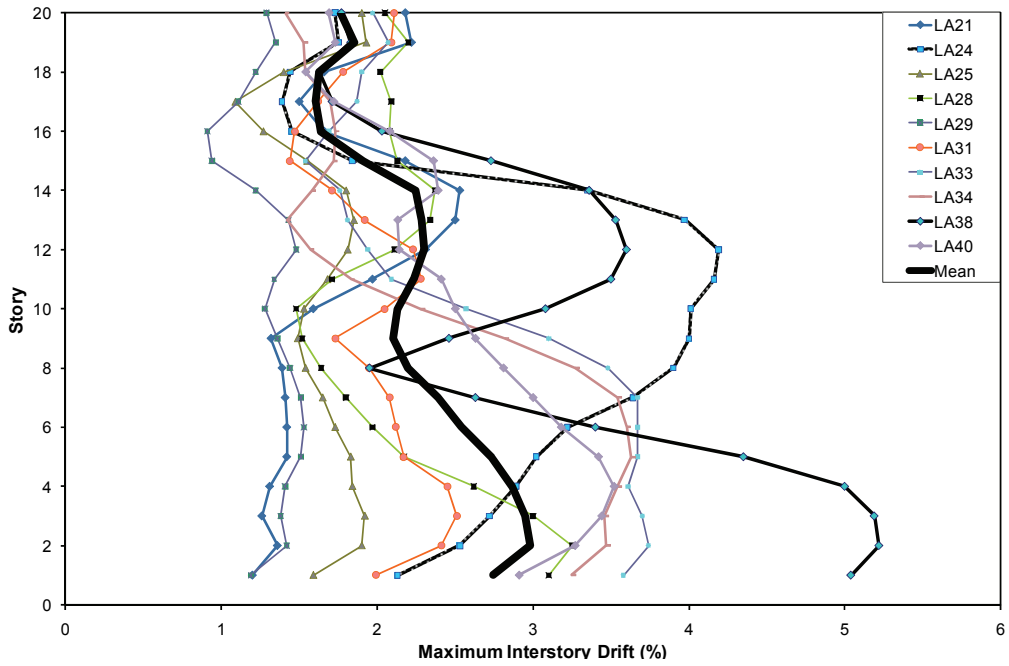

(a)

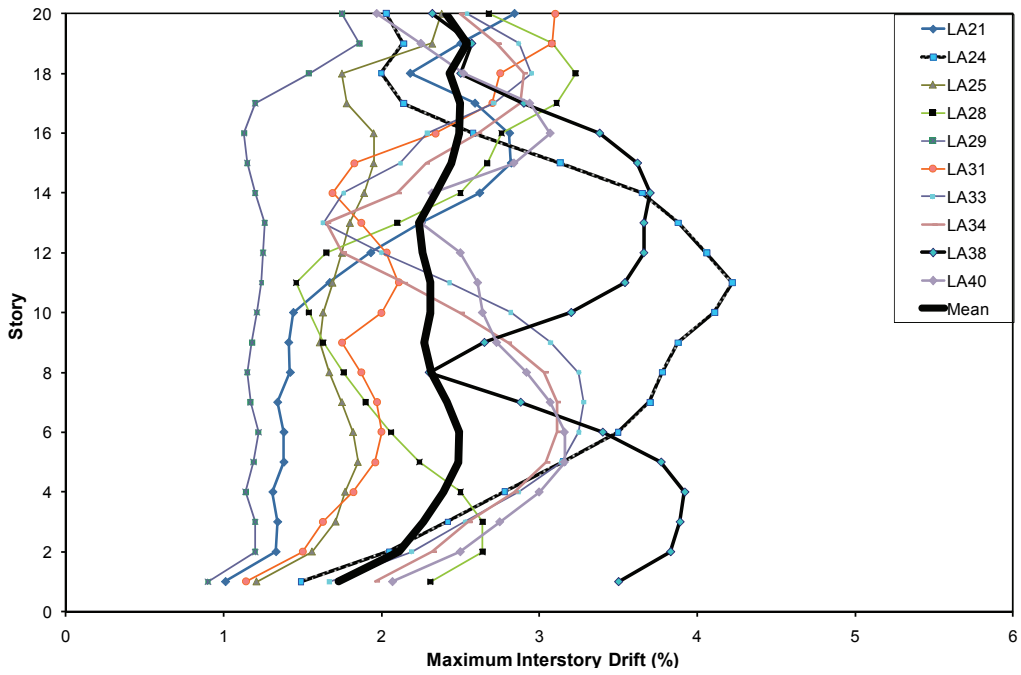

(b)

Figure 7.23. Maximum Interstory Drifts due to 2/50 Ground Motions: (a) SAC Frame; (b) PBPD Frame.

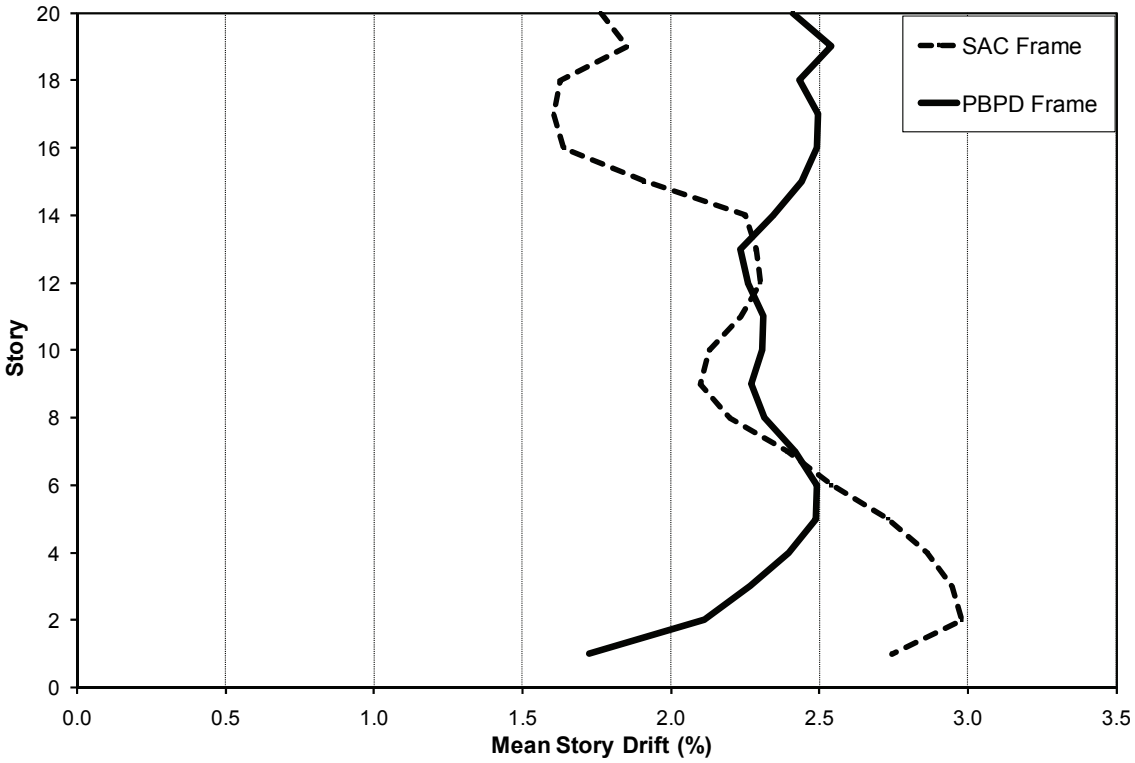

Figure 7.24. Mean Story Drifts under 2/50 Ground Motions.

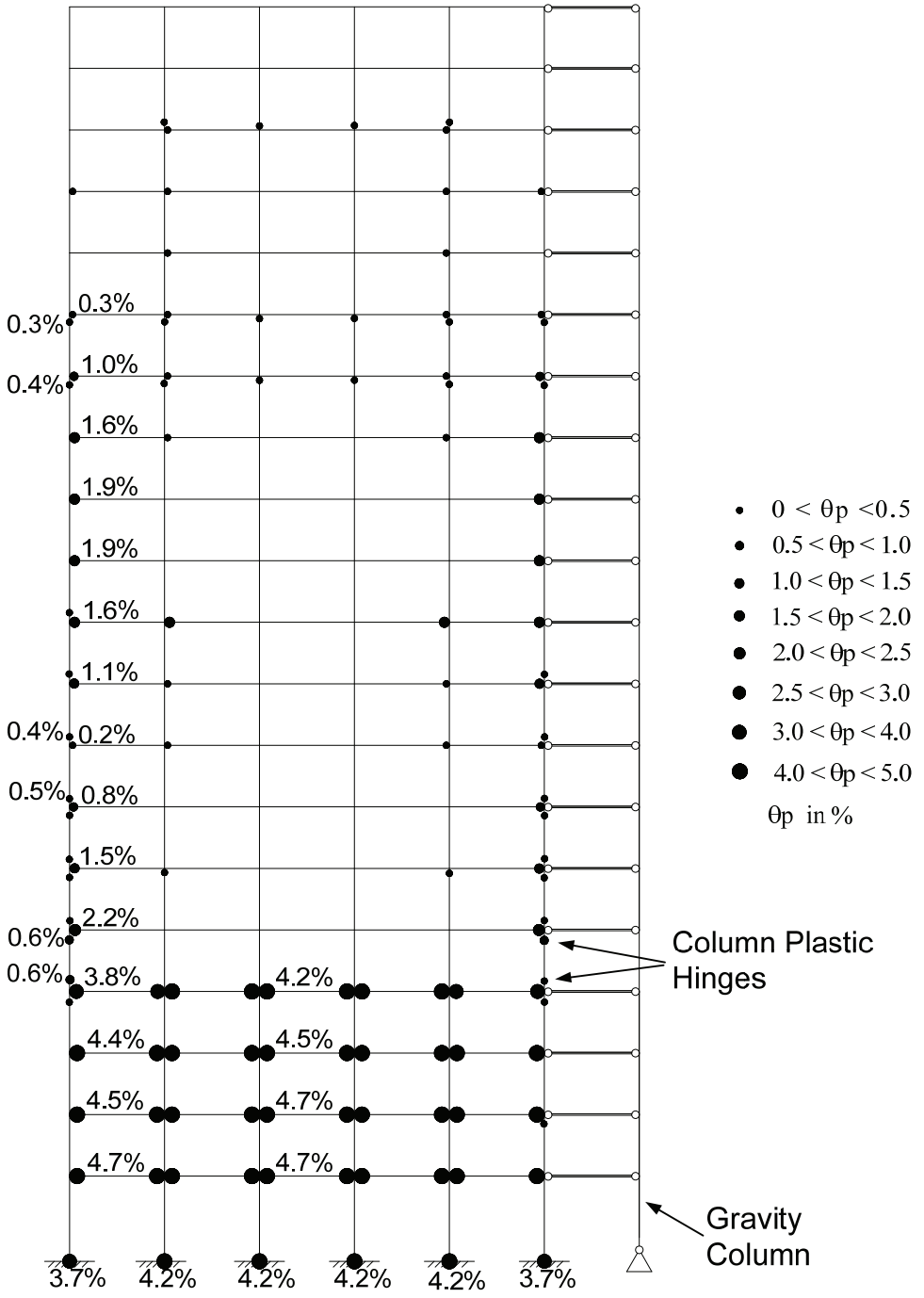

Figure 7.25. Plastic Hinge Locations for SAC Frame under LA38 Ground Motion.

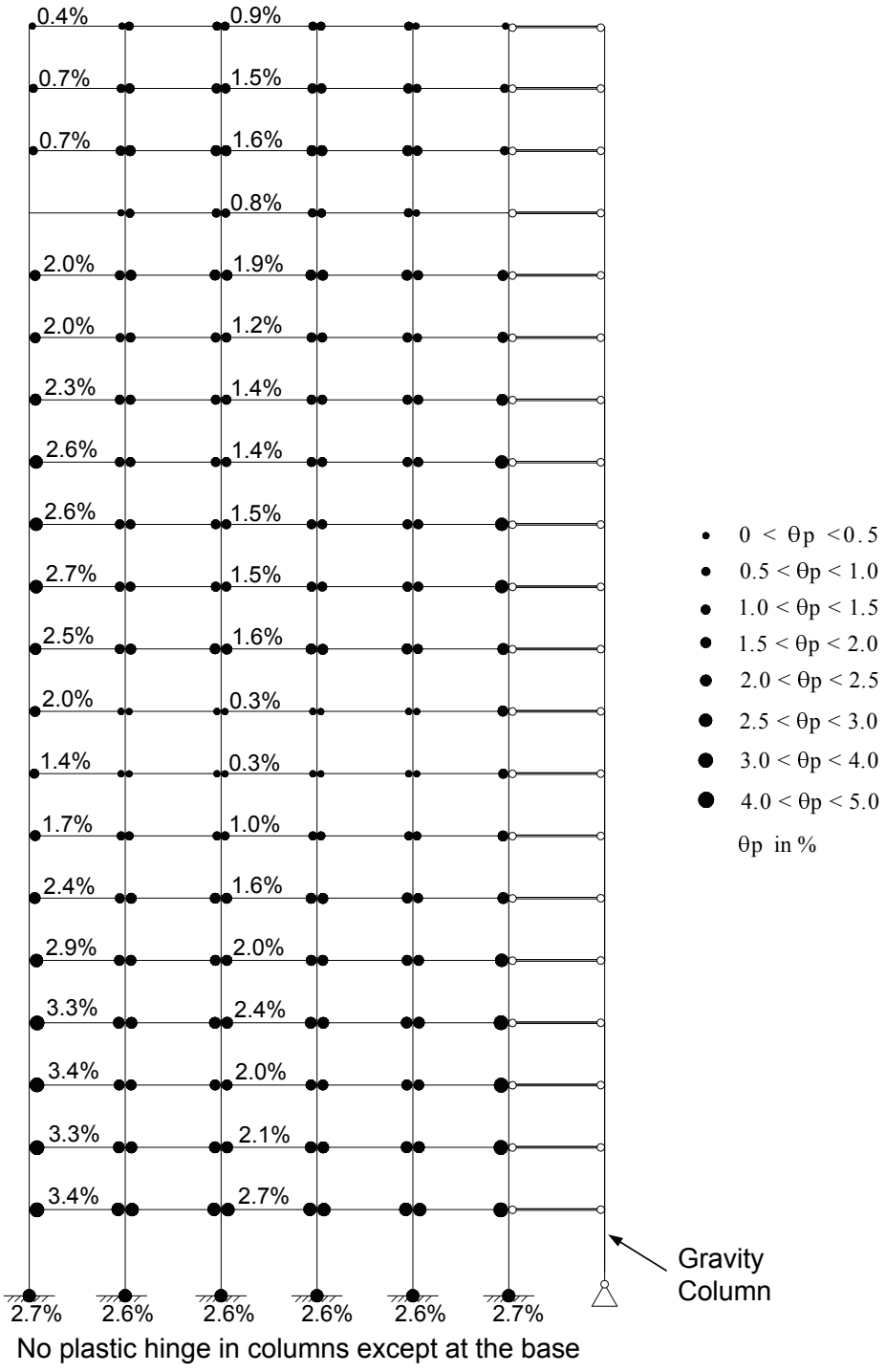

Figure 7.26. Plastic Hinge Locations for PBPD Frame under LA38 Ground Motion.

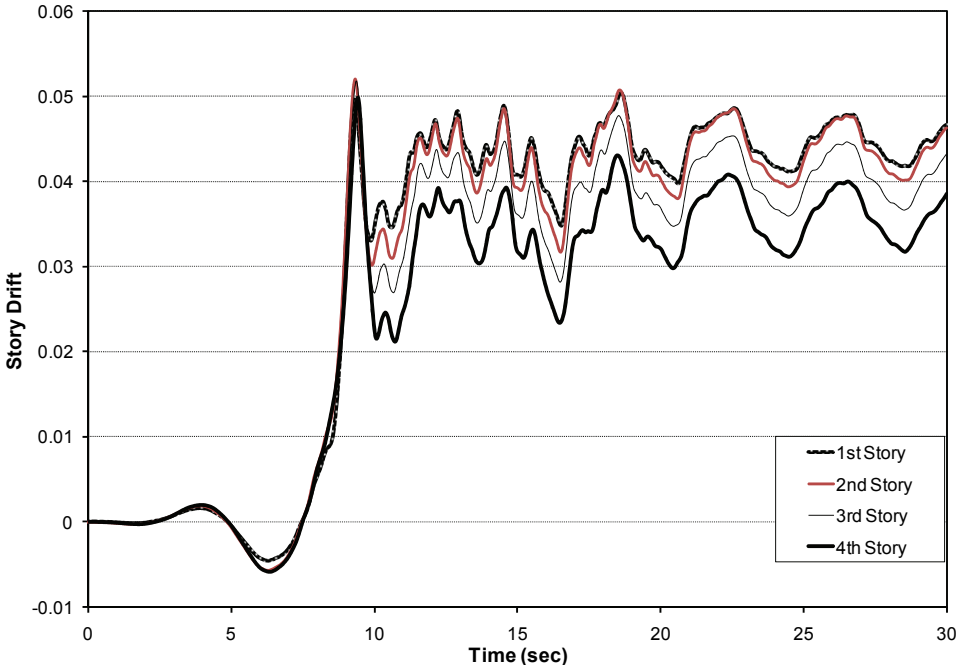

(a)

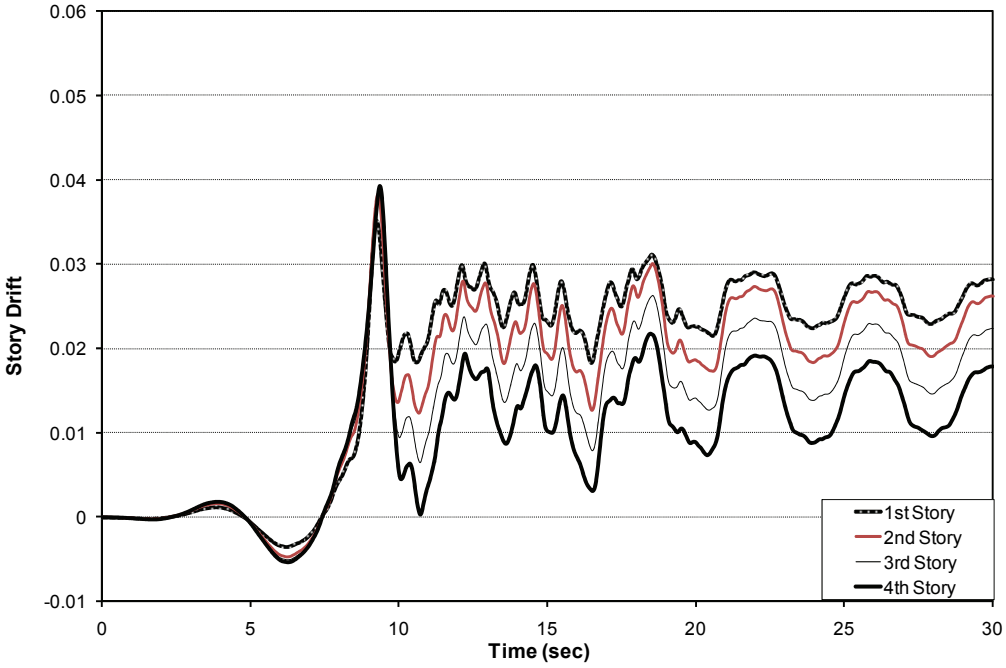

(b)

Figure 7.27. Story Drift-Time Plots under LA38 Ground Motion: (a) SAC Frame; (b) PBPD Frame.

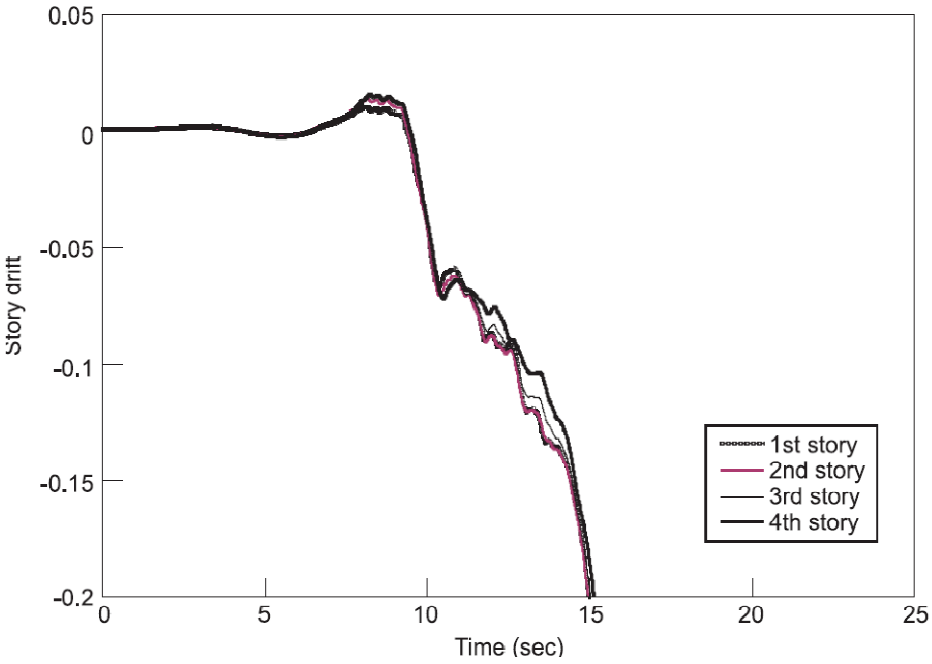

(a)

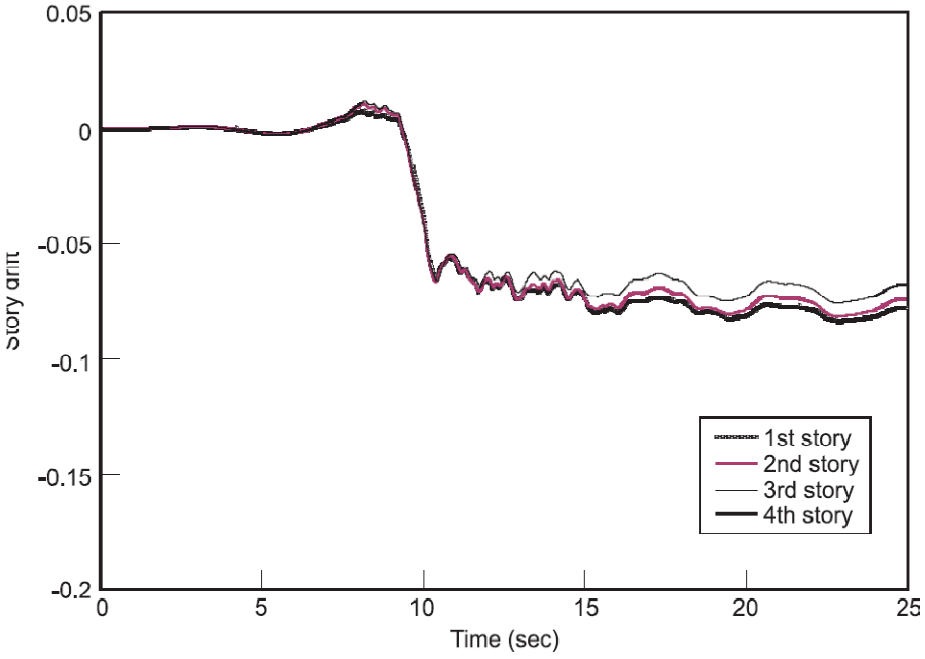

(b)

Figure 7.28. Story Drift-Time Plots under LA35 Ground Motion: (a) SAC Frame; (b) PBPD Frame.

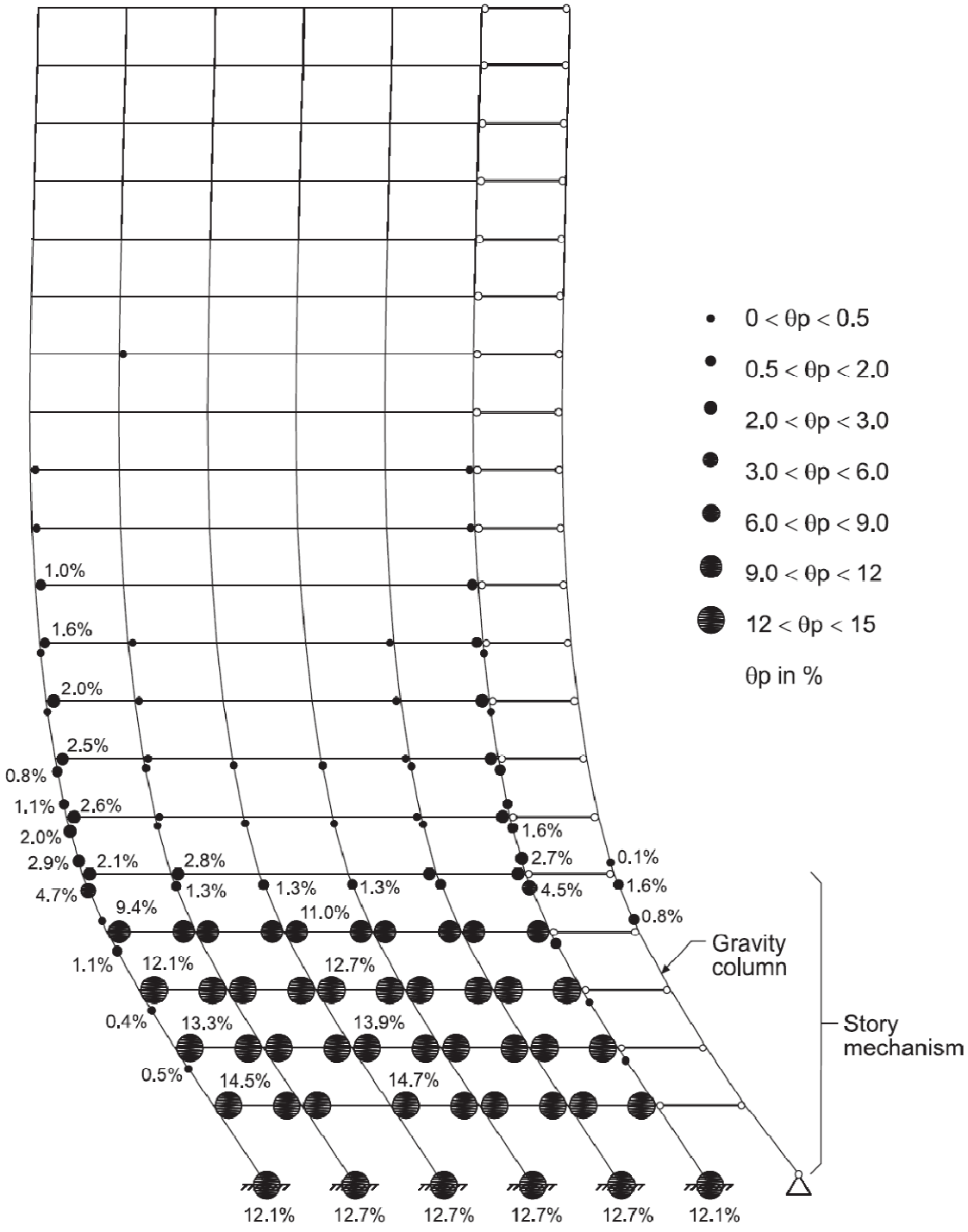

Figure 7.29. SAC Frame under LA35 Ground Motion at the Onset of Collapse (t=13.62 sec).

CHAPTER 8

DEVELOPMENT OF PBPD PROCEDURE FOR SEISMIC DESIGN OF STEEL PLATE SHEAR WALLS

8.1 General

Steel plate shear wall (SPSW) is an emerging steel structural element to resist lateral forces due to earthquakes. As has been demonstrated in recent experimental studies, SPSW can be used as seismic resistant element with stable hysteretic responses (Qu et al., 2008; Astaneh-Asl, 2001). Compared to other lateral load resisting systems, SPSW has the advantages of economy, rapid constructability, fewer detailing requirements, and stable ductile behavior. However, the behavior of SPSW systems is not well understood due to the lack of appropriate methodology to analyze and design such system. This has led to conservative design requirements (Berman et al., 2008). In addition, a pinched hysteretic response is expected in SPSW systems because the energy is dissipated through the post-buckling tension field action (Qu et al., 2008; Driver et al., 1998; Berman and Bruneau, 2005). This pinched behavior in turn leads to difficulty in predicting the maximum drift beyond first yield when the structure is designed by using the conventional elastic design approach, as commonly specified in current codes. Also, inelastic action or damage in SPSW systems could concentrate only at a few levels if the design is not carried out based on consideration of the overall yield mechanism.

In this chapter, the proposed Performance-Based Plastic Design (PBPD) procedure for seismic design of SPSW systems is presented. The developed PBPD procedure for SPSW structures offers a systematic approach for analysis and design of such systems. As was done with other systems, pre-selected target drift and yield mechanisms are used as performance limit states. The design lateral forces are derived by using an energy equation where the energy needed to push the structure up to the target drift is calculated as a fraction of elastic input energy which is obtained from the selected elastic design spectra. Plastic design is then performed to detail the frame members in order to achieve the intended yield mechanism and behavior. Moreover, with the proposed PBPD procedure, a dual level design based on appropriate target drift for each hazard level, can be easily implemented to obtain the desired performance at different hazard levels for SPSW systems. By using PBPD approach in design of SPSW structures, more insight and control over the design, less number of iterations, and direct drift control can be achieved.

In Section 8.2, the current AISC procedure for design of SPSW is briefly explained. The proposed PBPD procedure for SPSW with pinned beam-to-column connections is then presented in Section 8.3. In Section 8.4, the proposed procedure is applied to the design of an example 4-story SPSW considering different hazard levels.

In Section 8.5, the procedure for design of SPSW with moment resisting beam-to-column connections is presented. This procedure is then applied to the design of the example 4-story SPSW in Section 8.6.

To evaluate and compare the performances of the different designs, nonlinear time history analyses were carried out on all example SPSW frames. The modeling assumptions and the results are shown in Section 8.7.

8.2 Current AISC Procedure for Design of SPSW

Figure 8.1 shows the components of a typical SPSW frame. The slender and unstiffened steel web plates (infill paltes) yield and buckle at the very early stages of the lateral loading. These web plates are surrounded by beams or Horizontal Boundary Elements (HBE) and column or Vertical Boundary Elements (VBE). Each web element must be surrounded by boundary elements (AISC, 2005a).

AISC *Seismic Provisions* (AISC, 2005a) provides the design criteria for SPSW systems. According to Sect. 17 of these provisions, under design earthquake, the SPSW are expected to undergo significant inelastic deformations in the web while the HBE and VBE are designed to remain mainly elastic-except the plastic hinging at the ends of HBE. All HBE should be rigidly connected to the VBE with moment resisting connections with the ability to develop the expected plastic moment of the HBE. The current procedure for design of SPSW is described below.

8.2.1 Design Base Shear

Similar to other structural systems, the design base shear for SPSW is obtained according to the ASCE 7-05 procedure. In this method, the fundamental period of the structure is estimated based on the proper code formula. The minimum required design

base shear can then be calculated from the general equation of $V = C_s W$. The seismic response coefficient, C_s, can be obtained from the given elastic design response spectrum, considering R, the response modification factor, and I, the occupancy importance factor.

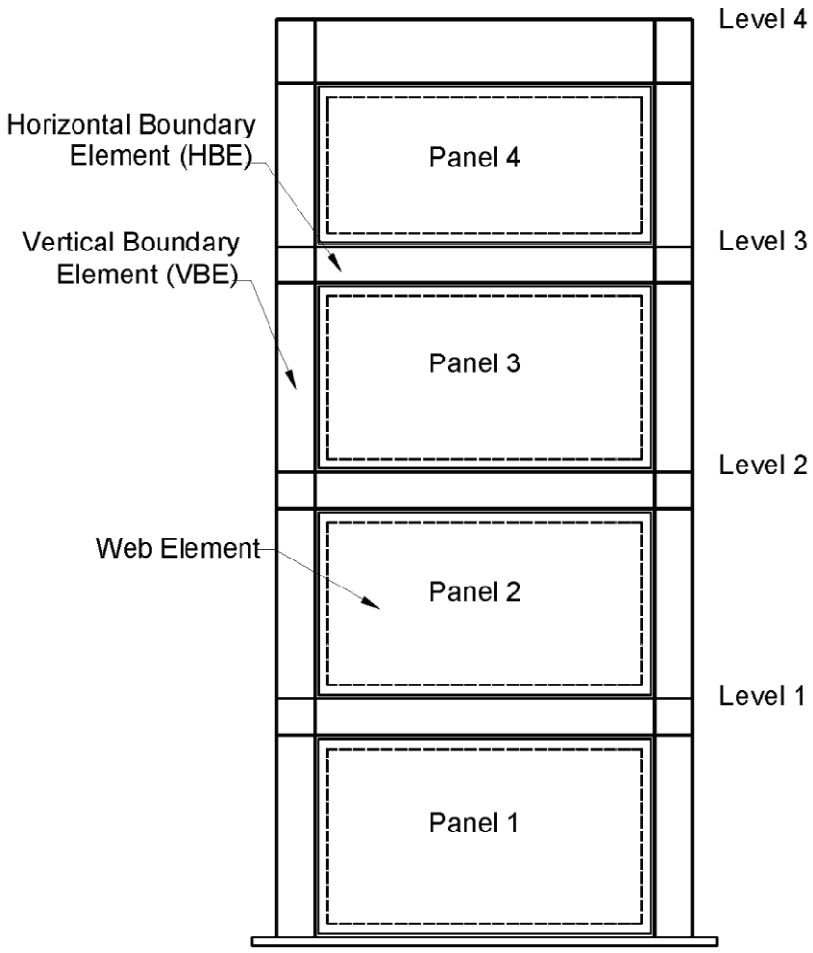

Figure 8.1. Elements of a Typical Special Plate Shear Wall (AISC, 2005a).

8.2.2 Design of the Steel Web Plates

Once the required design base shear is obtained, the required story shears at each story can be calculated using the code given lateral distribution. The web plates can then

be sized by comparing the total shear strength demand (V_u) to the design shear strength of the plate, ϕV_n as given by:

$$V_n = 0.42 F_y t_w L_{cf} \sin 2\alpha \qquad (8.1)$$

$$\phi = 0.90$$

where t_w is the thickness of the web and L_{cf} is the clear distance between VBE flanges. F_y is the nominal yield strength of the plate, and α is the angle of web yielding in radians (measured relative to the vertical) and is given by:

$$\tan^4 \alpha = \frac{1 + \frac{t_w L}{2A_c}}{1 + t_w h\left(\frac{1}{A_b} + \frac{h^3}{360 I_c L}\right)} \qquad (8.2)$$

where:

h = distance between HBE centerlines

A_b = cross-sectional area of HBE

A_c = cross-sectional area of VBE

I_c = moment of inertia of a VBE taken perpendicular to the direction of the web plate line

L = distance between VBE centerlines

It should be noted that the web plates are basically designed to carry the total lateral load. This means that the additional strength provided by the boundary moment

resisting frame is neglected in the current code procedure, resulting in larger system over-strength for such systems.

8.2.3 Design of Horizontal and Vertical Boundary Elements

In general, capacity design approach based on the maximum forces developed by the tension field action in fully yielded web plates should be considered in design of HBE and VBE. Therefore, the axial forces, shears, and moments in the boundary elements are due to the overall overturning and shear, as well as the tension field action in the web plates (AISC, 2005a). It should be noted that actual thickness of the web plates should be used for such capacity design approach.

The HBE should have the sufficient strength such that full tensile yielding in the web plate can develop. Plastic hinges are not allowed to form anywhere in HBE except at the two ends. Special attention should be given to the top and bottom HBE so that they have sufficient strength to anchor the vertical components of the tension field action in the fully yielded webs.

Three methods have been recommended in AISC *Seismic Provisions* (AISC, 2005a) to be used to achieve the capacity design for VBE. These methods are: (1) Nonlinear push-over analysis; (2) Combined linear elastic computer programs and capacity design concept; and (3) Indirect capacity design approach. The latter has been proposed by CSA-S16-02 [Canadian standard Association (CSA), 2001].

A more accurate capacity design method for VBE, recently suggested by Berman and Bruneau (2008) considers the whole length of VBE as a continuous member on multiple elastic supports. This method will be explained more in detail in Section 8.3.

The AISC *Seismic Provisions* also provides a stiffness requirement for VBE to prevent excessive in-plane flexibility and bucking of these elements under the tension field forces in plates. This requirement can be expressed as:

$$I_c \geq \frac{0.00307 t_w h^4}{L} \tag{8.3}$$

This design capacity approach has also been presented in the AISC Steel Design Guide#20 (Sabelli and Bruneau, 2007) for capacity design of VBE.

The HBE-to-VBE connection, which should be rigid according to AISC *Seismic Provisions*, should comply with the requirements of Ordinary Moment Frames (OMF), Section 11.2 of AISC Seismic Provisions.

It should be noted that since the drift control has been considered only indirectly in this procedure, iterations may be needed in order to achieve a final design which meets the desired performance criteria.

8.3 Proposed PBPD Design Procedure for Steel Plate Shear Wall Frames

The PBPD procedure for design of SPSW with pinned HBE-to-VBE connection is presented herein. First, the design base shear is obtained using the target drift and yield mechanism as the design criteria. The pinched hysteresis behavior of the SPSW system and also the varying yield drift are taken into account in this procedure. Using the PBPD

lateral force distribution, the web plates are then designed by plastic design method. After sizing of the web plates, the HBE and VBE are designed by following the capacity design procedure.

It is noted that pinned HBE-to-VBE connection was considered so that the procedure can be first developed for the simplest form of SPSW structure, although such connections are not allowed according to AISC *Seismic Provisions*. In the following section, the procedure will be modified such that it can be used for SPSW with moment-resisting HBE-to-VBE connections.

8.3.1 Design Target Drift and Yield Mechanism

Target drift and yield mechanism are the two main criteria in the PBPD method. A reasonable value for the target drift (considering the behavior of the structure and the desired performance objective) and also the desired yielding mechanism should be assumed at the very beginning of the PBPD procedure. As was shown in Chapter 3, the PBPD design base shear is calculated based on these two main criteria.

In the case of SPSW structures, the targets drift under design level seismic hazard (DBE, 10% probability of exceedance in 50 years) can be considered as 2%, same as the value suggested by the structural codes (FEMA-450, FEMA 2003). Severe yielding of steel web plates and also yielding in the HBE-to-VBE connection (in the case of moment-resisting connection), without major loss of strength are expected at this level of interstory drift for a reasonably detailed SPSW. The 2% drift limit would also minimize the damage to non-structural components under design level earthquake. Under the MCE

hazard level (2% probability of exceedance in 50 years), the appropriate value for target drift can be estimated based on the results of large scale experimental studies recently carried out on SPSW systems. The results of two large scale experimental studies are shown in Figures 8.2 and 8.3. Figure 8.2 shows the hysteretic behavior of the 1st story of the 2-story SPSW with reduced beam section connections and composite floors (Qu et al., 2008). As can be seen in this figure, the strength starts to decrease at about 3% story drift. The strength continued to drop in the following cycles with larger story drifts.

The hysteretic behaviors of three different SPSW specimens tested by Vian et al. (2009) are shown in Figure 8.3. These tests were done at the NCREE facility in Taiwan. The specimens include the Perforated Panel specimen, the Cutout Corner-Reinforced specimen, and the Reference specimen. As can be seen in parts (b), (d) and (f) of this figure, the lateral strength starts to drop at about 3% story drift for all three systems.

Based on these experimental results, the post-yield negative stiffness of the backbone curve begins at nearly 3% story drift. Hence, a collapse prevention target story drift of 3% is selected for SPSW structures under MCE (2% in 50 years) hazard level.

The desirable yield mechanisms for SPSW systems with pinned as well as moment-resisting HBE-to-VBE connections are shown in Figure 8.4. As can be seen, the web plates are fully yielded and the tension field action has been developed at mechanism. The plastic hinges should form at the end of HBE in order to have a full mechanism in the case of moment-resisting HBE-to-VBE connection. Since formation of plastic hinge in VBE (except at the base) and anywhere in HBE except at the ends would lead to degrading behavior of SPSW under lateral loading (e.g. Sabelli and Bruneau,

2007), such plastic hinging should be prevented. It should also be noted that the first story web plate can be anchored to the bottom HBE or else fixed to the ground (e.g. welded to an embedded plate in the foundation or basement wall).

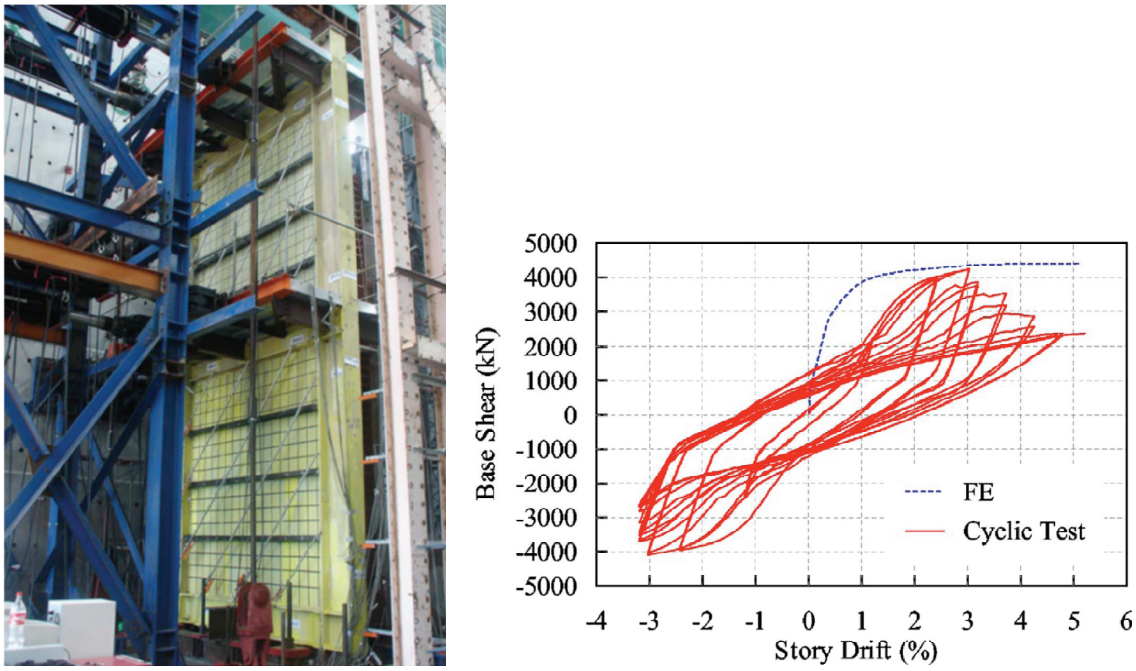

(a) (b)

Figure 8.2. Test of 2-Story SPSW in NCREE, Taiwan (Qu et al., 2008): (a) Test Specimen; (b) Cyclic Response of the 1st Story.

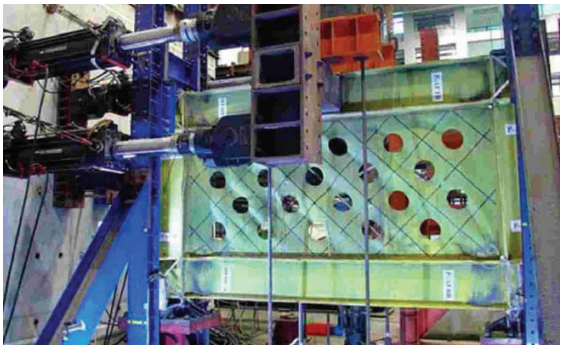

(a)

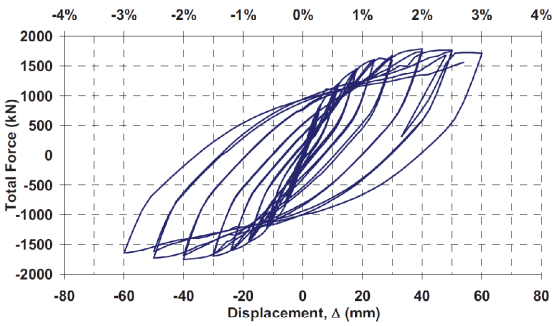

(b)

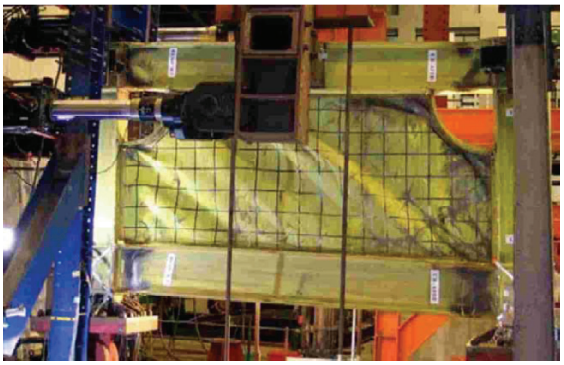

(c)

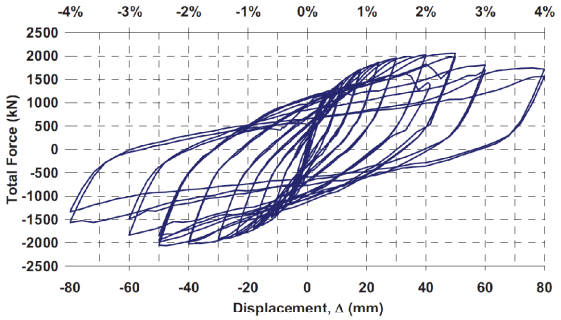

(d)

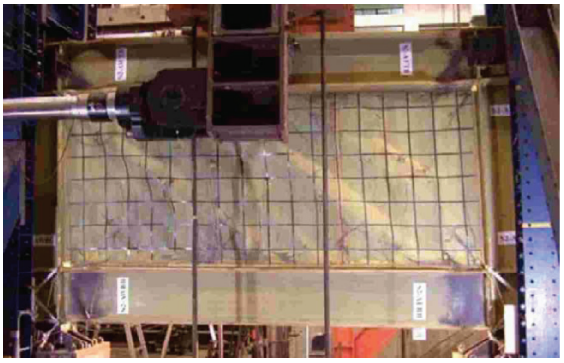

(e)

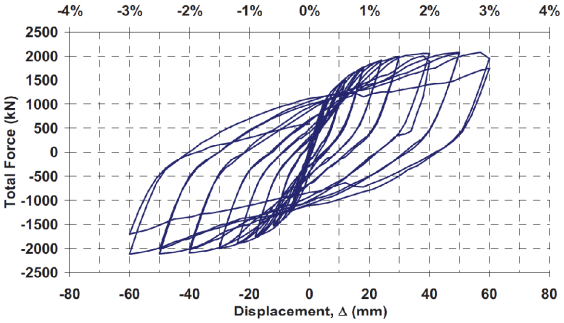

(f)

Figure 8.3. Three Test Specimens in Vian et al. (2009) Study, carried at at NCREE, Taiwan: (a) and (b) Perforated Panel Specimen; (c) and (d) Cutout Corner-Reinforced Specimen; (e) and (f) Reference Specimen.

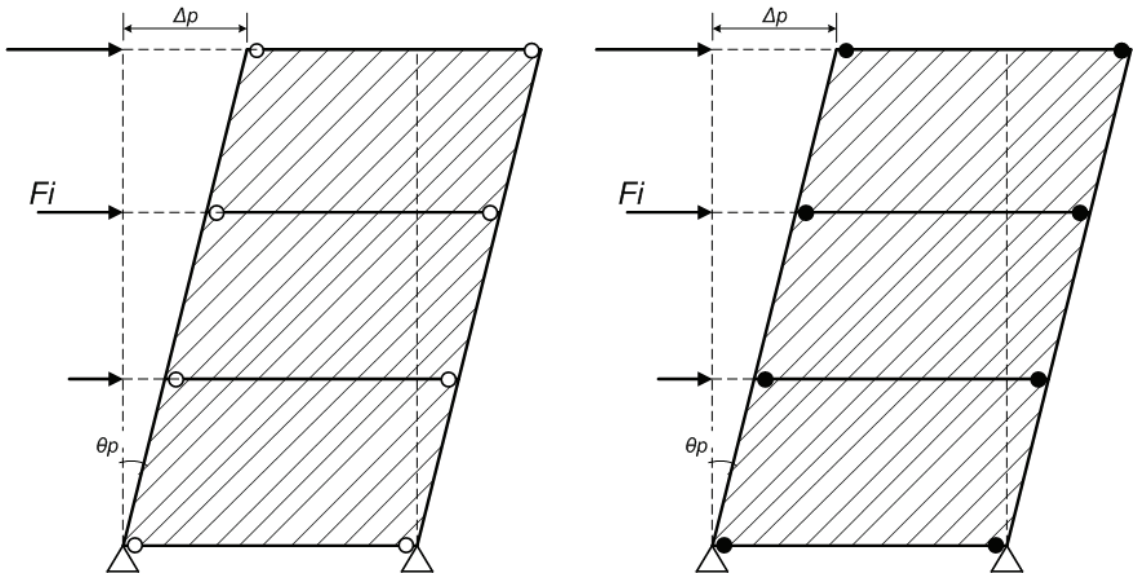

(a) (b)

Figure 8.4. Desired Yield Mechanism for SPSW Structures: (a) Pinned HBE-to-VBE Connection; (b) Moment-Resisting HBE-to-VBE Connection.

8.3.2 Yield Drift Estimation

Similar to the yield drift estimation suggested in Chapter 5 for CBF systems, the yield drift for SPSW systems can be obtained. The lateral deformation of a SPSW frame comes from shear and flexural deformations. The contribution of the shear deformation to the total lateral deformation can be obtained in a similar method shown in Chapter 5. This deformation is shown in the following equation, with angle α showing the angle of web yielding measured from vertical:

$$\frac{\Delta_s}{h} = \frac{2\varepsilon_y}{sin2\alpha} \tag{8.4}$$

where ε_y is the yield strain of the steel web plates. Although the angle α is not constant for different SPSW systems, it can be shown that for $40° \leq \alpha \leq 50°$, the variation in $1/\sin 2\alpha$ is only about *1.5%*. Therefore, an initial value of *45°* for α can be a good estimation. By putting $\alpha = 45°$, the shear part of the yield drift can be written as:

$$(\theta_y)_s \simeq 2\varepsilon_y \tag{8.5}$$

Depending on the variation of column sections along the height of VBE in the SPSW, the flexural contribution to the lateral deformation can be estimated by considering an average axial stress on columns at the yield mechanism state, similar to what was done for CBF in Chapter 5. Having the average axial stress, σ_{avg}, the flexural component of the yield drift can be obtained as:

$$(\theta_y)_f = \frac{\sigma_{avg}}{E} \times \frac{h}{L} \tag{8.6}$$

The yield drifts are obtained for two example SPSW frames in the following and then the estimated values are compared to the yield drifts obtained from the actual pushover curves. In Case I, column sections at each story are assumed to be designed according to their axial force demands. In Case II, column sections are kept the same for each two stories. The building considered is the 4-story MCEER demonstration hospital (Yang and Whittaker, 2002) which has been redesigned by Berman and Bruneau (2008) using SPSW as the lateral load resisting system. The average axial stress for these two cases can be calculated as follows:

$$\text{Case I}: \ \sigma_{avg} \approx (1.0) \times (0.85) \times (0.9)\sigma_y = 0.765\sigma_y \tag{8.7.a}$$

Case II : $\sigma_{avg} \approx (0.75)\times(0.85)\times(0.9)\sigma_y = 0.574\sigma_y$ (8.7.b)

Then the total yield drift for these cases can be estimated as:

Case I :

$$(\theta_y)_s \simeq 2\varepsilon_y = 2\times(1.3\times 36/29000) = 0.323\%$$

$$(\theta_y)_f = \frac{\sigma_{avg}}{E}\times\frac{h}{L} = \frac{0.765\sigma_y}{E}\times\frac{h}{L} = \frac{0.765\times 50}{29000}\times\frac{h}{L} = 0.001319\times\frac{h}{L} \quad (8.8)$$

$$h = 51\ ft\ ;\ L = 24.5\ ft$$

$$(\theta_y)_f = 0.275\%$$

$$\theta_y = (\theta_y)_s + (\theta_y)_f = 0.323\% + 0.275\% = 0.60\%$$

Case II :

$$(\theta_y)_s \simeq 2\varepsilon_y = 2\times(1.3\times 36/29000) = 0.323\%$$

$$(\theta_y)_f = \frac{\sigma_{avg}}{E}\times\frac{h}{L} = \frac{0.57\sigma_y}{E}\times\frac{h}{L} = \frac{0.57\times 50}{29000}\times\frac{h}{L} = 0.000983\times\frac{h}{L} \quad (8.9)$$

$$h = 51\ ft\ ;\ L = 24.5\ ft$$

$$(\theta_y)_f = 0.205\%$$

$$\theta_y = (\theta_y)_s + (\theta_y)_f = 0.323\% + 0.205\% = 0.53\%$$

It should be noted that the full height of the columns are used in yield drift calculation for SPSW since there is substantial axial force in the top story column and therefore its axial deformation contributes to the lateral drift. It should be also mentioned that the restraining effect of the plate was neglected in calculating the axial deformation of columns.

Figure 8.5 shows the pushover curves for the two SPSW cases considered above. The analyses have been done using Perform3D software (CSI, 2007). As can be seen in this figure, the proposed estimation for yield drifts matches quite well with the actual pushover results.

In Figure 8.5, the slope of the post yield line (post yield stiffness) is selected such that the area under the two curves becomes equal, meaning both systems have equal energy capacity (FEMA, 2000a). The second line is drawn from target drift (3% here) on the pushover curve.

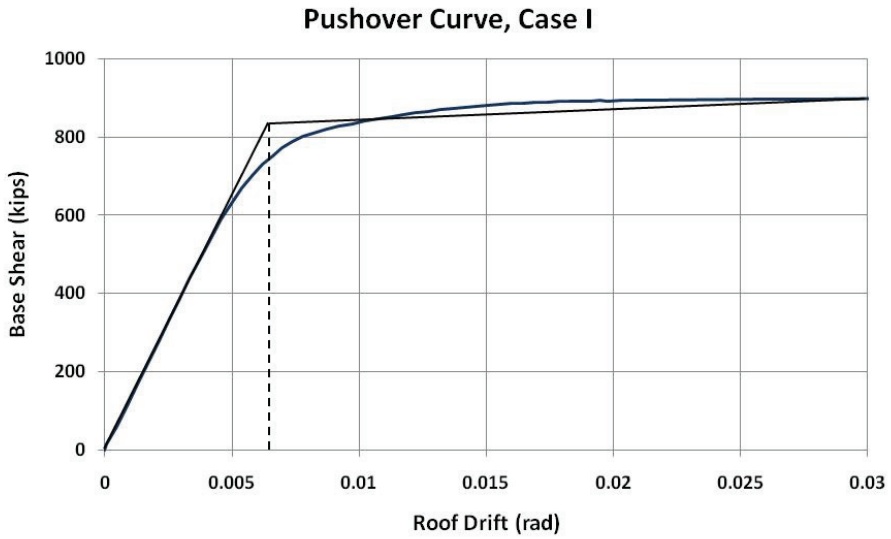

(a)

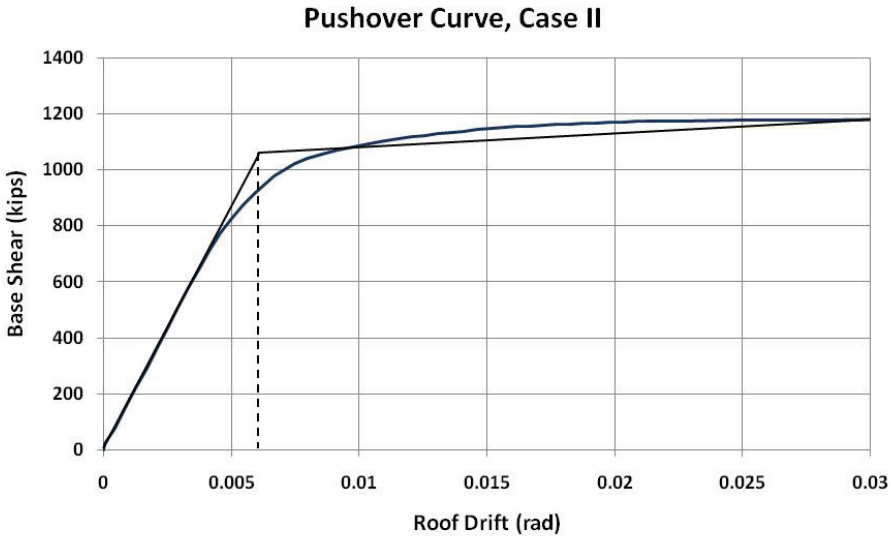

(b)

Figure 8.5. Pushover Curves and Yield Drifts for the 4-Story SPSW Structure: (a) Case I; (b) Case II.

8.3.3 Design Base Shear Calculation

Having the target drift and the desired yield mechanism, as considered in Section 8.3.1, and also by estimating the yield drift with the suggested method in Section 8.3.2, the required PBPD design base shear can be calculated following the general steps presented in Chapter 3. For SPSW systems, these steps are:

1. Select the target drift and yield mechanism. The target drift should be selected according to the seismic hazard level considered.
2. Estimate the fundamental period, T, of the structure.
3. Estimate the yield drift of the structure by adding shear and flexural deformations at yield mechanism.
4. Modify the target drift to account for pinched hysteretic behavior. This can be done similar to the method used for CBF by dividing the original target drift to C_2 factor (see Figure 5.15).
5. Using the design spectral acceleration value, S_a, calculate the PBPD design base shear, V_y, by equating the work needed to monotonically push the structure up to the target drift (no pushover analysis needed) to the energy needed by an equivalent EP-SDOF to be displaced up to the same drift (PBPD work-energy concept). Modified target drift should be used in these calculations.

The next two steps are done in PBPD procedure of SPSW after the design base shear is calculated. In these steps, the web plates and boundary elements will be designed according to the PBPD lateral forces.

6. By using PBPD lateral force distribution, plastic design method will be used to design the structural members that are expected to dissipate the earthquake energy

inelastically (DYMs, web plates), while keeping the vertical distribution of lateral strength of the structure close to the design lateral force distribution.

7. The boundary elements (HBE and VBE), which are basically the Non-DYMs, can then be designed by following capacity design approach based on the expected ultimate forces from fully yielded tension field action.

It should be noted that by using this method, a dual (or multiple) level seismic hazard design can be easily implemented, with the largest design base shear as the governing design force. Appropriate target drifts should be used for each hazard levels.

8.3.4 Design of Steel Web Plates

The design of web plates will be done by using the plastic design approach. External work done on the yield mechanism during the plastic deformation equals internal work (see Figure 8.4). The work equation for a general SPSW frame with moment-resisting HBE-to-VBE connections and fixed base can be written as:

$$\sum_i F_i h_i \theta_p = 2M_{pc}\theta_p - \sum_i 2M_{pi} \times \left(\frac{L}{L'}\right)\theta_p + F_y L \sin\alpha.\cos\alpha \times \theta_p \sum_i (t_i - t_{i+1})h_i \qquad (8.10)$$

By assuming that the strength of DYMs (web plates) follows the PBPD lateral force distribution, the thicknesses of the plates at each story can be obtained based on the thickness of the web plate at the top story, t_b, as:

$$t_i = \beta_i t_b \qquad (8.11)$$

substituting Equation (8.11) into (8.10), the required thickness of the web plate at the top story can be obtained as:

$$t_b = \frac{\Sigma F_i h_i - 2M_{pc} - \Sigma 2M_{pi} \times L/L'}{\frac{1}{2} F_y L \sin 2\alpha \, \Sigma(\beta_i - \beta_{i+1}) h_i} \tag{8.12}$$

The required thickness of the web plates for other stories can be obtained using Equation (8.11). For the SPSW with pinned HBE-to-VBE connections, Equation (8.12) becomes:

$$t_b = \frac{\Sigma F_i h_i}{\frac{1}{2} F_y L \sin 2\alpha \, \Sigma(\beta_i - \beta_{i+1}) h_i} \tag{8.13}$$

The web plates should be sized to the smallest available thickness. Conservative web plate design leads to heavier boundary elements (HBE and VBE) since they should be designed for the ultimate expected forces of the web plates according to the capacity design approach.

8.3.5 Design of Horizontal Boundary Elements (HBE)

The HBE are designed based on the capacity design approach. The capacity design of HBE should be done based on the forces corresponding to the expected yield strength of the tension field in the web plates, considering the actual thickness of these plates.

In addition to the flexure due to the difference in the above and below web plate tensions, substantial axial forces exist in HBE. The axial forces are mainly coming from VBE under the effect of plate yield forces as well as from the horizontal component of

the difference between plate yield forces above and below the HBE (Sabelli and Bruneau, 2007).

A practical method for capacity design of HBE is suggested by AISC Design Guide on SPSW (Sabelli and Bruneau, 2007). In this method, the required mid-span bending moment is obtained as:

$$M_u = \frac{(w_u + w_g)L_h^2}{8} + \frac{P_u L_h}{4} \tag{8.14}$$

where

w_u = the vertical component of the difference between plate yield forces above and below

w_g = distributed gravity load on the beam

L_h = the distance between plastic hinges at two ends of the beam

P_u = concentrated gravity load on the beam

The axial force in the HBE has two sources. One is the reaction forces from VBE under the effect of tension field in web plates. The other source for axial force is the horizontal component of the difference between the plate yield forces above and below the HBE. These axial forces can be respectively obtained by the following equations:

$$P_{HBE(VBE)} = \sum \frac{1}{2} R_y F_y \sin^2(\alpha) t_w h \tag{8.15}$$

$$P_{HBE(web)} = \frac{1}{2} R_y F_y \left[t_i \sin(2\alpha_i) - t_{i+1} \sin(2\alpha_{i+1}) \right] L_{cf} \tag{8.16}$$

where

L_{cf} = the clear length of the web panel between VBE flanges

It should be noted that the axial force in Equation (8.15) has been estimated by assuming that the VBE distributes the forces equally to the top and bottom HBE.

Once the HBE are sized, the VBE can be designed using the ultimate forces coming from web plates and HBE.

8.3.6 Design of Vertical Boundary Elements (VBEs)

A method similar to the column-tree analysis approached previously used for other systems (e.g. MF) can be used for capacity design of VBE in SPSW. In such method, the equilibrium of the whole column-tree under ultimate forces caused by web plate yielding and HBE should be considered. One such method has been recommended by Berman and Bruneau (2008). In this method, the free body diagram of the whole length of VBE with the applied forces, as shown in Figure 8.6 for the right VBE, is considered to obtain the design forces. Based on this free body diagram, the axial and shear forces as well as the moments in the VBE can be calculated.

The following equations show the equivalent distributed load of horizontal and vertical components of the plate yield forces at the *i*th story (Berman and Bruneau, 2008):

$$\omega_{yci} = \frac{1}{2} F_{yp} t_{wi} \sin 2\alpha \tag{8.17}$$

$$\omega_{xci} = F_{yp} t_{wi} \sin^2 \alpha \tag{8.18}$$

$$\omega_{ybi} = F_{yp} t_{wi} \cos^2 \alpha \tag{8.19}$$

$$\omega_{ybi} = \frac{1}{2} F_{yp} t_{wi} \sin 2\alpha \tag{8.20}$$

The distributed loads of ω_{yci} and ω_{xci} are applied to the VBE while ω_{ybi} and ω_{xbi} are applied to HBE.

The SPSW structures designed following the above suggested procedure are expected to meet the desired performance objectives under different seismic hazard levels, without the need to perform several analysis/design iterations.

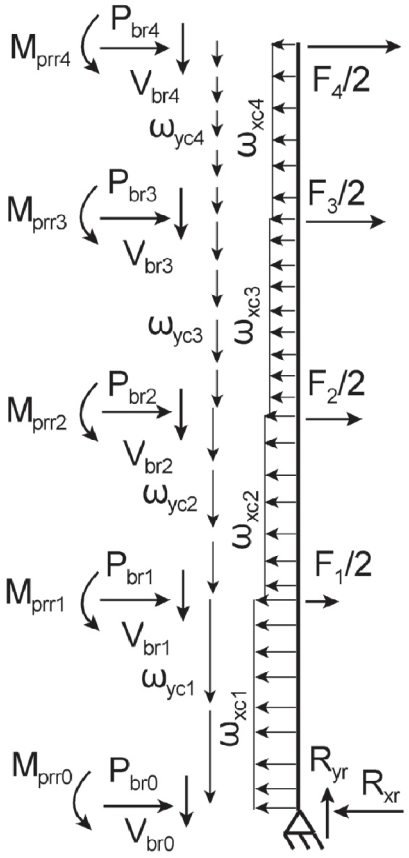

Figure 8.6. Free Body Diagram of the Right VBE (figure from Berman and Bruneau, 2008).

8.4 Design Example: 4-Story SPSW Structure with Pinned HBE-to-VBE Connections

8.4.1 Assumptions and Design

The proposed PBPD procedure will be applied to design of a 4-story office building with SPSW as the lateral load resisting system. The building considered is the 4-story MCEER demonstration hospital (Yang and Whittaker, 2002) which has been redesigned by Berman and Bruneau (2008) using SPSW as the lateral load resisting system. This 4-story building will be designed in this section as an office building. Four SPSW frames are assumed to carry the seismic forces.

The plan and elevation views of the example building are shown in Figures 8.7 and 8.8, respectively. As can be seen in Figure 8.7, there are four SPSW in N-S direction carrying seismic load.

Table 8.1 shows the height of the floors and their seismic weights. The general design parameters are shown in Table 8.2. The R and I factors in this table are used for the code design.

It should be noted that three different designs are considered herein so that their seismic performance can be later compared under actual earthquake ground motions. These designs are: (1) the code design; (2) the DBE design; and (3) the MCE design. The code design is done based on the AISC Seismic Provisions (AISC, 2005a) guidelines and also the recommendations by AISC Design Guide on SPSW (Sabelli and Bruneau, 2007). The DBE design is done using the PBPD method by assuming a design hazard level (10% in 50 years). And the MCE design is performed by using PBPD procedure under the MCE hazard level (2% in 50 years). With these three designs, the difference between

the performances of the code designed and the PBPD designed SPSW structures can be compared. In addition, the validity of applying a dual hazard level design with the PBPD method can be evaluated.

Table 8.3 shows the design parameters used in the PBPD procedure. As can be seen, the required PBPD design base shears are obtained for two different hazard levels of DBE and MCE. The target drift for these two hazard levels are assumed as 2% and 3%, respectively, based on the discussion in Section 8.3.1. A C_2 factor of 1.2 has also been applied (see Figure 5.15) on these target drifts to obtain the effective target drift accounting for the pinching behavior. The required design base shear under MCE hazard level (*V/W = 0.261*) has come out to be larger compared to the DBE one (*V/W = 0.213*). Therefore, the MCE hazard level governs if dual level design is considered.

The required design base shears for the three different designs are shown in Table 8.4. As can be seen, the code design has the lowest design base shear of *V/W = C/(R/I) = 1.17/(7.0/1.0) = 0.167*. These design base shears are then used to find the required thicknesses for the web plates for each design.

The final design results for the three designs considered are shown in Table 8.5 and Figures 8.9 and 8.10.These results include the thickness of the web plates, the HBE and the VBE sizes for each design. As can be seen, the plate thicknesses and also the size of boundary elements are obtained to be larger for the MCE design compared to the other two designs, which was expected due to its larger design base shear. It should also be noted that the actual thicknesses obtained from the calculations have been used in all

three designs (as compared to using the available commercial thicknesses) for the purpose of having fair comparison between these designs.

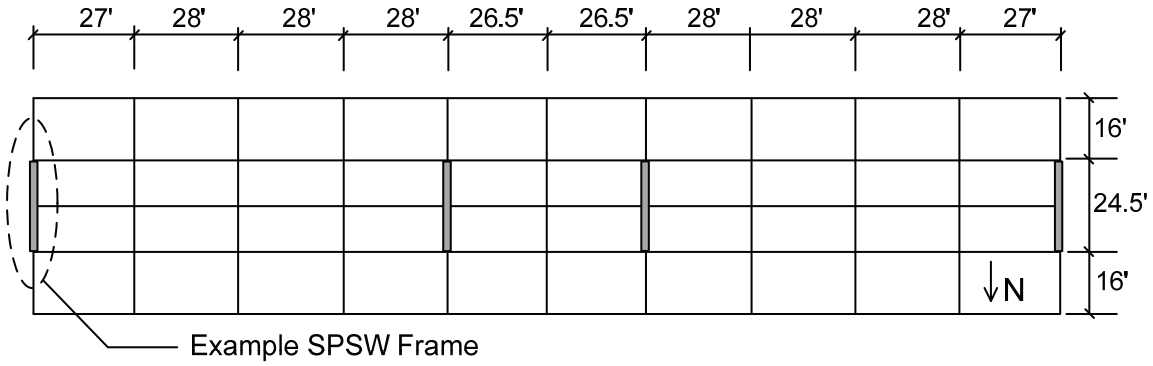

Figure 8.7. Plan View of the MCEER Demonstration Building (Yang and Whittaker, 2002).

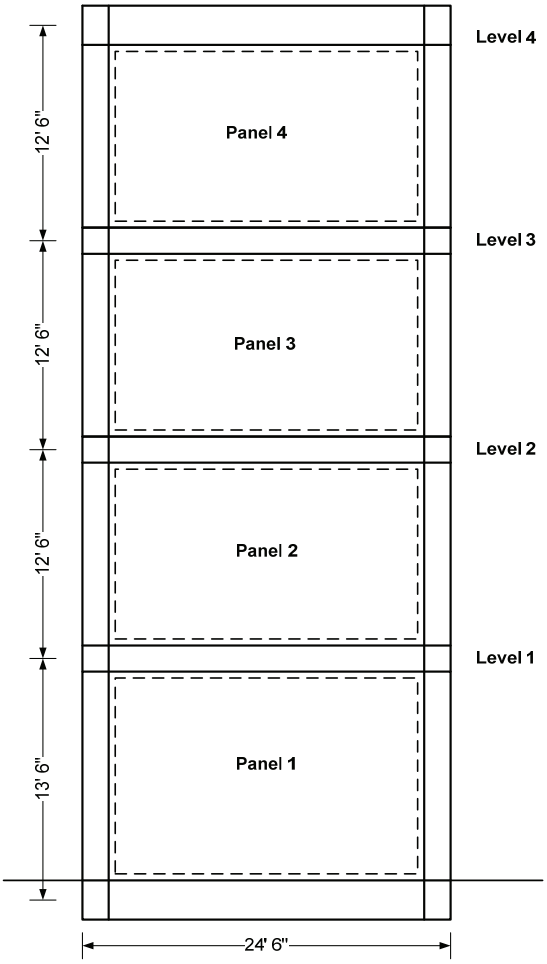

Figure 8.8. Elevation View of the Example 4-Story SPSW Frame (Berman and Bruneau, 2008).

Table 8.1. Floor Heights and Seismic Weights (Berman and Bruneau, 2008).

Floor	h_j (ft)	w_j (kips)
Roof	51	2613
4	38.5	2542
3	26	2542
2	13.5	2103
Total		9800

Table 8.2. General Design Parameters (Berman and Bruneau, 2008).

Parameters from FEMA 450 (FEMA, 2003)	
S_{DS}	1.17g
S_{D1}	0.44g
Site Class	D
Building Height	51 ft
T	0.38 sec.
R	7.0
Importance Factor, I	1.0
Total Seismic Weight W	9800 kips

Table 8.3. PBPD Design Parameters for the 4-Story SPSW.

Design Parameters	10% in 50 Years Hazard (2/3 MCE)	2% in 50 Years Hazard (MCE)
S_a	1.17g	1.755g
T	0.38 sec.	0.38 sec.
Yield Drift Ratio θ_y	0.7%	0.7%
Target Drift Ratio θ_u	2%	3%
Inelastic Drift Ratio $\theta_p = \theta_u - \theta_y$	1.3%	2.3%
$\mu_s = \theta_u / \theta_y$	2.38	3.57
$\underline{R_\mu}$	1.94	2.48
$\lambda (=C_2)$	1.2	1.2
γ	1.0	1.0
α	6.203	11.546
V/W	0.213	0.261
Design Base Shear V	2087 kips	2558 kips (governs)

Table 8.4. Design Base Shear for Three Different Designs.

Model	*V/W*	*V* (kips)- one frame
Code design, (R=7)	**0.167**	**409**
PBPD (DBE)	**0.213**	**490**
PBPD (MCE)	**0.261**	**639**

Table 8.5. Summary of Three Different Designs for the 4-Story SPSW.

Story	Code Design			PBPD- DBE Design			PBPD- MCE Design		
	t_p (in)	HBE	VBE	t_p (in)	HBE	VBE	t_p (in)	HBE	VBE
		W30x148			W30x108			W30x108	
4	**0.04**	W30x132	W14x120	**0.05**	W24x94	W14x82	**0.06**	W24x94	W14x176
3	**0.07**	W30x99	W14x120	**0.09**	W24x84	W14x132	**0.11**	W24x94	W14x176
2	**0.09**	W24x76	W14x193	**0.11**	W24x76	W14x193	**0.15**	W24x94	W14x342
1	**0.11**	W40x235	W14x193	**0.13**	W36x160	W14x257	**0.17**	W36x170	W14x342

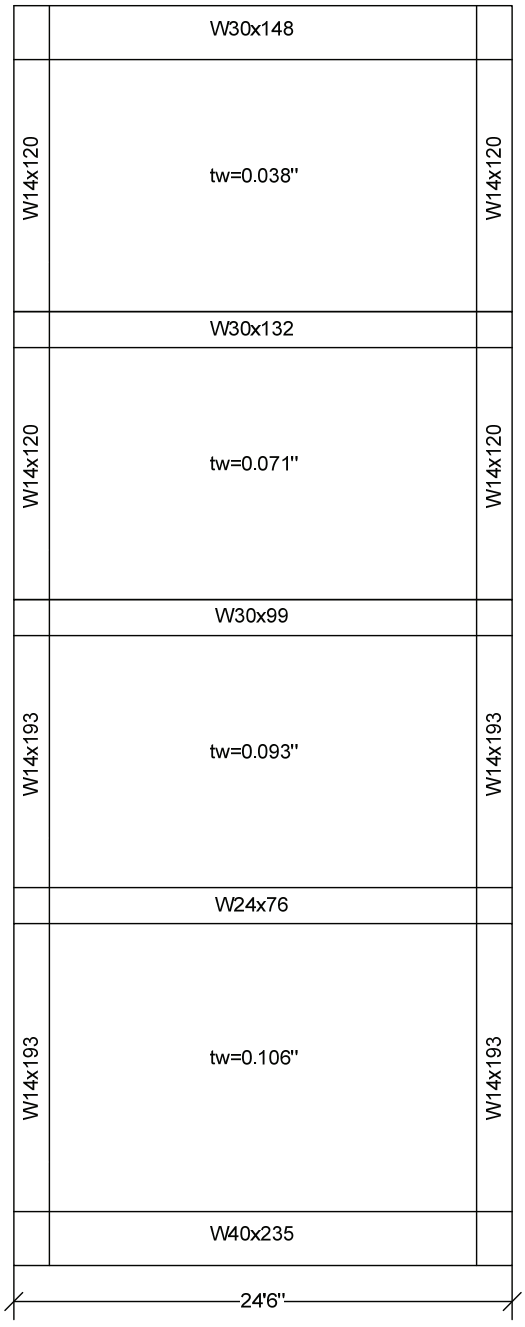

Figure 8.9. Code Designed SPSW.

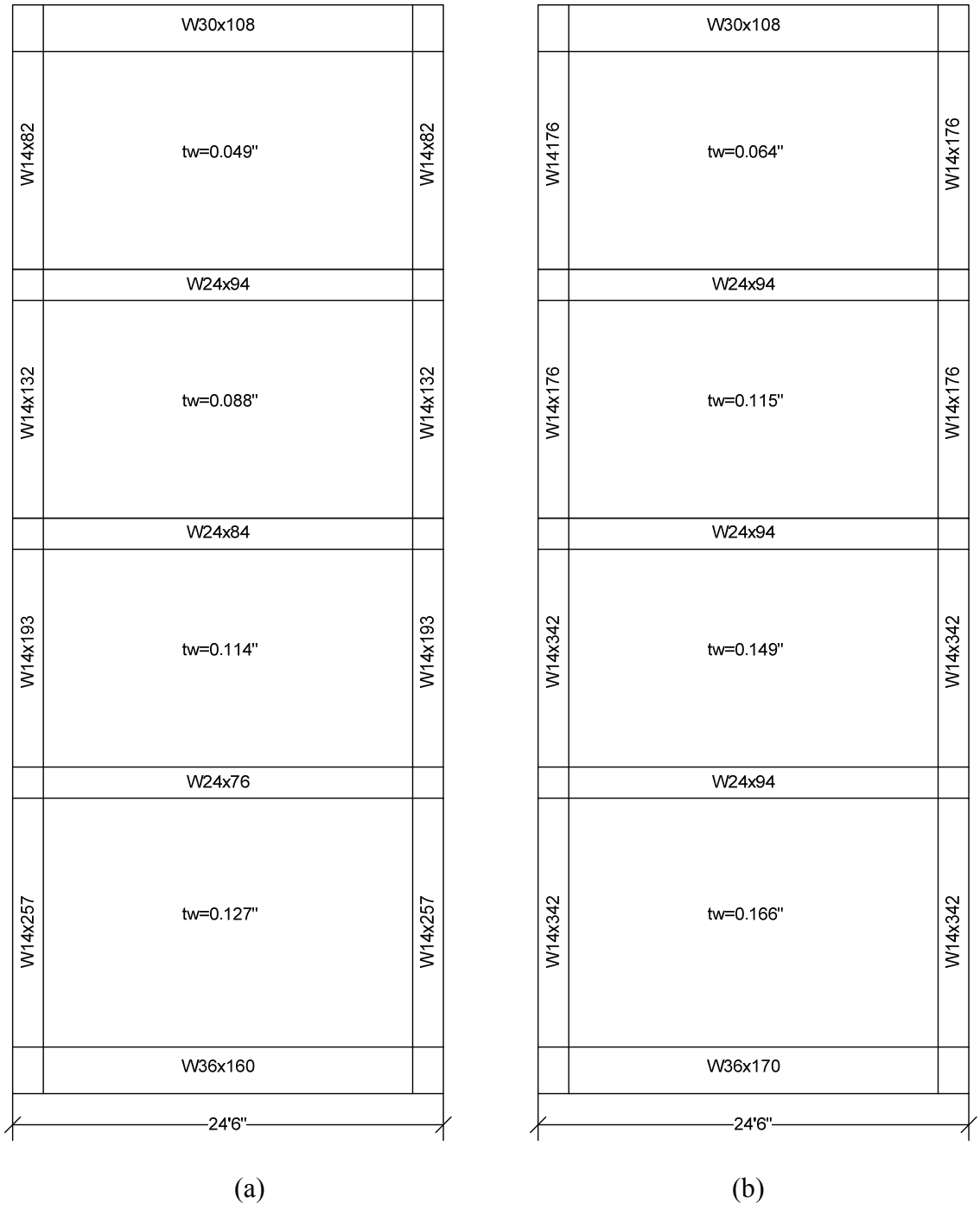

Figure 8.10. PBPD Designed SPSWs: (a) PBPD-DBE Design; (b) PBPD-MCE Design.

8.4.2 Performance Evaluation Using Nonlinear Time-History Analysis

Nonlinear static and dynamic time-history analyses were carried out on three different designs of the previous section in order to compare their performances. Perform-3D software (CSI, 2007) was used for modeling and analysis of these SPSW systems.

In modeling with Perform-3D, tension-only strips in both directions were used to capture the post-buckling behavior of web-plates. These tension strips are shown in Figure 8.11. As shown in this figure, totally 18 tension strips were used in each direction to model the web plates. It has been shown that modeling the web plates using such strips leads to results which are in good agreement with the experimental data (Qu et al., 2008).

Since A36 steel was used for web plates, an over-strength factor of R_y = 1.3 was considered in modeling these tension-only strips. Pinned connections were modeled between HBE and VBE as was the assumption in the design. Also, the column bases were modeled as pin support. PMM type plastic hinges were considered throughout the length of HBEs and VBEs in order to capture any yielding over the length of these members. P-Delta effects were included by considering a lumped gravity column rigidly connected to the SPSW.

Figure 8.12 shows the pushover curves for the three different SPSW designs. As was expected, the ultimate strength of the PBPD-MCE design is higher than the other two designs. All three models formed the desired uniform yield mechanism under pushover loading.

Two sets of SAC ground motions for LA site (Somerville et al., 1997), with the probability of exceedances of 10% in 50years and 2% in 50 years, have been used for performance evaluation of these SPSW.

Figure 8.13 shows the maximum story drifts under 10%/50yrs and 2%/50yrs SAC LA ground motions for the code designed SPSW. As can be seen, under 10%/50yrs ground motions, the mean story drift is somewhat close to the target drift of 2%, but under 2%/50yrs ground motions, the mean drifts are much larger than the target drift of 3%. The maximum story drifts under the same sets of ground motions have been also found for the other two designs of PBPD-DBE and PBPD-MCE in Figures 8.14 and 8.15, respectively. For PBPD-DBE design, as can be seen in Figure 8.14.a, the response is well controlled under 10%/50yrs ground motions. Somewhat smaller and also more uniform story drifts can be observed in this design compared to the Code design. However, the mean drifts under 2%/50yrs ground motions are larger than the corresponding target drift of 3%. Therefore, while the PBPD-DBE design performs well under DBE level ground motions, the response under MCE level ground motions is inadequate. This observation is quite consistent with the design base shear calculations done in Section 8.4.1, in which MCE level design base shear governed. As can be seen in Figure 8.15.b, the mean story drift for the PBPD-MCE design is quite close to the target drift of 3%. Therefore this design can be considered adequate under MCE level ground motions. Again, this is consistent with the dual level design that was considered from the beginning in the calculation of design base shear.

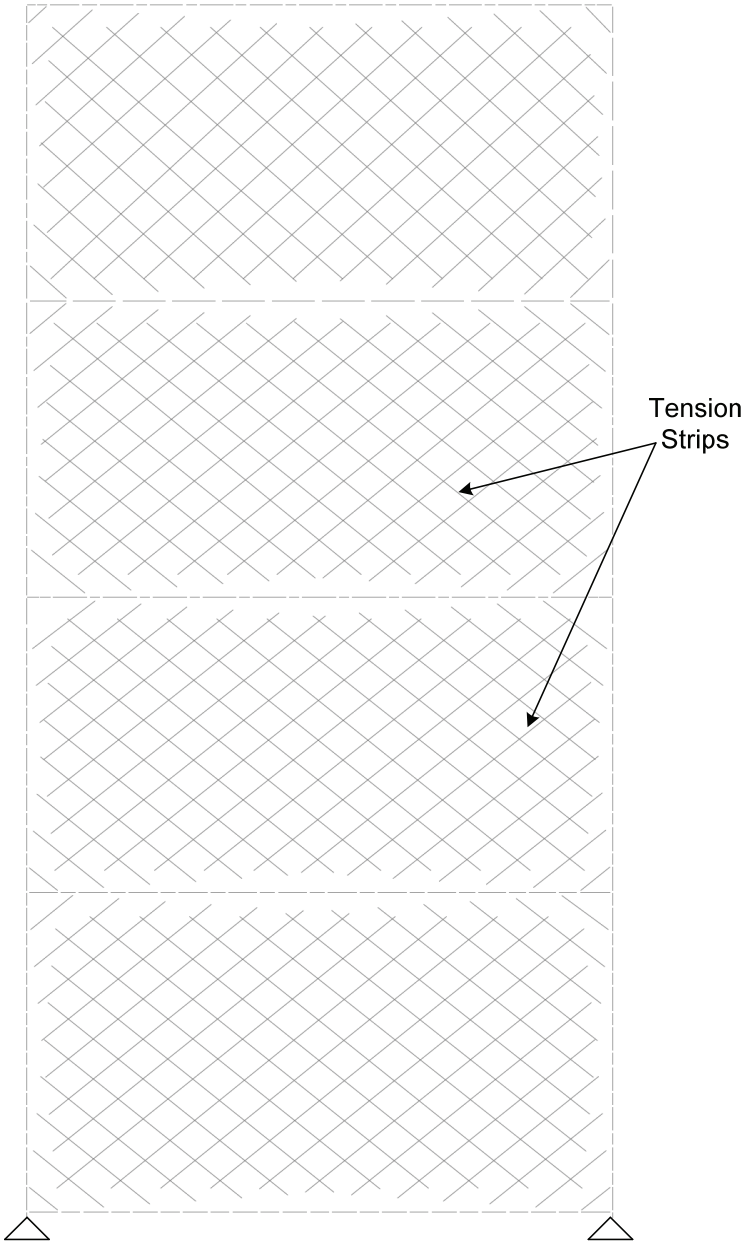

Figure 8.11. Dual Strip Model used for Dynamic Analysis (Tension Strips in Both Directions).

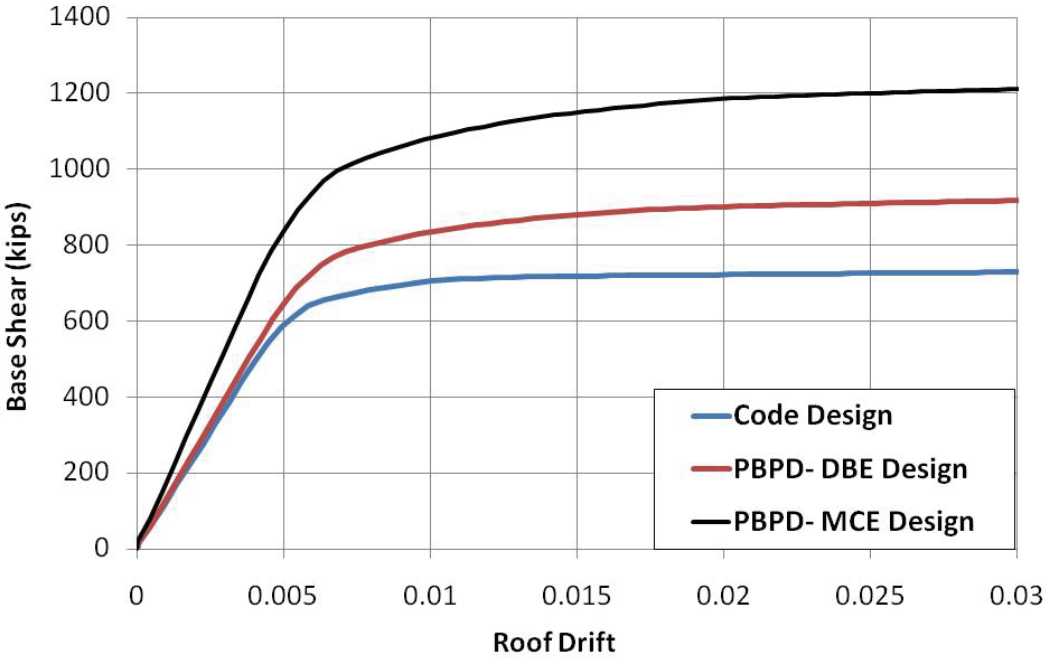

Figure 8.12. Pushover Curves for Three SPSW Designs.

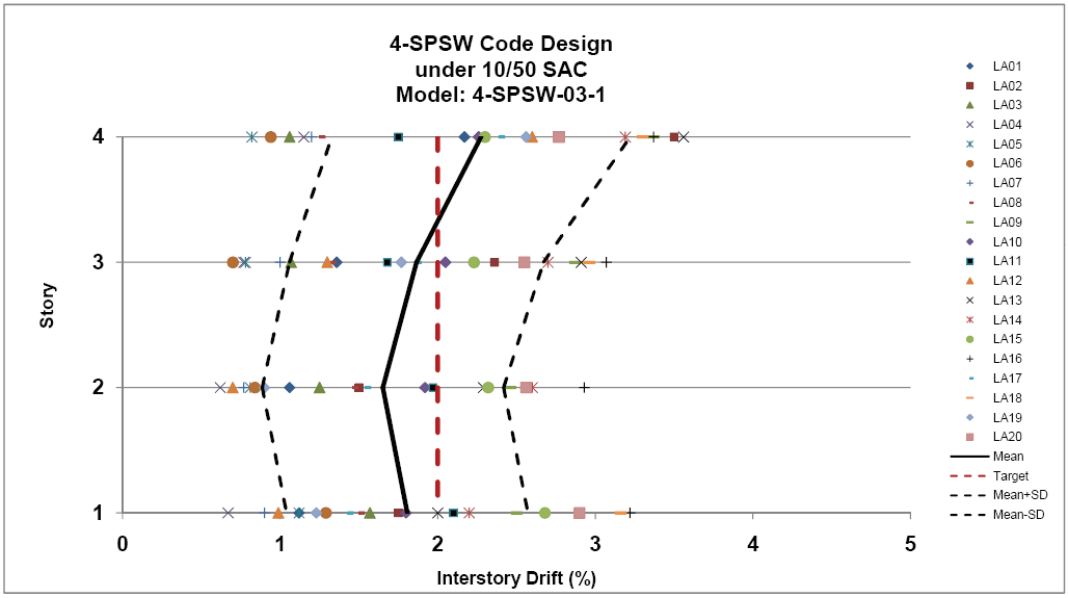

(a)

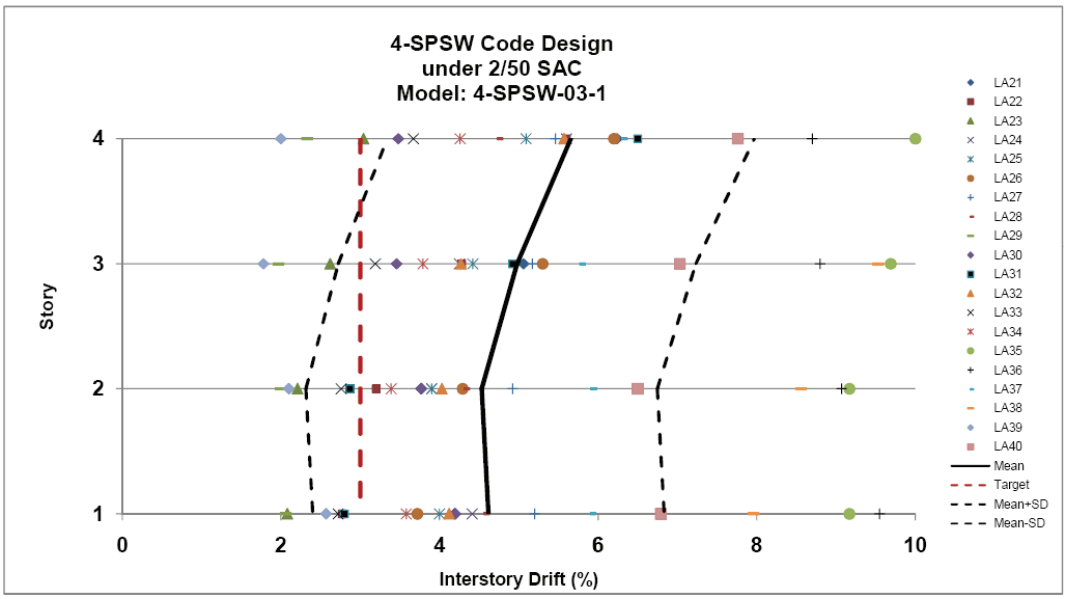

(b)

Figure 8.13. Maximum Story Drifts for Code Designed SPSW under: (a) 10/50 SAC; and (b) 2/50 SAC Ground Motions.

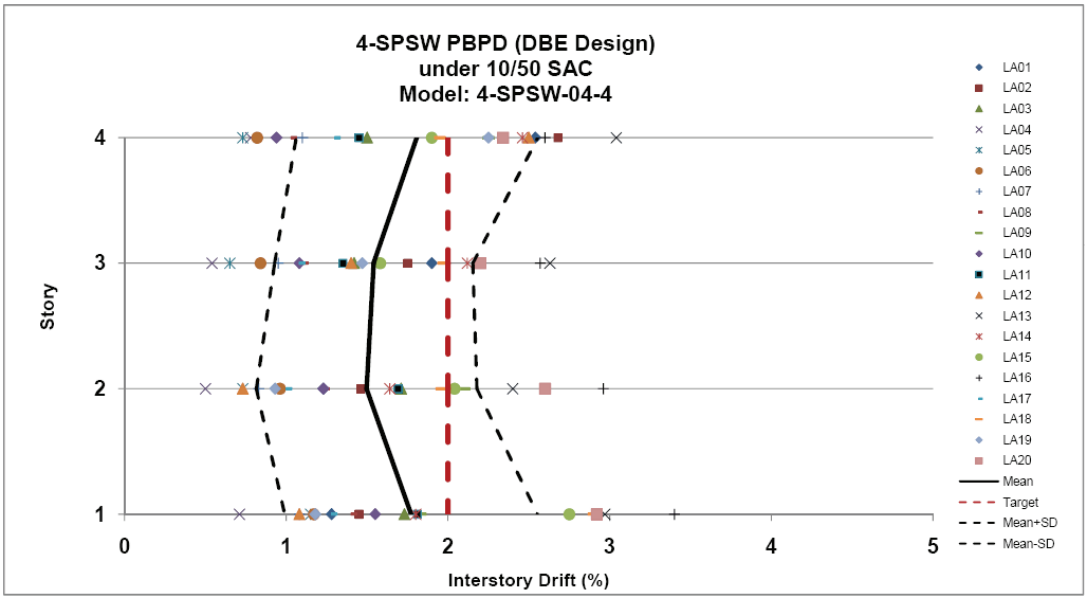

(a)

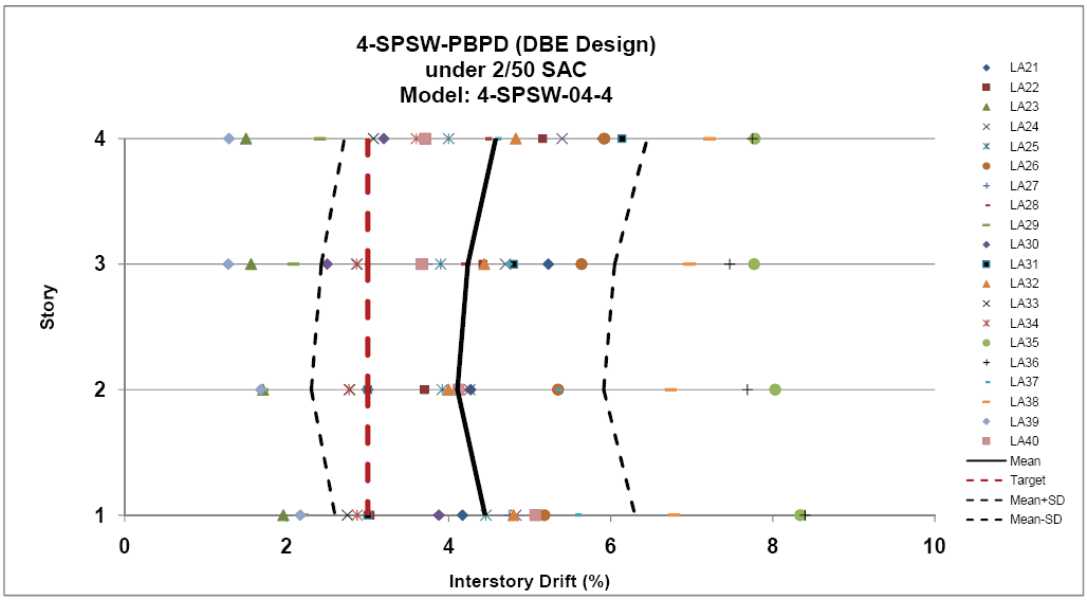

(b)

Figure 8.14. Maximum Story Drifts for PBPD-DBE SPSW under: (a) 10/50 SAC; and (b) 2/50 SAC Ground Motions.

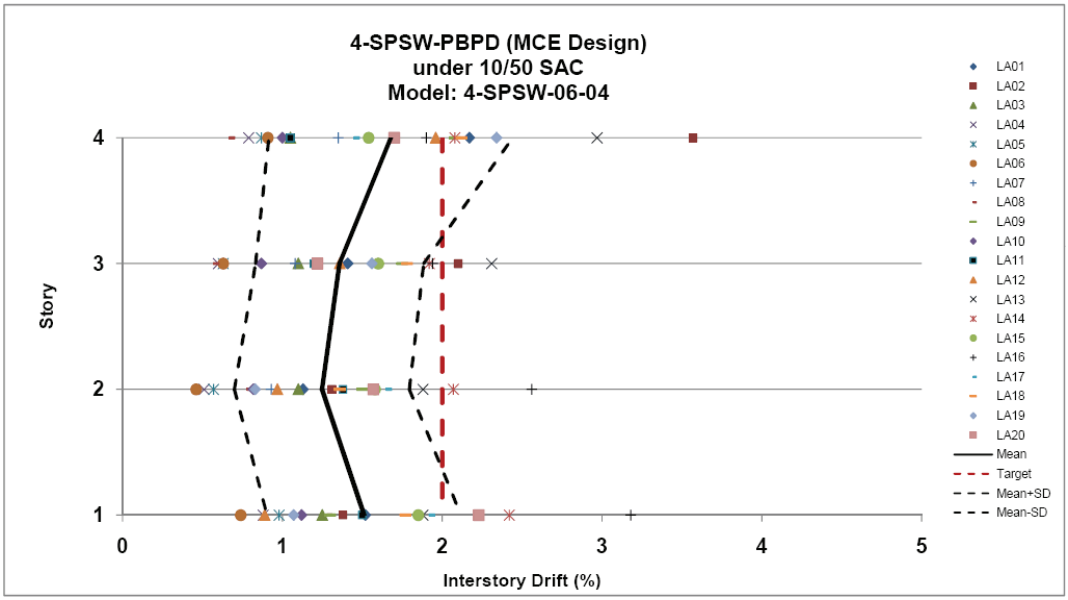

(a)

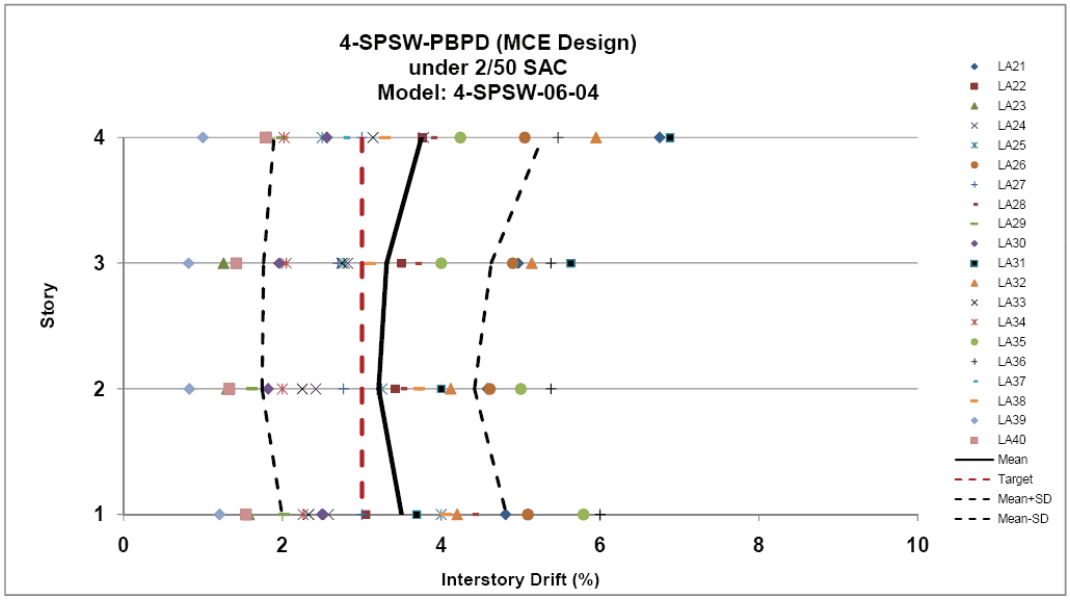

(b)

Figure 8.15. Maximum Story Drifts for PBPD-MCE SPSW under: (a) 10/50 SAC; and (b) 2/50 SAC Ground Motions.

8.5 Summary and Concluding Remarks:

In this chapter, the PBPD procedure for design of SPSW, an emerging lateral load resisting system, was developed. The pinched hysteretic behavior of SPSW leads to difficulty in predicting the maximum drift beyond first yield when the structure is designed by using the conventional elastic design approach. Also, inelastic action or damage in SPSW systems could concentrate only at a few levels if the design is not carried out based on consideration of the overall yield mechanism.

By using target drift and yield mechanism as key performance limit states, the proposed PBPD procedure provides a systematic approach for analysis and design of such systems. The pinching behavior of SPSW is directly accounted for in this method. Moreover, with the proposed PBPD procedure, a dual level design based on appropriate target drift for each hazard level, can be easily implemented to obtain the desired performance at different hazard levels for SPSW systems.

The proposed PBPD procedure was applied into design of example 4-story SPSW frames for different hazard levels. To evaluate and compare the performances of the different designs, nonlinear static and time-history analyses were carried out on all example SPSW frames. Dual tension-only strips (in both directions) were used to model the cyclic behavior of steel web plates in SPSW frames. The maximum story drifts under time-history analyses were obtained for under SAC LA ground motions (both DBE and MCE hazard levels).

Based on the results of this study, it was shown that the proposed PBPD procedure works quite well for design of SPSW frames. The intended target drifts and

yield mechanisms were successfully achieved for the PBPD designs. In addition, the proposed procedure was successfully applied for consideration of dual seismic hazard level in design. In general, the PBPD designed frames showed quite improved performance compared to the code designed SPSW frame, especially under MCE ground motions.

CHAPTER 9

SUMMARY AND CONCLUSIONS

9.1 Summary

9.1.1 Introduction

Current seismic design practice is generally based on elastic structural behavior and inelastic behavior is only considered indirectly through certain modification factors. However, it is known that structures designed by current codes experience large inelastic deformations during major earthquakes. As a result, the behavior of structures under design level ground motions can be somewhat unpredictable and uncontrolled even after all the current code criteria are satisfied. Inelastic activity, including severe yielding and buckling of structural members can be unevenly distributed in the structure which may result in global collapse or costly repair work. Therefore, the current design approaches may not lead to structures with intended behavior under major ground motions. Recently, a new design method has been developed at the University of Michigan, called Performance-Based Plastic Design (PBPD) method (Goel and Chao, 2008). This method directly accounts for inelastic behavior and eliminates the need for any assessment after initial design. The method uses pre-selected target drift and yield mechanism as key performance limit states. In this method, control of drift and yielding is built into the design process from the very start, eliminating or minimizing the need for lengthy iterations to arrive at the final design.

In the present research work, the application of PBPD method was extended to design of mid to high-rise CBF structures by proposing several important modifications in calculation of design base shear. These includes the modification on yield drift estimation for taller CBF structures to include column axial deformations, on lateral force distribution to prevent large story drifts at upper stories due to the higher mode effects, and on target drift by adjusting it with the proposed λ-factor to account for pinching. These proposed modifications were applied to design of 9-story SAC building and resulted in satisfactory seismic performance.

Moreover, different methods were proposed to enhance the confidence level of mid to high-rise CBF structures. These methods include the increase in design base shear by using new λ-factor (in Chapter 6), using Split-X configuration for braces, and increasing the minimum required fracture life, N_f, from 100 to 200. The effect of each of these suggested methods on increasing the confidence level of the 9-story CBF structure were evaluated.

In addition, the application of PBPD method in design of tall MF structures was successfully carried out. Modifications for design of tall MF systems, primarily on design of columns, were proposed to achieve this goal. The current PBPD procedure for design of columns in steel MF structures, although works very well for low-rise frames, but results in quite overdesign sections for mid to high-rise frames. It was shown that by applying the proposed modifications in design of tall MF, excellent seismic performance under pushover as well as time-history analyses can be achieved.

Furthermore, the PBPD procedure for design of Steel Plate Shear Wall (SPSW) frames was developed in this research work. The procedure presents a systematic approach for analysis and design of such systems, using target drift and yield mechanism as key performance limit states. The pinching behavior of SPSW is directly accounted for in this method by using the proposed λ-factor method. Using the developed PBPD method, a dual level design based on appropriate target drift for each hazard level can be easily implemented to obtain the desired performance at different hazard levels for SPSW systems. The proposed procedure is then applied to design of SPSW structures and the performances of these systems are evaluated using nonlinear static and dynamic analyses.

9.1.2 Review of Related Literature on Seismic Performance of MF, CBF, and SPSW Systems and the PBPD Method

Review of the current seismic procedures was done in Chapter 2. Previous studies on the problems with the current code procedures along with the new PBPD method were summarized. In addition, the performances of steel MFs and CBFs in past earthquakes were reviewed. Related experimental and analytical studies found in the literature were briefly presented. Moreover, the analytical and experimental studies on Steel Plate Shear Wall (SPSW) systems were reviewed.

In Chapter 3, the outline for the PBPD procedure was presented along with along with the discussion on different components of this method.

9.1.3 Reliability-Based Seismic Performance Evaluation of CBF Structures

In Chapter 4, the reliability-based performance evaluation (confidence level analysis) was done for two sets of CBF structures, the NEHRP design and the PBPD design. The NEHRP frames, originally designed by Sabelli (2000), were shown to have quite low confidence level against collapse by Uriz and Mahin (2004). In this regard, the PBPD procedure for design of CBF was briefly described. Then, a summary of the reliability-based performance evaluation procedure developed as part of the FEMA/SAC Steel Project (FEMA, 2000) was presented. The confidence level analysis procedure was then applied to the PBPD designed CBF structures. The results can be summarized as follows:

- Reliability-based evaluation by using the FEMA 351 procedure, which accounts for randomness and uncertainty in the estimation of seismic demand and drift capacity, showed that steel concentrically braced frames (CBFs) designed by the performance-based plastic design (PBPD) method can have dramatically higher confidence levels against global collapse than those of CBFs designed in current practice. Also, those confidence levels can be similar to the target confidence levels for SMFs in current practice, *i.e*., 90% or above.

- Significant improvement in the confidence level (C.L.) can be seen for the 3V-PBPD compared to 3V-NEHRP. This C.L. is indeed comparable to those of MFs designed by 1997 NEHRP code (Yun et al., 2002). On the other hand, the 3V-NEHRP shows extremely low confidence level against global collapse. It can also be seen that

although the median drift capacities for the two 3-story frames are somewhat close, they show quite different drift demands under MCE ground motions.

- The C.L. for 6V-NEHRP frame was somewhat better than that of the 3V-NEHRP frame, but was still much less than the 90% satisfactory level as suggested by FEMA 351. Significant difference can still be observed between the C.L.s of 6V-NEHRP and 6V-PBPD, with the latter having a confidence level quite close to 90%.

9.1.4 Modifications on the PBPD Procedure for Design of CBF Structures

In Chapter 5, the PBPD procedure for CBF systems was evaluated and several modifications have been proposed. A new configuration for the gusset plate connection, in which the gusset plate is only connected to the column, is proposed such that the total unbalanced moment on the column would be reduced. Also, the current capacity design method for columns in CBFs based on the accumulative axial forces has been evaluated by comparing the column moments from pushover and dynamic analyses. In addition, a proposed method to account for pinching hysteretic behavior of CBFs in PBPD approach, with the capability to be applied to other types of systems with degrading behavior is introduced. For design base shear calculation in CBF systems, a procedure to estimate the varying yield drift ratio (due to flexural deformation caused by axial deformation of columns) at the beginning of design for braced systems is introduced. The target drift ratio for such systems has been modified accordingly, based on the original definition of the target drift used in the work-energy equation in PBPD. Finally, the suggested PBPD approach is utilized to design the 9-story SAC building by using CBF as the lateral load

resisting system. The performance of this design has then been evaluated using both DBE and MCE SAC LA ground motions. The major findings in Chapter 5 are:

1) Although there is some eccentricity in the proposed connection of gusset plate to column, the total unbalanced moment transferred to the column is smaller in the newly proposed configuration. This is due to the fact that the shear splice in this configuration is much closer to the column centerline. More importantly, the moments produced by the axial force in the brace and those produced by the shear force at the shear splice act oppositely to each other. This would further reduce the unbalanced moment on the column. Since the columns are designed solely based on their accumulative axial force in the PBPD procedure, having less moment demand on columns would ensure their better performance and safety.
2) Even with only considering axial forces in column design in CBF, good performance can still be expected for the PBPD frame. The main reason for this conclusion is that although the bending moments were not considered in columns during the design, since the maximum moments and maximum axial forces in columns are not occurring at the same time, the columns are still behaving fine. Also, the axial force used in column design is based on the assumption that all braces buckle and yield at the same time, which applies the largest possible axial demand on columns. A practical conclusion is that since it is known that there would be some bending moments in columns due to unbalanced moments transferred to the column and also from the continuity of the column itself under dynamic analysis, it is better to use a W-sections with larger depth (with almost

the same weight) whenever possible, so that additional bending capacity can be provided.

3) A new approach was proposed to account for the pinched hysteretic behavior of CBF systems in PBPD procedure. The method can be easily applied to other degrading systems as well. This proposed method has been shown to result in reasonable PBPD design base shear values for low-rise as well as high-rise CBF structures. The proposed modifications on yield drift and target drift should also be included in the modified procedure.
4) The proposed modifications were applied in the design of the 9-story SAC LA frame with CBF as the lateral system. The results from nonlinear static and dynamic analyses showed the desirable performance of the designed structure under both DBE and MCE hazard levels, proving that the dual level design concept has been properly considered.

9.1.5 Enhancement of Confidence Level of Mid to High-Rise CBF Structures Against Collapse

The main objective of the study presented in this chapter was to improve the confidence level (C.L.) for the 9-story CBF against collapse. Several modifications were proposed. The first modification was in the design base shear (DBS) calculation. A slightly larger λ-factor was suggested for mid to high-rise CBF frames to offset the detrimental effect of P-Delta overturning forces in the calculation of DBS.

The effect of using Split-X (two story X bracing) configuration on seismic performance and C.L. of CBF was also studied. In addition, the effect of increasing brace fracture life, N_f, on seismic performance and C.L. was evaluated.

The main conclusions from the results presented in this chapter are:

1) Higher values of design base shear (DBS) for 9-story (and taller) CBF were obtained using the proposed new λ-factor in PBPD method. This new λ-factor results in larger design base shear for mid to high-rise CBF structures.
2) The 9-story Chevron CBF design based on the new DBS showed smaller story drifts under both DBE (10%/50 yrs) and MCE (2%/50 yrs) ground motions compared to the 9V-PBPD-A frame designed in Chapter 5.
3) Higher levels of confidence level (C.L.) against collapse were obtained using the new DBS for Chevron configuration. The C.L. of 52% obtained in Chapter 5 for 9V-PBPD-A increased to 68.6% by using the new DBS in 9V-PBPD-B.
4) Improvement was seen in C.L. of the Chevron frame designed by using increased N_f (of more than 200) for fracture life of the braces. This increase in N_f resulted in increase of C.L. of the 9-stoy Chevron CBF from 68.6% to 79.4% (about 11%).
5) It was shown that C.L. of 9-story CBF improved by only changing the brace configuration to Split-X. The C.L. increased from 68.6% to 77.4% (about 10%) by using Split-X instead of Chevron configuration. The same brace sections were used. However, much lighter beams are needed in the Split-X configuration. The C.L. obtained for the Split-X design with original N_f values was almost equal to that of Chevron design with increased N_f.

6) Increasing the design base shear did not have much effect on drift capacity of the 9-story CBF frames obtained from IDA. However, larger design base shear resulted in lower drift demands with reduced scatter under MCE ground motions which basically translates into higher confidence level.
7) Increase in design base shear based on the new λ-factor was seen to be the main factor in reducing the story drifts under MCE level ground motions. Better controlled drift demands resulted in higher confidence level.
8) Increase in N_f value (brace fracture life factor) did not have significant effect on drift response under MCE level SAC LA ground motions since the maximum story drifts generally occur at the early stages for such near-field ground motions.

9.1.6 Application of PBPD Procedure to Tall Moment Frames

In Chapter 6, modifications were proposed to the current PBPD procedure for design of Non-Designated Yielding Members (Non-DYMs), such as columns, in tall MF structures such that their final design better matches with the expected performance. Two main issues are addressed in this chapter: (1) Calculation of base column plastic moment, M_{pc}, to prevent formation of soft-story mechanism and also to achieve a more realistic column design moment profile over the height of the structure; and (2) P-Delta effect for design of Non-DYMs. These modifications are then applied to redesign the 20-story SAC LA building by the PBPD method using suggested modifications. The performance of the original SAC frame and the PBPD frame under nonlinear static and dynamic analyses are then evaluated and compared. The major findings can be summarized as:

1) The column tree analysis results amplified by B_2-factor give the most appropriate design moments for columns in all stories, while also being slightly conservative. This can also be confirmed by comparing the performances of the frames designed by these three methods under dynamic analysis.
2) Pushover method for obtaining column design moments underestimates the required column moments, which in turn leads to a weak and flexible structure. Also, having insufficient column strength/stiffness in the upper stories by using results of pushover analysis can lead to undesirable performance under dynamic analysis due to higher mode effects, especially for mid to high-rise structures.
3) As targeted in the design, absence of plastic hinges in columns of the PBPD frame (except at the base) can be noticed under pushover analysis at 3.5% roof drift. In contrast, significant plastic hinging in the columns in the lower stories is observed, which also shows up in the differences in deformed shape of the two frames, i.e., concentration of drift in the lower stories of the SAC frame.
4) Several plastic hinging can be observed in the original SAC frame under 10%/50yres (or DBE) and 2%/50yrs (or MCE) ground motions. In contrast, even under MCE ground motions there is no plastic hinging in the columns of the PBPD frame except at the base as intended in design. Also, larger residual drifts are seen in the SAC frame compared to those from PBPD frame.

5) The responses under LA35, LA36, and LA38 were found to be more severe, resulting in larger story drifts for the PBPD frame, but resulted in complete collapse for the SAC frame.

9.1.7 Development of PBPD Procedure for Seismic Design of SPSW Frames

In this chapter, the PBPD procedure for design of SPSW, an emerging lateral load resisting system, was developed. The pinched hysteretic behavior of SPSW leads to difficulty in predicting the maximum drift beyond first yield when the structure is designed by using the conventional elastic design approach. Also, inelastic action or damage in SPSW systems could concentrate only at a few levels if the design is not carried out based on consideration of the overall yield mechanism.

By using target drift and yield mechanism as key performance limit states, the proposed PBPD procedure provides a systematic approach for analysis and design of such systems. The pinching behavior of SPSW is directly accounted for in this method. Moreover, with the proposed PBPD procedure, a dual level design based on appropriate target drift for each hazard level, can be easily implemented to obtain the desired performance at different hazard levels for SPSW systems.

The proposed PBPD procedure was applied into design of example 4-story SPSW frames for different hazard levels. To evaluate and compare the performances of the different designs, nonlinear static and time-history analyses were carried out on all example SPSW frames. Dual tension-only strips (in both directions) were used to model the cyclic behavior of steel web plates in SPSW frames. The maximum story drifts under

time-history analyses were obtained for under SAC LA ground motions (both DBE and MCE hazard levels).

Based on the results of this study, it was shown that the proposed PBPD procedure works quite well for design of SPSW frames. The intended target drifts and yield mechanisms were successfully achieved for the PBPD designs. In addition, the proposed procedure was successfully applied for consideration of dual seismic hazard level in design. In general, the PBPD designed frames showed quite improved performance compared to the code designed SPSW frame, especially under MCE ground motions.

9.2 Concluding Remarks

- It has been shown that the PBPD procedure is a powerful and reliable design method for different steel structural systems, resulting in structures with superior seismic performance.

- As was shown in the development of the design procedure for SPSW system, the PBPD method has the capability of being applied to various structural systems due to its strong theoretical basis. In addition to the conventional systems, innovative structural schemes can be developed by selecting suitable yielding members and/or devices and placing them at strategic locations, while the designated non-yielding members can be detailed for no or minimum ductility capacity. All of this would translate into enhanced performance, safety, and economy in life-cycle costs.

- The target drift and yield mechanism design criteria used in PBPD procedure were shown to work quite well for taller frames as well. Accordingly, this method can provide the much needed initial guidance on proportioning the member sizes at the beginning of the design, especially when the deformations are governing the design, such as in MF system.

- It was shown that the conventional thinking of CBF structures as systems with inferior seismic performance and reliability under severe ground motions can be dramatically altered by using PBPD criteria in their design. In many cases, the PBPD designed CBF structures showed the confidence levels on the order of those from MF systems while being evaluated against global collapse.

- Application of the PBPD method on taller CBF systems was achieved using the proposed modifications to the calculation of the PBPD design base shear. These modifications were suggested to account for the pinched hysteretic response and also the varying yield drift ratios due to column axial deformation, and selection of proper target drift for such systems. The modifications were especially beneficial in applying the PBPD method to taller CBF structures. Moreover, different methods to increase the confidence level of mid to high-rise CBF structures against collapse were proposed and their efficiencies in enhancing the confidence level are evaluated.

- It was shown in the design of CBF and SPSW systems that the dual level design based on appropriate target drift for each hazard level can be easily and reliably implemented in the PBPD procedure to obtain the desired performance at different hazard levels.

9.3 Suggested Future Studies

Some aspects of the research work presented herein needs to be further studied. Some suggestions for future studies on these topics are:

- More comprehensive performance evaluation of the CBF structures designed by suggested PBPD method can be done by using the newly published FEMA P695. The validity of the suggested modifications can also be evaluated using the procedure introduced in this document.

- The developed PBPD procedure for SPSW frames can be extended to design of SPSW with moment resisting connections. For an efficient design, the contributions of each system (steel web plates and frame action) on resisting lateral loads should be estimated at the beginning of design.

- The application of PBPD on dual systems can be considered in the next step of the research. Proper modifications in the design parameters should be made based on the combined behavior of the two lateral force resisting systems.

- Developing the PBPD procedure for design of Coupled SPSWs can be considered in future. This system is quite beneficial especially for tall SPSW frames. However, some challenges exist in terms of estimation of PBPD design parameters as well as proper design of Non-Yielding members.

- Another interesting topic related to the current work that can be done in future is applying PBPD based Energy Evaluation method to obtain maximum drift demand for SPSW and CBF structures (systems with pinched hysteretic behavior).

REFERENCES

AISC. (1997), Seismic Provisions for Structural Steel Buildings, American Institute of Steel Construction, Chicago, Illinois.

AISC. (2005a), ANSI/AISC 341-05, *Seismic Provisions for Structural Steel Buildings*, American Institute of Steel Construction, Chicago, Illinois.

AISC. (2005b), ANSI/AISC 360-05, *Specification for Structural Steel Buildings*, AmericanInstitute of Steel Construction, Chicago, Illinois.

Akiyama, H. (1985), "Earthquake-Resistant Limit-State Design of Buildings." University of Tokyo Press, Japan.

Applied Technology Council. (1978), "Tentative Provisions for the Development of Seismic Regulations for Building," *ATC 3-06 Report*, NBS Special Publication 510, NSF Publication 78-08.

Applied Technology Council. (2005), "Improvement of Nonlinear Static SeismicAnalysis Procedures," FEMA 440 Report, Applied Technology Council, Redwood City,California and Federal Emergency Management Agency, Washington, D. C.

ASCE. (2000), "Prestandard and Commentary for the Seismic Rehabilitation of Buildings," FEMA 356 Report, prepared by the American Society of Civil Engineers, published by Federal Emergency Management Agency, Washington, D. C.

ASCE. (2005), Minimum Design Loads for Buildings and Other Structures, SEI/ASCE 7-05, American Society of Civil Engineers, Reston, VA.

Aslani, F. and Goel, S.C. (1991), "Stitch Spacing and Local Buckling in Seismic Resistant Double Angle Bracing Members," *Journal of Structural Engineering*, ASCE, Vol. 177, No. 8, August, Reston, VA.

Astaneh-Asl, A. (1998). "Seismic Design and Behavior of Gusset Plates." Structural Steel And Education Council {Steel Tips}, 209 Vernal Drive, Alamo, California 94507.

Astaneh-Asl, A., Goel, S., and Hanson, R. D. (1985). "Cyclic out-of-plane buckling of double-angle bracing." *ASCE Journal of Structural Engineering*, 111(5), 1135- 1153.

Astaneh-Asl, A., (2001). "Seismic Behavior and Design of Steel Shear Walls", *Steel TIPS Report*, Structural Steel Educational Council, CA.

Bayat, M.R., Chao, S-H., Goel, S.C. (2010), "Further Development of Performance-Based Plastic Design Method for Concentrically Braced Frame." *9th US National and 10th Canadian Conference on Earthquake Engineering,* July 2010, Toronto, Canada.

Bayat, M.R., Goel, S.C., Chao, S-H. (2010). "Performance-Based Plastic Design of Earthquake Resistant Concentrically Braced Steel Frames "*Report No. UMCEE 10-02*, Department of Civil and Environmental Engineering, University of Michigan, Ann Arbor, MI.

Berman, J.W., and Bruneau, M. (2003), "Experimental Investigation of Light-Gauge Steel Plate Shear for the Seismic Retrofit of Buildings", *Technical Report No. MCEER-03-0001*, Multidisciplinary Center for Earthquake Engineering Research, Buffalo, NY.

Berman, J. W., Celik, O.C., Bruneau, M., (2005), "Comparing Hysteretic Behavior of Light-Gauge Steel Plate Shear Walls and Braced Frames." *Engineering Structures*, 27(3):475- 485.

Berman, J. W. and Bruneau, M. (2005), "Experimental Investigation of Light-Gauge Steel Plate Shear Walls." *Journal of Structural Engineering*, ASCE, Vol. 131, No. 2, pp. 259–267.

Berman, J. W., and Bruneau, M. (2008), "Capacity Design of Vertical Boundary Elements in Steel Plate Shear Walls." *Engineering Journal.*, 45(1), 55–71.

Berman, J. W., Lowes, L. N., Okazaki, T., Bruneau, M., Tsai, K-C., Driver, R. G., Sabelli, R. (2008). "Research Needs and Future Directions for Steel Plate Shear Walls." *Proceedings of 2008 ASCE Structure Congress*, Vancouver, Canada.

Bertero, V. V., Anderson, J. C., Krawinkler, H, Miranda, E. (1991). "Design Guidelines for Ductility and drift Limits." *Report No. UCB/EERC-91/15*. University of California, Earthquake Engineering Center, Berkeley, CA, 1991.

Bondy, K. D. (1996), "A More Rational Approach to Capacity Design of Seismic Moment Frame Columns." *Earthquake Spectra*, EERI, 12(3), 395-406.

Building Seismic Safety Council (BSSC). (2003a), "National Earthquake Hazard Reduction Program (NEHRP) Recommended Provisions for Seismic Regulations for New Buildings and Other Structures—Part 1: Provisions (FEMA 450-1)," Federal Emergency Management Agency, Washington, D. C.

Building Seismic Safety Council (BSSC). (2003), "National Earthquake Hazard Reduction Program (NEHRP) Recommended Provisions for Seismic Regulations for

New Buildings and Other Structures—Part 2: Commentary (FEMA 450-2)," Federal Emergency Management Agency, Washington, D. C.

Building Seismic Safety Council (BSSC). (2006), "NEHRP Recommended Provisions: Design Examples (FEMA 451)." Federal Emergency Management Agency, Washington, D. C.

Caccese, V., Elgaaly, M., and Chen, R., (1993), "Experimental Study of Thin Steel-Plate Shear Walls Under Cyclic Load", *Journal of Structural Engineering*, ASCE, Vol. 119, No. 2, Feb. 1993, pp. 573-587.

Calvi, G. M., Priestley, M. J. N., Sullivan, T. J., and Happold, B. (2006). Development of Displacement-Based Design and Assessment Methods; Progress Review: Year 1. *Presentation, European Centre for Training and Research in Earthquake Engineering (EUCENTRE), Nov 2006. (url:* http://www.reluis.it*).*

Chao, S.-H., and Goel, S. C. (2005), "Performance-Based Seismic Design of EBF Using Target Drift and Yield Mechanism as Performance Criteria," *Report No. UMCEE 05-05*, Department of Civil and Environmental Engineering, University of Michigan, Ann Arbor, MI.

Chao, S-H., and Goel, S. C., (2006a), "Performance-Based Plastic Design of Seismic Resistant Special Truss Moment Frames (STMF)." *Report No. UMCEE 06-03*, Department of Civil and Environmental Engineering, University of Michigan, Ann Arbor, MI.

Chao, S-H., and Goel, S. C., (2006b), "A seismic design method for steel concentric braced frames for enhanced performance." *4th International Conference on Earthquake Engineering,* Taipei, Taiwan.

Chao, S.-H., and Goel, S.C., Lee, S.-S., (2007), "A Seismic design lateral force distribution based on inelastic state of structures." *Earthquake Spectra* 23 (3), 547-569.

Chao, S.-H., and Goel, S. C. (2008), "Performance-Based Plastic Design of Special Truss Moment Frames," *AISC Engineering Journal,* 2nd quarter, 127-150.

Chao, S.-H., Bayat, M. R., and Goel, S.C., (2008), "Performance-Based Plastic Design of steel concentric braced frames for enhanced confidence level." *14th World Conference on Earthquake Engineering,* Beijing, China.

Choi, I.-R., and Park, H.-G., (2008), "Ductility and Energy Dissipation Capacity of Shear-Dominated Steel Plate Walls." *Journal of Structural Engineering*, ASCE, Vol. 134, No. 9, pp. 1495-1507.

Chopra, A. K. (2000), *Dynamics of Structures- Theory and Applications to Earthquake Engineering*, 2nd edition, Prentice Hall, Englewood Cliffs, New Jersey, 844 pp.

Clough, R.W., and Penzien, J. (1993), *Dynamics of Structures*, 2nd edition., McGraw-Hill,Inc., New York, 739 pp.

CSA, (2001), *Limit States Design of Steel Structures*, CAN/CSA S16-01, CanadianStandards Association, Willowdale, Ontario, Canada.

CSI (2007). *Perform-3D v.4.0 User Manual*. Computers & Structures Inc., Berkeley, CA.

Dasgupta, P., Goel, S.C., and Parra-Montesinos, G. (2004) "Performance-Based Seismic Design and Behavior of a Composite Buckling Restrained Braced Frame (BRBF)", Paper No. 497, *Proceedings of 13WCEE*, Vancouver, BC, August 1-6, 2004.

Driver, R. G., Kulak, G. L., Kennedy, D. J. L., and Elwi, A. E. (1997). "Seismic behavior of steel plate shear walls." *Structural Engineering Rep. No. 215*, Univ. of Alberta, Edmonton, Alberta, Canada.

Driver, R.G., Kulak, G.L., Kennedy, D.J.L., and Elwi, A.E. (1998), "Cyclic Test of Four-Story Steel Plate Shear Wall", *Journal of Structural Engineering*, ASCE, Vol. 124, No. 2, Feb. 1998, pp 112-130.

Englekirk, R. (1994). *Steel Structures: Controlling Behavior Through Design.* John Wiley & Sons, Inc.

FEMA 356. (2000a), "Prestandard and Commentary for the Seismic Rehabilitation ofBuildings," Federal Emergency Management Agency, Washington, D. C.

FEMA. (2000b). FEMA 351: Recommended Seismic Evaluation and Upgrade Criteria for Existing Welded Steel Moment Frame Buildings, Federal Emergency Management Agency, Washington, DC.

FEMA. (2000c). "FEMA 355E: State of the Art Report on Past Performance of Steel Moment-Frame Buildings in Earthquakes." D. Bonowitz and R. Evans, (Team Leader) Federal Emergency Management Agency, Washington, D.C.

FEMA (2004), FEMA 440, *Improvement of Inelastic Seismic Analysis Procedures*, Federal Emergency Management Agency, Washington, D.C.

Foutch, D. and Shi, S. (1998), "Effects of Hysteresis Type on the Seismic Response of Buildings." *Proceedings of the 6th US National Conference on Earthquake Engineering*.

Goel, S.C., (1992a). "Cyclic Post-Buckling Behavior of Steel Bracing Members." In *Stability and Ductility of Steel Structures under Cyclic Loading*. Ed. Y. Fukumoto and G. C. Lee. Boca Raton, FL, CRC Press: 75-84.

Goel, S. C. (1992b). "Earthquake Resistant Design of Ductile Braced Steel Structures." In *Stability and Ductility of Steel Structures under Cyclic Loading*, Ed. Y. Fukumoto and G. C. Lee. Boca Raton, FL, CRC Press, pp. 297-308.

Goel, S.C., and Lee, S. (1992), "A Fracture Criterion for Concrete-Filled Tubular Bracing Members Under Cyclic Loading." *Proceedings of the 1992 ASCE Structures Congress*, ASCE, pp. 922-925, Reston, VA.

Goel, S. C., and Itani, A. M. (1994). "Seismic-Resistant Special Truss-Moment Frames," *Journal of Structural Engineering*, ASCE, 120 (6), 1781-1797.

Goel, S.C., and Leelataviwat, S. (1998). "Seismic Design by Plastic Method." *Engineering Structures*, Elsevier Science, 20(4-6), 465-471

Goel, S.C. and Chao, S-H., (2008). *Performance-Based Plastic Design: Earthquake Resistant Steel Structures*, International Code Council.

Gupta, A. and Krawinkler, H. (1999). "Seismic Demands for Performance Evaluation Steel Moment Resisting Frame Structures." *Report No. 132*, The John A. Blume Earthquake Engineering Center, Dept. of Civil and Env Eng., Stanford University.

Gupta, A., and Krawinkler, H. (2000). "Dynamic P-delta effects for flexible inelastic steel structures." *ASCE Journal of Structural Engineering*, 126(1), pp. 145-154.

Gupta, B and Kunnath, S.K. (1998), "Effects of Hysteresis Model Parameters on Inelastic Seismic Demands." *Proceedings of the 6th US National Conference on Earthquake Engineering.*

Hamburger, R., Rojahn, C., Moehle, J., Bachman, R., Comartin, C., and Whittaker, A. (2004), "The ATC-58 Project: Development of Next-Generation Performance-Based Earthquake Engineering Design Criteria for Buildings," *13th World Conference on Earthquake Engineering*, Paper No. 1819, Vancouver, B. C., Canada.

Hassan, O. F., and Goel, S. C. (1991). "Modeling of Bracing Members and Seismic Concentrically Braced Frames." *UMCE 91-1*, University of Michigan, College of Engineering, Ann Arbor, MI 48109-2125.

Housner, G. W. (1956), "Limit Design of Structures to Resist Earthquakes," *Proceedings of the First World Conference on Earthquake Engineering*, Berkeley, CA: Earthquake Engineering Research Institute.

Housner, G. W. (1960). "The Plastic Failure of Frames During Earthquakes," *Proceedingsof the Second World Conference on Earthquake Engineering*, Tokyo: Internationa Association of Earthquake Engineering :pp. 997-1012.

International Code Council (ICC). (2006), *International Building Code*, ICC, Birmingham, AL.

Krawinkler, H., and Miranda, E. (2004). *Performance-Based Earthquake Engineering. Earthquake Engineering—from Engineering Seismology to Performance-Based Engineering*, Edited by Bozorgnia, Y. and Bertero, V. V., CRC Press.

Lacerte, M., Tremblay, R. (2006), "Making Use of Brace Overstrength to Improve the Seismic Response of Multistory Split-X Concentrically Braced Steel Frames.", *Canadian Journal of Civil Engineering*, 33 (8), 1005-1021.

Lee, H.-S. (1996). "Revised Rule for Concept of Strong-Column Weak-Girder Design." *Journal of Structural Engineering*, ASCE, Vol. 122, No.4, pp. 359-364.

Lee, S-S., and Goel, S. C. (1987), "Seismic Behavior of Hollow and Concrete-Filled Square Tubular Bracing Members," *Report No. UMCE 87-11*, Department of Civil and Environmental Engineering, University of Michigan, Ann Arbor, MI.

Lee, H.-S, and Goel, S. C. (1990), "Seismic Behavior of Steel Built-Up Box-Shaped Bracing Members and Their Use in Strengthening Reinforced Concrete Frames," *Report No. UMCE 90-7*, Department of Civil and Environmental Engineering, University of Michigan, Ann Arbor, MI.

Lee, S.-S. and Goel, S.C. (2001). "Performance-Based Design of Steel Moment Frames Using Target Drift and Yield Mechanism", *Report No. UMCEE 01-17*, Dept. of Civil and Environmental Engineering, University of Michigan, Ann Arbor, MI.

Leelataviwat, S.(1998), "Drift and Yield Mechanism Based Seismic Design and Upgrading of Steel Moment Frames", *PhD Dissertation*, University of Michigan, Ann Arbor, MI.

Leelataviwat, S., Goel, S. C., and Stojadinovic, B., (1999). "Toward Performance-Based Design of Structures." *Earthquake Spectra* 15 (3): 435-461

Liu, Z. and Goel, S.C. (1987), "Investigation of Concrete Filled Steel Tubes under Cyclic Bending and Buckling." *Report No. UMCEE 87-03*, Department of Civil and Environmental Engineering, University of Michigan, Ann Arbor, MI.

Liu, Z. and Goel, S.C. (1988), "Cyclic Load Behavior of Concrete-Filled Tubular Braces," *Journal of the Structural Division*, ASCE, Vol. 114, No. 7, Reston, VA.

Lubell, A.S., Prion, H.G.L., Ventura, C.E., and Rezai, M. (2000), "Unstiffened Steel Plate Shear Wall Performance Under Cyclic Loading", *Journal of Structural Engineering*, ASCE, Vol. 126, No.4, pp. 453-460.

MacRae, G.A., Kimura, Y., Roeder, C. (2004), "Effect of Column Stiffness on Braced Frame Seismic Behavior." *Journal of Structural Engineering*, 130(3), 381-391.

Malley, J., Yu, Q-S., and Moore, K. (2004). Seismic Design of Steel Moment Frames. *Earthquake Engineering—from Engineering Seismology to Performance-Based Engineering*, Edited by Bozorgnia, Y. and Bertero, V. V., CRC Press.

Medina, R. A. and Krawinkler, H. (2004). "Influence of Hysteretic Behavior on the Nonlinear Response of Frame Structures", *Proceedings of the 13th World Conference on Earthquake Engineering*, 13WCEE, Vancouver, B.C., Canada, Paper # 239, August 1-6.

Medina, R. A., and Krawinkler, H. (2005), "Strength Demand Issues Relevant for the Seismic Design of Moment-Resisting Frames", *Earthquake Spectra*, Vol. 21 No. 2, pp. 415-439.

Miranda, E., and Akkar, S. D. (2006). "Generalized Interstory Drift Spectrum", *Journal of Structural Engineering*, ASCE, Vol. 132, No.6, pp. 840-852.

Miranda, E. and Bertero. (1994). "Evaluation of Strength Reduction Factors for Earthquake-Resistant Design", *Earthquake Spectra*, Vol. 10, No. 2, 357-379.

NCREE website, National Center for Research on Earthquake Engineering, Taipei, Taiwan, *url:* http://w3.ncree.org/

NEHRP (National Earthquake Hazards Reduction Program). (1997). FEMA 302: Recommended Provisions for Seismic Regulations for New Buildings and Other Structures. Washington, D.C., Federal Emergency Management Agency.

Newmark, N. M., and Hall, W. J. (1973). "Seismic Design Criteria for Nuclear Reactor Facilities." *Report No. 46*, Building Practices for Disaster Mitigation, National Bureau of Standards, U.S. Department of Commerce.

Newmark, N.M. and Hall, W.J. (1982). *Earthquake Spectra and Design*, Earthquake Engineering Research Institute, El Cerrito, CA.

Park, H.-G., Kwack, J.-H., Jeon, S.-W., Kim, W.-K., Choi, I.-R. (2007), "Framed Steel Plate Wall Behavior under Cyclic Lateral Loading." *Journal of Structural Engineering*, ASCE, Vol. 133, No. 3, pp. 387-388.

Park, R., and Pauley, T. (1975). *Reinforced Concrete Structures*. John Wiley and Sons Inc., New York, New York.

Paulay, T., and Priestley, M. J. N. (1992), "Seismic design of reinforced concrete andmasonry buildings," Wiley, New York.

Qu, B., Bruneau, M., Lin, C-H., and Tsai, K.-C., (2008). "Testing of Full-Scale Two-Story Steel Plate Shear Wall with Reduced Beam Section Connections and Composite Floors." *Journal of Structural Engineering*, 134 (3): 364-373.

Rahnama, M., and Krawinkler, H. (1993), "Effects of soft soil and hysteresis model on seismic demands", *Report No. 108,* John A. Blume Earthquake Engineering Center Department of Civil and Environmental Engineering, Stanford University, Stanford, California.

Rai, D.C., Goel, S. C. and Firmansjah, J. (1996). "SNAP-2DX: General Purpose Computer Program for Static and Dynamic Nonlinear Analysis of Two Dimensional Structures", *Report No. UMCEE 96-21*, Dept. of Civil and Environmental Eng., University of Michigan, Ann Arbor, MI.

Redwood, R. G., and Channagiri, V. S. (1991), "Earthquake Resistant Design of Concentrically Braced Steel Frames," *Canadian Journal of Civil Engineering*, Vol. 18, pp. 839-850.

Rezai, M. (1999), "Seismic Behavior of Steel Plate Shear Walls by Shake Table Testing", *Ph.D. Dissertation*, University of British Columbia, Vancouver, British Columbia, Canada.

Richards, P. (2009). "Seismic Column Demands in Ductile Frames." *Journal of Structural Engineering*, ASCE, 135 (1), 33-41.

Roberts, T.M., and Sabouri-Ghomi, S. (1992), "Hysteretic Characteristics of Unstiffened Perforated Steel Plate Shear Walls", *Thin Walled Structures*, Vol. 14, pp. 139- 151.

Ruiz-Garcia, J., Miranda, E. (2005), "Performance-based assessment of existing structures accounting for residual displacements", *Report TR-153*, The John A. Blume Earthquake Engineering Center, Stanford University, Stanford, CA.

Sabelli, R., (2000). "Research on Improving the Design and Analysis of Earthquake Resistant Steel Braced Frames", *FEMA/EERI Report*, Washington, D. C.

Sabelli, R., Mahin, S., and Chang, C. (2003). "Seismic Demands on Steel Braced Frame Buildings with Buckling-Restrained Braces," *Engineering Structures*, Vol. 25, pp. 655-666.

Sabelli, R., and Bruneau, M. (2007). *Steel Plate Shear Walls (AISC Design Guide # 20)*, American Institute of Steel Construction, Chicago, IL.

Shaback, B., and Brown, T. (2003). ”Behaviour of Square Hollow Structural Steel Braces with End Connections under Reversed Cyclic Axial Loading,” *Canadian Journal of Civil Engineering*, Vol. 30, pp. 745-753.

Somerville, P.G., Smith, M., Punyamurthula, S. and Sun, J. (1997). “Development of Ground Motion Time Histories for Phase 2 of the FEMA/SAC Steel Project”, *Report No. SAC/BD-97/04*, SAC Joint Venture, Sacramento, CA.

Tang, X., and Goel, S. C. (1987), “Seismic Analysis and Design Considerations of Braced Steel Structures,” *Report No. UMCEE 87-04*, Department of Civil and Environmental Engineering, University of Michigan, Ann Arbor, MI

Tang, X., and Goel, S. (1989). "Brace Fractures and Analysis of Phase I Structure."*ASCE Journal of Structural Engineering*, 115(8), 1960-1976.

Thorburn, L.J., Kulak, G.L., and Montgomery, C.J. (1983), "Analysis of Steel Plate ShearWalls", *Structural Engineering Report No. 107*, Department of Civil Engineering,Universtiy of Alberta, Edmonton, Alberta, Canada.

Timler, P.A. and Kulak, G.L. (1983), "Experimental Study of Steel Plate Shear Walls", *Structural Engineering Report No. 114*, Department of Civil Engineering, University of Alberta, Edmonton, Alberta, Canada.

Tremblay, R. and Robert, N. (2000), “Seismic Design of Low- and Medium-Rise Chevron Braced Steel Frame.” *Canadian Journal of Civil Engineering*, 27(6), 338-360.

Tromposch, E.W., and Kulak, G.L. (1987), “Cyclic and Static Behaviour of Thin Panel Steel Plate Shear Walls”, *Structural Engineering Report No. 145*, Department of Civil Engineering, University of Alberta, Edmonton, Alberta, Canada.

Uang, C.-M., and Bertero, V. V. (1988), “Use of Energy as a Design Criterion in Earthquake-Resistant Design,” *Report No. UCB/EERC-88/18*, Earthquake Engineering Research Center, University of California, Berkeley, CA.

UBC (1994). *Uniform Building Code*, International Conference of Building Officials, Whittier, California.

UBC (1997). *Uniform Building Code*, International Conference of Building Officials, Whittier, California.

Uriz, P., Mahin, S.A. (2004). “Seismic Performance Assessment of Concentrically Braced Frames”. Paper No. 1639, *13th World Conference on Earthquake Engineering*, Vancouver, B. C., Canada.

Uriz, P. (2005). "Towards Earthquake Resistant Design of Concentrically Braced Steel Structures", *Ph.D. Thesis*, University of California, Berkeley.

Vamvatsikos, D. and Cornell, C.A. (2002). "Incremental Dynamic Analysis". *Earthquake Engineering and Structural Dynamics*, 31, 491-514.

Vian, D., and Bruneau, M. (2005). "Steel plate shear walls for seismic design and retrofit of building structure." *Technical Rep. No. MCEER- 05-0010*, Multidisciplinary Center for Earthquake Engineering Research, Buffalo, N.Y.

Vian, D., Bruneau, M., Tsai, K. C., and Lin, Y. C. (2009). "Special perforated steel plate shear walls with reduced beam section anchor beams. I: Experimental investigation." *Journal of Structural Engineering*, 135(3), 211– 220.

Wallace, B. J. and Krawinkler, H. (1985), "Small-Scale Model Experimentation on Steel Assemblies," *John A. Blume Earthquake Engineering Center Report No. 75*, Stanford University, Department of Civil Engineering, Palo Alto, CA.

Yang, Y.T. and Whittaker, A.S. (2002), "MCEER Demonstration Hospitals, Mathematical Models and Preliminary Analysis Results," *Technical Report*, Multidisciplinary Center for Earthquake Engineering Research, Buffalo, NY.

Yun, S.-Y., Hamburger, R.O., Cornell, C.A. and Foutch, D.A. (2002). "Seismic Performance Evaluation for Steel Moment Frames.' *Journal of Structural Engineering*, 128: 4, 534-545.

BIOGRAPHICAL INFORMATION

Mohammad Reza Bayat received his BS Degree in Civil Engineering from Shiraz University, Shiraz, Iran, in September 2003 and MS Degree in Structural Engineering from Sharif University of Technology, Tehran, Iran, in February 2006. He completed his Ph.D. Degree in Civil Engineering/Structures at the University of Texas at Arlington in December 2010. He was the recipient of the most outstanding graduate student award in Department of Civil Engineering at UT Arlington, in recognition of academic excellence in 2009-2010 academic year. His research interests include performance-based earthquake engineering, nonlinear analysis of structures, structural stability, performance-based plastic design, and behavior of steel and composite structures.